RECORD
2023/6

6IAS: PILBARA CRATON, EVOLVING ARCHEAN TECTONIC STYLES — FIELD GUIDE

MJ Van Kranendonk and RH Smithies

Government of Western Australia
Department of Mines, Industry Regulation and Safety

Geological Survey of Western Australia

Government of **Western Australia**
Department of **Mines, Industry Regulation and Safety**

RECORD 2023/6

6IAS: PILBARA CRATON, EVOLVING ARCHEAN TECTONIC STYLES – FIELD GUIDE

MJ Van Kranendonk* and RH Smithies

* Australian Centre for Astrobiology, University of New South Wales Sydney, Kensington NSW 2052

PERTH 2023

Geological Survey of Western Australia

REFERENCE
The recommended reference for this publication is:
Van Kranendonk, MJ and Smithies, RH 2023, 6IAS: Pilbara Craton, evolving Archean tectonic styles — field guide: Geological Survey of Western Australia, Record 2023/6, 88p.

ISBN 978-1-74168-008-9
ISSN 2204-4345

Grid references in this publication refer to the Geocentric Datum of Australia 1994 (GDA94). Locations mentioned in the text are referenced using Map Grid Australia (MGA) coordinates, Zone 50. All locations are quoted to at least the nearest 100 m.

About this publication
This field guide relates to a pre-conference field trip planned from 17 to 23 July 2023, for the Sixth International Archean Symposium.

Much of the isotope and element analyses were conducted using the GeoHistory laser-ablation ICP-MS and SHRIMP ion microprobe facilities at the John de Laeter Centre (JdLC), Curtin University, with the financial support of the Australian Research Council and AuScope National Collaborative Research Infrastructure Strategy (NCRIS).

The TESCAN Integrated Mineral Analyser (TIMA) instrument was funded by a grant from the Australian Research Council (LE140100150) and is operated by the JdLC with the support of the Geological Survey of Western Australia, The University of Western Australia and Murdoch University.

Acknowledgement of Country
We respectfully acknowledge Aboriginal peoples as the Traditional Custodians of this land on which we deliver our services to the communities throughout Western Australia. We acknowledge their enduring connection to the lands, waterways and communities and pay our respects to Elders past and present.

Published 2023 by the Geological Survey of Western Australia
This Record is published in digital format (PDF) and is available online at <www.dmirs.wa.gov.au/GSWApublications>.

Further details of geoscience products are available from:
First Floor Counter
Department of Mines, Industry Regulation and Safety
100 Plain Street
EAST PERTH WESTERN AUSTRALIA 6004
Telephone: +61 8 9222 3459 Email: publications@dmirs.wa.gov.au
www.dmirs.wa.gov.au/GSWApublications

Cover image: Aerial view of the boxwork set of hydrothermal chert–barite veins that directly underlie and are synchronous with deposition of the c. 3.48 Ga Dresser Formation of the Pilbara Craton. They are host to the world's oldest and most convincing evidence of life. They were visited during the 6IAS Field trip 1 across the Pilbara Craton. Field of view about 500 m. Photo by Martin Van Kranendonk

Contents

Figures

6IAS: Pilbara Craton, evolving Archean tectonic styles — field guide

MJ Van Kranendonk* and RH Smithies

Abstract

This field guide was prepared for a seven-day excursion across the Pilbara Craton associated with the Sixth International Archean Symposium. The guide visits localities that exemplify the lithostratigraphy and tectonic evolution of the northern Pilbara Craton and its evidence for ancient life, based on extensive field and analytical data collected by the Geological Survey of Western Australia (GSWA) and others mainly between 1995 and 2010, but including the results of additional studies thereafter. Comprehensive reviews of the lithostratigraphy and tectonic evolution of the northern Pilbara Craton are presented by Van Kranendonk et al. (2002, 2007b, 2019b) and by Hickman (2016, 2021).

Introduction: Evolution of the Pilbara Craton

The Pilbara region of Western Australia provides extensive exposures of well-preserved Paleoarchean to early Paleoproterozoic crust from which extensive information about the evolution of crustal processes, the biosphere and the atmosphere has been obtained. The region contains two major tectonic divisions: i) the Paleo- to Mesoarchean Pilbara Craton, composed of early (largely hidden) crust (3.80 – 3.53 Ga), well-exposed granite–greenstone terranes (3.53 – 3.07 Ga), syn-tectonic volcano-sedimentary basins and granites (3.05 – 2.93 Ga), and post-orogenic granites (2.89 – 2.83 Ga); ii) the Neoarchean to Paleoproterozoic (2.78 – 2.2 Ga) Mount Bruce Supergroup, consisting of the Fortescue, Hamersley and Turee Creek Basins, which are composed of a thick succession of interbedded volcanic, clastic and chemical sedimentary rocks.

The Pilbara Craton is a 250 000 km^2 ovoid segment of 3800–2830 Ma Archean crust underlying the northwestern part of Western Australia (Fig. 1). The craton is well exposed over 60 000 km^2, with only minor cover by younger successions. The southern 70% of the craton is predominantly concealed by unconformably overlying rocks of the Mount Bruce Supergroup, except for small domes that occupy the cores of ovoid-shaped fold structures.

Mapping and geochronology have revealed that the exposed portion of the Pilbara Craton is composed of five distinct tectonic terranes (Fig. 1). The ancient (3.52 – 3.18 Ga) East Pilbara Terrane forms the nucleus of the craton, onto which the other terranes accreted over the period 3.15 – 2.91 Ga, followed by the emplacement of a major suite of post-orogenic Sn–Ta–Li-bearing granites during 'cratonization' at c. 2.85 Ga (Fig. 2).

Rifting of the Pilbara Craton at c. 2775 Ma and outpouring of Fortescue Group continental flood basalts (Thorne and Trendall, 2001) mark the beginning of a new stage in the evolution of the crust underlying the Pilbara region. The distinctive granite dome and greenstone syncline geometry of the East Pilbara Terrane was reactivated during deposition of the lowermost (unnamed: see Localities 4.1, 4.2, 4.4) part of the >2775–2630 Ma Fortescue Group, but this deformation was comparatively minor and occurred throughout deposition of the group.

The basement rocks of the northern Pilbara Craton comprise seven main tectonostratigraphic units (Fig. 2; Van Kranendonk et al., 2007b, 2010). In order of decreasing age, these are:

1. Early, 3800–3530 Ma, crust of the East Pilbara Terrane: remnants are only very rarely exposed, its original extent is unknown, and its existence is inferred mainly from xenoliths and geochronological data on inherited zircons and isotopic data (Van Kranendonk et al., 2002, 2007b; Kemp et al., 2015; Hickman, 2021).
2. East Pilbara Terrane, 3525–3235 Ma: a granite–greenstone terrane consisting of the predominantly volcanic succession of the Pilbara Supergroup (comprising, from oldest to youngest, the Warrawoona, Kelly and Sulfur Springs Groups) and four contemporaneous granitic supersuites (from oldest to youngest the Callina, Tambina, Emu Pool and Cleland Supersuites).
3. A c. 3.2 Ga rift succession in both the West Pilbara Superterrane (Regal Basalt and Dixon Island Formation: Smithies et al., 2007a; Kiyokawa et al., 2002) and East Pilbara Terrane (Soanesville Group: Rasmussen et al., 2007; Van Kranendonk et al., 2010).

* Australian Centre for Astrobiology, University of New South Wales Sydney, Kensington NSW 2052

4. West Pilbara Superterrane, 3270–3070 Ma: three granite–greenstone terranes, independently formed between 3270 and 3100 Ma, in part built on older crust to 3450 Ma, and accreted by plate convergence at 3070 Ma.
5. The southeastern Kurrana Terrane, 3200–2895 Ma: two granitic supersuites, with greenstones of uncertain age.
6. De Grey Superbasin, 3050–2930 Ma: five depositional basins, and three contemporaneous, mainly granitic, supersuites (from oldest to youngest the Orpheus, Maitland River and Sisters Supersuites).
7. Split Rock Supersuite, 2890–2830 Ma: late- to post-tectonic S–Ta–Li-bearing granitic intrusions.

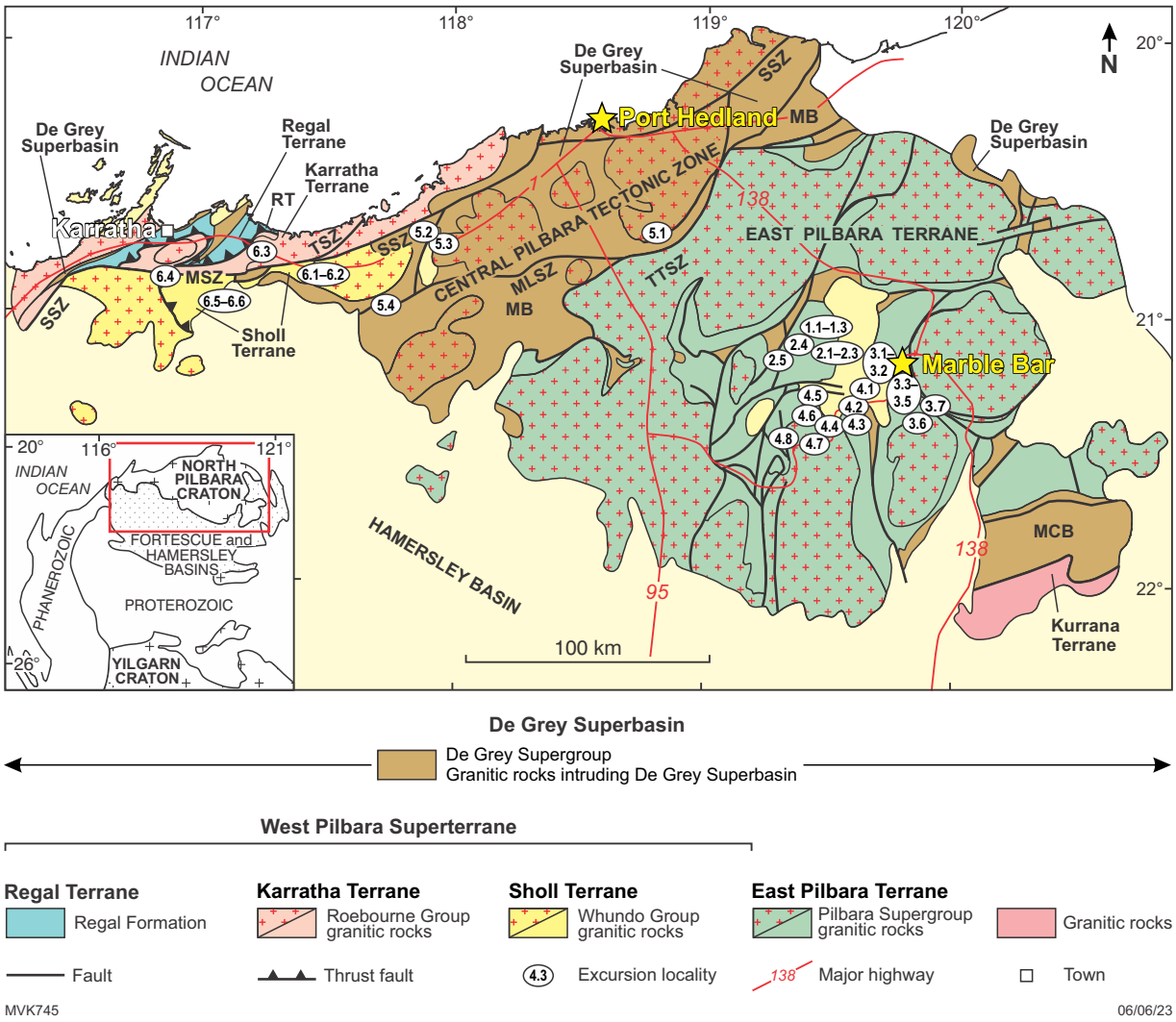

Figure 1. Lithotectonic map of the Pilbara Craton, showing identified terranes, major shear zones and excursion localities: red for East Pilbara Terrane (Days 1–4); green for central Pilbara and West Pilbara Superterrane (Days 5, 6). Abbreviations: MB = Mallina Basin; MCB = Mosquito Creek Basin; MSZ = Maitland Shear Zone; SSZ = Sholl Shear Zone; TTSZ = Tabba Tabba Shear Zone; RT = Regal Thrust; TSZ = Terenar Shear Zone; MLSZ = Mallina Shear Zone. Modified from Van Kranendonk et al. (2007b)

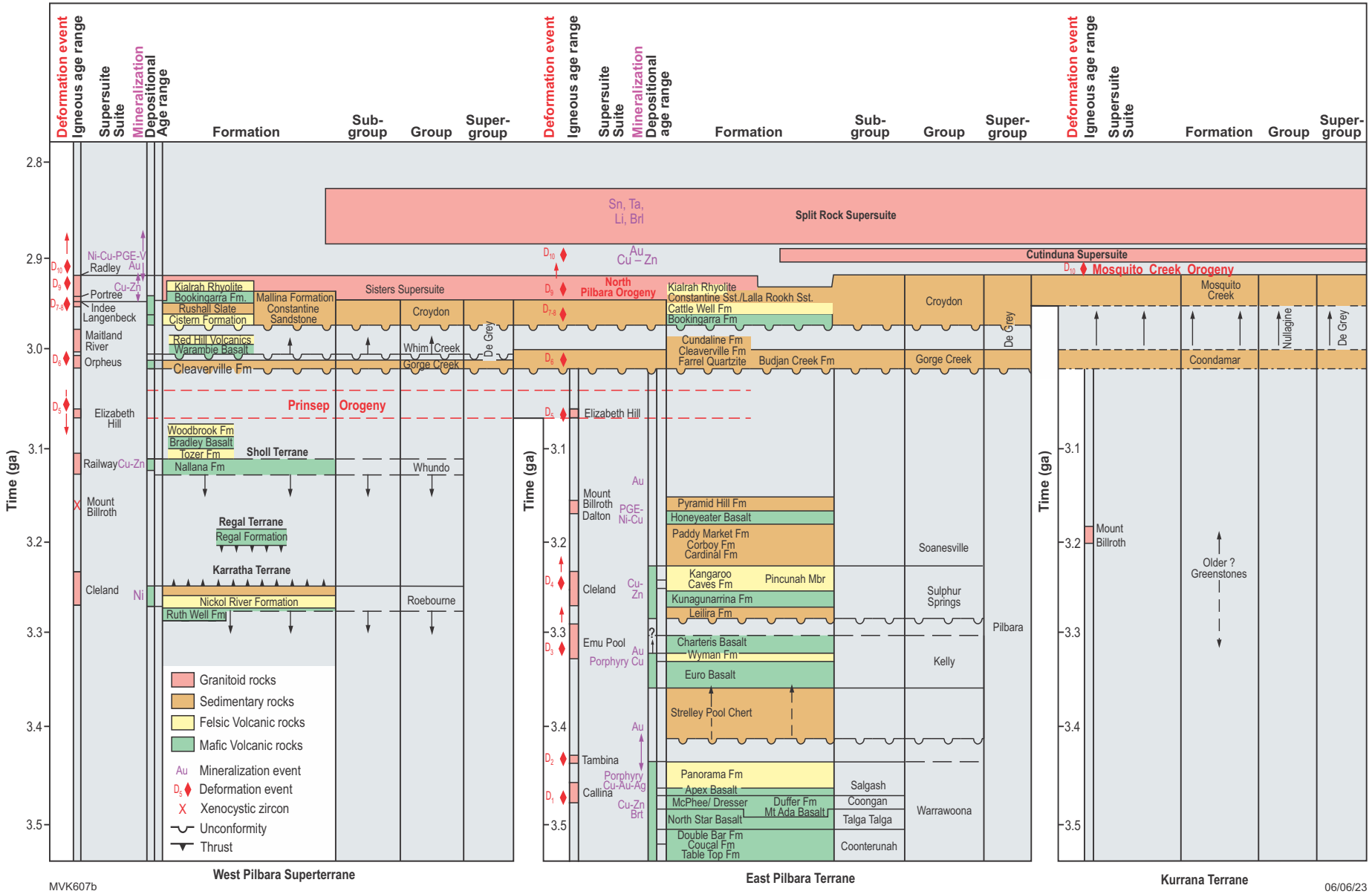

Figure 2. Time–space diagram of lithostratigraphic, plutonic, deformation and mineralization events for the Pilbara Craton, showing the distinct early histories of the terranes and the common history of the craton after c. 3.02 Ga. The Split Rock Supersuite comprises post-tectonic granites emplaced across all of the terranes of the craton. From Van Kranendonk et al. (2007b)

Field trip localities: Part 1 East Pilbara

Day 1: Depositional environments of early life in the c. 3480 Ma Dresser Formation

The North Pole Dome

The North Pole Dome in the middle of the East Pilbara Terrane (Fig. 1) is a structural dome of well-preserved 3.52 – 3.32 Ga, dominantly mafic, volcanic rocks of the Warrawoona Group, the Strelley Pool Formation and the Kelly Group that wrap around a central nucleus occupied by the c. 3.45 Ga North Pole Monzogranite (Fig. 3; age from Thorpe et al., 1992a). Younging directions from pillow basalts and from graded bedding in volcaniclastic rocks indicate that all the rocks young away from the core of the dome in a radial pattern that is disrupted in the western part by the Antarctic Fault, a curviplanar, post-2.7 Ga, structure with west-side-down displacement (Van Kranendonk, 2000). Available geochronology supports an upward-younging succession within the dome, from c. 3490 Ma to 3320 Ma, supported by geochemical data that indicates continuous upward change (Smithies et al., 2007a,b). These data, combined with additional field observations (Van Kranendonk, 2000; Van Kranendonk et al., 2008, 2015, 2019b) discount previous interpretations of a thrust-repeated ocean plate stratigraphy in the North Pole Dome (Kitajima et al., 2001; Terabayashi et al., 2003).

The dip of strata increases outwards from gentle dips of 20–40° in the core of the dome to dips of 80° at the outer edges of the dome where remnants of younger rocks of the De Grey Supergroup and Fortescue Group are preserved (Van Kranendonk, 1999). North Pole Dome rocks have been metamorphosed to prehnite–pumpellyite to lower greenschist facies, with a lower amphibolite facies contact metamorphic aureole around the North Pole Monzogranite (Van Kranendonk, 1999; Brown et al., 2005). Regional low-grade metamorphism and deformation was episodic, with pulses at c. 3450 Ma and at c. 3240 Ma (Caruso et al., 2021). Metamorphic mineral assemblages vary across the stratigraphy, controlled by zoned hydrothermal alteration that took place in multiple episodes during the accumulation of the volcanic stratigraphy (Terabayashi et al., 2003; Brown et al., 2005; Van Kranendonk, 2006; Caruso et al., 2021). The largest of these hydrothermal systems is associated with the Dresser Formation. *We will visit this unit on Days 1 and 2.*

The majority of the North Pole Dome is underlain by pillowed mafic volcanic rocks that vary from dominantly tholeiitic, with typical mid-oceanic ridge basalt (N-MORB) rare earth element (REE) profiles, to komatiitic basalts (Smithies et al., 2005b). The stratigraphy of the greenstones includes the lowermost, c. 3490 Ma, North Star Basalt surrounding the North Pole Monzogranite in the core of the dome (Fig. 3). Overlying this are two main bedded chert ± barite horizons that sandwich pillowed basalts and dolerite; these collectively belong to the Dresser Formation (Van Kranendonk and Morant, 1998; Van Kranendonk, 2000; Van Kranendonk et al., 2002, 2008). Pb–Pb model ages of c. 3490 Ma on galena in syngenetic barite gave a close estimate for the age of the formation (Thorpe et al., 1992b), while more recent SHRIMP U–Pb zircon dating of a felsic volcaniclastic sandstone from the top of the lowermost chert unit of the formation has yielded a maximum depositional age of 3481 ± 2 Ma (Van Kranendonk et al., 2008). The Dresser Formation overlies, and is partially cut by, a dense network of syndepositional hydrothermal chert ± barite veins (Nijman et al., 1998; Van Kranendonk et al., 2019a; Tadbiri and Van Kranendonk, 2020).

A thick succession of mafic volcanic rocks belonging to the Mount Ada Basalt overlies the Dresser Formation. This includes a thin unit of felsic sandstone and layered blue, grey and red chert known as the Antarctic Creek Member (Van Kranendonk, 1999, 2000), which is known to contain impact-generated spherules (Byerly et al., 2002). This unit has yielded a conventional U–Pb zircon date of 3470 ± 2 Ma (Byerly et al., 2002), although this may represent the age of the target rock rather than the age of the impact event itself, but it does reflect the known age of this unit.

Overlying the Mount Ada Basalt are up to 1.3 km of felsic volcanic and volcaniclastic rocks of the 3.47 Ga Duffer Formation, including up to 150 m of the Marble Bar Chert Member, and the 3.45 – 3.43 Ga Panorama Formation. A sample of massive rhyolite from the lower part of the felsic volcanic rocks in the southern part of the belt has been dated at 3458 ± 2 Ma, within error of the age of the North Pole Monzogranite (Thorpe et al., 1992a). A sample of bedded tuff with local pumice layers from the upper part of the volcaniclastic apron of the Panorama volcano in the northwestern part of the dome returned a SHRIMP U–Pb zircon date of 3434 ± 5 Ma (Fig. 3; Nelson, 2000d; Van Kranendonk, 2000).

Unconformably overlying the Panorama Formation is the Strelley Pool Formation, with its diverse assemblage of stromatolites (e.g. Lowe, 1983; Hofmann et al., 1999; Van Kranendonk et al., 2003; Allwood et al., 2006, 2007, 2009, 2010; Van Kranendonk, 2007, 2011), some of which contain preserved organic matter (OM) (Bontognali et al., 2012; Flannery et al., 2017). This unit is recognized across the entire 220-km diameter of the East Pilbara Terrane (Van Kranendonk et al., 2002, 2019b). Across the North Pole Dome, the Strelley Pool Formation lies on the underlying rocks across a northeast–southwest downcutting angular unconformity on previously metamorphosed and locally deformed stratigraphy. The Strelley Pool Formation contains

a basal unit of cobble conglomerate and quartz sandstone that is up to 1 km thick and contains detrital zircons dated at ≥3414 Ma, which provides a maximum age of deposition (Gardiner et al., 2019). Overlying this is a <10 m-thick succession of thinly bedded stromatolitic dolostones and evaporative crystal splays, and then a disconformably overlying coarse clastic succession. *We will visit this unit on Day 2.*

Conformably overlying the Strelley Pool Chert is the Euro Basalt, a thick succession of interbedded high-Mg and tholeiitic basalts and chert that reaches a maximum total thickness of 9.4 km in the southwestern extension of the North Pole Dome. This unit forms the lower part of the Kelly Group, dated as c. 3350 Ma (Van Kranendonk et al., 2007a).

Remnants of the unconformably overlying c. 2.7 Ga Fortescue Group cover succession are present in a few places across the North Pole Dome (Fig. 3).

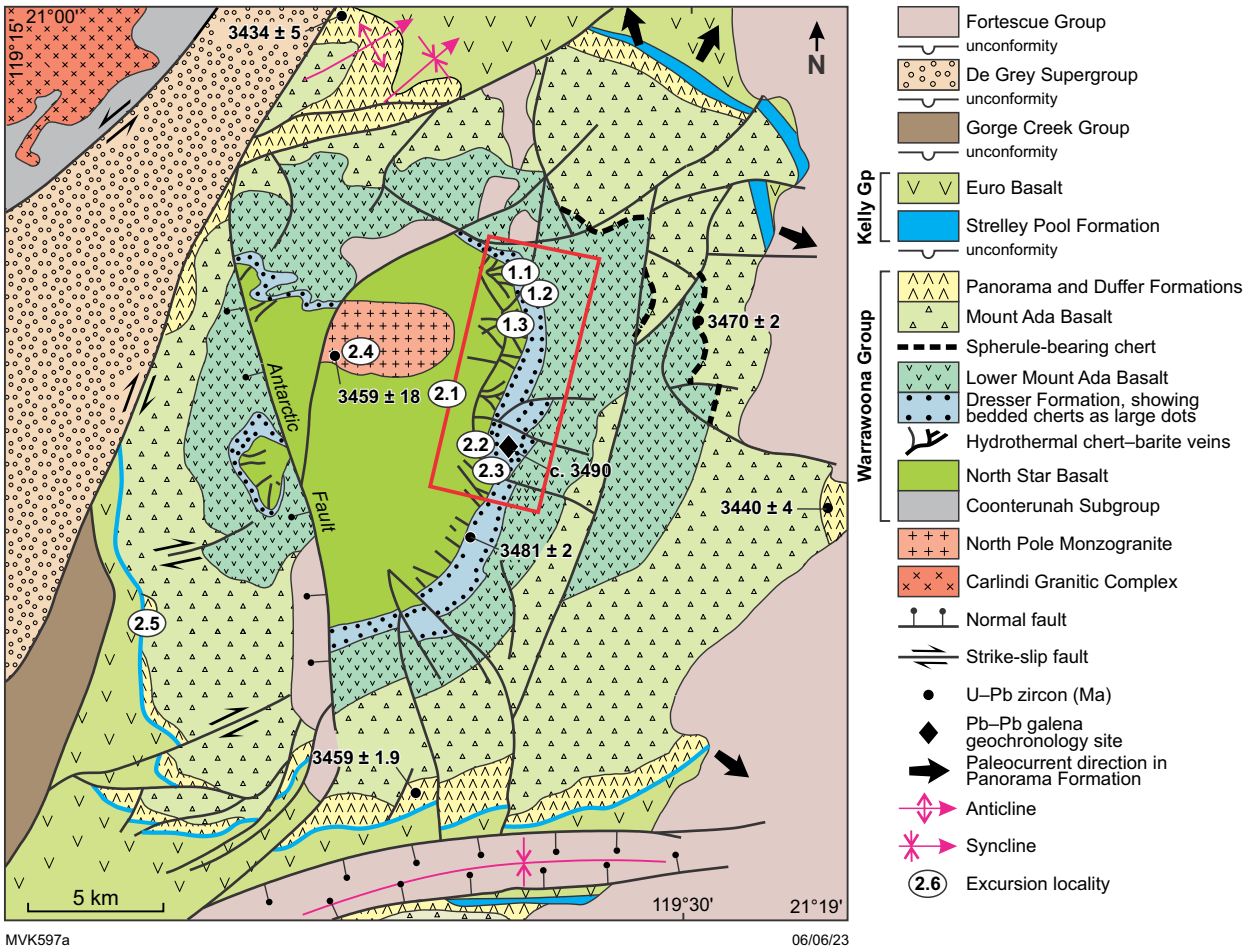

Figure 3. Geological map of the North Pole Dome, showing the distribution of the Dresser Formation and its underlying hydrothermal vein network. Red rectangle denotes location of Figure 4

Dresser Formation

The Dresser Formation consists of three units that include: i) the lower, polylithic, stromatolite-bearing North Pole Chert Member; ii) a middle unit of massive to pillowed komatiitic basalt and a thin bed of jaspilitic chert with basal pebble conglomerate; iii) an upper unit of centimetre-bedded grey-white chert (Fig. 4). The apparent occurrence of multiple units of chert and basalt/dolerite in the uppermost chert to the north of the Dresser mine area is due to a combination of splitting apart of the single, upper chert unit by intrusive dolerite, as well as duplication by localized reverse faulting (Fig. 4).

The North Pole Chert Member crops out across a 14-km diameter within the North Pole Dome, east and west of a late strike-slip fault (Fig. 3). Exceptionally good exposures can be found on the eastern flank of the dome where stromatolites were first described (Lambert et al., 1978; Walter et al., 1980; Buick et al., 1981; Groves et al., 1981; Buick and Dunlop, 1990). The North Pole Chert Member varies dramatically in thickness, sometimes over only a few metres, from a minimum of 1–2 m total thickness, to a maximum of 208 m across horst-and-graben block faults occupied by hydrothermal chert ± barite veins (Nijman et al., 1998; Van Kranendonk et al., 2008; Djokic et al., 2021). Regionally, the thinnest part of the North Pole Chert Member is over the widest and longest hydrothermal chert vein in the central part of the Dresser Formation (Fig. 4). The succession becomes progressively thicker on the flanks on either side (north and south) of this vein, extending south to the large listric growth fault that bounds the northern side of the Dresser mine. This suggests that the central part of uplift during magmatic inflation of the Dresser caldera was in the area of the largest hydrothermal chert vein, with flanking basins on either side. However, unit thicknesses also change dramatically over short distances within smaller fault-bounded blocks within these broad flank regions, indicative of a more complex geometry consistent with a piecemeal-type caldera (Tadbiri and Van Kranendonk, 2020).

Lithology within the North Pole Chert Member includes green volcaniclastic sandstone and conglomerate, felsic tuffs, bedded carbonates, finely laminated sulfidized stromatolites, and grey-white and jaspilitic cherts (Buick, 1985; Van Kranendonk et al., 2008, 2019a; Djokic et al., 2017, 2021). Layers of coarse crystalline barite that lie generally parallel to bedding have been interpreted as either evaporitic deposits (Groves et al., 1981; Buick and Dunlop, 1990), or as hydrothermal veins emplaced parallel to bedding (Van Kranendonk et al., 2008). The latter interpretation is based on observations of discordant relationships between bedding-parallel barite and sedimentary strata, and on observed barite crystal growth within layers that indicate both upwards and downwards growth into pre-existing sediment (Van Kranendonk et al., 2008). Nevertheless, there is textural evidence for the growth of some barite crystals in wet sediment, during early diagenesis, and before the deposition of overlying beds (see Locality 1.1; Van Kranendonk et al., 2008).

Previous authors have recognized either three or four lithostratigraphic assemblages within the North Pole Chert Member (Nijman et al., 1998; Van Kranendonk, 2006; Van Kranendonk et al., 2008). The most recent, detailed mapping has recognized four main lithostratigraphic assemblages, as follows (Fig. 5; Van Kranendonk et al., 2019a; Djokic et al., 2021).

Assemblage 1, at the base, may reach up to 20 m thick and consists of bedded and cross-bedded sandstones; silicified mudstone; jaspilitic chert; and volcaniclastic conglomerate, breccia and sandstone. Volcaniclastic conglomerates in this assemblage locally contain clasts of bedded jaspilitic chert, coarse crystalline barite, and stromatolitic laminates, all within a felsic tuffaceous matrix. These clasts provide evidence for an even older, or laterally equivalent, succession that has largely been uplifted and eroded away, broken up by an eruptive event, and/or is not exposed. Jaspilitic cherts from this part of the stratigraphy have a distinct geochemistry and isotopic composition that indicates deposition in a transitional land–sea environment (Johnson et al., 2022).

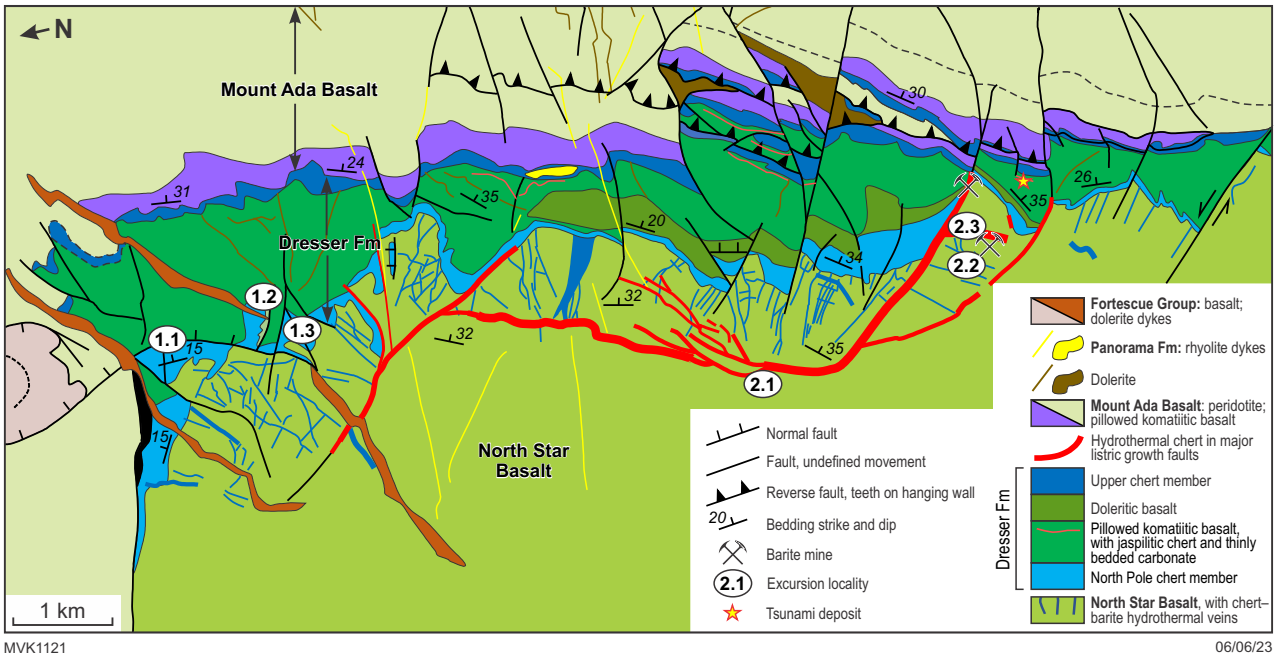

Figure 4. Geological map of the Dresser Formation on the eastern limb of the North Pole Dome (see Fig. 3 for location)

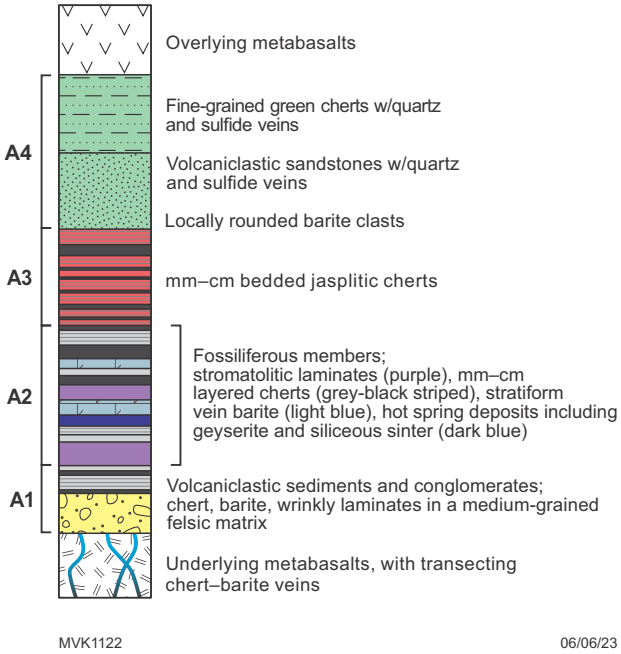

Figure 5. Generalized stratigraphy of the North Pole Chert Member, showing four main lithostratigraphic assemblages (A1–A4). From Djokic et al. (2021)

Assemblage 2 contains widely distributed stromatolite horizons and newly discovered hot spring deposits (Djokic et al., 2017, 2021; Van Kranendonk et al., 2019a, 2021a,b), in addition to a number of other distinctive rock types. The components of this assemblage vary considerably across strike and, although distinctive individual rock types are recognized in several places across the map area, they are not present everywhere due to either syndepositional block faulting, non-deposition(?), and/or erosion by overlying units.

A widespread facies near the base of Assemblage 2 is a rhythmically bedded carbonate–chert 'zebra rock' unit, up to 1 m thick, consisting of repeated couplets of Fe-rich carbonate beds, 1–5 cm thick, that grade up across flocculated contacts into 1–2 cm-thick beds of green chert that have sharp upper contacts with overlying carbonate of the next couplet (Garcia-Ruiz et al., 2003; Van Kranendonk et al., 2019a). Both chert and carbonate beds contain radiating crystal splays of what was previously inferred as gypsum but has recently definitively been identified as aragonite (Van Kranendonk et al., 2008; Otálora et al., 2018). More detail on this unit is provided in the description of Locality 1.2.

Stromatolites lie directly above the 'zebra rock' unit, across up to 10 cm of rippled sandstone. Characteristically composed of wrinkly laminated red–black weathering mats, they vary in morphology to columnar, domical and coniform structures (Walter et al., 1980; Buick and Dunlop, 1990; Van Kranendonk, 2006, 2011). *We will visit the stromatolites at Localities 1.1 and 1.2.*

At three localities, stromatolites have been found to be overlain by, or interbedded with, siliceous hot spring deposits that include geyserite, siliceous sinter and ferruginous tourmaline-bearing hot spring crusts (Djokic et al., 2017, 2021; Van Kranendonk et al., 2019a, 2021a). Geyserite consists of alternating silica-rich black and white microlaminations (2–30 µm thick) with distinct botryoidal to stratiform layering (Djokic et al., 2017, 2021). The black laminations contain concentrated microscopic grains (~2 µm) of the mineral anatase (the low-temperature polymorph of TiO_2). The white layers are composed of K–Al-rich flaky aggregates and tabular shaped grains of kaolinite and illite. These textures and identical mineral assemblages are known from modern hot spring fields, including Sulphur Springs, New Mexico (Charles et al., 1986) and Soufriere Hills volcano, Montserrat (Boudon et al., 1998).

Assemblage 3 dominantly consists of centimetre-layered chert, including mostly white-grey layered cherts but also, characteristically, hematitic chert, or jaspilite (e.g. Van Kranendonk et al., 2008; Djokic et al., 2021). The jaspilitic chert in this part of the stratigraphy is typically very finely bedded and lacks any indications for current reworking that, together with geochemistry (Johnson et al., 2022), suggests that it was deposited in a deep, quiet water setting.

Assemblage 4 is a 0–100 m-thick, fining-up, succession of silicified green volcaniclasitc conglomerate, sandstone and siltstone that unconformably overlies the lower assemblages, as well as most of the hydrothermal chert–barite veins (Fig. 6; Dunlop and Buick, 1981; Buick and Dunlop, 1990; Van Kranendonk and Pirajno, 2004; Van Kranendonk, 2006; Van Kranendonk et al., 2008, 2019a). Comprising predominantly clasts of komatiitic basalt and basalt, these rocks are preserved in sedimentary wedges across the map area that thicken southward against bounding, long-lived listric normal growth faults, indicative of deposition during extensional basin formation and/or caldera collapse (Fig. 4; Van Kranendonk et al., 2019a; Tadbiri and Van Kranendonk, 2020). This assemblage locally contains rounded clasts of coarsely crystalline hydrothermal barite and is cut by quartz sulfide — but not by barite — veins, indicative of deposition under deeper water conditions after the cessation of barite mineralization (Barley et al., 1979; Van Kranendonk et al., 2019a).

Hydrothermal chert ± barite veins

A dense network of large chert ± barite ± pyrite ± epithermal quartz hydrothermal veins immediately underlies the Dresser Formation, cutting through and causing alteration of the footwall North Star Basalt. These veins extend up to the base of, and almost exclusively terminate within, the lower parts (Assemblages 1 and 2, lesser in 3, but not in 4) of the North Pole Chert Member (Fig. 4). However, some of the largest veins that occupy major, long-lived listric growth faults extend up to the top of the Dresser Formation (i.e. to the level of the upper Dresser chert) (red units on Fig. 4).

The main set of hydrothermal veins extends for a maximum of up to 2 km beneath the base of the Dresser Formation and can be up to a maximum of 300 m wide, as swarms of veins (Fig. 4). Typically, however, veins are approximately 1 km deep and 2–10 m wide. All veins are carrot shaped, with narrow bases of generally white quartz and/or chert that thicken upwards towards the paleosurface. Most of the length of the veins are composed of one or more generations of dark blue-black, OM-bearing chert, sometimes with small amounts of fine, cubic pyrite. All black chert veins contain dispersed OM that studies have shown to have a biological origin (Morag et al., 2016), although some components of

OM in vein chert may have an abiological origin (Rasmussen and Muhling, 2023). Barite only occurs in veins within the top 75 m of the paleosurface, becoming a more significant component of veins further towards the paleosurface. The upper parts of many chert veins contain both chert and barite, commonly as intergrown phases that may include barite at the edges and chert in the cores, or the reverse (Fig. 7a). The central core zone of many black chert veins near their upper limit commonly contain patches, or more continuous veins (to 20 cm wide) of chalcedonic white quartz that are classic examples of epithermal infilling of open space (Fig. 7b; Van Kranendonk and Pirajno, 2004; Harris et al., 2009). Fluid inclusion analysis of vein phases show a change in temperature going up the veins, from a maximum of 350 °C at the base, to 150 °C at the tops, the latter temperature consistent with precipitation of barite (Harris et al., 2009; Caruso et al., 2021). Phreatic brecciation is a common feature near the tops of many veins and indicates that chert (+barite) precipitated out of solution of hydrothermal fluids near-instantaneously as a result of boiling and volatile release (crack-seal) from fluids kept under pressure by sealed caprocks (Van Kranendonk, 2006; Caruso et al., 2021).

A recent, detailed study of the veins recognized three main sets that were emplaced before a last set (set four) of veins was emplaced within large listric growth faults (Fig. 4; Tadbiri and Van Kranendonk, 2020). Back-rotation of the dipping Dresser strata and underlying veins back to the paleo-horizontal reveals that hydrothermal vein sets 1–3 were all emplaced within vertical fractures, indicative of a vertical maximum stress direction (σ1) during vein emplacement. Whereas veins across most of the Dresser Formation exposure area define a single orientation, conjugate vein sets are developed in two areas with the densest network of veins (Fig. 4). This pattern is fully consistent with a nested caldera depositional model, within what has been classified as a piecemeal caldera, which is one that is characterized by floors that are heavily faulted and divided into multiple blocks (cf. Branney and Kokelaar, 1994; Cole et al., 2005).

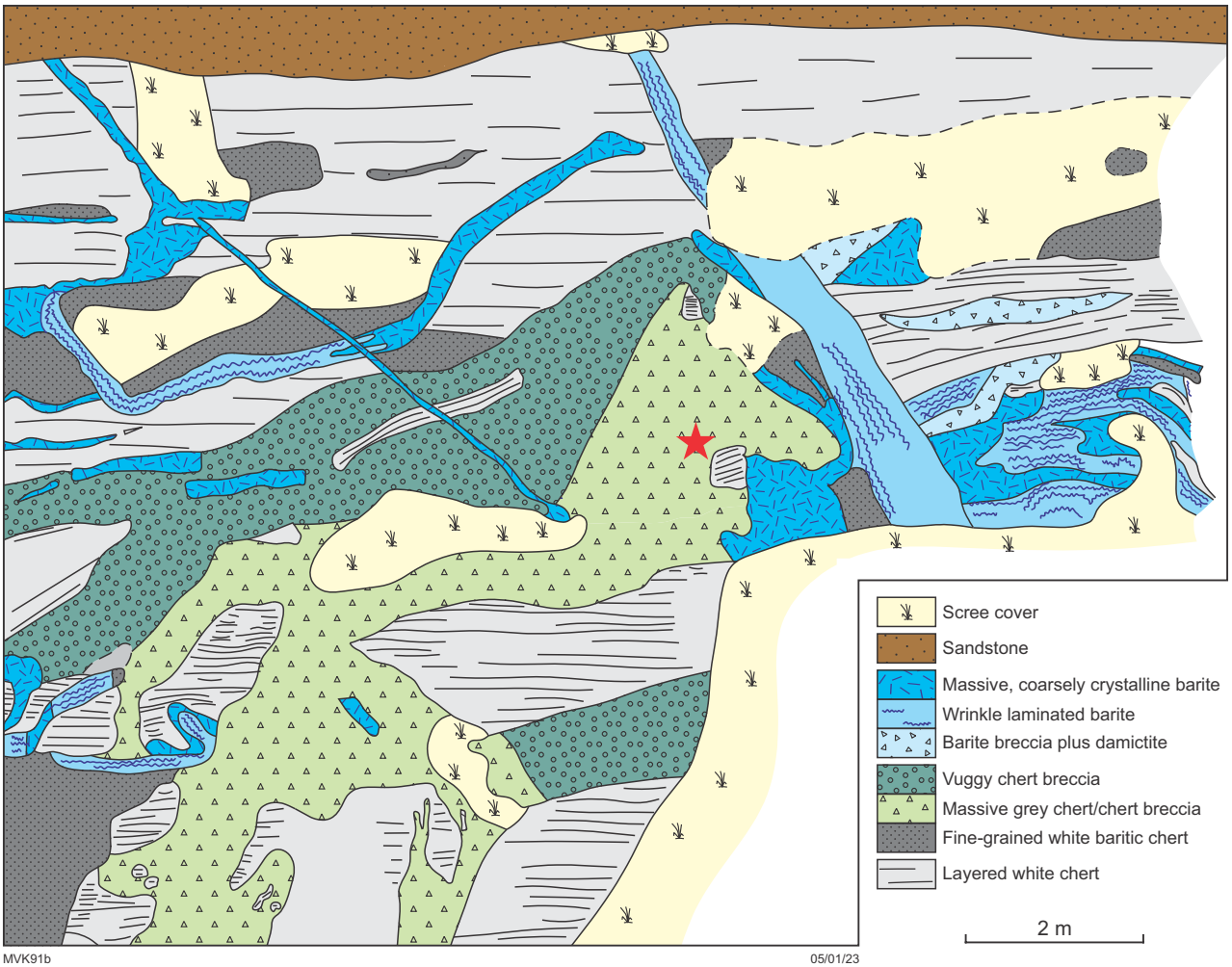

Figure 6. Detailed geological map of part of the North Pole Chert Member, showing the unconformable relationship of overlying green volcaniclastic sandstones of Assemblage 4 with layered cherts cut by hydrothermal barite veins and chert breccia veins. Red star denotes location of hydrothermal kaolinite veinlets. From Van Kranendonk and Pirajno (2004)

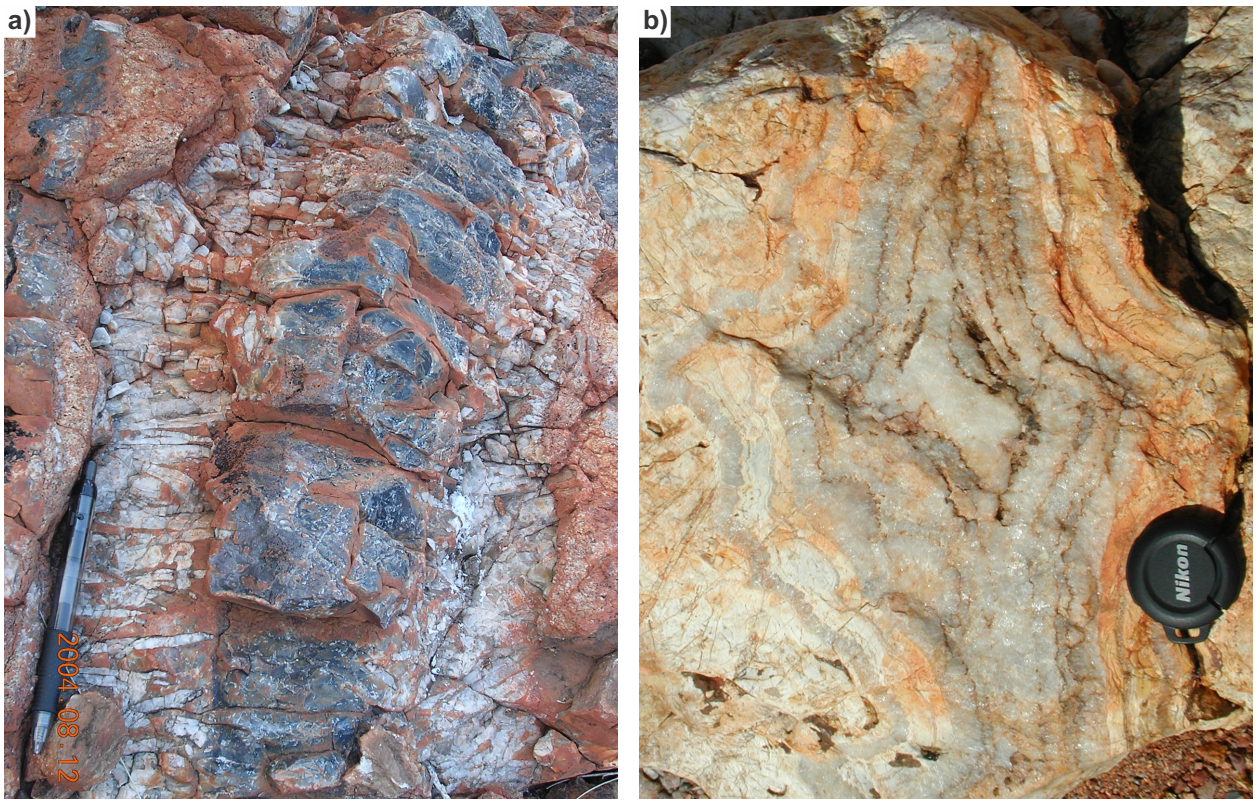

Figure 7. Close-up views of textures in Dresser hydrothermal chert–barite veins: a) zoned chert-barite vein; b) classic epithermal quartz filling central void space in chert–barite vein

Hydrothermal alteration

Pillow basalts underlying the Dresser Formation are strongly affected by hydrothermal alteration that is strongly zoned away from individual hydrothermal veins (Van Kranendonk, 2006; Caruso et al., 2021). The most intense alteration is at the sites where barite was mined, reflecting the largest volume of hydrothermal fluid flow within the Dresser system. At these sites, perfectly preserved pillow basalts are pure white, and composed of hydrothermal kaolinite–illite–quartz, indicative of high-sulfidation, steam-heated acid-sulfate (argillic) alteration (see Locality 2.3). Pyrophyllite, indicative of advanced argillic alteration, is developed along the flanks of larger hydrothermal chert–barite veins (Caruso et al., 2021). Progressively further away from the veins are white mica dominated alteration zones, and then carbonate–white mica–chlorite, the widespread chlorite–carbonate–epidote (i.e. propylitic) alteration, and actinolite alteration at the base. The zoned hydrothermal alteration identified in the vicinity of the Dresser mine is similar to that associated with epithermal mineral deposits from throughout the geological record (Fig. 8) and matches the range of temperature estimates (150–350 °C) obtained from fluid inclusions in hydrothermal veins by Harris et al. (2009).

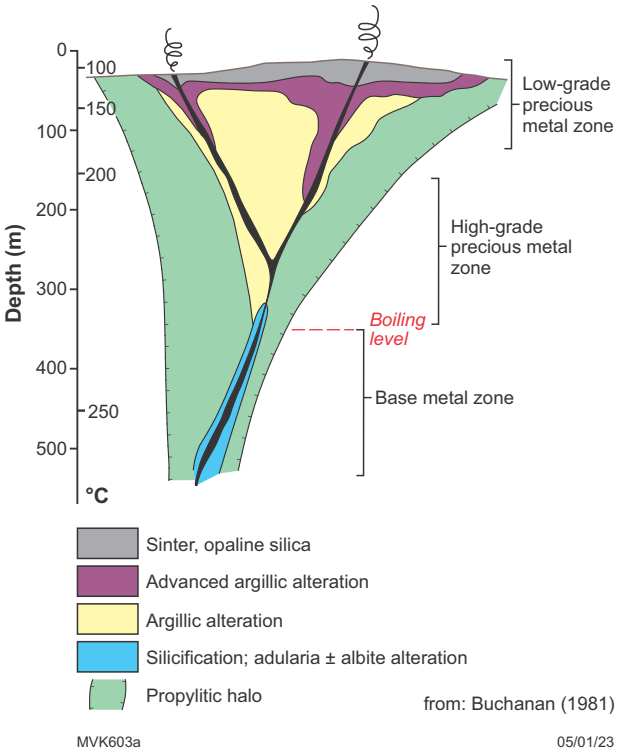

Figure 8. Zoned alteration associated with epithermal mineralization and surficial hot spring deposits. After Buchanan (1981)

Depositional model

Whereas original studies suggested deposition of the Dresser Formation in a quiet, restricted shallow marine basin analogous to Shark Bay, Western Australia, where stromatolites thrive today (Groves et al., 1981; Buick and Dunlop, 1990), more detailed recent studies indicate deposition within a dynamic volcanic caldera affected by syndepositional growth faults and voluminous hydrothermal circulation (Fig. 9; Nijman et al., 1998; Van Kranendonk, 2006; Van Kranendonk et al., 2008, 2019a). Lithofacies analysis of the North Pole Chert Member indicates a progressive rise from submarine conditions at the base (underlying pillow basalt and cross-bedded sandstones), through shallow water and even temporarily (or locally) exposed conditions when the 'zebra rock' evaporative facies and hot spring deposits were laid down, and back to marine conditions during deposition of Assemblages 3 and 4. Whereas this 'rise and fall' of the land surface could arise from marine regression/transgression, a more likely cause — given the environment — is local surface uplift arising from magma recharge, followed by eruption and surface collapse. At least some of the collapse may have been caused by, or accompanied, regional extension, when the large listric growth faults of the Dresser Formation were active.

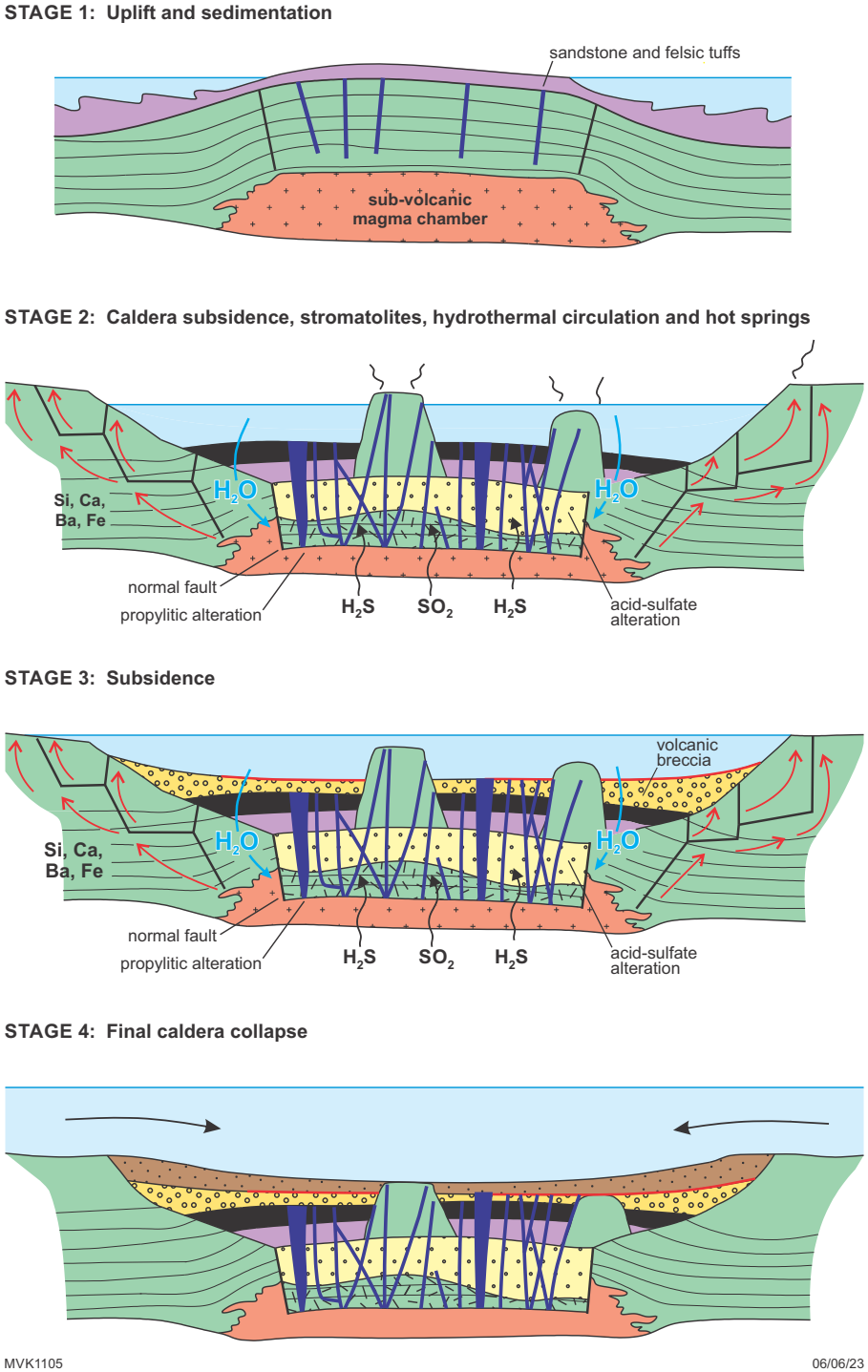

Figure 9. Depositional model for the North Pole Chert Member of the Dresser Formation in a low-eruptive, piecemeal volcanic caldera, showing the progressive rise and fall of the land surface. Stages 2 and 3 were accompanied by extensive block faulting and voluminous hydrothermal fluid circulation. From Van Kranendonk et al. (2019a)

Locality 1.1: Dresser Formation stratiform and domical stromatolites, and rippled sandstones (location withheld to protect location)

Note: This locality is of major geological significance and lies within the Buick State Geoheritage Reserve (R44710).

IT IS ILLEGAL TO ACCESS THIS RESERVE WITHOUT PRIOR APPROVAL.

Hammering, sample collecting, camping and driving off pre-existing tracks is strictly not permitted within the bounds of this Reserve.

More information on the location and significance of localities on the Register of State Geoheritage Sites can be accessed via GeoVIEW, the Geological Survey of Western Australia (GSWA) online mapping platform; more general information on geoheritage and the Reserve permitting system can be found on the Department of Mines, Industry Regulation and Safety (DMIRS) website.

Note that the export of geological material out of Australia, particularly fossils and meteorites, is strictly controlled by the Federal Protection of Cultural Moveable Heritage Act 1986. *Approval is required from the Federal Office of the Arts for the permanent export of Class B objects.*

The hill rising up behind this locality to the west is predominantly composed of bedded grey and white chert of the c. 3480 Ma Dresser Formation, which dips down towards this locality at an angle of 34° to the east. Bedding is broadly warped on east-northeasterly plunging axes, but apart from this, the rocks have been unaffected by penetrative deformation despite their great antiquity. A variety of macroscopic stromatolites may be observed at this locality, including wrinkly laminated mats, broad domes and columnar forms (Fig. 10; Walter et al., 1980; Buick et al., 1981; Walter, 1983; Van Kranendonk, 2006, 2011; Van Kranendonk et al., 2008).

MVK1123 13.12.22

Figure 10. Wrinkly laminated stratiform and broad domical stromatolites of the Dresser Formation at Excursion Locality 1.1

Silicified clastic rocks immediately underlying stratiform to domal stromatolites display well-preserved evidence of very shallow water deposition (Fig. 11). This includes cross-stratification with straight to bifurcating, asymmetrical ripple crests and radiating aragonite crystal splays (Otálora et al., 2018) that are apparent in some ripple crests at this locality. Along strike are local desiccation cracks (Van Kranendonk, 2006). Also visible here are early diagenetic barite crystals that grew in what was still wet sediment. Collectively, these features are indicative of very shallow water, to periodically exposed, conditions.

The stromatolites preserved here are composed of red- and black-weathering material that was of unknown protolith until the 2004 Pilbara drilling project revealed that equivalent rocks from below the effects of oxidative weathering along strike to the south were composed predominantly of pyrite, with subordinate sphalerite and dolomite (Fig. 12a; Van Kranendonk et al., 2008). Further investigations have revealed that the sulfides comprising the bulk of the stromatolites have a nanoscale porosity filled by OM (Fig. 12b; Baumgartner et al., 2019), that the sulfidized stromatolites contain ropy textured kerogen filaments that are interpreted as remnants of microbial extra-polymeric substances (EPS) of the organisms that built these structures (Fig. 12c; Baumgartner et al., 2019), that there is fine-scale elemental layering within the sulfides (Fig. 12d; Baumgartner et al., 2020a), and that clumps of thermally mature OM contain microspherulitic barite that is known only from modern settings with biological OM (Fig. 12e; González-Muñoz et al., 2003, 2013; Torres-Crispo et al., 2015; Martinez-Ruiz et al., 2018a,b; Baumgartner et al., 2020b). Sulfur isotopic data from pyrite of the stromatolites fall within the range $\delta^{34}S$ = +2‰ to −8‰ and $\Delta^{33}S$ = +0.1‰ to −1.0‰, values that are consistent with, but not exclusively indicative of, precipitation as a result of microbial sulfate reduction (Baumgartner et al., 2020c).

At the top of the hill to the north is an excellent exposure that displays a cross-section through the most important units within the North Pole Chert Member. Rock types exposed here include the carbonate–chert 'zebra rock' with its aragonite 'starburst' mineral splays — although it is silicified at this locality — the unit of wrinkly laminated stratiform to domical stromatolites, edgewise conglomerate and potential hot spring deposits (Fig. 13a).

There are two main aspects to focus on at this locality. One is identification of different textures and how these distinct units extend, or do not extend along strike, and how they each relate to overlying and underlying units. The other main aspect to focus on is the wrinkly laminated stromatolites and their relationship to bounding sedimentary units. Of specific importance is to recognize the abiogenic (i.e. purely physical or geological) components vs the biological components preserved in the rocks, and identify the places where, and the way in which, they interfere (Fig. 13a). It is this interference that is a major factor in support of biogenicity, as witnessed from modern examples of microbialites from Shark Bay (Fig. 13b). A similar interference relationship between biological and abiological components can be seen at this outcrop, supporting biogenicity (cf. Van Kranendonk, 2011). We will see similar relationships at Locality 2.5.

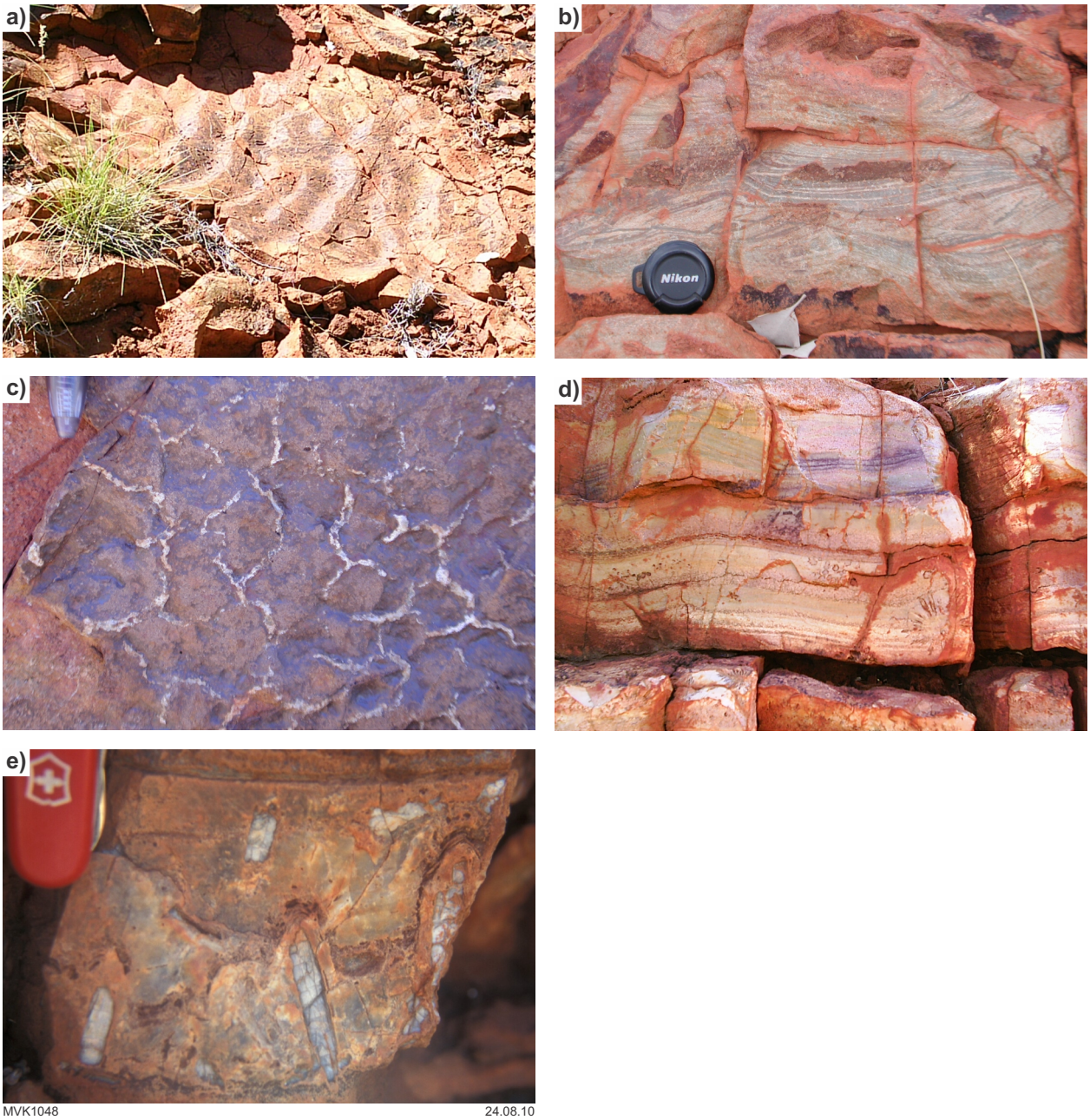

Figure 11. Features of the North Pole Chert Member at Locality 1.1: a) curved ripple crests of clastic sedimentary rocks immediately below the stromatolites; b) cross-laminated clastic sedimentary rocks immediately below the stromatolites; c) bedding surface with quartz-filled desiccation cracks in fine-grained sedimentary rock; d) silicified bedded carbonate with radiating crystal splays of former aragonite; e) diagenetic barite crystals that grew in wet sediment and microbial mat immediately beneath the stromatolites

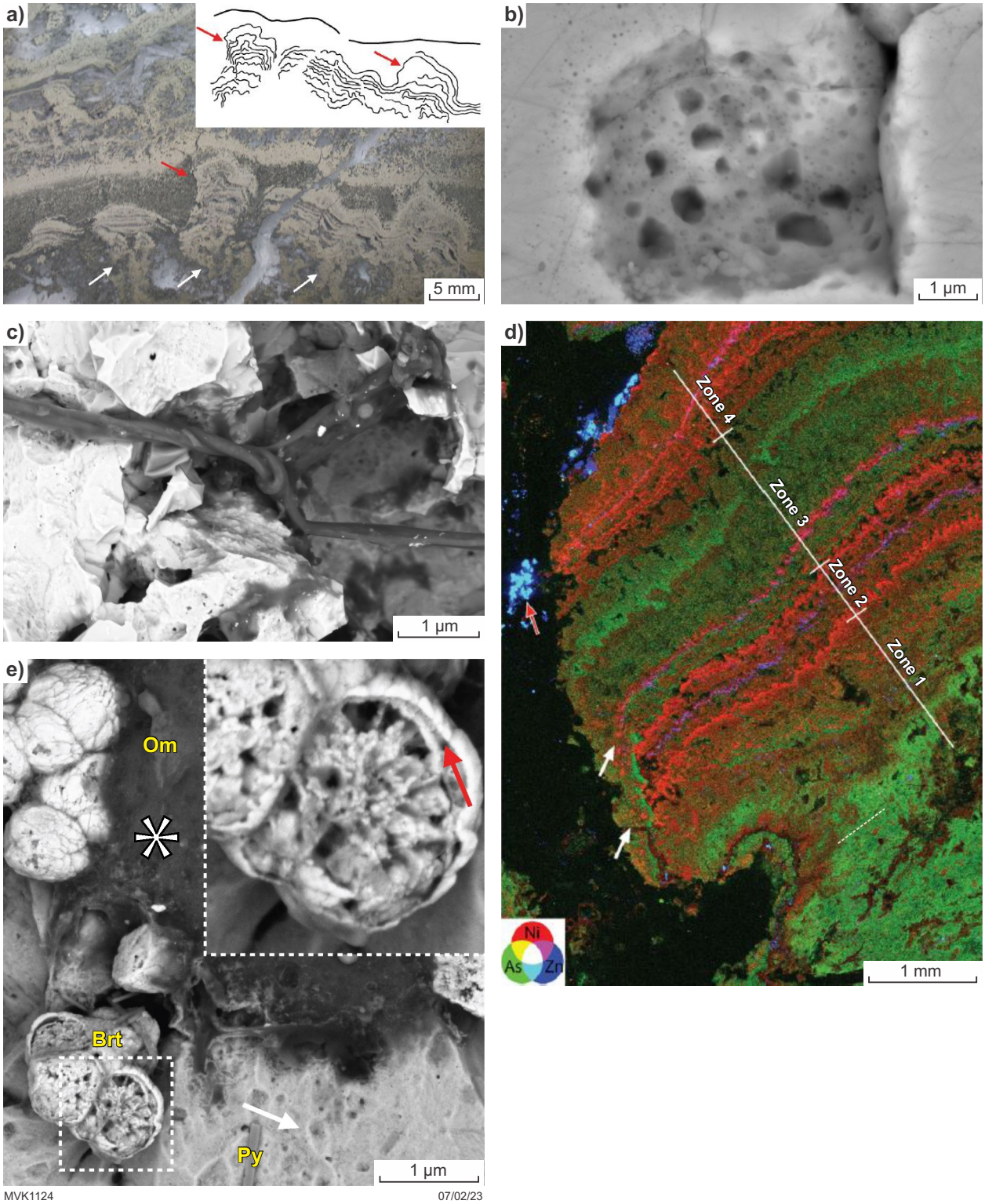

Figure 12. a) Thin section view of sulfidized columnar stromatolite from the Pilbara Drilling project: width of view is 3 cm. From Van Kranendonk et al. (2008). Inset sketch highlights the crinkly nature of laminations. From Baumgartner et al. (2019); b) backscattered electron image of nanoporous sulfides in the sulfidized stromatolites. Note the gradation of pyrite textures: Py1 → Py2 → Py3, and the void trails along pyrite pseudo-grain boundaries. From Baumgartner et al. (2019); c) ropy textured, thermally mature organic matter (OM) within nanoporous pyrite (py) of the Dresser sulfidized stromatolites, interpreted as remnants of microbial EPS. From Baumgartner et al. (2019); d) qualitative elemental distribution map of Ni, As and Zn (green, red, purple) for a laminated, sulfidized columnar stromatolite. Note the cyclical nature of As, Ni and Zn enrichments and the overgrowth relationship (white arrows). From Baumgartner et al. (2020a); e) microspherulitic barite (Brt), pyrite (Py) and organic matter (Om) in Dresser stromatolites: white arrow indicates nanoporous pyrite enriched in OM; red arrow in the inset indicates the outer shell of a barite microspherulite; asterisk indicates the location of Raman spectroscopy analysis of OM. From Baumgartner et al. (2020b)

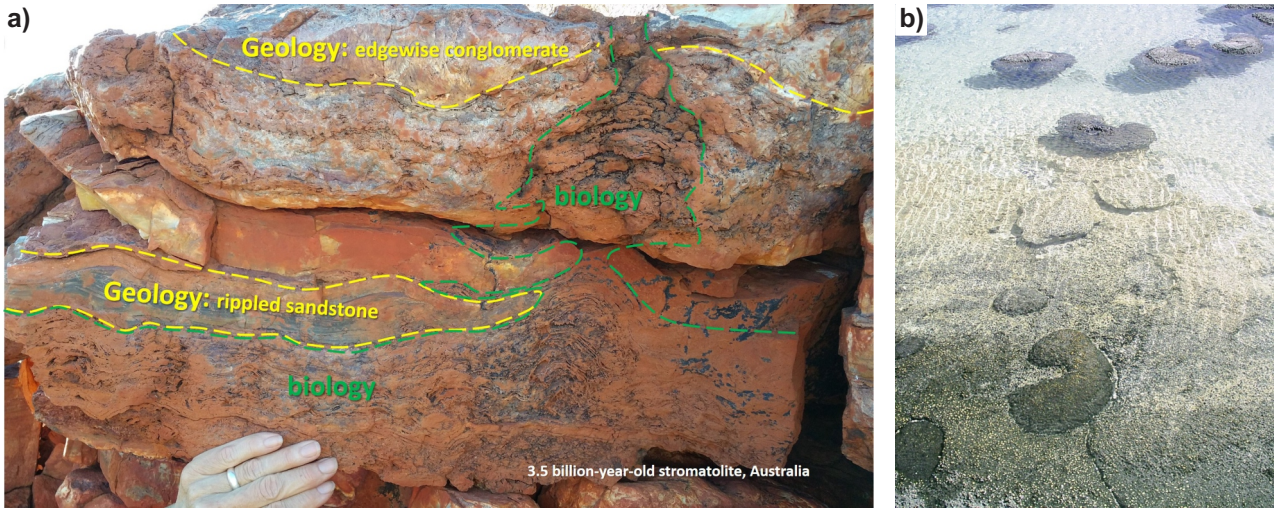

Figure 13. Comparison of ancient and modern stromatolites and their host rocks: a) wrinkly laminated stratiform stromatolite (across base) and a large wrinkly laminated columnar stromatolite (right) that extends continuously upward through beds of rippled sandstone, edgewise conglomerate and capping hot spring silica sinter; b) recent stromatolites at Shark Bay, showing transition from living forms growing up above sediment–water interface in rear, and dead, lithified stromatolites in foreground encased in lithified coquina

Sulfide micromineralogy

High-resolution mineralogical analysis reveals that the Dresser Formation stromatolites are predominantly composed of nanoscale porous pyrite (Fig. 12a; Baumgartner et al., 2019), a texture know to precipitate within low-temperature biofilms (cf. MacLean et al., 2008). In fact, three main pyrite generations can be recognized in the stromatolites (Fig. 14; Baumgartner et al., 2019). The earliest generation of irregular nanoporous pyrite (Py1) comprises anhedral to rounded pyrite grains, usually <0.1 to 1 µm in diameter. Zoned nanoporous pyrite (Py2) that typically mantles Py1 exhibits concentric banding defined by nanoscale porosity. Py1 and Py2 are overgrown by nonporous, massive pyrite (Py3). Importantly, the Py1–Py2 assemblages are the main architectural elements of the stromatolites, and they are the mineralogical hosts of the transition metal and metalloid enrichments seen in the elemental mapping, as described below.

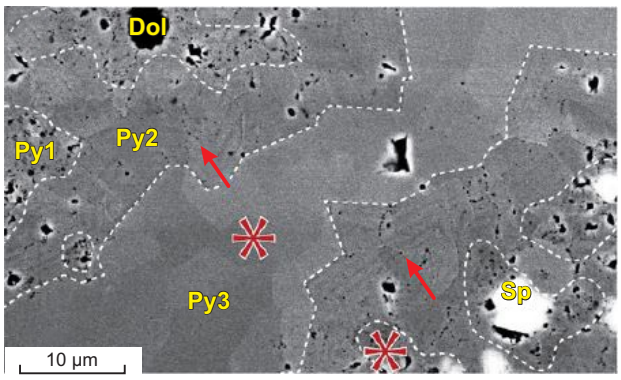

Figure 14. Backscattered electron image of representative pyrite assemblages, ranging from irregular (Py1) to zoned (Py2) nanoporous pyrite, to later overgrowths of non-porous, massive pyrite (Py3). Fine-scale zonation within Py2 is indicated (red arrows). Note the grains of dolomite (Dol) and sphalerite (Sp) that are associated with Py1 and Py2. Asterisks indicate the locations of Raman spectroscopy analyses in Baumgartner et al. (2019)

Enrichments of transition metals and metalloids

Qualitative elemental mapping using synchrotron radiation X-ray fluorescence (XRF) microscopy reveals complex variations in transition metal and metalloid concentrations within stromatolite microtextures (Fig. 12d; Baumgartner et al., 2020a). For example, the sulfidized branching to columnar stromatolites in Figure 15 shows As-rich pyrite in its base, grading up into increasing Ni concentrations at the top of the branches. The branching lower stromatolites are capped by wrinkly laminated microbialite that extends across two separate columns, with cyclically repeated Ni- and Zn-rich laminae with locally microdigitate-like, or tufted, distributions of Ni (Baumgartner et al., 2020a).

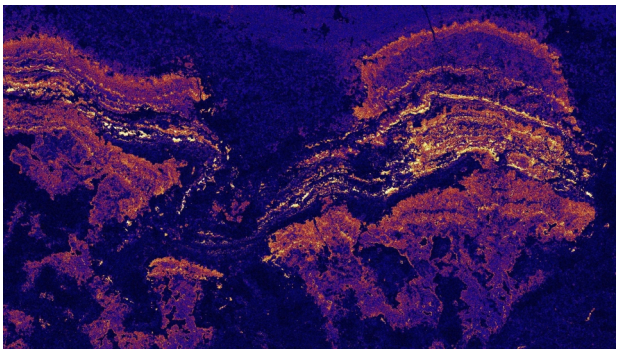

Figure 15. Synchrotron X-ray fluorescence microscopy image of arsenic enrichment in branching and columnar sulfidized stromatolite of the Dresser Formation showing Ni enrichments within As-rich pyrite

Laser-ablation inductively coupled plasma mass spectrometry trace element mapping of the columnar stromatolites reveals that As, Ni and Zn are coupled with other minor and trace elements, as follows: i) Ni + Co; ii) As + Mo; iii) Zn + Sn + Hg (Baumgartner et al., 2020a). It was also found that there is an additional association of iv) Cu + Ag + Sb + Te + Pb within the laminations. These elemental maps also highlight fine-scale structures within the laminae, including millimetre-scale columnar structures oriented perpendicular to the main stromatolite lamination. Such element enrichments are characteristic of microbial biofilms from a variety of habitats (e.g. Labrenz et al., 2000; Lalonde et al., 2007; Huerta-Diaz et al., 2011, 2012). In particular, Ni and Zn enrichments point to the activity of sulfate-reducing bacteria (cf. Gramp et al., 2007), as deduced for other settings in the Dresser Formation (Shen et al., 2001, 2009).

Organic matter

Morag et al. (2016) examined the carbon isotopic composition of kerogen preserved within bedded samples of the Dresser Formation from drillcores collected from below the effects of surface weathering. As explained for the kerogen from hydrothermal chert veins at Locality 2.3, variations in carbon isotopic signatures for microstructure-specific occurrences of kerogen in bedded sediments, together with the $\delta^{13}C$ values themselves (ranging from −33.6 to −25.7‰), and the relatively shallow water depth inferred for the Dresser environment and the restricted occurrence of stromatolites to shallow water deposits in this unit, led these authors to conclude that the preserved OM in Dresser sedimentary rocks was produced via photosynthesis.

Raman spectroscopy analysis, plus ion mapping by nanoscale secondary ion mass spectroscopy, indicates that nanoporous pyrite in the stromatolites hosts thermally mature, N-bearing OM within the nanoscale porosity of this mineral phase (Fig. 16). The relative heights and shapes of the disorder-induced 'D' (~1315 Δcm^{-1}) and order-induced 'G' (~1600 Δcm^{-1}) Raman bands of this OM (Morag et al., 2016; Baumgartner et al., 2019) are consistent with thermally mature Archean OM elsewhere in the Dresser Formation (compare with data in Harris et al., 2015).

Bulk OM extracted from a millimetre-thick volume cut from a sulfidized stromatolite drillcore sample yields relatively high (0.3%) total organic carbon that has a $\delta^{13}C_{OM}$ value of −29.6 ± 0.3‰ Vienna Peedee belemnite (VPDB; Baumgartner et al., 2019). This isotopic signature, which is within the range of previous data from the Dresser Formation (OM in bedded chert with −33.6 to −25.7‰ $\delta^{13}C_{OM}$; Morag et al., 2016), is typical of biomass derived from microorganisms, although similar values have also been reported from abiotic OM synthesis (McCollom and Seewald, 2006).

Nitric acid etching reveals that the majority of OM within the nanoporous pyrite of the stromatolites occurs as irregular masses. However, OM is also present as complexly twisted, rope-like filaments that are usually <1 µm in diameter, but that extend for tens of microns (Fig. 12c). Occasionally sinusoidal and axially arranged, finely striated, and partially calcified OM strands reach lengths of up to approximately 20 µm (Baumgartner et al., 2019). Both the OM strands and rope-like filaments are embedded in Py1 and pass across grain boundaries of Py2. This characteristic, in addition to Raman spectroscopy signatures that are equivalent to OM in unetched sulfide, indicate that the OM strands and rope-like filaments are autochthonous, and that they have not been altered substantially through nitric acid etching.

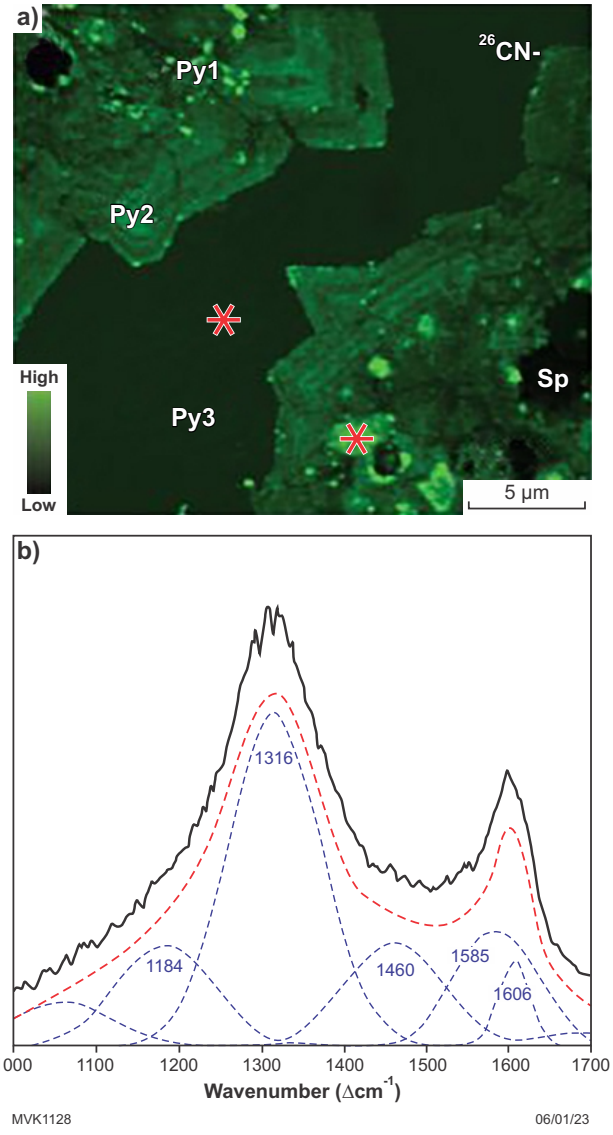

Figure 16. Investigations of pyrite in Dresser Formation stromatolites: a) ion map of $^{26}CN^-$ in pyrite; b) deconvoluted Raman spectra of OM-rich nanoporous pyrite indicating overlaps of D1 (~1316 Δcm^{-1}) and G (~1585 Δcm^{-1}) with disorder-induced 'D2' (~1606 Δcm^{-1}), 'D3' (~1460 Δcm^{-1}), and 'D4' (~1184 Δcm^{-1}) bands. The cumulative fit is indicated by red dashed line. From Baumgartner et al. (2019)

Locality 1.2: Hydrothermally fed, evaporative volcanic caldera lake facies (Zone 50, MGA 753884E 7665553N)

Note: This locality lies within the Buick State Geoheritage Reserve (R44710).

IT IS ILLEGAL TO ACCESS THIS RESERVE WITHOUT PRIOR APPROVAL.

Hammering, sample collecting, camping and driving off pre-existing tracks is strictly not permitted within the bounds of this Reserve.

More information on the location and significance of localities on the Register of State Geoheritage Sites can be accessed via GeoVIEW, GSWA's online mapping platform; more general information on geoheritage and the Reserve permitting system can be found on the DMIRS website.

Note that the export of geological material out of Australia, particularly fossils and meteorites, is strictly controlled by the Federal Protection of Cultural Moveable Heritage Act 1986. *Approval is required from the Federal Office of the Arts for the permanent export of Class B objects.*

At this locality, the cliffbank of a creek exposes the almost flat-lying North Pole Chert Member of the Dresser Formation where it is only 5 m thick. In the creek bed, highly altered basalts of the underlying footwall are cut by a complex network of black chert–barite hydrothermal veins.

At the top of the cliff is a unit of interbedded carbonate and chert 'zebra rock' that is conformably overlain by black-and-red weathering wrinkly stromatolites similar to the stromatolites of the last stop and correlated stratigraphically with them across much of the Dresser Formation. The stromatolitic laminites at this locality are directly overlain by basalt with large, undeformed pillows. The low strain of both the underlying and overlying rocks indicates that this is a primary stratigraphic succession, whereas the relative thinness of the entire chert unit here, compared with the last and next stops, suggests that this was a horst block during deposition.

The primary bedded carbonate–chert 'zebra rock' is widespread in Dresser exposures across the eastern limb of the North Pole Dome and lies at the base of lithostratigraphic Assemblage 2. This unit consists of interbedded couplets of very dark-brown carbonate and light-green chert (Fig. 17a).

Carbonate–chert couplets are 3–6 cm thick. Thicker, basal Fe- and Mn-rich carbonate layers are dominantly ankerite, with the rest consisting of chert and trace berlinite (Al–phosphate). These layers pass upwards across flocculated, gradational contacts, into thinner, pale green chert layers (0.6 – 1.5 cm thick) that commonly have sharp upper contacts (Fig. 17b). Radiating, starburst-like splays (0.6 – 4 cm in diameter) of aragonite crystals (Van Kranendonk et al., 2008; Otálora et al., 2018) occur most commonly at the top of the chert beds, but also within carbonate beds. Layering at the top of this facies displays gentle peaks and troughs, suggestive of crude ripples, and this passes up into 10–20 cm of rippled carbonate sandstone that is directly overlain by wrinkly laminated stromatolite (Fig. 18).

Carbonate from this facies has seawater-like REE + Y patterns, but contrasts with shallow marine dolostones of the Strelley Pool Formation in having overall higher concentrations of these elements and smaller Y anomalies (Fig. 19; Van Kranendonk et al., 2003). The distinctive pattern suggests a strong influence from hydrothermal fluids. Stable isotopic compositions yield mantle-like $\delta^{13}C$ values from –4.16 to –6.3‰ (Lindsay et al., 2005), providing further evidence of a large hydrothermal component. Geochemical analyses show that carbonate layers contain significant enrichments in Ba and Zn (0.6 and 0.2 wt%, respectively; Van Kranendonk et al., 2021a), sourced from the hydrothermal fluids, and consistent with the occurrence of barite and sphalerite in the hydrothermal veins (Van Kranendonk et al., 2008).

Figure 17. The carbonate–chert 'zebra rock', North Pole Chert Member: a) outcrop of 'zebra rock' carbonate–chert; b) cut section showing flocculated texture between lower carbonate and upper chert couplets, and sharp upper contacts of chert layers. Note evaporitic crystal splays in middle of sample

Figure 18. Bedding plane view of low-amplitude domical stromatolites at Locality 1.2

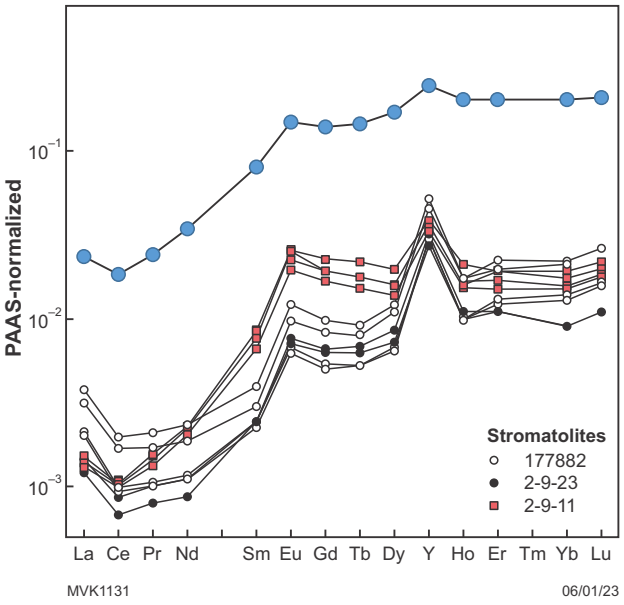

Figure 19. Post-Archean average shale normalized (PAAS) REE + Y pattern of 'zebra rock' carbonate (blue dots) compared with stromatolitic dolostones of the Strelley Pool Formation (black: see Locality 2.5), documented to have a characteristic early Archean seawater pattern. Modified from Van Kranendonk et al. (2003)

The concentration of Fe (and Mn?) in the carbonate layers, together with the REE + Y pattern from these rocks, indicates deposition from concentrated seawater. In contrast, the mantle-like carbon isotopic signatures and enrichments of Ba and Zn point to significant addition of hydrothermal fluids. The development of carbonate–chert couplets and lack of any cross-stratification indicates quiet water conditions. However, rather than deep water, the presence of evaporative crystal splays and overlying ripples indicates shallow to very shallow evaporative conditions of deposition for this facies.

As a result, this facies is interpreted to represent a closed lacustrine basin, possibly in a volcanic caldera, with trapped seawater that was subject to evaporation and recharge by hydrothermal springs. The alternation between carbonate and chert precipitation in this facies was most likely controlled by fluctations in pH, as gleaned from modern systems, arising in some cases from wet season / dry season variations in lake levels (e.g. Casanova, 1986; Renault and Jones, 1997). The overlying transition through rippled carbonate sandstone to stromatolite reflects Walther's Law of increasing proximity to a shoreline colonized by stromatolites. The setting is thus analagous to that described for Lake Bogoria in the East African Rift Valley, where high evaporation competes with rainfall to control water levels and pH in a lake fed by numerous flanking hot springs (Fig. 20; Renaut and Jones, 1997).

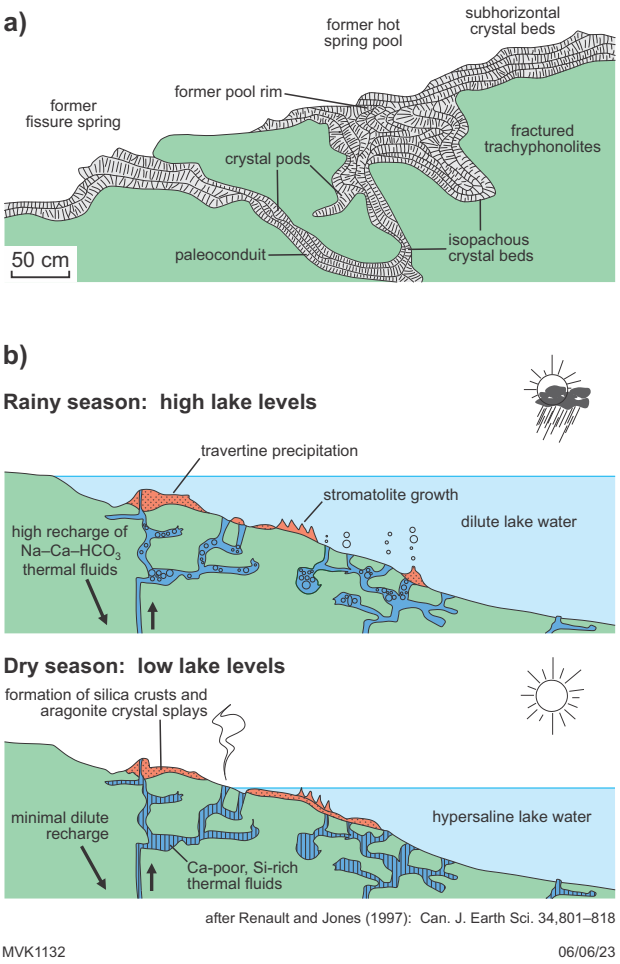

Figure 20. Lake Bogoria, Kenya: a) depositional setting; b) schematic model of seasonal controls on lake levels and the precipitation of silica and travertine from hot springs that flank the lake. From Renaut and Jones (1997)

Locality 1.3: Dresser Formation hot spring pool with collapsed sinter rim (Zone 50, MGA 753526E 7665002N)

Note: This locality lies within the Buick State Geoheritage Reserve (R44710).

IT IS ILLEGAL TO ACCESS THIS RESERVE WITHOUT PRIOR APPROVAL.

Hammering, sample collecting, camping and driving off pre-existing tracks is strictly not permitted within the bounds of this Reserve.

More information on the location and significance of localities on the Register of State Geoheritage Sites can be accessed via GeoVIEW, GSWA's online mapping platform; more general information on geoheritage and the Reserve permitting system can be found on the DMIRS website.

Note that the export of geological material out of Australia, particularly fossils and meteorites, is strictly controlled by the Federal Protection of Cultural Moveable Heritage Act 1986. *Approval is required from the Federal Office of the Arts for the permanent export of Class B objects.*

In a groundbreaking paper, Nijman et al. (1998) showed that the Dresser Formation was deposited during growth faulting and exhalations of sulfate- and silica-rich hydrothermal fluids. This model was further developed by Van Kranendonk (2006), who showed that deposition was in a dynamic, low-eruptive felsic caldera setting affected by uplift (magma inflation) to shallow water conditions when the stromatolites were deposited, and downdrop (post-eruption) when the uppermost (Assemblage 4) coarse volcaniclastic rocks were deposited. Part of the evidence for this change of view from the original model of deposition in quiet, shallow water lagoonal conditions (Groves et al., 1981; Buick and Dunlop, 1990) is evident at this locality.

Here, we delve into a gully that exposes a cross-section through the North Pole Chert Member. Most of the unit near the entrance to the gully consists of gently dipping grey and white, and rare jaspilitic layered cherts, whose protoliths have not been studied in detail. However, deeper in the gully, subhorizontally bedded grey-white cherts abut against a coarse breccia unit that, in addition to numerous other large, subrounded to angular blocks of bedded chert and hydrothermal barite, contains a 10 m-long, steeply dipping block of bedded chert, coarsely crystalline barite and wrinkly laminite (Fig. 21). The breccia and the bedded cherts along strike are overlain by additional layered grey and white chert, the bedding of which indicates recovery up-section from steep dips back to the shallow dips that characterize the cherts adjacent to the breccia. All of these rocks are cut by a 2 m-wide, vertical vein of coarsely crystalline barite.

The fallen block and breccia at this locality closely resemble the collapsed sinter rims that commonly form around the edges of hot spring pools in modern geothermal fields (Fig. 22). Collapsed rims form around modern springs because they build inwards from the edge of the pool through a combination of evaporative and microbial precipitation of sinter.

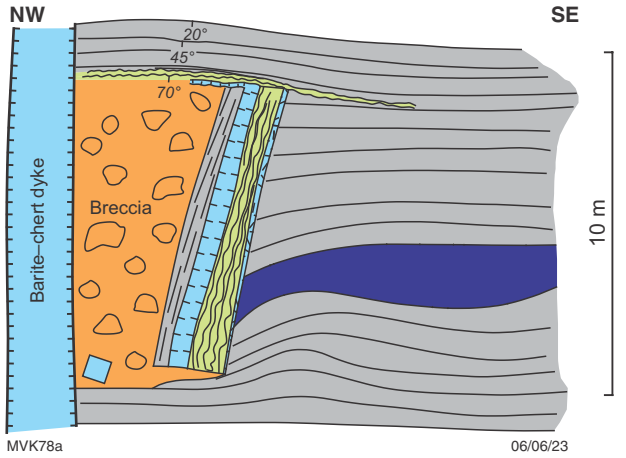

Figure 21. Simplified sketch showing coarse breccia that abuts horizontally bedded grey-white chert at Locality 1.3. Note the recovery wedge of the overlying sedimentary units and the cross-cutting chert–barite vein

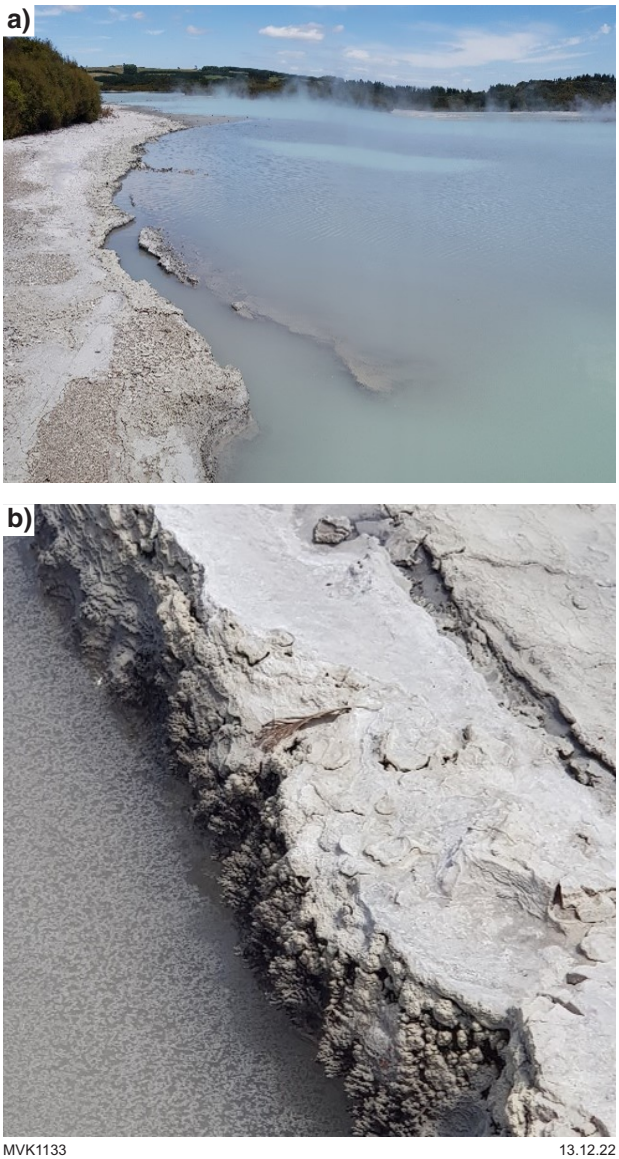

Figure 22. The hot spring Lake Rotokawa, Rotorua, New Zealand: a) collapsed sinter terrace rim on the edge of the hot spring; b) close-up view of microbialite textures on uptilted edge of the collapsed sinter terrace rim in a)

Looking across the gully to the south, you can see a set of thick barite veins, the main one of which occupies a syndepositional growth fault that separates bedded cherts of the Dresser Formation from altered basalts of the footwall (Fig. 23). Along the eastern margin of the vein, drag folds of the bedded cherts can be seen, indicating Dresser Formation (i.e. east side-down displacement) across this vein-occupied fault.

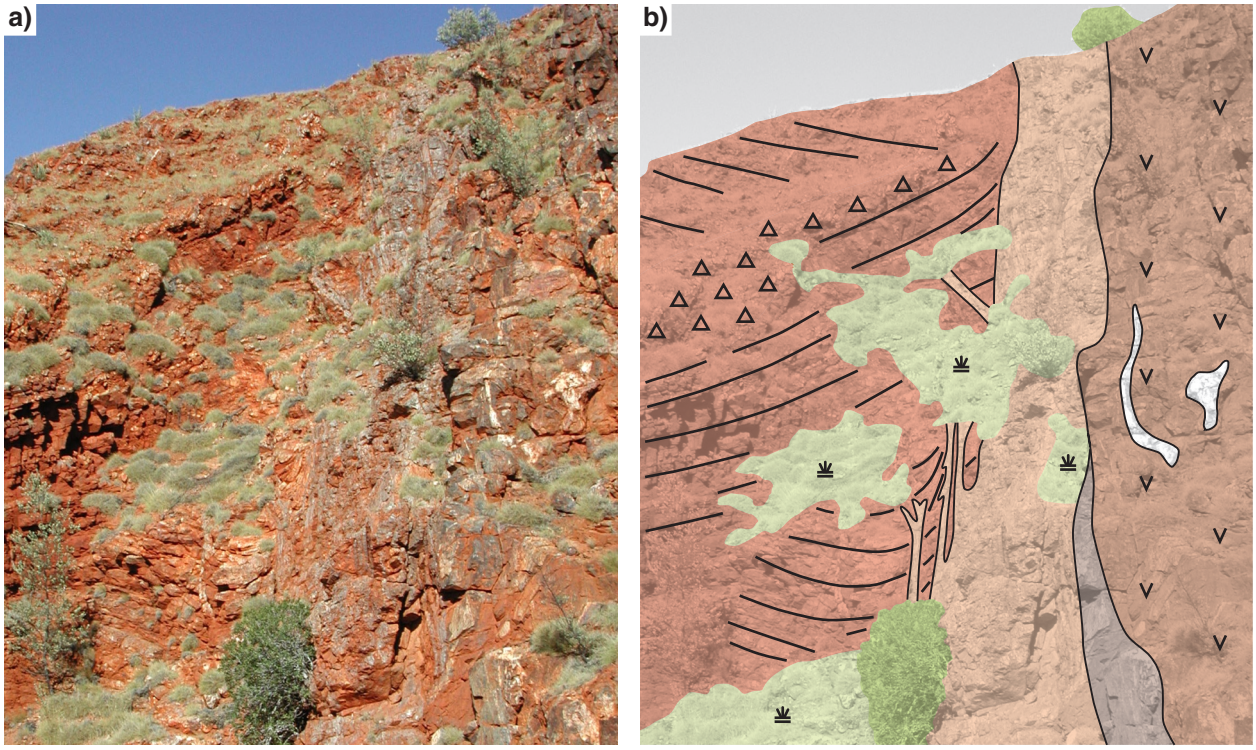

Figure 23. Locality 1.3: a) outcrop view of the cliff opposite the collapsed sinter terrace; b) interpreted sketch of the outcrop view. Hydrothermal vein (peach) cuts up within a fault that has dragged the lower sedimentary rocks upwards and juxtaposes them against footwall basaltic rocks to the right. Note the unit of olistostrome breccia (triangles) in the upper part

Day 2: Heart of the Dresser Formation hydrothermal system

Locality 2.1 (Drive-by): Chert–barite veins in the footwall of the Dresser Formation (Zone 50, MGA 751187E 7661455N)

This roadside stop presents a classic view of the Dresser hydrothermal system, viewed from structurally below the Dresser Formation (i.e. nearer to the core of the structural dome). Looking east, the hillside displays several narrow black ridges running up to the flat crest of the hill that is composed of bedded Dresser Formation cherts, dipping 30° away from the viewer (Fig. 24). The ridges are black hydrothermal chert–barite veins and they can be seen to penetrate up through the footwall basalts into the lower part of the sedimentary succession, but do not pass up through it. Looking closely, one can see offsets of the basal contact of the Dresser cherts, indicating the veins (which include multiple sets) were emplaced within growth faults active during sediment deposition, as described by Tadbiri and Van Kranendonk (2020).

Locality 2.2: Dresser mine hydrothermal black chert vein (Zone 50, MGA 752521E 7659377N)

This road cutting heading into the main pit of the Dresser barite mine passes directly through a large hydrothermal black chert vein, characteristic of the several hundreds of veins in this system (Fig. 25). Such black chert veins typically contain OM, as clots and strings of kerogen (Fig. 26a,b; Morag et al., 2016; Duda et al. 2018). Here, you can also see a narrow epithermal quartz core zone of the veins, which is typical higher up in the veins, towards the paleosurface (Van Kranendonk and Pirajno, 2004; Harris et al., 2009).

The OM present in the black chert veins has been the subject of three independent studies, both of which present evidence in favour of a biological origin (Ueno et al., 2004; Morag et al., 2016; Duda et al., 2018). These studies show that the OM is distributed as either wispy, dispersed kerogen, or as distinct clots, with Raman spectra characteristic of thermally mature OM, consistent with metamorphic temperatures of c. 300 °C in the lower parts of the veins (Fig. 26c; Harris et al., 2009; Duda et al., 2018). An alternative interpretation for some of the OM in hydrothermal veins can be found in Rasmussen and Muhling (2023).

Morag et al. (2016) found that average $\delta^{13}C_{OM}$ values in specific microstructural types range between −32 and −25‰ (Fig. 27). No correlation was seen between measured $\delta^{13}C$ values and H/C ratios in the studied OM microstructures. This lack of correlation and the low metamorphic grade of the rocks studied were used to argue against significant modification of OM isotopic composition by later metamorphic alteration. It was concluded that the range of $\delta^{13}C$ values represented primary OM isotopic variability, a feature inconsistent with solely abiotic OM formation via Fisher-Tropsch type reactions. These authors concluded that chemolithosynthesis was likely within the veins, due to the abundance of OM.

Duda et al. (2018) investigated kerogen from a hydrothermal black chert vein from just north of Dresser mine pit #2 (Fig. 25). Catalytic hydropyrolysis (HyPy) of this kerogen yielded *n*-alkanes up to *n*-C_{22}, with a sharp decrease in abundance beyond *n*-C_{18} (Fig. 28). This distribution (≤*n*-C_{18}) is very similar to that observed in HyPy products of recent bacterial biomass, which was used as reference material. The result differs markedly from the unimodal distribution of abiotic compounds experimentally formed via Fischer-Tropsch type synthesis. These authors therefore proposed that the OM in the Dresser chert veins had a primarily microbial origin.

Ueno et al. (2006) studied fluid inclusions from a Dresser hydrothermal black chert vein and found that the extracted fluids contain microbial methane with carbon isotopic compositions of −35 to −56‰ included within original precipitates. This was used to argue for the oldest evidence of methanogenesis.

Glikson et al. (2008) produced transmission electron microscopy images of OM from Dresser hydrothermal chert veins that are suggestive of microbial remains and possible remnants of microbial cell walls, comparable to a potential modern analogue, the hyperthermophilic *Methanocaldococcus jannaschii*, derived from an active sea floor hydrothermal environment (Fig. 29).

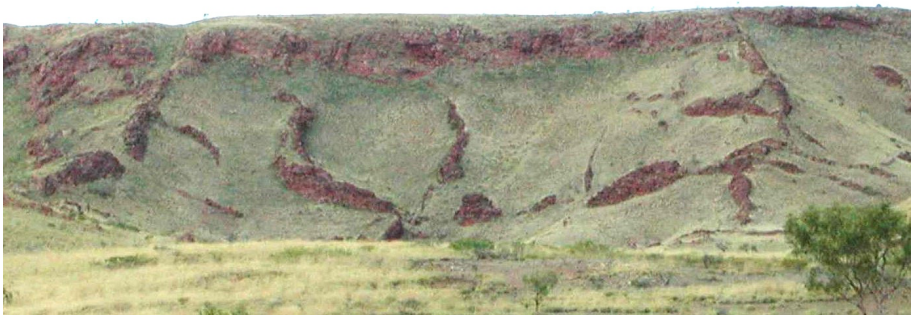

MVK1133 14.12.22

Figure 24. View looking west, at hydrothermal chert–barite veins (black ridges) cutting through altered volcanic rocks up to the base of bedded Dresser sedimentary rocks that cap the hill and dip away from the viewer (see Fig. 4 for location). Top of veins here include the sample location of Ueno et al. (2006) with evidence for methanogenesis. Note the fork-shaped set of central veins that compare with those in an analogue model of a collapsed caldera (see Fig. 31)

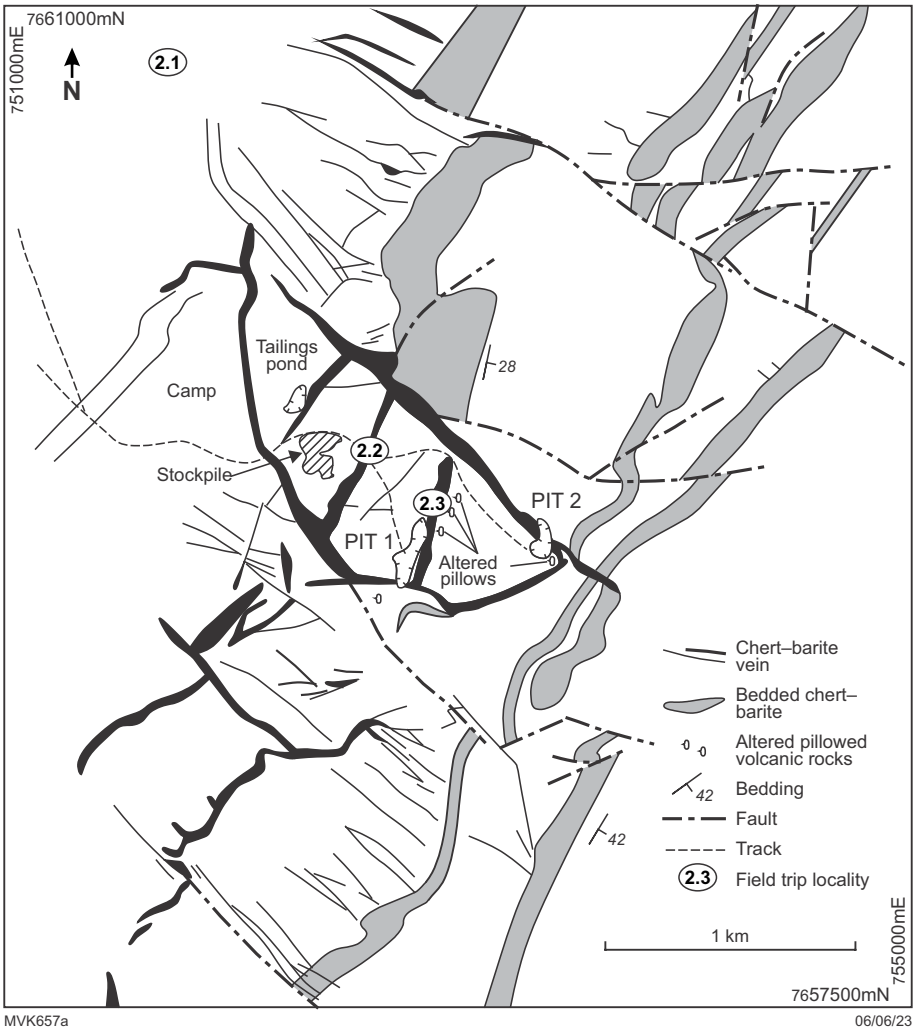

Figure 25. Simplified geological map showing the Dresser barite mine pits, hydrothermal veins and the bedded chert horizons of the Dresser Formation

Structural analysis shows there are three sets of early veins that were emplaced during repeated pulses of uplift and downdrop of the caldera system and deposition of the lower three lithofacies assemblages of the North Pole chert (Tadbiri and Van Kranendonk, 2020). A fourth set (red on Fig. 4) was emplaced into long-lived listric growth faults that were active through to the very top of the Dresser Formation, but not beyond.

Vein set orientations were used to test the volcanic caldera model of deposition (vertical σ1, σ2 = σ3 both horizontal; Van Kranendonk, 2006; Van Kranendonk et al., 2008, 2019a), in contrast to vein formation from either extension (i.e. vertical σ1, σ3 in one horizontal direction) or compression (i.e. σ1 in one horizontal direction). Untilting of dipping Dresser Formation bedding, and associated back-rotation of the veins, show that all veins were emplaced into vertical fractures prior to doming. Furthermore, the presence of conjugate vein sets in some structural blocks, and triple vein sets separated from each other by 120°, attests to a vertical σ1 and no preferred direction of horizontal extension (i.e. horizontal σ2 = σ3), which is consistent with the caldera model.

In fact, the Dresser veins show a north-to-south variation in orientation that correlate closely with the variations in orientation of fractures developed in a transect across the eastern limb of an analogue model of a collapsed caldera (Fig. 30; Troll et al., 2002; Tadbiri and Van Kranendonk, 2020). The collapsed caldera model shows essentially two sets of fractures — those that develop radially around the centre of the collapsed caldera, and a set of ring faults that encircle the centre point of the collapsed caldera. Directly east of the centre of the modelled collapsed caldera, radial faults form a conjugate set, similar to what is observed in Dresser structural block 4. To the north, ring faults strike west-northwest – east-southeast, as observed in Dresser structural blocks 1 and 2. To the south, ring faults strike northeast–southwest, as observed in Dresser structural blocks 6–8. Note also how local complexities in vein geometry in the analogue model (circled inset in Fig. 31) match those observed in the Dresser Formation (compare with Fig. 24).

In contrast, the veins emplaced within the younger, listric normal growth faults attest to uniaxial northerly directed extension at this time, in this locality.

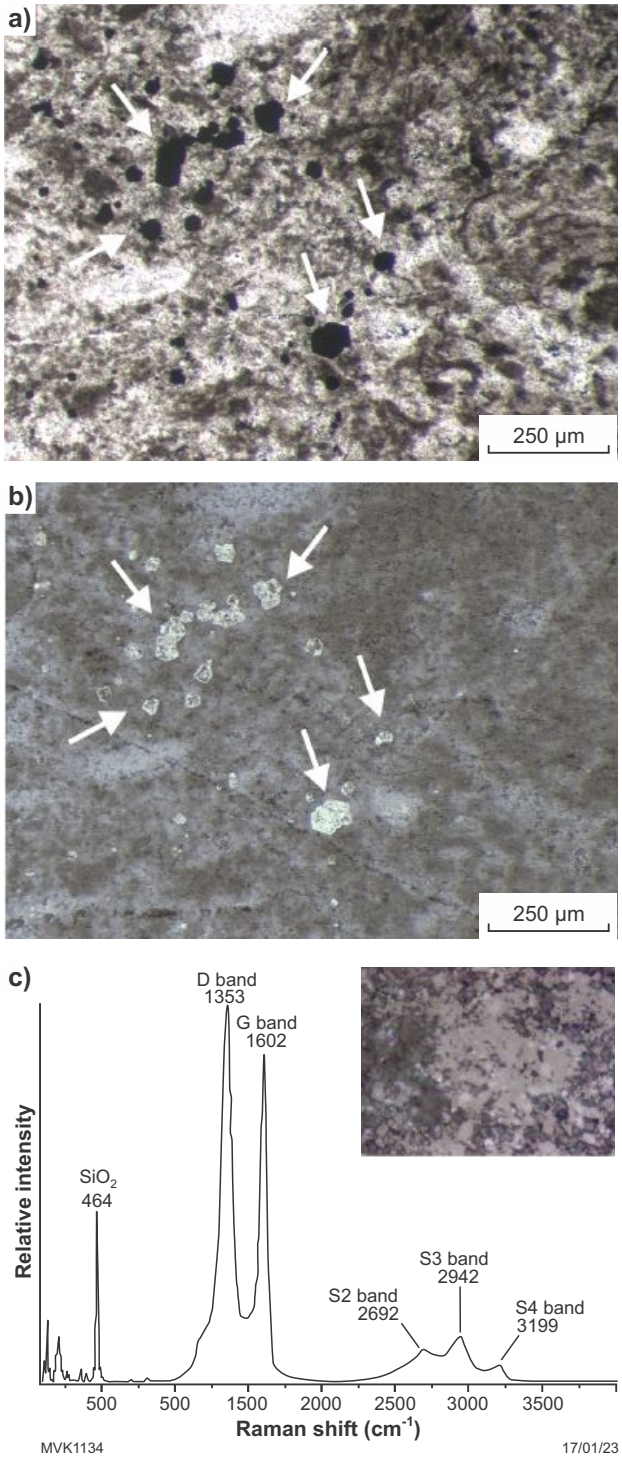

Figure 26. OM in black hydrothermal vein chert of the Dresser Formation: a–b) thin-section view of black hydrothermal vein chert containing dispersed OM and fresh pyrite (arrows); c) Raman spectra of the kerogen. From Duda et al. (2018)

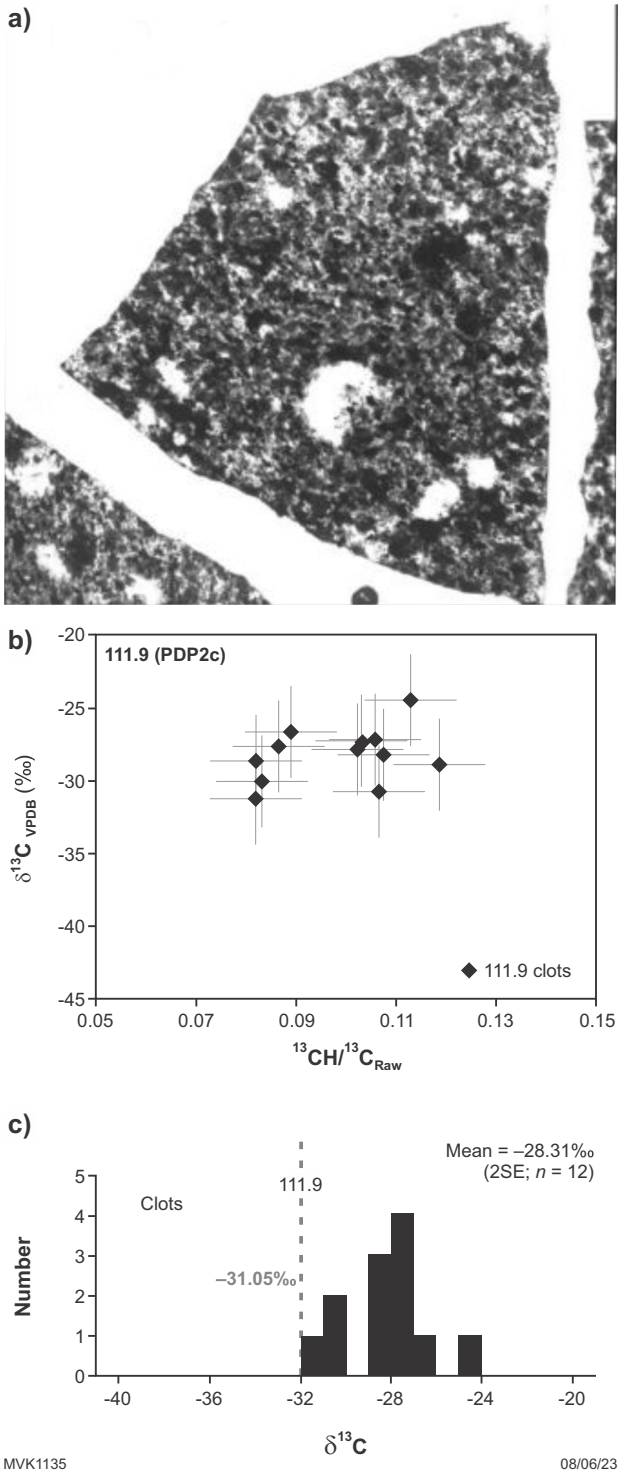

Figure 27. Carbon isotopic values of OM from Dresser hydrothermal vein chert: a) Dresser hydrothermal vein chert showing abundant OM as dark clots; b) SIMS $\delta^{13}C_{OM}$ (‰ VPDB) values plotted vs raw $^{13}CH/^{13}C$ ratios in the vein chert ; c) histogram of $\delta^{13}C$ values (‰ VPDB) for OM in Dresser hydrothermal vein chert. Dashed grey line with adjacent number indicates the bulk $\delta^{13}C$ value for insoluble OM . The $\delta^{13}C$ and $^{13}CH/^{13}C_{Raw}$ error bars indicate analytical uncertainty. From Morag et al. (2016)

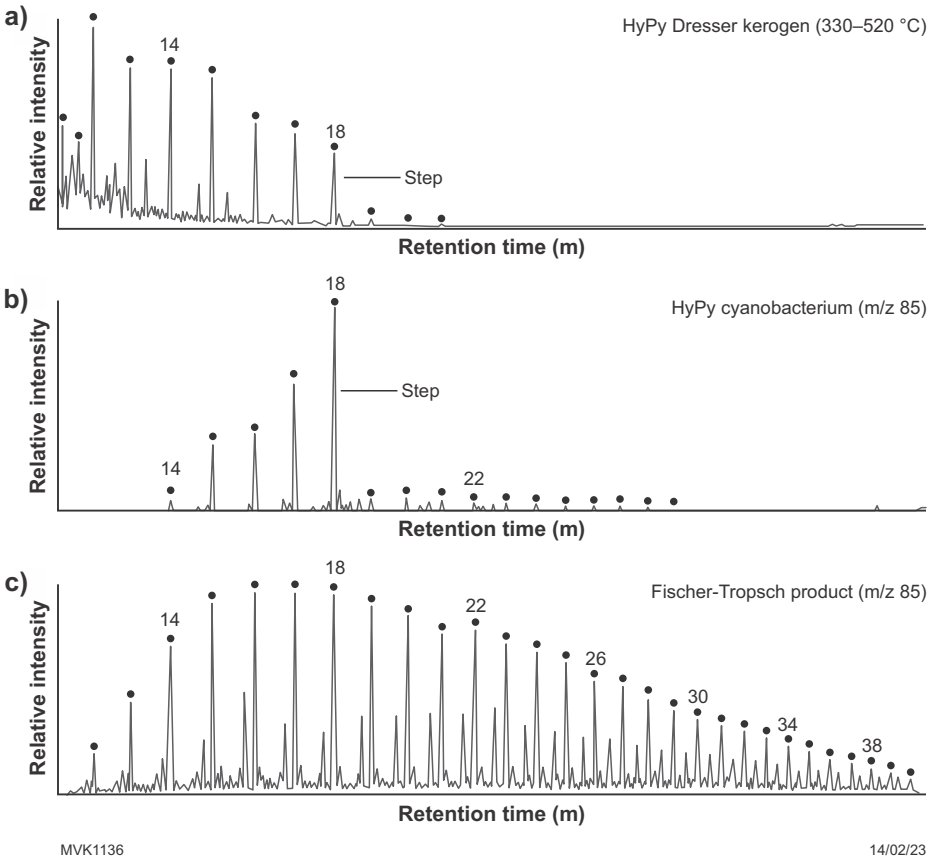

Figure 28. Organic geochemistry of Dresser Formation kerogen: a) high-temperature HyPy (330–520 °C) product of the Dresser kerogen, with blank subtracted; b) HyPy products of cell material of a heterocystous cyanobacterium. Note the sharp decrease in abundance of *n*-alkanes beyond *n*-C_{18} (arrow), similar to the *n*-alkane distribution of the Dresser kerogen; c) products of experimental Fischer-Tropsch type synthesis under hydrothermal conditions that is distinctly different from the Dresser kerogen. From Duda et al. (2018)

Locality 2.3: Barite veins and hydrothermal steam-heated acid-sulfate (argillic) alteration of footwall pillow basalts (Zone 50, MGA 752711E 7659199N)

This locality is in Dresser mine pit #1 (Fig. 25), where the largest volume of barite was mined from a large vein cutting strongly altered footwall rocks of the North Star Basalt. Dresser mine pit #2 to the east was situated in a 15–20 m-wide, subvertical barite vein from stratigraphically higher up, which cuts strongly altered pillowed, komatiitic basalts of the Dresser Formation. This latter vein is from within one of the late listric growth faults.

At this locality, we climb up the washed-out track towards a notch in the high hill to the east of the car park. Here, a zoned chert–barite vein cuts through perfectly preserved, but strongly altered, moderately east-dipping pillowed komatiitic basalts and flows (Fig. 32a,b). The pillows here are entirely white and contrast to the generally green-weathering nature of less altered pillow basalts that lie immediately above the Dresser Formation and elsewhere throughout the North Pole Dome. The white pillows are composed entirely of kaolinite–illite–quartz–anatase, yet retain perfectly primary pillow shapes, marginal vesicles and internal pyroxene–spinifex texture (Fig. 32c).

This style of alteration is unique within the North Pole Dome and consistent with argillic alteration caused by steam-heated acid-sulfate alteration at temperatures of approximately 150 °C within a high-sulfidation epithermal system (Fig. 8; Van Kranendonk and Pirajno, 2004; Van Kranendonk, 2006; Harris et al., 2009; Caruso et al., 2021).

Mapping of the vein array in the footwall shows that this style of alteration is part of a zoned alteration profile away from the largest veins (Fig. 33; Caruso et al., 2021). Immediately adjacent to the larger veins, relict pillows are composed predominantly of pyrophyllite, indicative of advanced argillic alteration. The white kaolinite–illite (argillic) alteration is the next alteration type, which passes laterally into dominantly sericite alteration, and then propylitic (chlorite–carbonate) alteration.

This hydrothermal alteration pattern is interpreted to have been caused by mixing of circulating groundwater with H_2S derived from the magmatic vapour plume derived from an unexposed synvolcanic mafic intrusion at depth that had differentiated to felsic compositions. This mixing generated H_2SO_4 and resulted in the steam-heated acid-sulfate alteration, as shown schematically in Figure 8 (Van Kranendonk, 2006). Downward penetration of meteoric water was probably facilitated by episodic faulting associated with felsic volcanic eruptive events and extension within the inferred piecemeal caldera setting. This activity was repeated numerous times, resulting in the many cross-cutting relationships seen between footwall silica–barite veins.

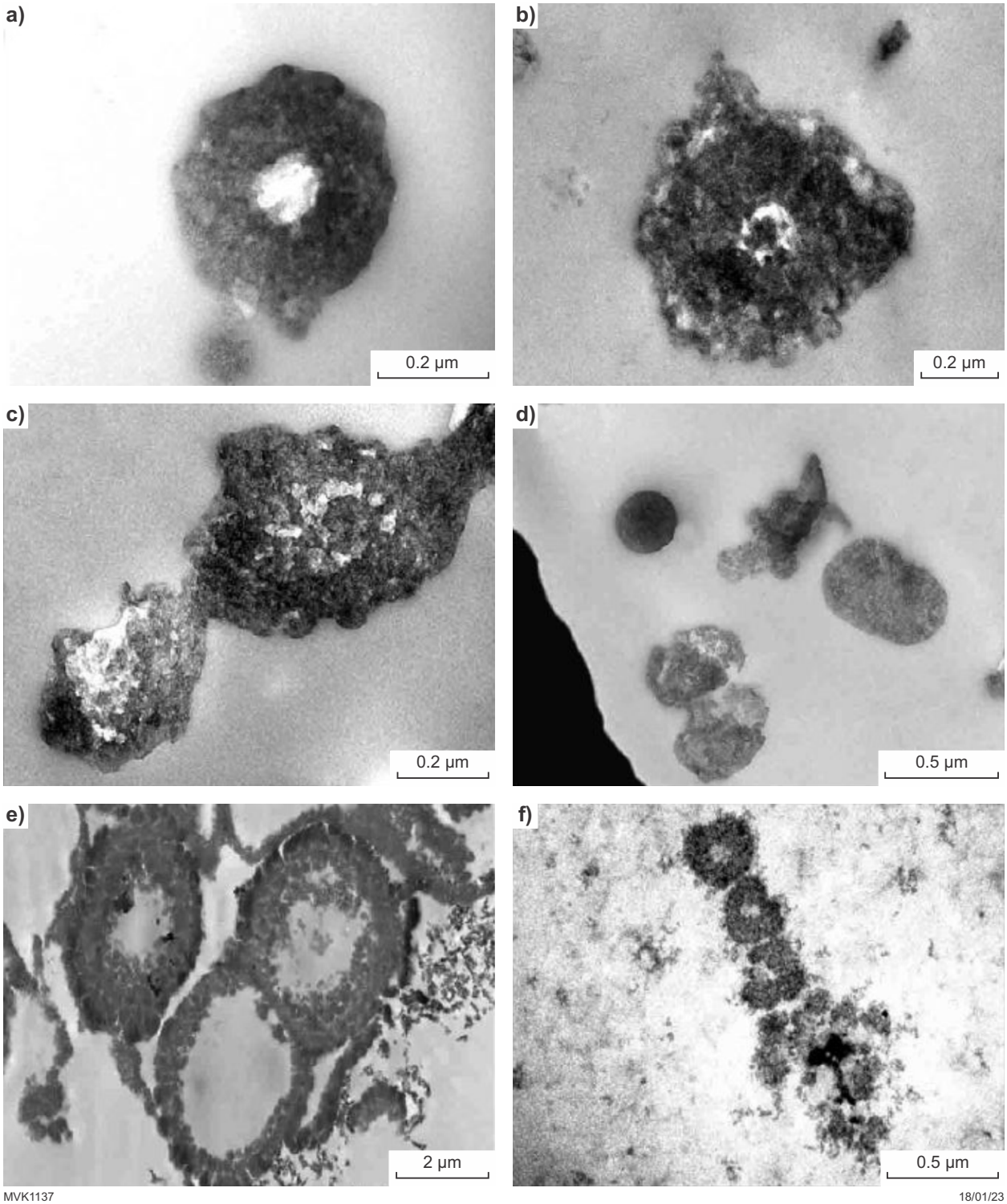

Figure 29. TEM micrographs of thermally degraded carbonaceous matter from Dresser cherts compared with modern microbes: a–e) thermally degraded carbonaceous matter concentrate after demineralization of Dresser cherts, showing possible cell-like wall segments; f) cell wall of *M. jannaschii* harvested after being autoclaved at 132 °C, showing nanoporosity following breakdown and ejection of cellular material. Shrinkage, deformity of cells and amorphous material formation following thermal stress is evident as is contraction of cell cavity into a tiny central hollow. From Glikson et al. (2008)

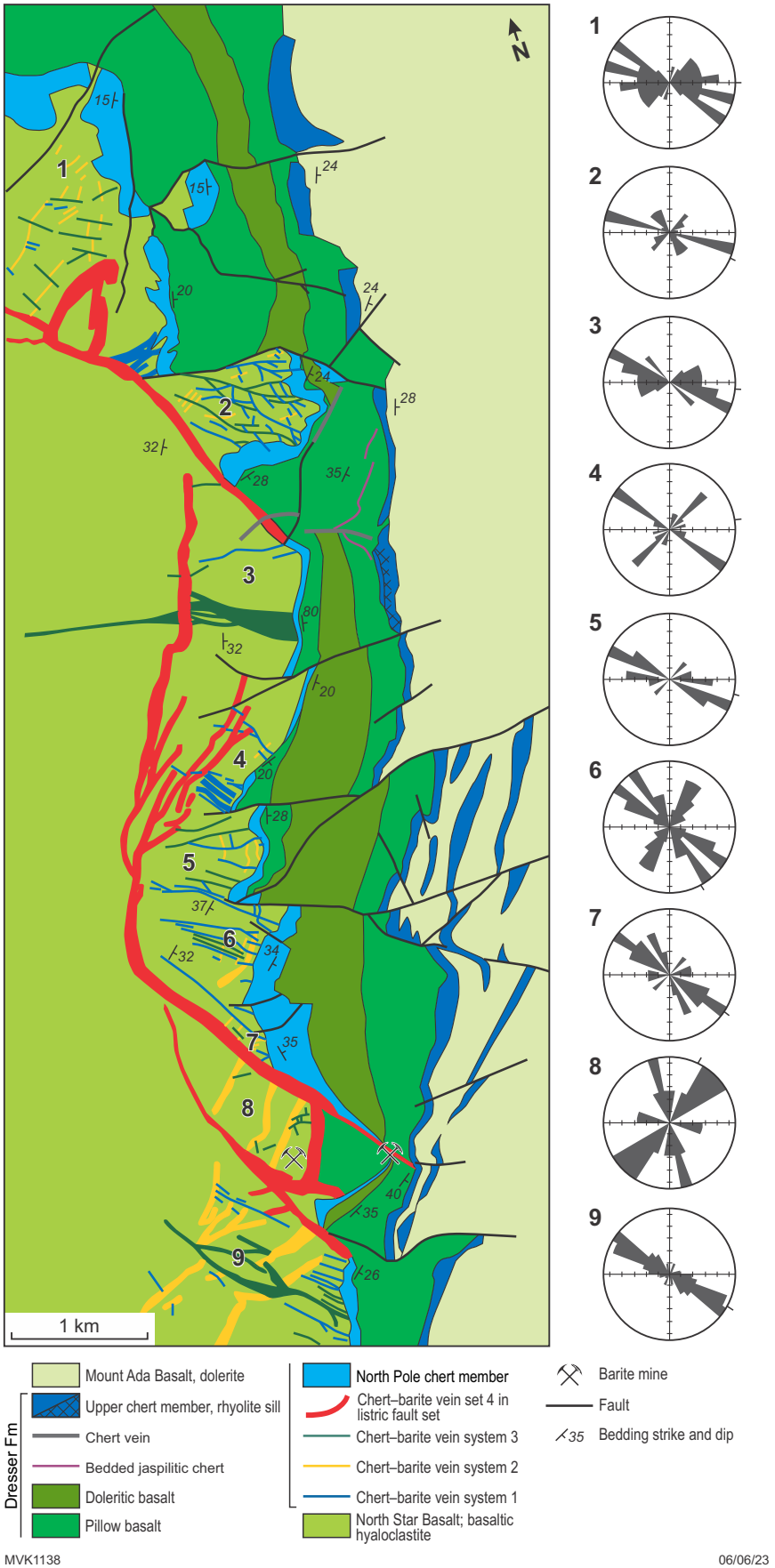

Figure 30. Rose diagrams showing orientations of back-rotated, early hydrothermal vein sets (blue, yellow and green) in structural blocks 1–9 along the Dresser Formation on the eastern limb of the North Pole Dome. Note that all back-rotated veins are vertical and the presence of conjugate vein sets in structural blocks 4 and 6, and 120° vein sets in structural blocks 2 and 8, indicative of vertical σ1. From Tadbiri and Van Kranendonk (2020)

A hydrothermal origin for the kaolinite at this locality — as opposed to formation through weathering — is indicated by four separate pieces of evidence: i) kaolinite is restricted to the area of highest paleofluid flow in the Dresser Formation and is found nowhere else in all greenstone belts of the East Pilbara Terrane; ii) the X-ray diffraction spectra of the kaolinite from this locality is distinctive of that produced by hydrothermal (not weathering) processes; iii) kaolinite has been observed within near-surface Dresser hydrothermal veins (Van Kranendonk and Pirajno, 2004) and in hot spring geyserite (Djokic et al., 2017); iv) Ar–Ar dating of the illite that is intergrown with the kaolinite from this locality has returned an age of c. 3240 Ma, which is the known age of the last major thermal overprint in the East Pilbara Terrane (Van Kranendonk et al., 2007a, 2019b) and demonstrates that the mineral assemblage is indeed ancient, and not due to much younger weathering processes (Caruso et al., 2021).

Several studies have provided evidence for the activity of sulfate-reducing and or elemental sulfur-utilizing bacteria in the barite-bearing hydrothermal veins (Shen et al., 2001, 2009; Philippot et al., 2007; Ueno et al., 2008; Baumgartner et al., 2020c).

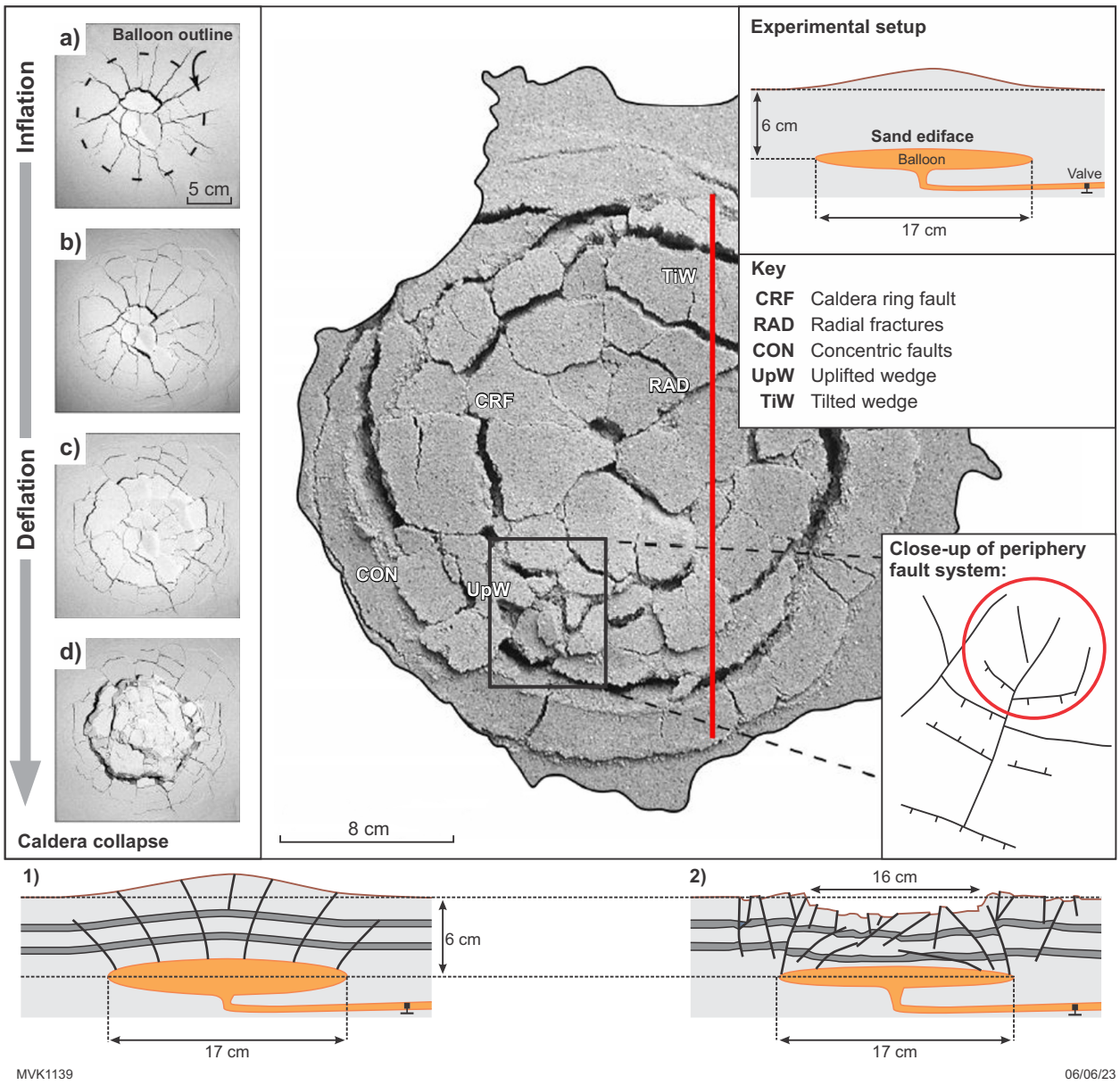

Figure 31. Sand analogue model of caldera collapse, showing radial and ring-shaped faults. The red line denotes the interpreted section represented by the exposure of the Dresser Formation on the eastern limb of the North Pole Dome. Compare geometry of circled veins of the inset with Dresser veins in Figures 4 and 30. Modified from Troll et al. (2002)

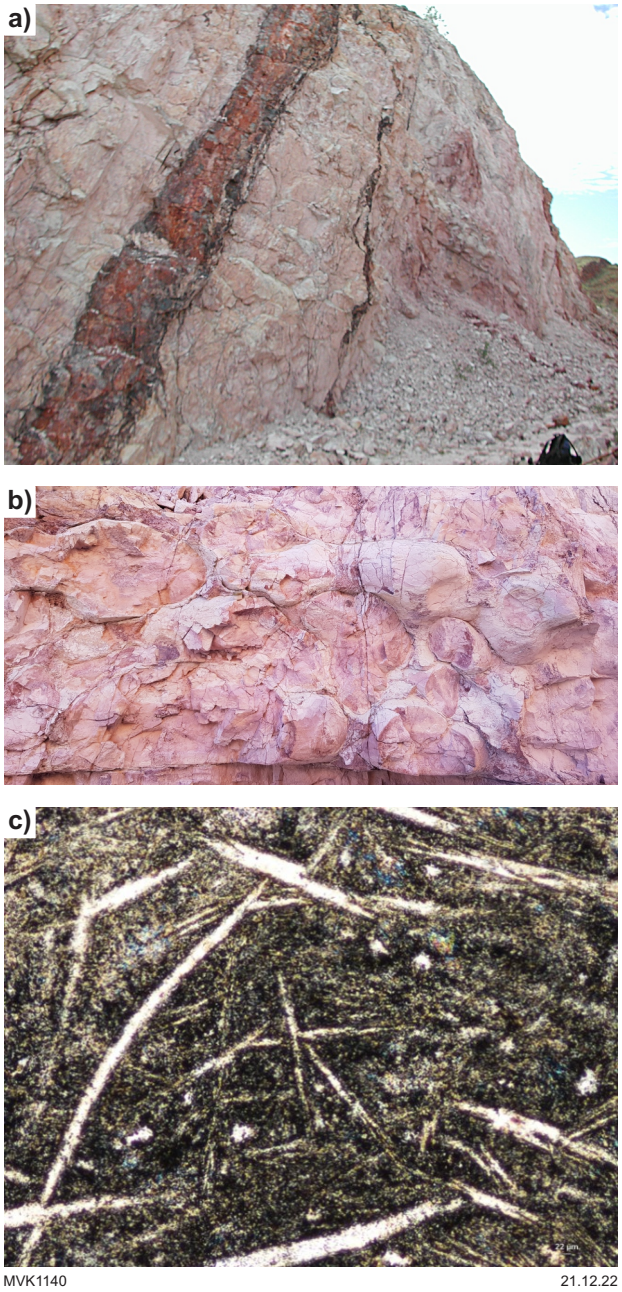

Figure 32. Kaolinite–illite basalts of the footwall to the Dresser Formation in the Dresser mine: a) zoned chert–barite vein cutting through kaolinite–illite steam-heated acid-sulfate altered pillowed komatiitic basalts of the footwall; b) detail of white kaolinite–illite altered pillowed komatiitic basalt, showing perfectly preserved pillow shapes with smooth, convex tops and irregular tails; c) thin section photomicrograph of kaolinite–illite altered pillowed komatiitic basalt, showing relict pyroxene–spinifex texture. Width of view approximately 1 mm

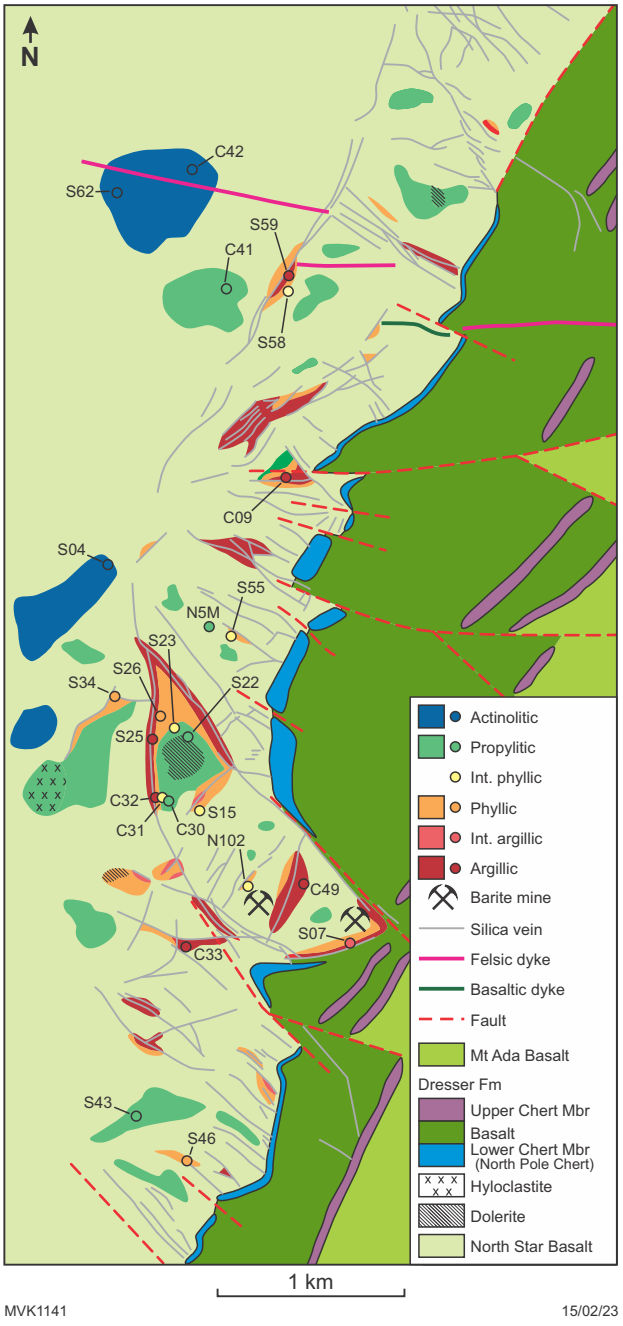

Figure 33. Alteration map of the eastern Dresser Formation, with sample locations (from Caruso et al., 2021)

Locality 2.4: The c. 3.45 Ga North Pole Monzogranite (Zone 50, MGA 746581E 7663261N)

The c. 3.45 Ga North Pole Monzogranite crops out over an oval (4.6 × 2.8 km) area in the core of the North Pole Dome (Fig. 3). It is a remarkable unit for a rock of this age on account of its potassic composition, and its state of preservation, containing centimetre-scale euhedral K-feldspar phenocrysts, unstrained quartz and miarolitic cavities.

At this locality, the monzogranite is cut by a northeast-striking dolerite dyke interpreted as belonging to the c. 2.77 Ga Black Range Dolerite Suite. The irregular intrusive contact of the granite with amphibolite facies metabasalts of the c. 3.49 Ga North Star Basalt can be seen on the hillside to the south.

This site is also the locality of turn-of-the-century gold processing from the North Pole Mining Centre located 2.6 km to the northwest. The tanks at the top of the hill were for cyanide, which was poured down onto a mercury-lined table across which pulverized ore from the stamp battery was passed, liberating the gold. The site was chosen here on account of a permanent water source in the creek just to the south.

The North Pole Mining Centre was named by the miners who were fascinated by Peary's attempt to reach the North Pole in 1909. The North Pole Mining Centre consists of five historical prospects from which 400.52 oz of gold was mined from 1899 to 1931. The prospects are in sheared and altered metabasalts on either side of a chert bar. The Breens Reward mine is adjacent to a 3432 ± 7 Ma felsic porphyry, which is interpreted to have been the source for the Au, Cu, Ag and Bi mineralization. This porphyry is one of several veins that emanate radially outward from the North Pole Monzogranite, across older lithology (see Fig. 4), and up to the level of the unconformity at the base of the Strelley Pool Formation where they are locally associated with pyrophyllite alteration (Van Kranendonk, 1999, 2000). These veins are interpreted to be feeders to the eruptive felsic volcanic rocks of the 3.45 – 3.43 Ga Panorama Formation at the top of the Warrawoona Group.

Gold processing continued at this site after the closure of the North Pole Mining Centre, when mining at Normay, located in sheared metabasalt near the northern contact of the North Pole Monzogranite, was instigated in 1940–41, which saw 70.1 t of ore treated to retrieve 0.966 kg of gold at an average grade of 13.79 g/t Au. In 1949–51, a further 3781.55 t of ore was treated for 46.62 kg Au and 8.089 kg Ag, at an average grade of 12.33 g/t Au. From 1952 to 1957, 44.664 kg Au and 54.59 kg Ag were extracted at the high grade of 54.59 g/t Au. The mine was reopened in 1971–72, when 4.54 kg of gold was extracted from 679.1 t of ore, but by far the largest amount was mined between 1988 and 1995 when 809 kg of gold was produced. The Normay mine was operational until placed under care and maintenance in 1994. Gold and silver mineralization at Normay are in quartz veins, together with minor pyrite and copper–lead–zinc sulfides at depth, within a steeply dipping, narrow shear that extends for up to 1 km along strike to the east, until it is cut out by a gabbro dyke of the Fortescue Group.

Locality 2.5: The c. 3.4 Ga Strelley Pool Formation at the Trendall locality on the Shaw River (Zone 50, MGA 739582E 7652496N)

Note: This locality is of major geological significance and lies within the Trendall State Geoheritage Reserve (R50149).

IT IS ILLEGAL TO ACCESS THIS RESERVE WITHOUT PRIOR APPROVAL.

Hammering, sample collecting, camping and driving off pre-existing tracks is strictly not permitted within the bounds of this Reserve.

More information on the location and significance of localities on the Register of State Geoheritage Sites can be accessed via GeoVIEW, GSWA's online mapping platform; more general information on geoheritage and the Reserve permitting system can be found on the DMIRS website.

Note that the export of geological material out of Australia, particularly fossils and meteorites, is strictly controlled by the Federal Protection of Cultural Moveable Heritage Act 1986. *Approval is required from the Federal Office of the Arts for the permanent export of Class B objects.*

The Trendall locality in the Strelley Pool Formation, together with the Buick locality in the Dresser Formation, are the best-known stromatolite localities in the Pilbara. This locality is named after the late Alec Trendall, geologist and former director of the GSWA. He discovered the outcrop one evening in 1979 after driving down the sandy Shaw River and stopping to look for a campsite. He noticed the outcrop and its odd, inverted V-shaped structures. He took a photo and sent it to the survey's palaeontologist, Kath Grey, who later dismissed them as being stromatolites as they had too-consistent laminations and lacked an axial bulge (Grey, 1984) that is a characteristic of phototrophic stromatolites made by gliding filamentous cyanobacteria. Alec did not agree and sent photos of the disputed stromatolites to Hans Hofmann, who visited the site in the early 1990s and subsequently published a paper citing a variety of lines of evidence supporting biogenicity (Hofmann et al., 1999), which has since been vindicated by a host of further studies, as detailed below.

In fact, stromatolites had been described from the Strelley Pool Chert (later renamed the Strelley Pool Formation) by Lowe (1980, 1983), although it was not known at that time that the locality where Lowe described his stromatolites and the Trendall locality were part of the same unit: this was only determined through later mapping (Van Kranendonk and Morant, 1998; Van Kranendonk, 1999, 2000). Lowe (1994) later recanted on his previous biological interpretation of the Strelley Pool Formation (and Dresser Formation) stromatolites, but the biogenicity of these structures has been confirmed by other, more recent and more detailed, studies.

Regional setting

The c. 3.4 Ga[1] Strelley Pool Formation is widespread across the whole 220-km diameter of the East Pilbara Terrane,

1 The exact age of the Strelley Pool Formation is disputed, as discussed at the end of this section.

deposited on rocks of the Warrawoona Group across a subaerial erosional unconformity that cuts down through a significant part of the Warrawoona Group stratigraphy (Fig. 34; Buick et al., 1995; Van Kranendonk, 2006; Allwood et al., 2007; Van Kranendonk et al., 2007a; Hickman, 2008; Wacey et al., 2010a). The oldest rocks that underlie the unconformity are the 3515 ± 3 Ma rocks of the Coonterunah Subgroup in the northwestern part of the East Pilbara Terrane, whereas the youngest rocks that underlie the unconformity are 3427 ± 2 Ma felsic volcaniclastic rocks of the Panorama Formation within the North Pole Dome (Nelson, 2001; Van Kranendonk et al., 2002, 2007a, 2019b).

Three geological settings have been proposed for the carbonates of the Strelley Pool Formation: i) a shallow, marine, evaporative basin (Lowe, 1980, 1983, 1994; Buick et al., 1995; Van Kranendonk, 2000, 2006); ii) a shallow, open marine environment (Hofmann et al., 1999; Van Kranendonk et al., 2003; Allwood et al., 2006; Duda et al., 2016); iii) a hydrothermal setting (Lindsay et al., 2005), in which carbonates were interpreted to have been deposited from hydrothermal solutions sourced from veins preserved locally in the footwall.

A characteristic feature of the Strelley Pool Formation is that it can be traced in good exposure for tens of kilometres along strike within greenstone belts, is recognized in all greenstone belts across the East Pilbara Terrane, and contains a recognizable and internally consistent stratigraphy in most of the belts. The only real changes within this unit across the different belts is the thickness of the lower clastic member, which varies from 0 to 1 m of boulder and pebble conglomerate to 1000 m of quartz-rich sandstone, reflecting local changes in depositional environments for this member from fluviatile to rocky shoreline and tide-dominated beach conditions (Lowe, 1983; Buick et al., 1995; Van Kranendonk, 1999, 2000; Allwood et al., 2006). In the far south, bedded carbonate sandstones of the formation lack stromatolites.

The widespread and consistent distribution of the carbonate lithofacies argues strongly against a hydrothermal setting of deposition, as these latter deposits occur within fault-bounded, active volcanic terrains and are characteristically highly variable in terms of thickness and composition along strike lengths of 0.1 – 10 km as, for example, is preserved in the Dresser Formation (see Days 1 and 2). Further evidence against a hydrothermal setting was provided by Van Kranendonk et al. (2003) and Allwood et al. (2010) in the form of trace element geochemical data on the carbonates, which demonstrated that they were precipitated from normal seawater, and not from hydrothermal solutions.

It is now clear from detailed studies that the Strelley Pool Formation was deposited during a basin-deepening event as a prelude to the onset of submarine basaltic volcanism, through a transition from a locally rocky shoreline to a hydrothermally influenced tide-dominated beach setting, to shallow marine conditions that included one or more periods of evaporative conditions and subaerial exposure, followed by basin collapse and deeper marine conditions (e.g. Allwood et al., 2006, 2007; Van Kranendonk, 2011; Sugitani et al., 2015a). Geochemical and geochronological data from the conformably overlying Euro Basalt has been used to suggest that the Strelley Pool Formation and conformably overlying Kelley Group succession can be related to the arrival (uplift and erosion) and eruption (basin deepening and pillow basalt) of a mantle plume (Van Kranendonk and Pirajno, 2004; Smithies et al. 2005b; Van Kranendonk et al., 2015, 2019b), whereas other studies have separated these events.

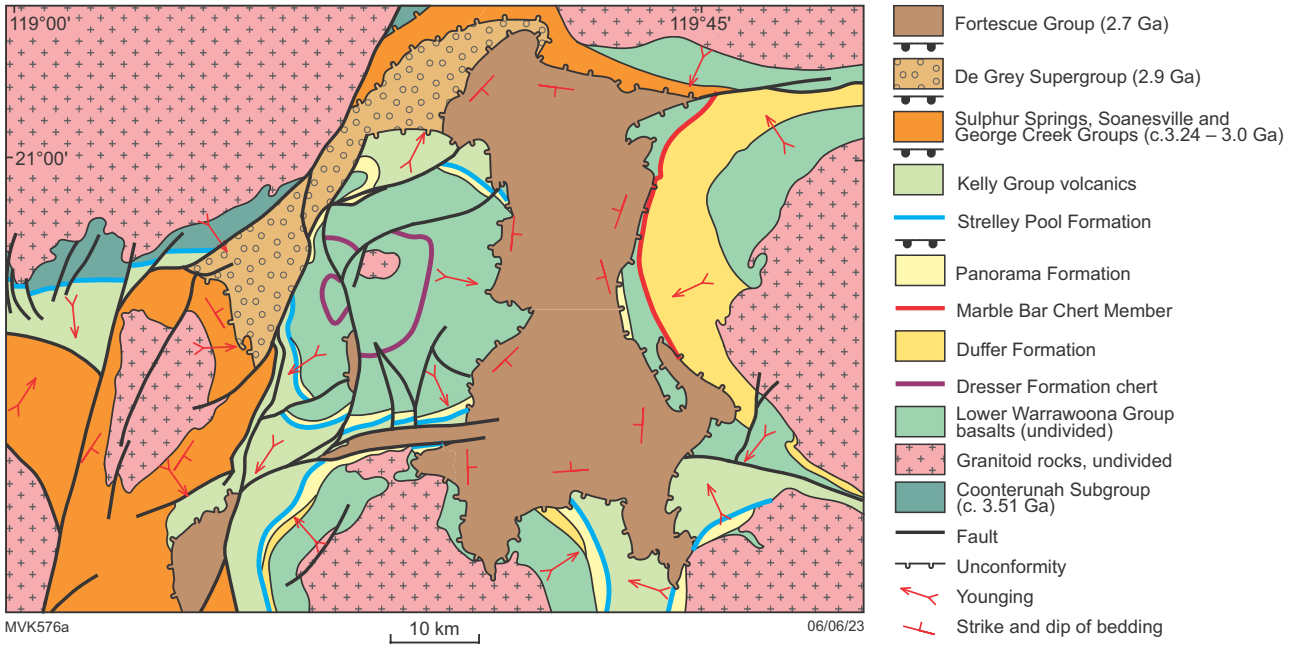

Figure 34. Simplified map of part of the East Pilbara Terrane, showing the distribution of major chert units, including the Strelley Pool Formation. Trendall locality is located in the southwestern corner of the North Pole Dome, which is in the centre of the map

Stromatolites

Coniform stromatolites are widespread in the Strelley Pool Formation across most of the 220 km diameter of the East Pilbara Terrane (Fig. 35). The stromatolites have been described in detail by several authors, who support a biogenic interpretation (Lowe, 1980; Hofmann et al., 1999; Van Kranendonk, 2000; Van Kranendonk et al., 2003; Allwood et al., 2006). Alternatively, Lowe (1994) and Lindsay et al. (2005) have suggested that coniform structures in the Strelley Pool Formation are abiogenic. Lowe (1994) suggested abiogenic formation of coniform structures through evaporitic precipitation of mineral crusts, whereas Lindsay et al. (2005) concluded that, because 'Laminations within the stromatolitic structures are conspicuously isopachous and comparable with abiotic structures formed by direct precipitation of carbonate … stromatolite structures described from the Strelley Pool Formation are abiotic features deposited by direct precipitation from hydrothermal solutions that were modified by ocean floor currents.' The biogenicity of Strelley Pool Formation stromatolites is discussed in more detail below and is a major focus of discussion at this locality.

MVK1142 21.12.22

Figure 35. View looking down onto a bedding plane surface of the Strelley Pool Formation with silicified coniform stromatolites of a variety of sizes

Geology of the Trendall locality

The Trendall locality is one of the prime localities in support of ancient life on early Earth and represents a key locality for understanding both the geological setting and biogenicity of ancient stromatolites. A detailed map of the outcrop is presented in Figure 36. At this locality, the formation lies across an unconformity on pyrophyllite-altered, schistose metabasalt of the Mount Ada Basalt and consists of four distinct members: i) a lower member of black-and-red layered chert boulder conglomerate that passes along strike uphill into a 1–2 m-thick unit of well-rounded chert pebble conglomerate; ii) a middle member of planar and stromatolitic carbonate laminites and coarse evaporitic crystal splays; iii) an approximately 1 m-thick unit of bedded black chert, which contains layers of fine-scale columnar stromatolites and casts of likely evaporative gypsum crystals; iv) an unconformably overlying upper unit of coarse- to fine-grained clastic sedimentary rocks, including beds with sparse to clastic OM (see also Allwood et al., 2009). All members of the formation are transected by a suite of zoned black chert and white quartz veins that extend up to the top of the formation but not into the overlying pillow basalts (Van Kranendonk, 2006, 2010) and reflects what elsewhere in the Strelley Pool Formation has been identified as part of a coastal hydrothermal field (Sugitani et al., 2015a). The Strelley Pool Formation is conformably overlain here, and elsewhere, by massive to pillowed basalts of the Euro Basalt.

Basal clastic member

Widely spaced boulders of laminated black-and-red chert line the base of the formation at the Trendall locality and pass along strike uphill to the south to 1–2 m of jasper chert round pebble conglomerate (Fig. 37). Boulders are encrusted by the overlying carbonate member. Chert boulders and pebbles in this basal member derive from units of layered red-and-black chert within the Mount Ada Basalt, visible along strike, across the Shaw River to the north. Indeed, stromatolitic carbonates of the middle member of the formation onlap Mount Ada cherts at a locality approximately 4.5 km along strike to the north, across a double unconformity (Hickman and Van Kranendonk, 2012). The boulder beds have been interpreted to represent the deposits on a rocky shoreline at the transition from a subaerial environment of erosion to shallow water deposition (Allwood et al., 2006). Wacey et al. (2010b) identified two coexisting sulfur metabolisms — microbial sulfate reduction and microbial disproportionation of elemental sulfur — from micron-sized pyrite intimately associated with organic material coating framework quartz grains in this member further to the north.

Middle carbonate member

Laminated carbonates

The dominant lithology of the middle carbonate member of the Strelley Pool Formation is millimetre-bedded, carbonate laminite. Planar laminite dominates but passes along strike into a texturally identical rock with a variety of structures formed by the growth of stromatolites (Fig. 38a; Hofmann et al., 1999; Van Kranendonk et al., 2003; Allwood et al., 2006). Detailed mapping shows that stromatolite forms vary along strike over distances of 1–1000 m (Allwood et al., 2006). In this outcrop, the largest and most complex stromatolites define three stacked, offset biostromes that dip to the north at an angle of up to 15° from the bedding and pass along strike into planar-bedded carbonate laminite (Fig. 36).

The dominant stromatolite morphology is that of stacked cones that locally display nearly isopachous lamination, although close inspection shows thicker beds in troughs between stromatolites than over the stromatolite crests (Fig. 38b). Conical stromatolites are characteristically elliptical in plan view, being elongate down the dip of bedding (Fig. 38a). Stromatolite elongation is not as a result of

tectonic strain, but rather reflects the original shape of the stromatolites and possibly a preferred direction of growth under flowing (tidal) water. Individual bedding planes may contain many cones of similar dimension (Fig. 38a), or of varied size (Fig. 39a). Cross-sectional views show that whereas the stromatolites are generally symmetrical, others are asymmetrical, with consistently longer northern limbs than southern limbs (Fig. 39b; Hofmann et al., 1999), suggesting growth on a local palaeoslope of 15° dip. Coniform stromatolites initiate from a flat generation surface and form structures that extend up-section for anywhere from a few centimetres up to a metre in height (Fig. 39b). Some coniform types show incipient branching and may form structures up to 35 cm in height (Fig. 39c). Rare branching columnar forms with convex lamination also occur (Fig. 39d). Others contain columnar branches off one side (Fig. 39e), with up to 10 small lateral branches having been observed on the flanks of the largest conical forms. Detailed investigation of Trendall locality coniform stromatolites has found that they do, indeed, contain an axial crest, suggestive of construction by gliding filamentous, and probably phototrophic, bacteria (Fig. 40; Hickman and Van Kranendonk, 2012).

Closer inspection of laminations shows that stromatolitic carbonates and their silicified equivalents display a variety of layering relationships, including onlap of sediment along the sides of coniform stromatolites (Fig. 41a,b; Van Kranendonk et al., 2003), and growth of coniform stromatolites within, and contemporaneous with (i.e. along strike of), sedimentary rocks deposited from strong currents (Fig. 42). These features show that the rocks are not abiogenic precipitates 'modified by ocean currents', as suggested by Lindsay et al. (2005), but rather are structures that formed ***during*** accumulation of clastic carbonate sand/silt that was deposited by strong currents. The interaction between stromatolite growth and water currents is most dramatically displayed in Figure 43, which shows a steep-sided coniform stromatolite that displays continuous growth upwards from fine to moderately laminated carbonates at the base, thorough an 8 cm-thick bed of flat pebble conglomerate, into finely laminated carbonates. This unequivocally demonstrates that coniform stromatolites are not precipitates from solutions of either evaporitic or hydrothermal origin and must have formed as a result of living microbial activity.This is a good example of the same relationship of the interference between biological and abiological processes as discussed on Day 1 at the Buick locality of the Dresser Formation.

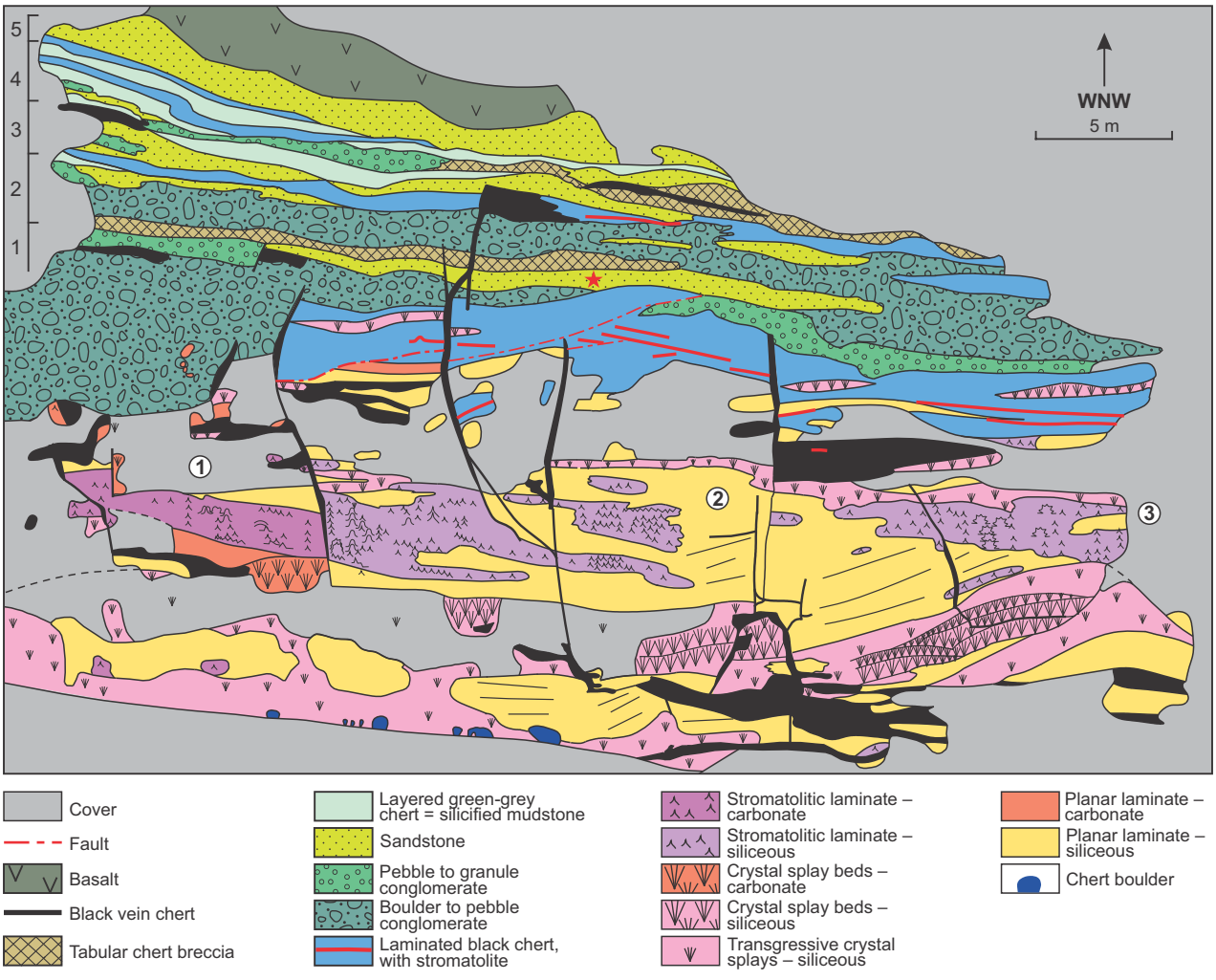

MVK175a 13/01/23

Figure 36. Geological map and legend of the Trendall locality of the Strelley Pool Formation, with the Shaw River to the right. The map shows the three main facies at this locality, including: lower boulder conglomerate; middle bedded carbonate, stromatolitic carbonate, and beds of crystal splays; upper coarse clastic succession with five repeated fining-up cycles (1–5). Circled numbers mark offlapping stromatolitic biostromes

MVK1143 21.12.22

Figure 37. Chert pebble (jasper, white and blue-grey) conglomerate at the base of the Strelley Pool Formation at the Trendall locality

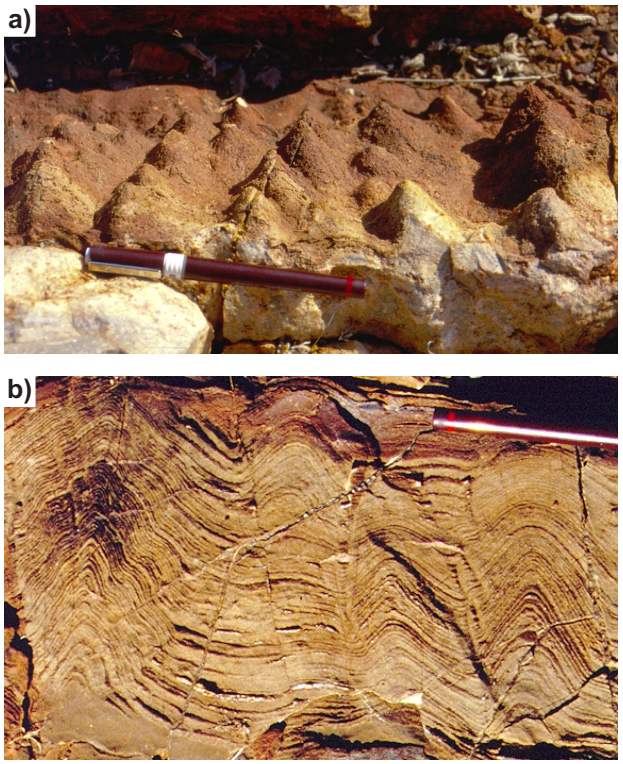

MVK1144 21.12.22

Figure 38. Outcrop views of coniform stromatolites of the Strelley Pool Formation at the Trendall locality: a) oblique view of 'egg-carton' coniform stromatolites exposed on a bedding plane. This exposure was collected for the Western Australian museum; b) cross-sectional view of coniform stromatolites with wavy, near-isopachous lamination, but note that bed thicknesses are greater in the troughs than over the crests of the stromatolites

In areas where carbonate is well preserved, laminae are defined by couplets of light-brown siderite/dolomite and dark-brown weathering, heavily silicified carbonate, dominated by polygonal microquartz. On the flanks of the large stromatolite shown in Figure 39c, repeated cyclical bundles of 7–11 carbonate–chert couplets are present, with each bundle capped by a slightly thicker dark-brown lamina. Although the cause of this cyclical bundling is unknown, consideration of the scale of the bundling suggests that the couplets may represent annual winter–summer cycles and that a possible cause of the bundling is variations in climatic effects due to varying insolation associated with the sunspot cycle, which operates on an 11-year cycle (e.g. Foukal, 2003).

Cammack et al. (2018) undertook a detailed analysis of oxygen isotopes of quartz materials at the Trendall locality. They recognized a number of petrographically distinctive quartz microtextures, none of which they determined were precipitated directly from seawater. In situ secondary ion mass spectrometry (SIMS) analyses yielded a range of $\delta^{18}O_{VSMOW}$ values of 7–31‰ in 'bedded' cherts at the Trendall locality, up to 9‰ above the secular-temporal oxygen isotope trend. The earliest generation of microquartz has maximum $\delta^{18}O_{Qz}$ of 22‰ by SIMS, interpreted to represent the effects of low-temperature hydrothermal activity. Quartz of clearly hydrothermal origin has a restricted range of $\delta^{18}O$, mostly from 16 to 19‰. Late cavity megaquartz that grows into late, open cavities has the highest $\delta^{18}O_{Qz}$ values reported from the Pilbara, up to 31.3‰.

Flannery et al. (2017) investigated the carbon isotopic composition of dolomite and kerogen within Strelley Pool Formation stromatolites. In situ SIMS analysis of microscale domains of organic material trapped within inorganic carbon matrixes yielded $\delta^{13}C$ values from −29 to −45‰, interpreted to indicate OM fixation and/or remobilization by at least one metabolism in addition to the Calvin-Benson cycle, possibly by the Wood-Ljungdahl pathway or methanogenesis–methanotrophy.

Bontognali et al. (2012) also investigated OM trapped within layers of the stromatolites from the Strelley Pool Formation, using in situ sulfur isotope measurements of the preserved organic sulfur. $\delta^{34}S_{CDT}$ values show large fractionations at very small spatial scales, including values below −15‰ that are interpreted as recording the process of sulfurization of OM by H_2S in heterogeneous mat pore-waters influenced by respiratory S metabolism.

Radiating crystal splays

A prominent feature of the Strelley Pool Formation in many localities is the widespread development of weakly upward-radiating crystal fans, up to 50 cm long (Fig. 36), indicative of periods of evaporation under extremely shallow to exposed conditions during accumulation of the carbonate member (Van Kranendonk et al., 2003; Allwood et al., 2006; Van Kranendonk, 2011).

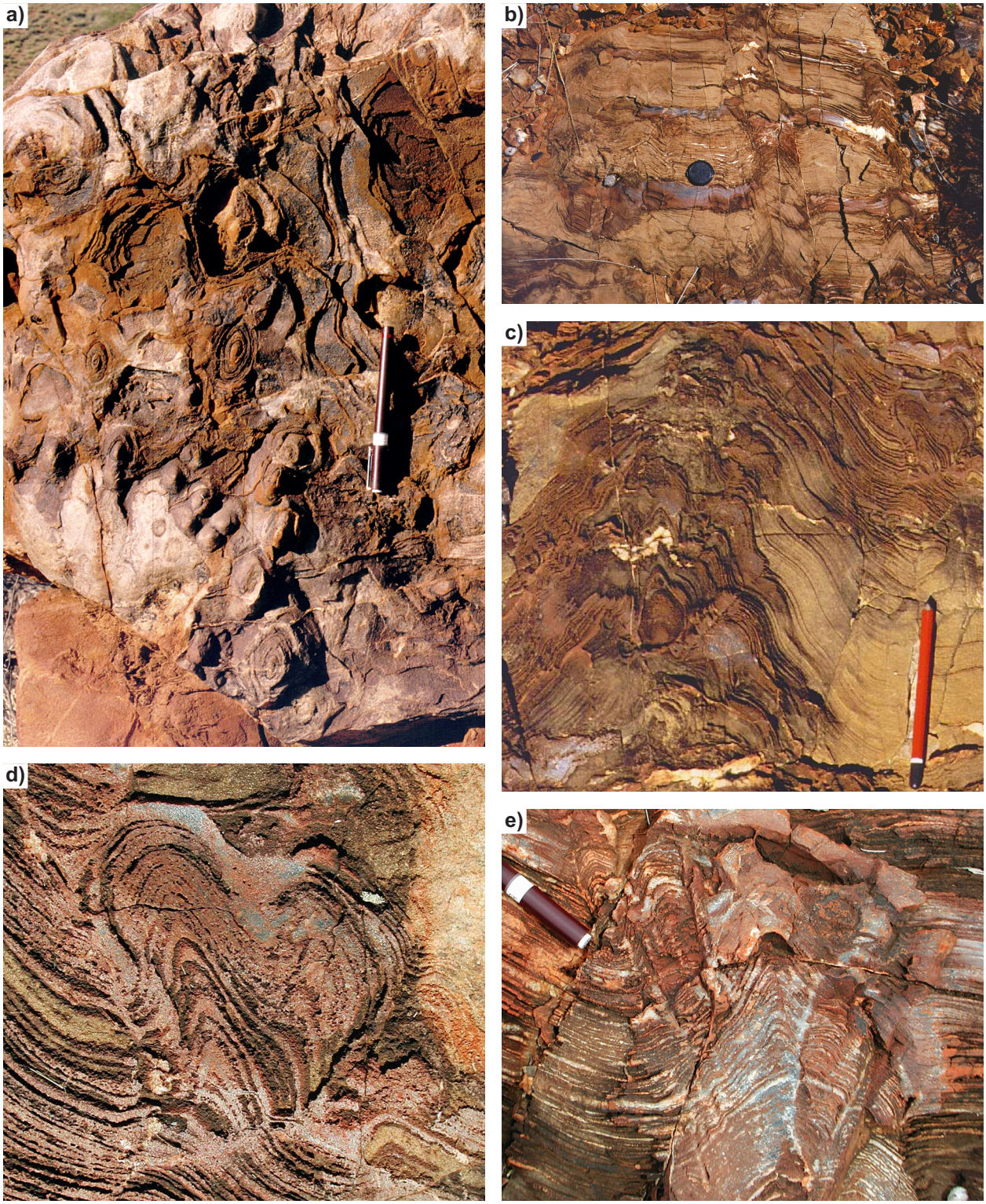

Figure 39. Outcrop views of stromatolite forms of the Strelley Pool Formation at the Trendall locality and along strike: a) bedding plane view of coniform stromatolites showing size variations and preferred elongation downdip; b) cross-section view of coniform stromatolites with >1 m of vertical inheritance and asymmetrical (short on left, long on right) limbs; c) large, incipiently branching coniform stromatolite, with doubly branched columnar stromatolite on right-hand flank; d) the 'Mickey Mouse Ears', a branched columnar stromatolite; e) incipient branching structures (just right of pen) off the top of a coniform stromatolite

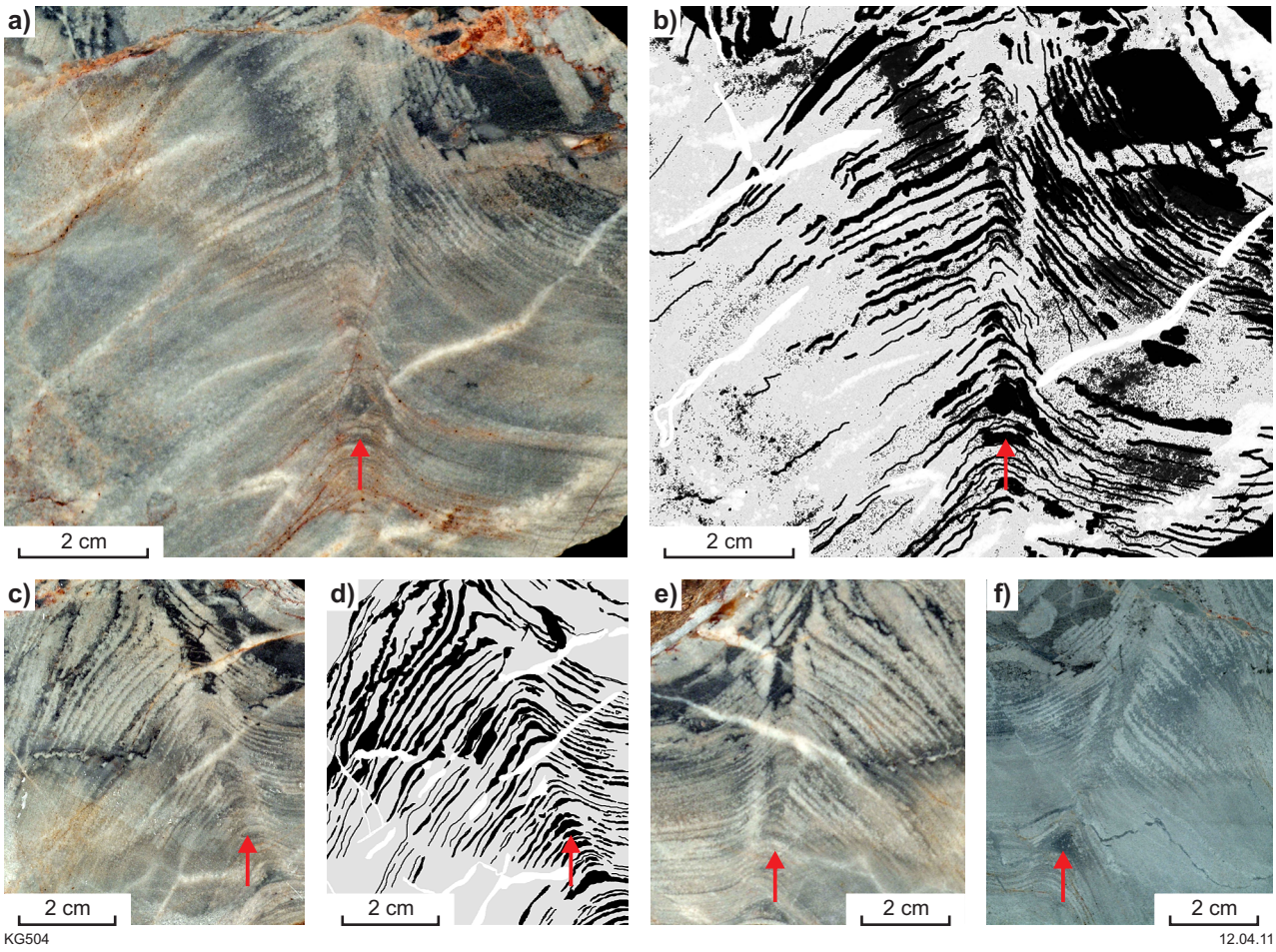

Figure 40. Cut polished axial sections (a, c, e and f), and derived line drawings (b, d) of Trendall locality coniform stromatolites, showing bulging of laminae in crestal regions. Analysis by Kath Grey, from Hickman and Van Kranendonk (2012)

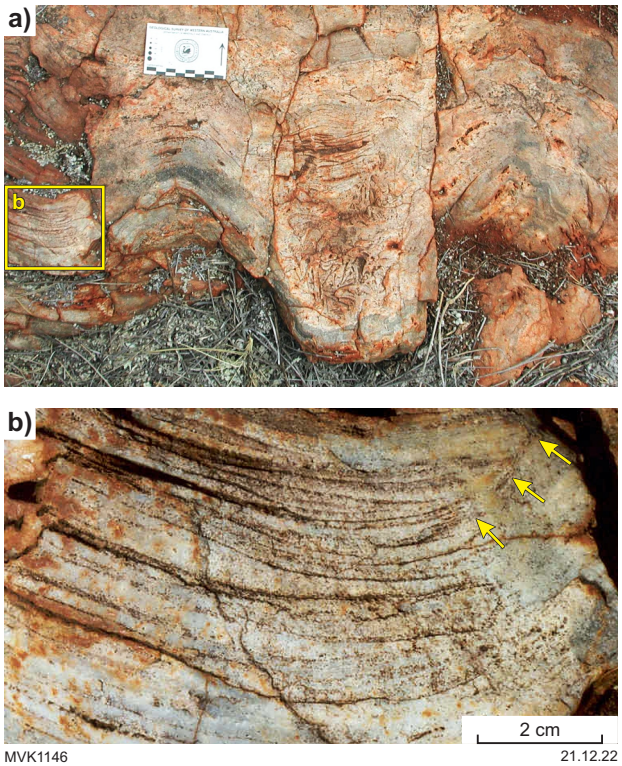

Figure 41. Views of two stromatolites at the Trendall locality: a) cross-sectional view of two large (silicified) coniform stromatolites, with edgewise conglomerate in the intervening trough. Rectangle indicates area shown enlarged in b); b) close-up view of the flank of a coniform stromatolite, showing onlap of bedded clastic sediment (arrows)

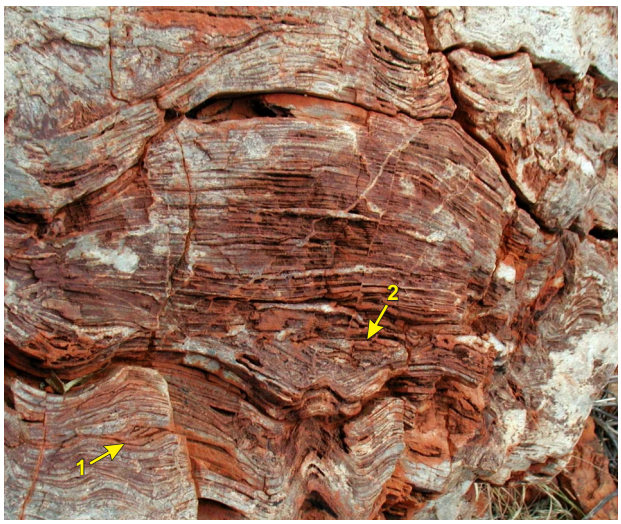

MVK1147 21.12.22

Figure 42. Large-scale swale overlying coniform stromatolite (bottom middle). Note the rippled sediment (arrow 1) adjacent to the stromatolite, and the wedge of conglomerate that directly overlies the stromatolite (arrow 2)

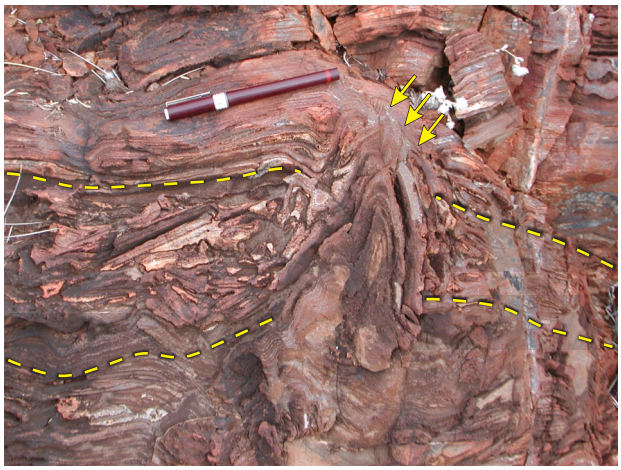

MVK1148 21.12.22

Figure 43. High-amplitude coniform stromatolite, centre, which has grown up from laminated carbonate through a conglomerate horizon (between dashed lines) and up into overlying laminated carbonate (arrows)

Two textural types of straight to weakly radiating vertical crystal splays have been recognized. One type grew across planar-bedded and stromatolitic laminites, such as those that occur throughout the lower part of the outcrop and those about halfway up the succession in the northern part of the outcrop (Fig. 44a). A second type includes the largest crystal splays, ≥50 cm long, in which no trace of bedding is evident (Fig. 44b). These include the coarse crystal splays in carbonate immediately adjacent to the black chert pebble vein that separates carbonate from siliceous laminites in the lower, southern part of the outcrop. Also included in this category are up to five sharp-bounded 'beds' of radiating crystal splays, 30 cm thick, that define a broad dome in the northern, more silicified part of the outcrop (Fig. 36). Although the original mineral species forming the crystal splays is unknown due to diagenetic carbonate alteration and silicification, preserved cross-sections of some large, silicified crystals are pseudo-hexagonal (Fig. 44c), suggesting the crystals were likely originally aragonite.

Significantly, stromatolite abundance is locally directly affected by the formation of crystal fan beds, with the latter forming a cap on the large biostromes at this locality (Fig. 36), above which stromatolite growth is much less abundant and of different morphology (small, domical forms above vs large coniform varieties below). More specific evidence of this was observed at a smaller scale in outcrop across the Shaw River, where a set of radiating crystals grew on top of a single stromatolite column and terminated its growth (Fig. 44d). This is used to argue that episodes of crystal splay growth represent periods of (at least) periodically evaporative conditions and, perhaps, subaerial exposure.

Bedded black chert

At the top of the stromatolitic carbonates is a 2–3 m-thick unit of almost massive, but in actuality thinly bedded black chert that contains a 20 cm-thick basal bed of coarse fanning crystal splays that have been replaced by white quartz (Fig. 36). In fact, this black chert unit represents a variety of rock types that have been extensively to wholly silicified by siliceous fluids that have penetrated into the rocks via a series of cross-cutting to low-angle discordant veins (Fig. 36). In small windows that have escaped complete replacement, sedimentary protoliths can be seen to include rippled carbonate sandstone and fine-grained carbonate mud.

Part of this unit is composed of laminated, very fine-grained black cherts with discontinuous white quartz layers and lenses that contain multiple layers of centimetre-high, domical, ferruginous stromatolites, as well as wind-blown crescentic ripples (Fig. 45a–c; Van Kranendonk, 2007). A comparison with modern sabkha environments suggests that the black chert units could have been organic-rich carbonate muds with evaporative gypsum crystals now represented by the layer with white quartz lenses (Van Kranendonk et al., 2021b).

Although the domical–columnar stromatolite forms of this unit display broadly isopachous laminations at outcrop scale, thin section observations show that these stromatolites display steep-sided growth walls that truncate laminae, internal discordances of laminae, and growth termination by influx of clastic sediment (Fig. 45d). These morphological features demonstrate dynamic growth within a changing environment and a compositional difference between the microbial precipitates and the sedimentary matrix, collectively supporting a biogenic origin for these structures.

Duda et al. (2016) studied these finely bedded cherts and interpreted them to have originally been microbial mats, based on their bulk carbon isotopic signature ($\delta^{13}C$ = −35.3‰), and the $\delta^{34}S$ values of abundant framboidal pyrite (= +3.05‰) that are consistent with microbial sulfate reduction. Similar cherts along strike across the Shaw River and in other greenstone belts were found to contain large, spindle-shaped microfossils (Fig. 45e; Sugitani et al., 2010, 2015a,b; Delarue et al., 2019).

Figure 44. Evaporative crystal splays from the lower part of the Trendall locality outcrop and from across the Shaw River: a) voids of eroded crystals that grew up through bedded carbonate laminate that has been silicified. From the lower part of the Trendall locality outcrop, near the Shaw River; b) long, weakly radiating crystal splays from the Trendall locality. Crystals are now composed of fine-grained dolomite; c) basal view of coarse crystals showing pseudo-hexagonal cross-section; d) small coniform stromatolite with radiating crystals growing off the crest. c) and d) are from across the Shaw River

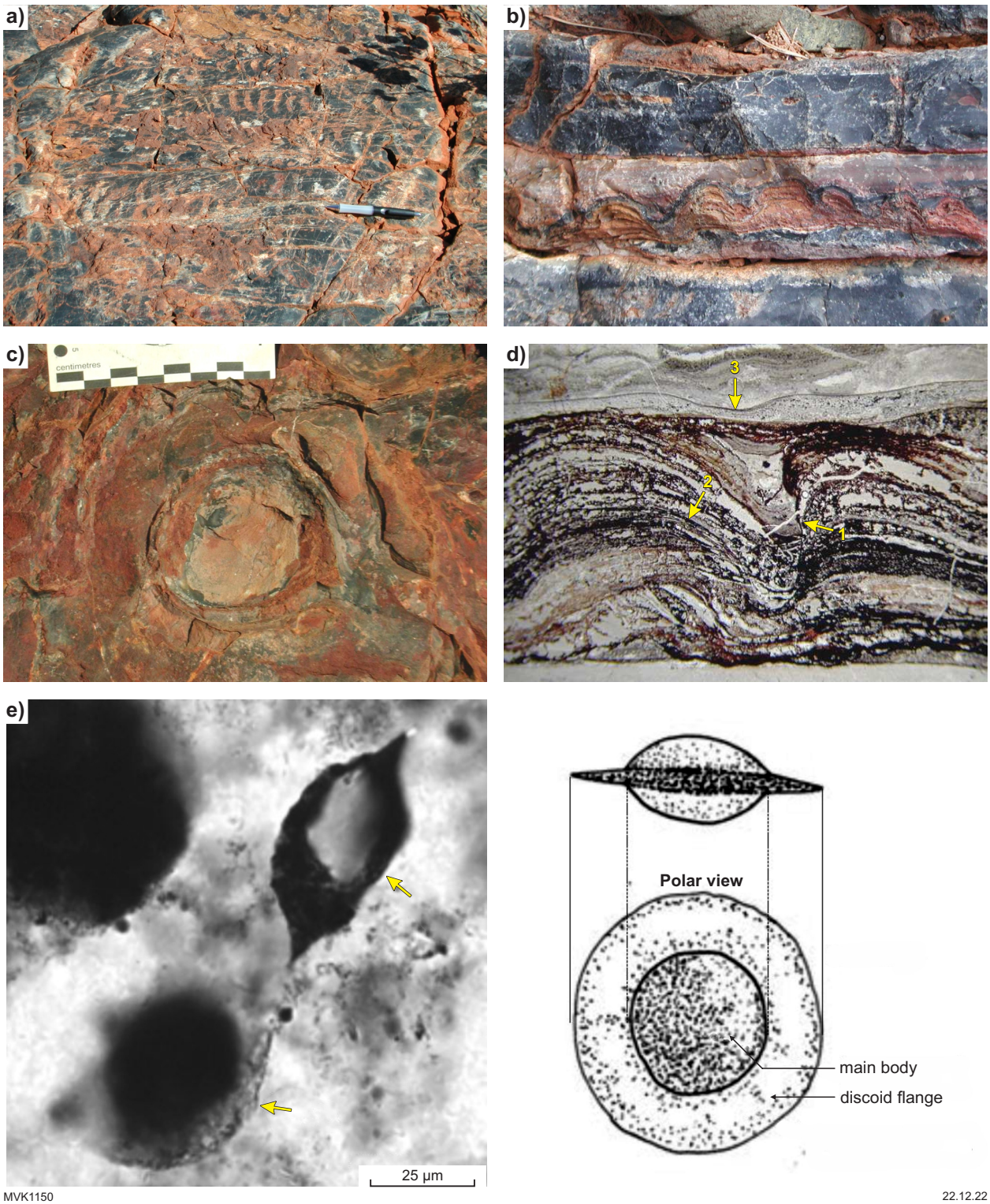

Figure 45. Features of the black chert horizon: a) crescentic windblown ripples; b) cross-sectional view of small domical stromatolites in black chert; c) top bedding plane view of small domical stromatolites in black chert; d) cross-sectional thin section view of small domical stromatolites, showing marginal growth walls (arrow 1), internal lamination (arrow 2), and overlying fine sand bed that truncates the stromatolites (arrow 3); e) plane-polarized light view (left) and interpreted sketch (right) of lenticular microfossils from the Strelley Pool Formation. From Sugitani et al. (2010). b–d) are from the Trendall locality; a) and e) from across the Shaw River

Upper clastic member

The upper clastic sedimentary member can be divided into five fining-up successions, interpreted as a series of receding alluvial fans (Fig. 36). A basal conglomerate is very coarse grained, with subrounded boulders up to 40 cm in diameter. Blocks of layered and massive blue-black chert are the dominant clast lithology, but boulders of dark-brown carbonate — some with stromatolites — are locally common, and fragments of komatiitic basalt were observed in an outcrop 250 m along strike to the south.

At the Trendall locality, the basal conglomerate fills a 6.2 m-deep channel that is bounded by normal faults lined by veins of black chert. These veins extend part-way up into, but terminate within, the conglomerate. The presence of vein chert along the channel-forming faults and the abundance of black chert clasts in the conglomerate suggest that at least some of the black chert veining was synchronous with accumulation of the formation.

Trough cross-bedding in sandstone and imbricate clasts from a conglomerate in this member indicate a palaeocurrent direction towards 132°, or towards the core of the North Pole Dome when bedding is rotated back to the horizontal. This is the opposite direction to the palaeocurrent data from the immediately underlying volcaniclastic rocks of the Panorama Formation, which are everywhere oriented pointing away from the centre of the North Pole Dome (DiMarco and Lowe, 1989).

One of the coarse sandy units part-way up in the member contains 2–5 mm-thick beds of blue-black chert with floating sand grains (Fig. 46a; thick red lines on Fig. 36). In thin section, the black chert beds are seen to consist of round, to elliptical, to wispy clasts of OM, floating sand grains, and what appear to have been gas bubbles that are suggestive of decayed OM (Fig. 46b,c; Van Kranendonk et al., 2021b).

Similar beds with clasts of OM from an outcrop across the Shaw River were studied by Marshall et al. (2007), who found — as Duda et al. (2018) did with Dresser Formation OM — that HyPy analysis of extracted bulk kerogen ($\delta^{13}C$ = −28.3 to −35.8‰) indicated that it was similar to kerogen extracted from younger rocks of known biological origin and thus likely to be of biological origin itself (Fig. 47).

Hydrothermal veins

A suite of black chert veins transects the outcrop and displays a variety of texture (Fig. 36). Whereas some are massive black chert, others are zoned with a white quartz core, sometimes with euhedral quartz crystals. Other zoned veins contain massive black chert margins and a core of pebble breccia derived through phreatomagmatic brecciation and thermal rounding of host rocks. One massive sill displays a pseudo-conglomeratic breccia texture derived from nearly in situ breakup of the country rock during chert intrusion (phreatic brecciation). Such black veins are common throughout the Pilbara Supergroup, but absent from rocks <3.2 Ga — what does this tell us about ocean/atmosphere conditions and/or tectonic processes in this type of terrain?

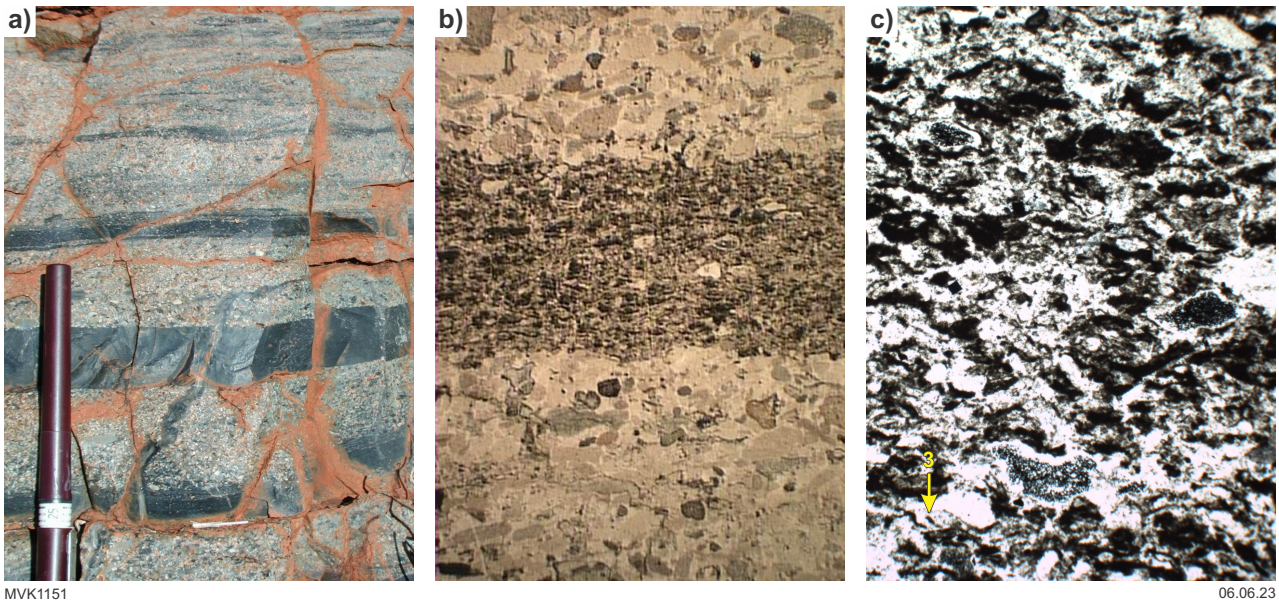

Figure 46. OM clastic beds in the upper siliciclastic member of the Trendall locality: a) OM clastic beds interbedded with coarse sandstone; b) thin section photomicrograph of an OM-rich bed, showing OM clasts with floating sand grains (bed is 1 cm thick); c) close-up photomicrograph of clastic OM with gas bubbles that are filled with silica and a fine-grained opaque material (width of view ~0.5 cm)

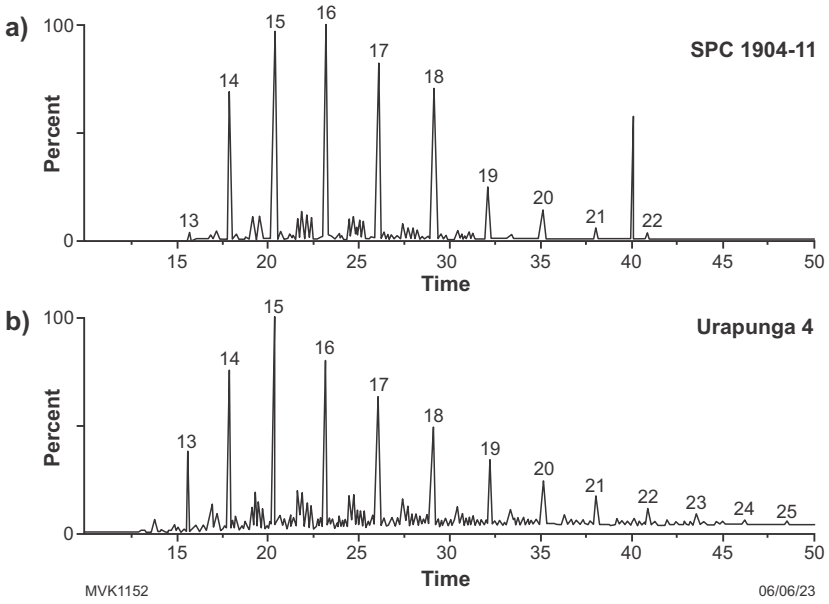

Figure 47. m/z 85 ion chromatograms for: a) Strelley Pool Formation (SPC 1904-11); b) Urapunga 4 (Mesoproterozoic) HyPy products. Chromatograms show similar distributions of *n*-alkanes and methyl-branched alkanes. Numbers 13–25 refer to the carbon chain lengths of *n*-alkanes. From Marshall et al. (2007)

Age of the Strelley Pool Formation

There is some discrepancy about the age of deposition of the Strelley Pool Formation. Van Kranendonk et al. (2002, 2007a,b, 2019b) considered it to be the basal component of the conformably overlying Kelly Group, the oldest age for which is 3350 ± 2 Ma from a felsic tuff within pillowed basalt near the base of the Euro Basalt (Nelson, 2005a), the formation that conformably overlies the Strelley Pool Formation across the East Pilbara Terrane. Allwood et al. (2006), however, interpreted the age of the Strelley Pool Formation to be significantly older, at c. 3.43 Ga, on the basis that '… the semilithified state of mudstones underlying the Strelley Pool Chert suggests a similarly short period of time passed between deposition from the mudstones (which belong to the 3.43 Ga Panorama Formation) and onset of Strelley Pool Chert deposition.' (Allwood et al., 2006 supplementary data.) This observation was made at an outcrop on the north side of the Shaw River, and the inferred age has been used in all successive works by this author and associated researchers.

Previous U–Pb studies of detrital zircons within sandstone units of the Strelley Pool Formation gave a youngest maximum depositional age of 3426 ± 10 Ma (2σ) in the Warralong Greenstone Belt (Nelson, 1998h). Recently, Gardiner et al. (2019) published detrital zircon age data from the Strelley Pool Formation, with the youngest group yielding an age of 3414 ± 34 Ma, and the youngest single, near-concordant grain at 3404 ± 7 Ma, providing the maximum age of deposition of the Strelley Pool Formation.

What has been missed in this debate is the relationship displayed at the base of the Strelley Pool Formation in outcrop on the northern side of the Shaw River, across from the Trendall locality. At this locality, there is evidence of a double unconformity, of the Strelley Pool chert on the Panorama Formation, and of the Panorama Formation on the Mount Ada Basalt (Fig. 48). This relationship, combined with regional stratigraphic relationships, clearly shows that the Strelley Pool Formation was deposited across a period of regional uplift and erosion that post-dates the youngest age of deposition of the Panorama Formation (i.e. 3427 ± 3 Ma), or the age of the youngest detrital zircon population from basal clastic rocks of the Strelley Pool Formation (3414 ± 34 Ma). Enough time must have passed after this age to develop significant doming related deformation and metamorphism, including differential regional uplift to develop an unconformity that cuts down to the lowest component of the stratigraphy — the 3515 Ma Coonterunah Subgroup of the Warrawoona Group.

Furthermore, the relationship of the Strelley Pool Formation to the overlying units clearly demonstrates that it was deposited as part of a single basin-deepening event linked to the Kelly Group. This commenced with deposition under subaerial (fluvial) to rocky shoreline conditions (basal clastic member 1 of the Strelley Pool Formation; Van Kranendonk, 2000, 2006; Allwood et al., 2006), continued through a shallow marine shelf (stromatolitic carbonates of Strelley Pool Formation member 2), and then via a period of rapid basin subsidence (clastic member 4 of the Strelley Pool Formation), to deep basin extension accompanied by the eruption of thick pillow basalts (Euro Basalt). As basin subsidence progresses rapidly once initiated, the best estimate for this basin-deepening event is given by the 3350 ± 2 Ma age of the felsic tuff near the base of the Euro Basalt.

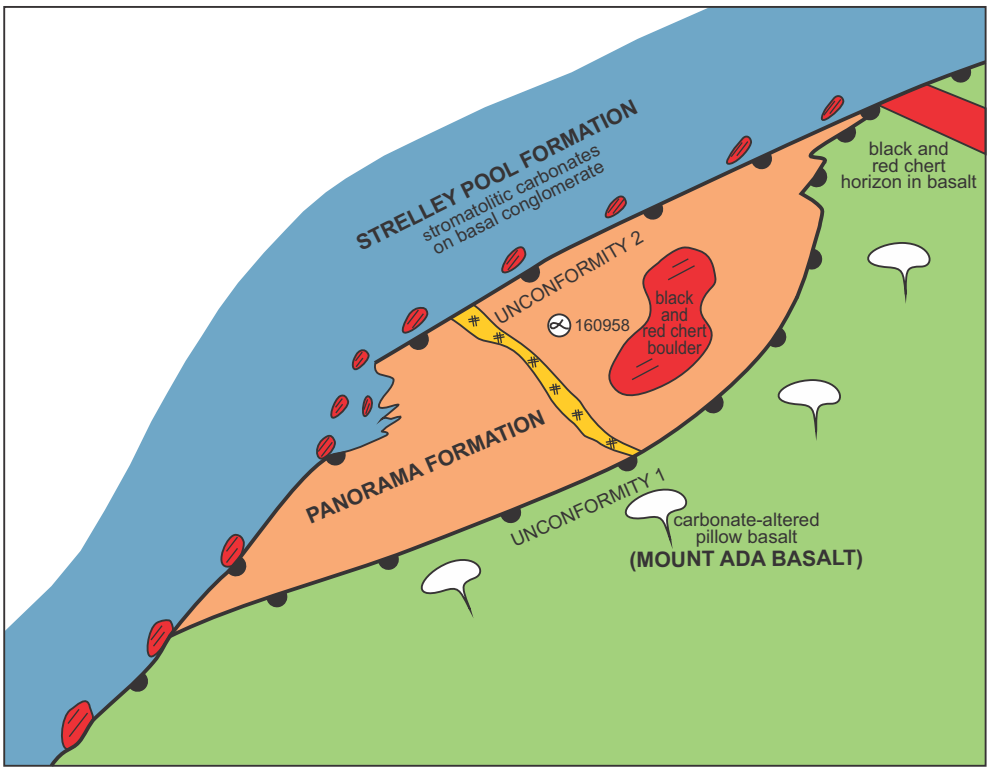

Figure 48. Geological sketch map of the double unconformity at the base of the Strelley Pool Formation on the north bank of the Shaw River, across from the Trendall locality. From Hickman and Van Kranendonk (2012). Note the location of the detrital zircon sample, which yielded a youngest population at 3430 Ma, which is here interpreted as the age of the Panorama Formation tuffaceous sandstone

Day 3: The 'Marble Bar' and Warrawoona Syncline

A remarkable feature of the Marble Bar greenstone belt is the transition in strain state along strike north to south, with a change from essentially undeformed rocks in the north across the main part of the belt, to penetratively deformed and highly transposed schists to the south and southeast into the Warrawoona Syncline. This change in strain state is accompanied by a dramatic structural thinning of the lithostratigraphy, from at least 12 km thick where it is little deformed north of the town of Marble Bar, to less than 1 km thick in the core of the Warrawoona Syncline, although the excision of stratigraphy in the syncline is also partly achieved by intrusion of c. 3300 Ma granitic rocks in both the Mount Edgar and Corunna Downs Granitoid Complexes (Fig. 49).

As the rocks become more intensely transposed from west to east into the core of the Warrawoona Syncline, metamorphic foliations are accompanied by the progressive development of mineral elongation lineations that gradually change orientation from moderately east plunging, to vertical in the core of the syncline, and moderately west plunging on the eastern side of the syncline (Fig. 50; Collins, 1989; Teyssier and Collins, 1990). Teyssier and Collins (1990) showed that in combination with the steepening of the lineations, fabric shape elements changed from S>L, to L>>S, to pure L-tectonites in a 'zone of sinking' (Fig. 50a,b), identical to the geometry predicted by centrifuge models of diapirs (Fig. 50c,d; Dixon and Summers, 1983). Collins et al. (1998) summarized this data and used it in support of partial crustal overturn, the high-grade part of which was interpreted from previous geochronology to have occurred at c. 3300 Ma (Williams and Collins, 1990). Additional structural evidence in support of partial crustal overturn was provided by Hickman and Van Kranendonk (2004) and Van Kranendonk et al. (2004). No other mechanism has been proposed to explain these fabric elements, and they cannot be explained by cross-folding as suggested by Blewett (2002) due to an absence of upright axial planar fabrics in the domes (see Van Kranendonk et al., 2004).

The Klondyke Shear Zone, just north of the axis of the Warrawoona Syncline, is a ring fault close to the southwestern margin of the Mount Edgar Dome, but mapping has shown it to terminate along the Salgash Fault, a scissor fault with east-side-up displacement (Fig. 49). The shear zone is host to numerous gold deposits mined at the turn of the last century, and similar mineralized shear zones are present in other greenstone belts of the East Pilbara Terrane.

There is a wedge of kyanite-bearing (Duffer Formation) schists in between the shear zone splays developed along the margin of the Mount Edgar Granitic Complex. Pressure–temperature estimates of 5.5 – 6 kbar and 500–600 °C have been obtained from the schists and associated metabasites (Delor et al., 1991) that indicate initial burial to depths of about 25 km. Collins and Van Kranendonk (1999) showed that these deeply buried rocks were exhumed within the kyanite stability field, and that this was consistent with heating along the side of a rising diapir as indicated by numerical modelling (Mareschal and West, 1980; Warren and Ellis, 1996).

Locality 3.1: Transect across the upper contact of the Duffer Formation to the Marble Bar Chert Member at Marble Bar Pool (Zone 50, MGA 781600E 7655700N)

Note: This locality falls within the Marble Bar and Chinaman Pool State Geoheritage Site (Geosite 74). The location is also within a State Class A Reserve (R24096). Hammering, sample collection, camping and driving off pre-existing tracks is strictly not permitted within the bounds of this Reserve.

More information on the location and significance of localities on the Register of State Geoheritage Sites can be accessed via GeoVIEW, GSWA's online mapping platform; more general information on geoheritage and the Reserve permitting system can be found on the DMIRS website.

Note that the export of geological material out of Australia, particularly fossils and meteorites, is strictly controlled by the Federal Protection of Cultural Moveable Heritage Act 1986*. Approval is required from the Federal Office of the Arts for the permanent export of Class B objects.*

This traverse along the east bank of the Coongan River starts in felsic agglomerate or volcaniclastic conglomerate (or both) at the upper contact of the c. 3.47 Ga Duffer Formation (Locality 3.1a on Fig. 51). The rock dominantly consists of angular to subangular boulders to cobbles of porphyritic dacite in a fine-grained dacitic matrix, but also includes scattered, rounded clasts of bedded jaspilitic chert. As you wander over the outcrop here, notice crude bedding in some packages that is locally at a distinct angle to bedding in adjacent packages, suggesting large-scale slumping. Note also the stream polish on upper horizontal surfaces caused by flooding events of the Coongan River.

Heading upstream to Locality 3.1b, we reach the contact between felsic volcaniclastic rocks and the discontinuous unit, about 3 m thick, of centimetre-layered blue, white and red chert of the Chinaman Pool Chert Member of the Duffer Formation. Both of these rocks are cut by dolerite sills that have sheared margins. The chert dips 80° towards the east-northeast and, as seen from pillow structures in overlying basalt, is overturned.

Immediately overlying the Chinaman Creek Chert Member is a unit of massive ultramafic rock (Locality 3.1c) with pseudo-pillow structure, the origin of which is interpreted to relate to alteration during metamorphic recrystallization. Internally, the texture is that of an olivine orthocumulate, but all olivine has been replaced by a mixture of serpentine, white mica and carbonate, and these lie within an altered matrix containing chlorite (Fig. 52).

Continuing up-section, you will pass through a unit of pillowed, variolitic komatiitic basalt (Locality 3.1d) that has well-preserved textures, including small vesicles around pillow margins, crackle rinds, interpillow hyaloclastite, and way-up structures from pillow tops and tails, despite minor to moderate flattening. The pillows are slightly overturned and dip to the east-northeast, but face west. Pillows here show distinctive ocellar structure (Fig. 53), whose origin is debated — is it due to primary liquid immiscibility (unmixing) of silicate fractions (e.g. Ferguson and Currie, 1972), hydrous melting of crustal xenoliths (e.g. Appel et al., 2009), devitrification, or H_2O saturation in basaltic melts (Ballhaus et al., 2015)?

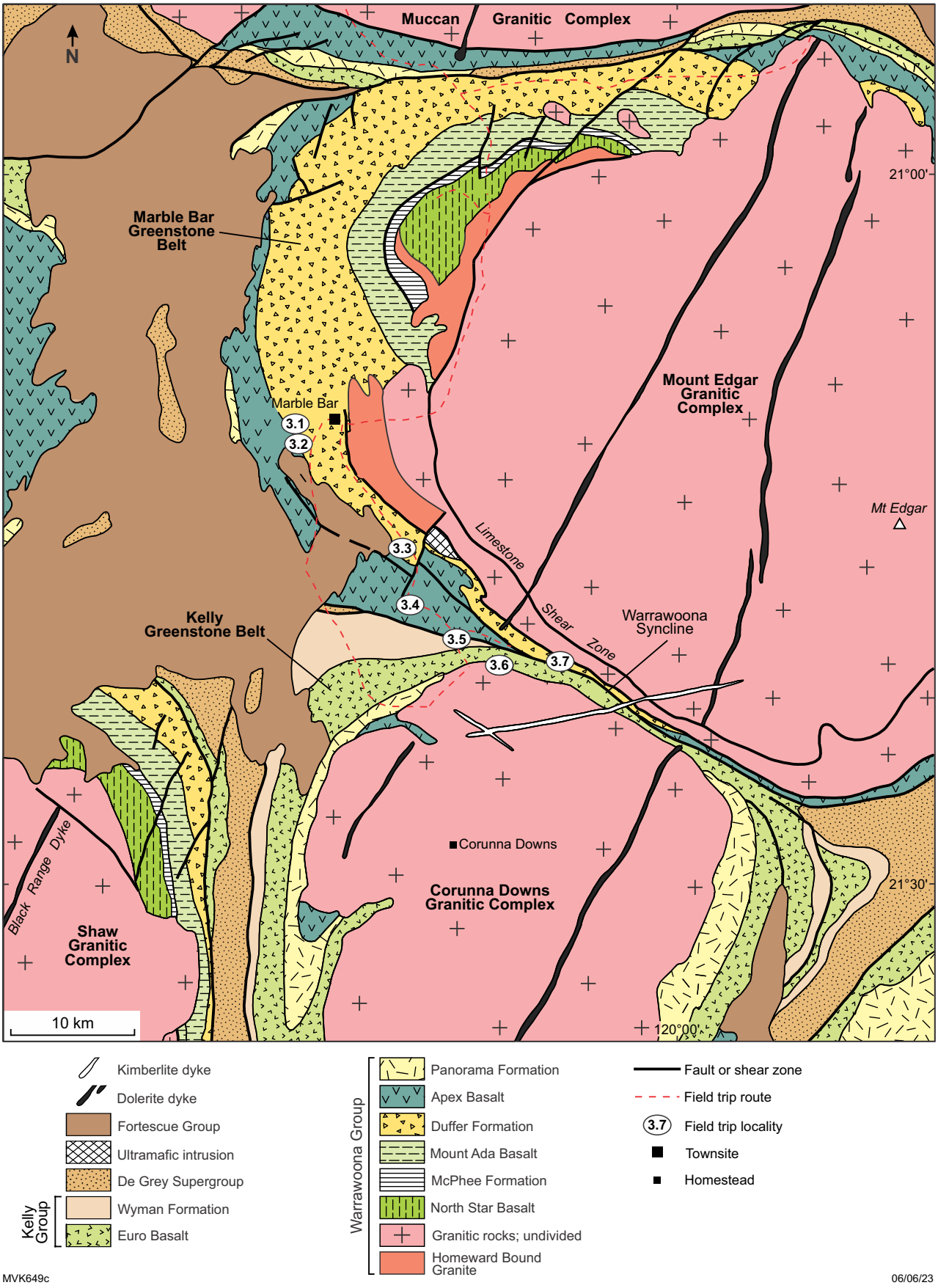

Figure 49. Geological map of the Marble Bar area, showing excursion localities of Day 3

Continuing south, the pillows become increasingly altered, with bleached pillow rinds and gas cavities in pillows filled by carbonate and quartz. At the southern end of the platform is a thick, almost undeformed, dolerite sill.

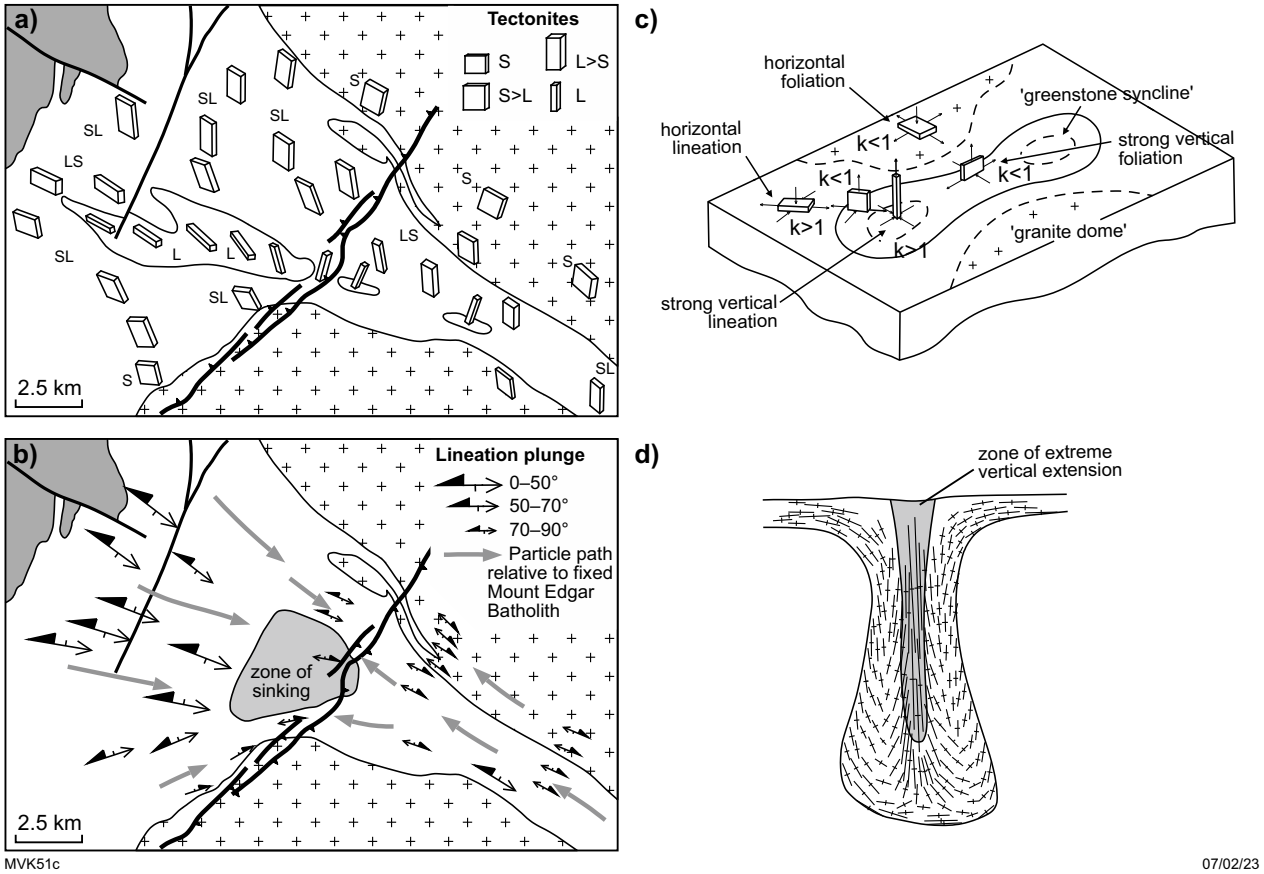

Figure 50. Strain patterns across the margin of Mount Edgar Granitic Complex and Warrawoona Syncline: a) strain pattern variation. L = lineation, S = schistosity (flattening component); b) lineation pattern showing convergence towards a central point along the synclinal axis; c) variation in strain across a modelled diapiric syncline. k = index of the relative prolateness or oblateness of the local strain ellipsoid. Note the similarity of the modelled strain relative to that in the Warrawoona Syncline shown in a); d) cross-sectional profile showing a zone of extreme vertical extension in the core of a modelled diapiric syncline. a) and b) after Teyssier and Collins (1990); c) and d) modified from Dixon and Summers (1983)

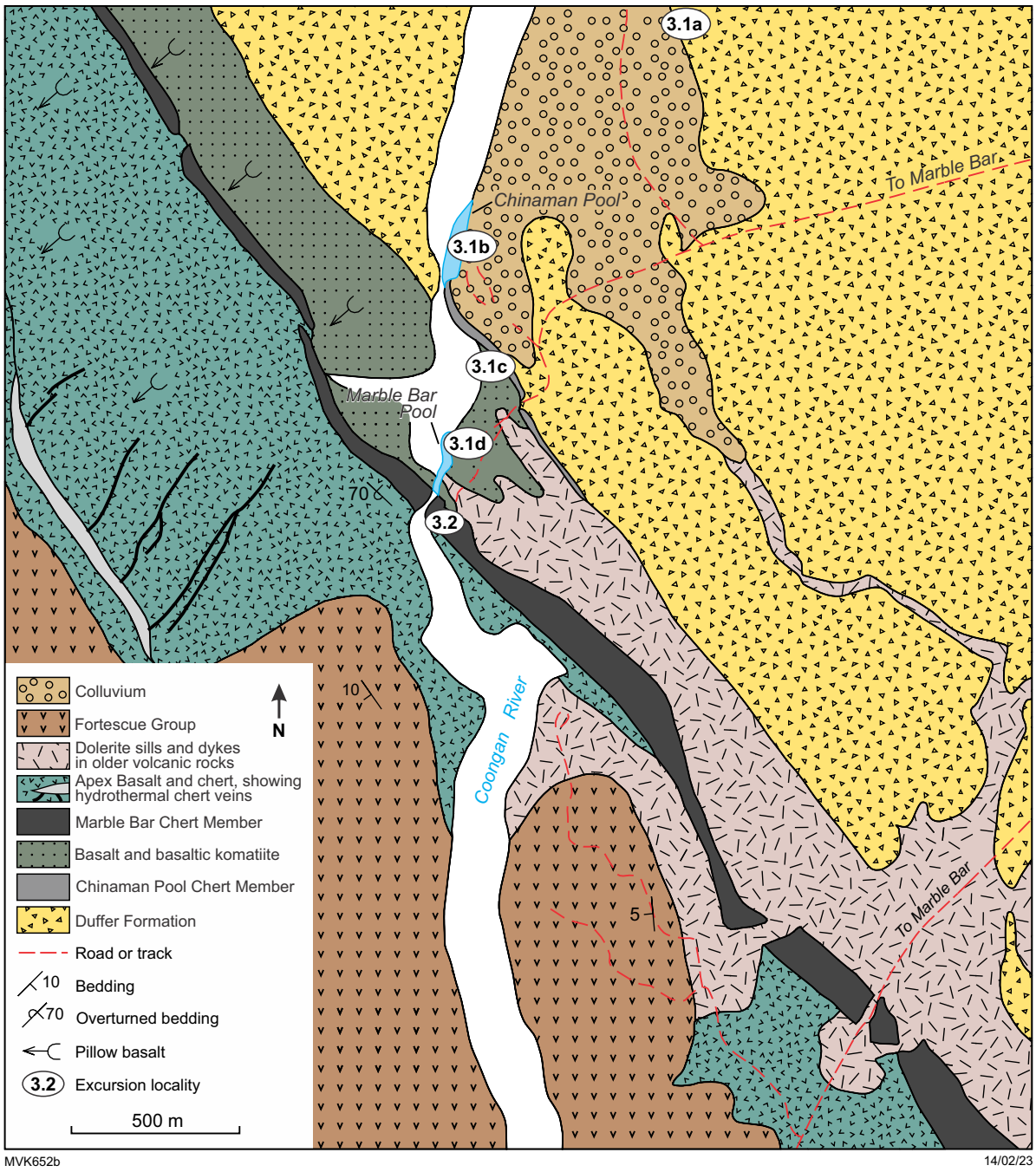

Figure 51. Geological map of the Marble Bar Chert Member at Marble Bar Pool, showing excursion localities commencing in Duffer Formation felsic volcanics, across the Chinaman Pool Chert Member, and extending across pillowed komatiitic basalts up into the Marble Bar Chert Member

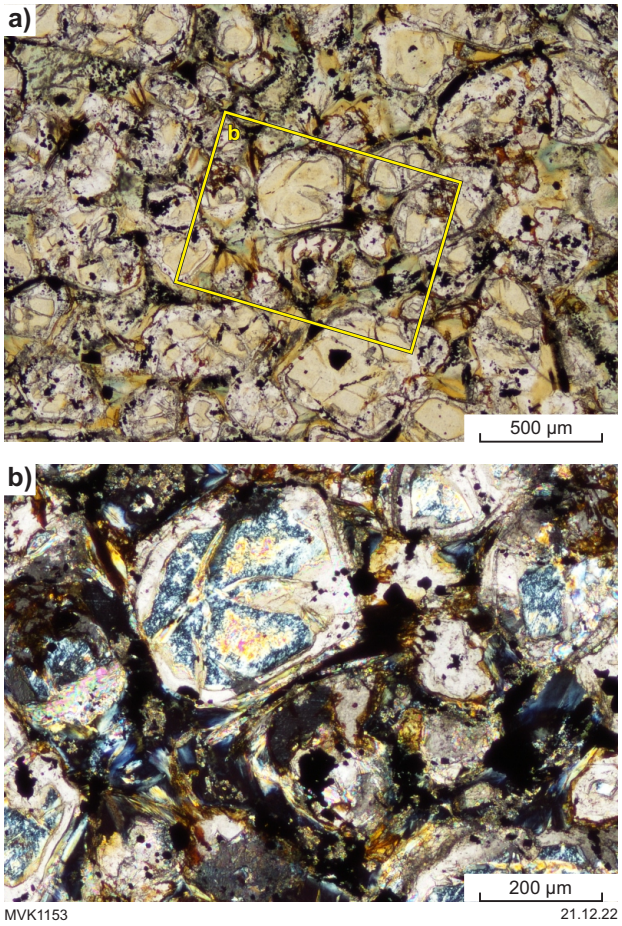

Figure 52. Thin section photomicrographs of olivine orthocumulate texture at the base of the flow that immediately overlies the Chinaman Pool Chert Member and that displays pseudo-pillow structure in outcrop: a) in plane-polarized light; b) in cross-polarized light. Note that the primary mineralogy is completely replaced by a mosaic of serpentine, carbonate, white mica and chlorite

Figure 53. Outcrop of ocellar-textured komatiitic basalt at Locality 3.1d in Figure 51

Locality 3.2: Marble Bar Chert Member at Marble Bar Pool (Zone 50, MGA 781500E 7654800N)

Across the parking lot at Marble Bar Pool is the well-known, water-polished outcrop of blue, white and red layered chert known as 'The Marble Bar', forming a bar across the Coongan River.

Note: This locality falls within the Marble Bar and Chinaman Pool State Geoheritage Site (Geosite 74). The location is also within a State Class A Reserve (R24096). Hammering, sample collection, camping and driving off pre-existing tracks is strictly not permitted within the bounds of this Reserve.

More information on the location and significance of localities on the Register of State Geoheritage Sites can be accessed via GeoVIEW, GSWA's online mapping platform; more general information on geoheritage and the Reserve permitting system can be found on the DMIRS website.

Note that the export of geological material out of Australia, particularly fossils and meteorites, is strictly controlled by the Federal Protection of Cultural Moveable Heritage Act 1986. *Approval is required from the Federal Office of the Arts for the permanent export of Class B objects.*

Formally named the Marble Bar Chert Member, this spectacular unit is here composed of three distinct colour varieties that are interlayered at a centimetre to decimetre scale: thinly bedded jasper, milky white chert, and blue-black chert (Fig. 54). Jasper is only present in the top third of the unit, whereas several hundred metres along strike (and more broadly across the East Pilbara Terrane) thinly bedded jasper comprises nearly all of the member and hydrothermal veining is less prevalent. The lower parts of the chert at this locality are composed of white and blue-black chert, commonly with highly disrupted layering, and all of it transected by hydrothermal veins of white, grey and black chert (Fig. 55).

Figure 54. Outcrop view of the top, jaspilitic, part of the Marble Bar Chert Member against a flooded Coongan River

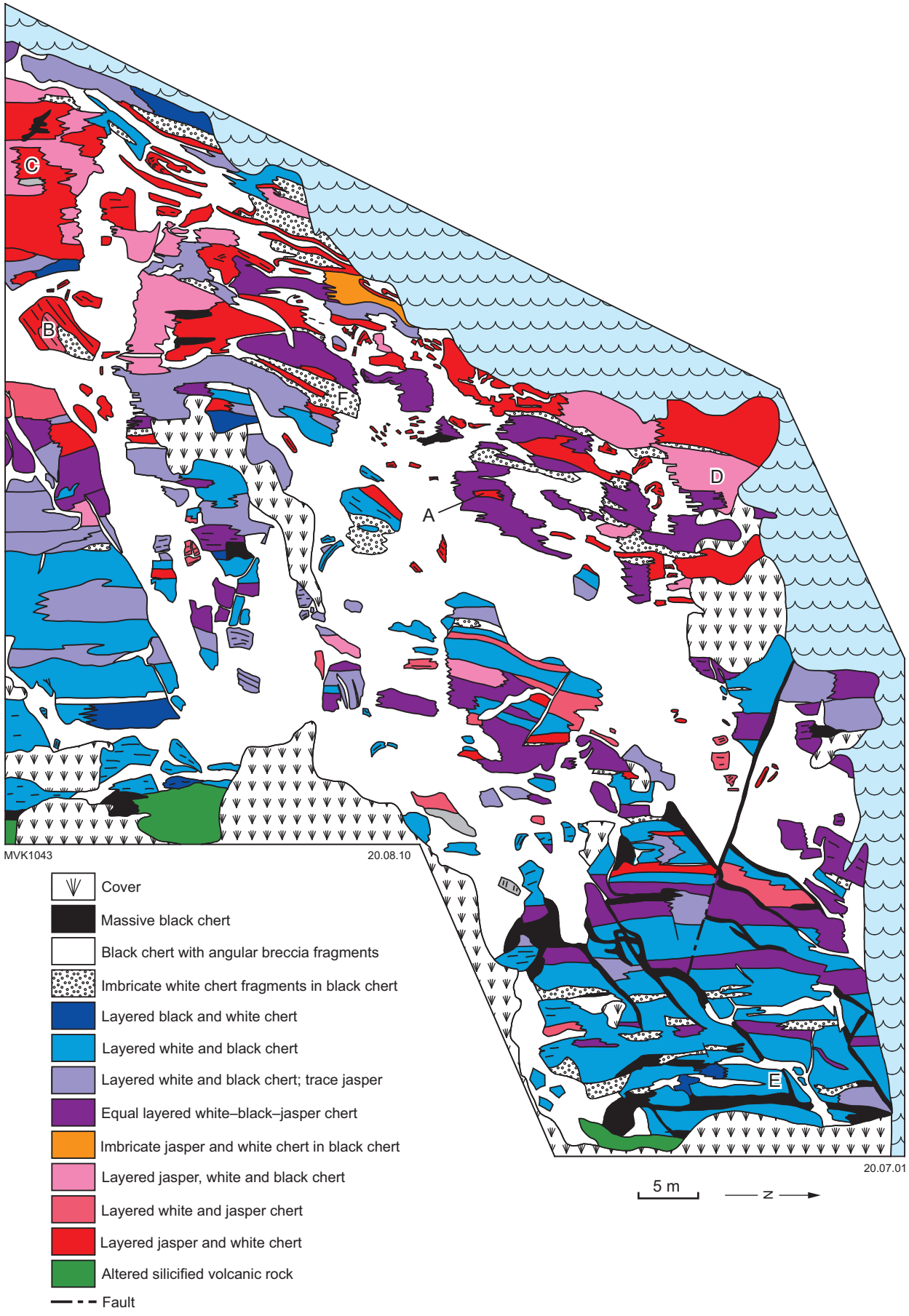

Figure 55. Geological map of the Marble Bar Chert Member on the east bank of Marble Bar Pool, from Van Kranendonk (2006). Note the increase in jasper to the top of the unit and the way that the colour variations change laterally along strike of bedding. See text for discussion of features

Jasper is bedded at a millimetre scale, defined by slight changes in colour and the degree of faint granularity. The fine layering of the jasper indicates deposition under quiet water conditions and the presence of pillowed basalts above and below suggests that this was probably in a deep marine setting.

At the basal contact of the chert, altered massive volcanic rocks are cut by an anastomosing network of weakly folded, massive blue-black chert veins (Fig. 56a). Near the basal contact of the chert, the veins contain numerous fragments of the country rock, many with a jigsaw-fit, consistent with phreatic brecciation during instantaneous, explosive boiling of hydrothermal fluids. Some of these veins extend up into the layered chert as breccia veins (Fig. 56b), some of which become quite large, up to 12.5 m wide. The white chert forms centimetre-thick layers spaced at irregular intervals through the jasper, although it is not bedded. Characteristically, the white chert forms lenses in the jasper, often with pinch-and-swell structures and, in many places, it may be observed that bedded jasper strikes directly into, and is replaced by, white chert (Fig. 55), much of which can be seen to emanate sideways from white to grey chert veins (Fig. 56c; Van Kranendonk, 2006).

In places, the white chert is clearly intrusive into the red jasper chert, but elsewhere clearly represents the product of an in situ chemical replacement of the jasper chert (Fig. 56d; Van Kranendonk, 2006). Bedding-subparallel breccia horizons in the layered white and jasper chert are composed of elongate, angular fragments of white chert within a homogeneous matrix of remobilized, homogeneous jasper or blue-grey chert. Detailed mapping shows that these horizons emanate out from discordant chert veins (Fig. 55) and thus represent the products of silica-saturated fluids emplaced into the chert under high fluid pressures, rather than primary sedimentary deposits.

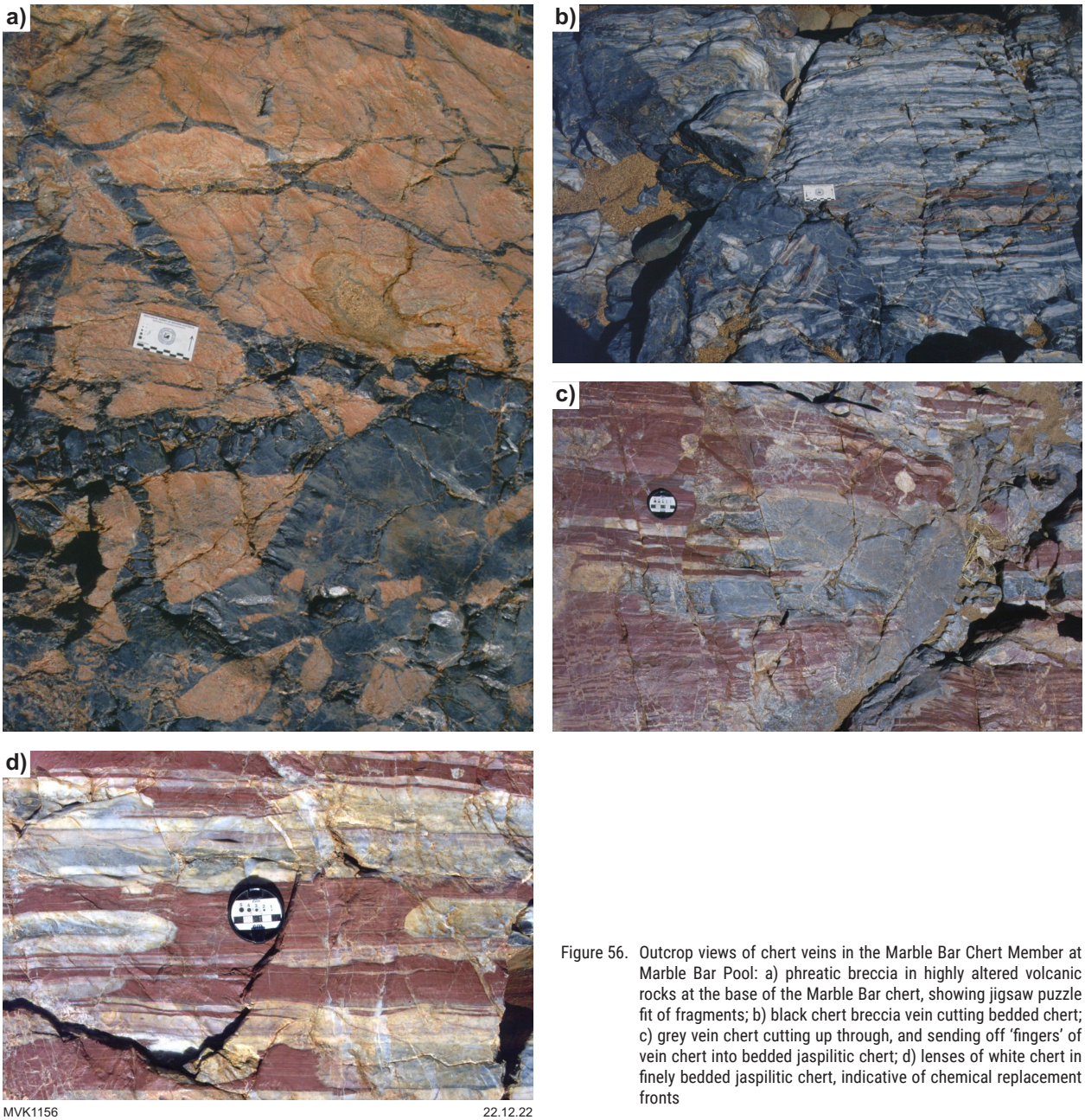

Figure 56. Outcrop views of chert veins in the Marble Bar Chert Member at Marble Bar Pool: a) phreatic breccia in highly altered volcanic rocks at the base of the Marble Bar chert, showing jigsaw puzzle fit of fragments; b) black chert breccia vein cutting bedded chert; c) grey vein chert cutting up through, and sending off 'fingers' of vein chert into bedded jaspilitic chert; d) lenses of white chert in finely bedded jaspilitic chert, indicative of chemical replacement fronts

Rasmussen et al. (2014) provided a high-resolution investigation of the jaspilitic layers of the Marble Bar Chert Member and concluded that the hematite was secondary and replaced primary iron-rich clays. In contrast, Li et al. (2013) studied jaspilite samples of the Marble Bar chert and showed that they have extreme heavy Fe isotope enrichment ($\delta^{56}Fe$ = +1.5‰ to +2.6‰). This range requires very low levels of oxidation in a Paleoarchean ocean that had high aqueous Fe(II) contents and indicates that the hematite did not form through recrystallization of siderite and that it formed from direct precipitation from hydrothermal fluids. U–Th–Pb isotope systematics of the same samples show that U contents in the Paleoarchean ocean were likely below 0.02 ppb, two orders of magnitude lower than the modern ocean. Collectively, the Fe and U data from this study indicate a reduced, Fe(II)-rich, U-poor Archean ocean likely inhabited by anoxygenic photosynthetic Fe(II) oxidizing microbes.

The top contact of the Marble Bar Chert Member is directly overlain by beautifully preserved pillowed basalt of the Apex Basalt. Pillows commonly contain one or multiple pillow shelves. No chert veins extend up through the chert into the pillow basalt, indicating that deposition of the basalt occurred ***after*** chert veining.

Part of the outcrop of Apex Basalt here contains conspicuous hematite alteration, which Hoashi et al. (2009) attributed to sea floor alteration in an oxygenated ocean. Subsequent U–Th–Pb isotope data, however, proved that the hematite formed through oxidation during the Phanerozoic (Li et al., 2012, 2013).

Locality 3.3: Stretched clasts in the upper Duffer Formation (Zone 50, MGA 789934E 7645932N)

This locality is the first of three excursion stops selected to show structural evidence, visible at outcrop scale, demonstrating that vertical tectonic processes (diapiric deformation) was primarily responsible for the regional dome-and-basin pattern seen in the East Pilbara Terrane (Hickman and Van Kranendonk, 2004; Van Kranendonk et al., 2004). Alternative models have attempted to explain the structural evolution of the terrane using Phanerozoic-style horizontal tectonic processes (Bickle et al., 1980, 1985, 1993; Boulter et al., 1987; Barley, 1993, 1997; Zegers et al., 1996, 2001; van Haaften and White, 1998; Kloppenburg et al., 2001; Blewett, 2002). These models differ in detail, but most include suggestions of Alpine-style thrusting at 3450 and 3300 Ma and subsequent periods of major regional extension during which the granitic domes formed as metamorphic core complexes. However, models of horizontal tectonics and core complex formation have been refuted for the reasons given in Van Kranendonk et al. (2004).

This locality shows small-scale structures within rhyolitic schist near the top of the Duffer Formation. At Marble Bar, the Duffer Formation is not strongly sheared and is approximately 8 km thick. Here, on the northern limb of the Warrawoona Syncline, the formation is both tectonically attenuated and intruded by the 3466 Ma Homeward Bound Granite, and as a result is only 1.8 km thick. Note that the felsic volcanic rocks of this area are strongly schistose (Fig. 57a). The schistosity is part of the steeply inclined to vertical tectonic foliation that rims the 50-km diameter granitic core of the Mount Edgar Dome. Sense of shear movement, demonstrated by changes in metamorphic grade and shear fabrics, is granite side up. At this locality, on the southwestern flank of the dome, the dominant foliation dips 80° towards 225°. The main foliation in the schists is locally axial planar to tight to isoclinal folds defined by layers of altered mafic rocks. Regional evidence indicates that the major deformation in this area occurred at c. 3.31 Ga (Williams and Collins, 1990).

The schist is a metamorphosed rhyolitic volcaniclastic rock containing clasts of vein quartz, felsic volcanic rock and chert. These clasts are stretched, with the long axis plunging 60° towards 115° (Fig. 57b). The same elongation direction is repeated at other localities on the northern limb of the syncline. Locality 3.4 shows stretching lineations with a similar southeasterly plunge. Eastwards from Locality 3.4, the stretching fabrics steepen to be almost vertical in the more highly deformed and deeper axial region of the syncline at Locality 3.5. The orientation of stretching is normal to the general plunge of the Warrawoona Syncline, and consistent with sinking of the greenstone succession relative to the adjacent granitic rocks in the Mount Edgar Dome (Collins, 1989; Collins et al., 1998). In detail, however, various minor folds within the northern limb of the Warrawoona Syncline plunge southeast as well as northwest indicating primary noncylindricality or superposed folding. Shear intensity in the greenstones varies with lithology and proximity to ring faults, but there is a general trend of increasing shear into the centre of the syncline, and into deeper structural levels of the syncline (east-southeastwards). The east-southeast plunging elongation of the clasts at Localities 3.3 and 3.4 is consistent with the diapiric model for development of the Warrawoona Syncline (Hickman, 1975, 1983, 1984; Collins, 1989; Collins et al., 1998), but is far less easily reconciled with the regional unidirectional southwest–northeast extension and stretching that is essential to the metamorphic core complex model (Kloppenburg et al., 2001).

Other significant features at this locality include the presence of secondary chert units along silicified shear zones in the felsic shists, and the observation that on the top of the ridge, a few hundred metres to the west of this locality, the Duffer Formation is separated from the Apex Basalt by only a few metres of ferruginous and grey and white layered chert (MGA 789709E 7645873N). This chert is at the same stratigraphic level as the Marble Bar Chert Member at Locality 3.2, but it is very much thinner and different in appearance. It is impossible to map lateral facies changes in the Marble Bar Chert Member over most of the 12 km in the Marble Bar greenstone belt due to the member being concealed by basalt of the Fortescue Group. However, it is clear that the Marble Bar Chert Member is not everywhere laterally continuous, but instead forms lenticular deposits at this stratigraphic level, the distribution of the lenses probably depending on local hydrothermal activity.

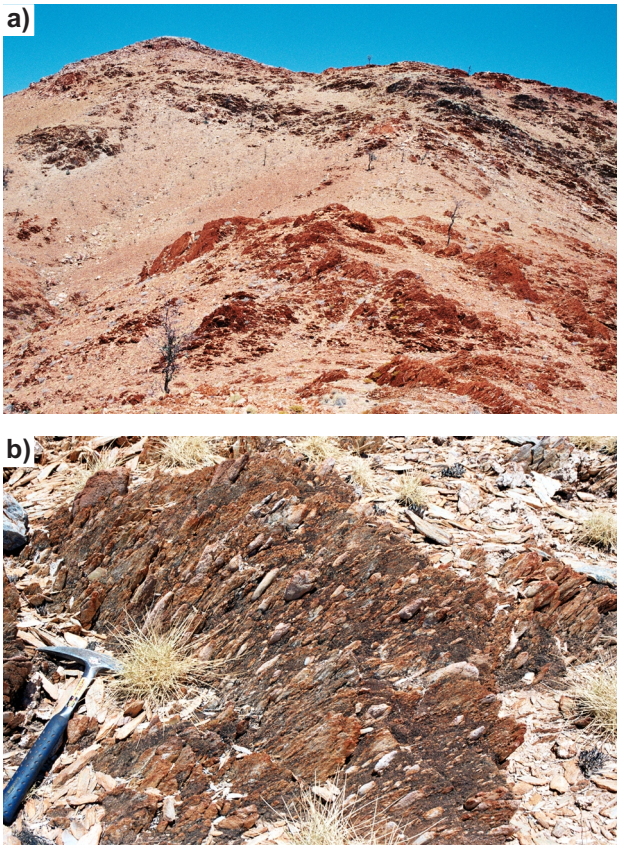

Figure 57. The upper Duffer Formation: a) view of the upper Duffer Formation at Locality 3.3; b) stretched clasts in volcaniclastic Duffer Formation. Photographs by AH Hickman

Figure 58. Outcrop views of lensoid quartz veins filling tension gashes: a) view, looking south, at a series of lensoid quartz veins filling tension gashes in ultramafic schists, indicating extension towards the zone of sinking that is located further to the east; b) strongly vertically lineated (pure shear) silicified rocks in the zone of sinking between the Mount Edgar and Corunna Downs Granitoid Complexes, in the middle of the Warrawoona Syncline

Locality 3.4: Shallow–moderate east-plunging lineations pointing towards the zone of sinking in the Warrawoona Syncline (Zone 50, MGA 790500E 7642205N)

The steep hill on the south side of the track contains a thin chert unit in metamorphosed schistose metabasalts. The rocks show well-developed elongation lineations plunging moderately to the east-southeast, parallel in trend to the axis of the Warrawoona Syncline and plunging towards the zone of vertical L-tectonites in the centre of the zone of sinking farther along strike to the east (see Locality 3.5; Collins, 1989; Collins et al., 1998). Note that at the top of the hill is a set of en echelon quartz veins in tension gashes that are oriented perpendicular to the lineation direction (Fig. 58a); these are interpreted as having formed during a late component of the stretching during sinking of the greenstones.

Locality 3.5: Zone of sinking vertical L-tectonites in the core of the Warrawoona Syncline (Zone 50, MGA 793940E 7640299N)

This locality is in the core of the Warrawoona Syncline in the centre of the zone of sinking of the greenstones (Fig. 50) and is less than 200 m south of the axial shear zone that separates the Mount Edgar and Corunna Downs granitic domes. This axial shear zone (which also marks the boundary between the Marble Bar and Kelly greenstone belts) excises at least 7 km of stratigraphy between the Apex Basalt and the top of the Wyman Formation. West of this locality, it is intruded by peridotite of the 3.18 Ga Dalton Suite. The rocks at this locality are characterized by vertical L-tectonite fabrics in silicified felsic tuffaceous rocks of the 3.32 Ga Wyman Formation (Fig. 58b). Although cleavages are visible cutting relict, highly transposed (millimetre-scale) bedding in the chert, the cleavages are in all directions and reflect equal compression from all directions during vertical stretching of the rock into the zone of sinking.

Once established, this post-3.32 Ga zone in the core of the syncline was reactivated during regional extension at 3.18 Ga (Dalton Suite), and very probably again after 3.02 Ga during renewed doming. Metasandstone and pelite of either the 3.2 Ga Soanesville Group or the 3.02 Ga Gorge Creek Group are displaced by later movement along the shear zone 10 km west of this locality.

Locality 3.6: Intrusive contact of the northern margin of the Corunna Downs Granitoid Complex (Zone 50, MGA 796611E 7636935N)

Outcrops of almost undeformed coarse-grained monzogranite here are characteristic of much of the Corunna Downs Granitoid Complex and have been dated in several places at c. 3310 Ma (Barley and Pickard, 1999; Nelson, 2000a). The granitoid rocks have weakly deformed to locally sheared intrusive contacts with little-deformed metavolcanic rocks of the Kelly Group in the Warrawoona Syncline. The low strain state of the granitic rocks and their envelope of greenstones contrasts sharply with the southern margin of the Mount Edgar Granitic Complex on the northern limb of the Warrawoona Syncline, which is strongly deformed and composed of reworked, c. 3450 Ma orthogneisses (Williams and Collins, 1990). Importantly, these younger (c. 3300 Ma) granitic rocks were emplaced to higher levels in the stratigraphy (Kelly Group) than their older granitic counterparts (c. 3450 Ma) in the Mount Edgar Granitic Complex into the Warrawoona Group (c. 3470 Ma) on the northern limb, giving an overall asymmetry to the syncline and indicative of greater relative uplift of the Mount Edgar Dome, which is consistent with the change in metamorphic grade across the syncline.

Locality 3.7: Gold mineralization in the Warrawoona Syncline (Calidus Resources)

Proceed for approximately 3 km east and turn left (north) towards the Warrawoona Range and to the parking lot for the Calidus Resources Ltd mine site. Follow all instructions prior to demounting from the vehicles. Calidus staff will lead us onto the site and provide information about the mining operation under way at this site, which is orogenic gold style mineralization in highly strained, vertically lineated rocks of the Warrawoona Group.

Calidus Resources will guide the field trip into their active mine site and provide an explanatory guidebook.

Day 4: The Fortescue Group and Shaw Granitic Complex

Locality 4.1: Basal pillow breccia of the c. 2.77 Ga Mount Roe Basalt (Zone 50, 771266E 7639443N)

At this locality, orange-weathering sandstones dip 30°N on the south side of the track in the southeastern corner of the Marble Bar Sub-basin of the Fortescue Group (Fig. 59). North of the track are some impressive outcrops of the pillow breccia unit that forms the base of what is interpreted here as the Mount Roe Basalt throughout the Marble Bar Sub-basin. This unit is 100–450 m thick and is conformably overlain by subaerial basalt flows. Indications are that the pillow breccia unit was likely deposited in a lacustrine setting. The pillow breccia contains rare, whole pillows, but much more commonly consists of angular pillow fragments surrounded by hyaloclastite (Fig. 60). The pillow basalt breccia and underlying sandstone unconformably overlies thick subaerial lavas that also have been ascribed to the Fortescue Group but that are, unlike all other localities of the Fortescue Group across the Pilbara, steeply dipping and tightly folded within the Marble Bar Sub-basin.

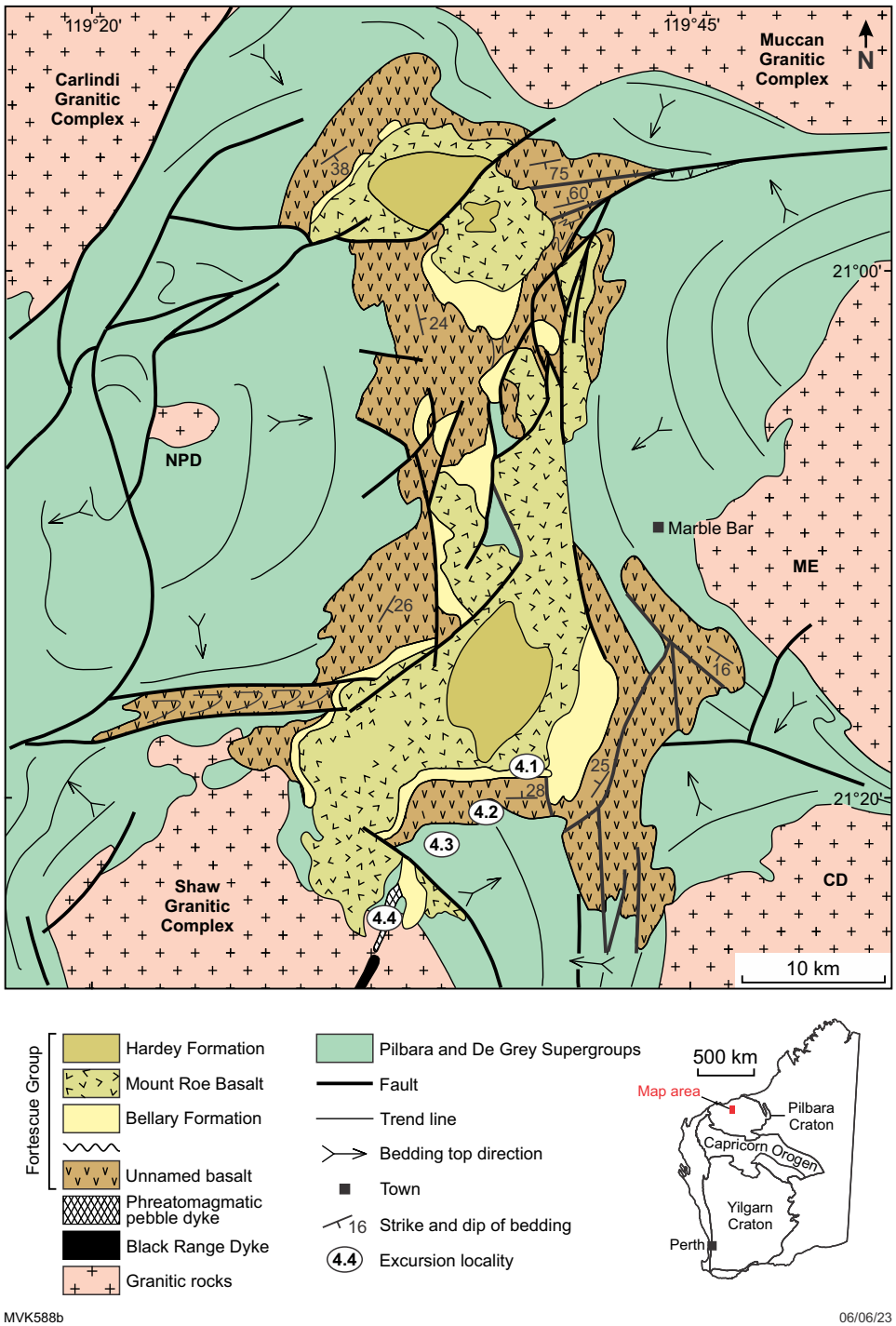

Figure 59. Simplified geological map of the Marble Bar Inlier of the Fortescue Group, showing excursion localities. Abbreviations: CD = Corunna Downs Granitic Complex; ME = Mount Edgar Granitic Complex; NPD = North Pole Dome

Indications from mapping (see Locality 4.2 and Van Kranendonk et al., 2006a) and paleomagnetic studies (Strik et al., 2003) indicate that the pillow breccia unit seen here is the basal unit of the Mount Roe Basalt and tied to eruption from the Black Range Dolerite dyke, whereas the unconformably underlying, more steeply dipping unit must represent an unnamed, older unit, whose age has not been determined.

Locality 4.2: Basal unconformity of the Fortescue Group in Glen Herring Gorge (Zone 50, 771233E 7636598N)

As you walk north from the parking area along the creek bed, you will walk over flows of vesicular basalt belonging to a basal, unnamed unit of the Fortescue Group in the Marble Bar Sub-basin (Fig. 59). These smooth, white-weathering rocks have been polished by the flow of the creek and carved into odd shapes. If you look closely at the rocks, you will notice they contain numerous small, white, round to irregular amygdales in fine-grained basalt; these magmatic vesicles are now filled by secondary minerals (quartz, calcite) precipitated out of solution from later circulating fluids. You will also notice red fractures and stains in the rock, which reflect the passage of highly oxidized groundwater through fractures in the rock caused by episodes of more recent faulting.

As you walk further north, down the gorge, notice that the rocks change from smooth-textured basalts to cobble and boulder conglomerate that was deposited under very high-energy conditions on a steep slope — probably conditions that were much the same as those you see around you today. Some of the fragments in the conglomerate are very large and probably derived from episodes of faulting. Even further north, in the heart of the gorge, the rocks change again. The steep cliff at the sharp bend of the river is part of the 3.32 Ga felsic volcaniclastic Wyman Formation, which forms the basement to the Fortescue Group at this locality and a paleoisland at the time of early Fortescue Group deposition.

MVK1159 22.12.22

Figure 60. Basaltic hyaloclastite with remnant, near-whole, pillows set within a matrix of pillow breccia and hyaloclastite; from the Mount Roe Basalt in the Marble Bar Inlier of the Fortescue Group

Locality 4.3: Pyroxene spinifex texture in 3.47 Ga Mount Ada Basalt (Zone 50, 766816E 7634880N)

In the low outcrops at this locality can be seen coarse (up to 15 cm) pyroxene–spinifex textured flows belonging to the Mount Ada Basalt (Fig. 61). These textured flows are interbedded with pillowed komatiitic basalts and carbonate-altered komatiitic basalts and intruded by subvolcanic sheets of quartz- and feldspar–porphyritic micromonzogranite emplaced during the eruption of the younger, overlying Duffer Formation.

MVK1160 23.12.22

Figure 61. Long pyroxene–spinifex texture in c. 3.47 Ga komatiitic basalt of the Mount Ada Basalt

Locality 4.4: The 2772 Ma Black Range Dolerite dyke and phreatomagmatic boulder conglomerate (Zone 50, MGA 763436E 7627340N)

The 2772 ± 2 Ma Black Range Dolerite dyke (Wingate, 1999) is the largest dyke of the Black Range Dolerite Suite, which was emplaced during eruption of the Mount Roe Basalt above the basal sedimentary rocks (Bellary Formation) of the Fortescue Group (Fig. 59). This locality lies within the core of a narrow zone of unusual boulder conglomerates that extends along-strike to the northeast of the Black Range Dolerite dyke for about 5 km, reaching 1 km wide (Fig. 62; Van Kranendonk et al., 2006a).

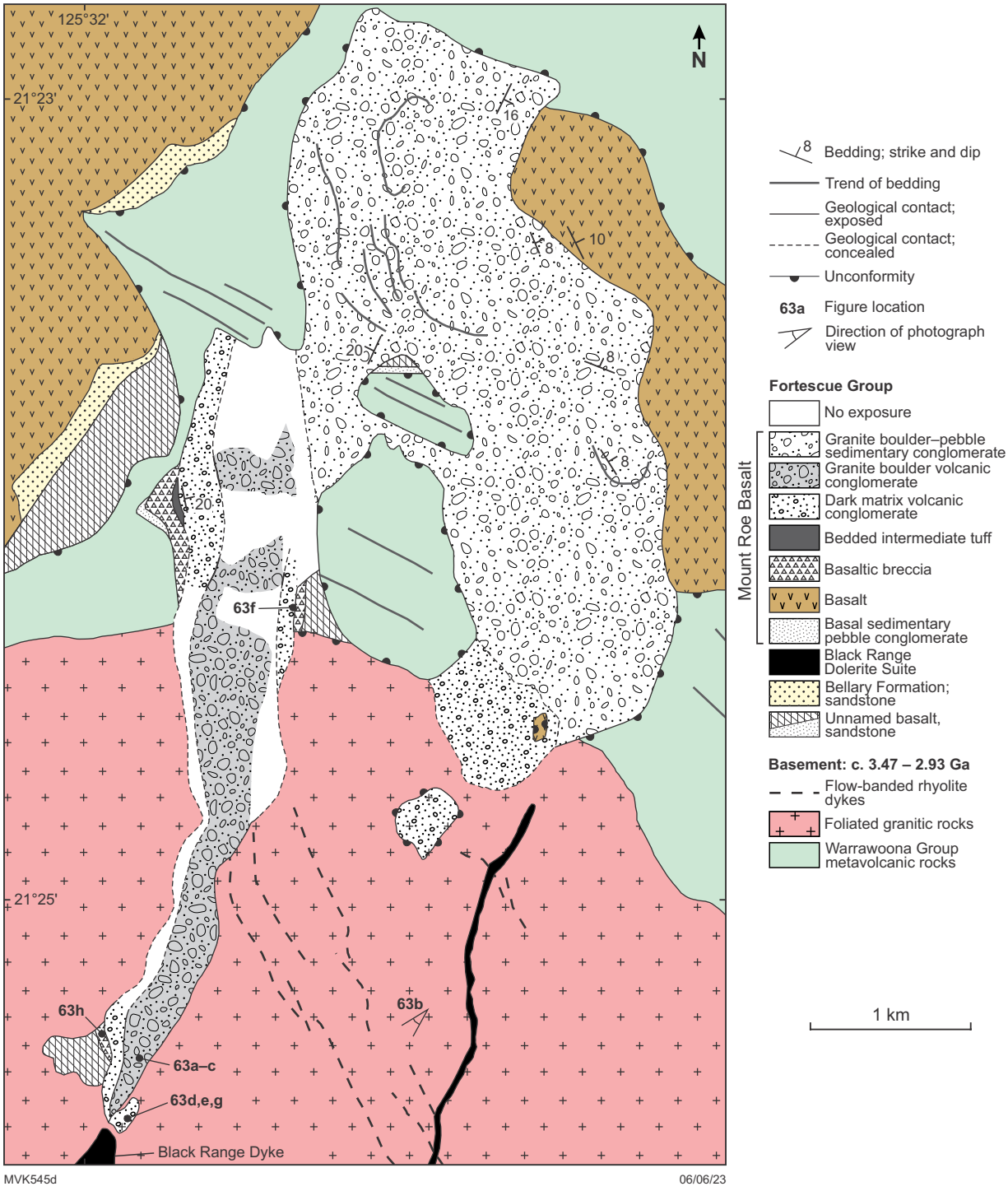

Figure 62. Geological map of the phreatomagmatic pebble dyke at the fracture propagation tip of the c. 2.77 Ga Black Range dyke. Modified from Van Kranendonk et al. (2006a)

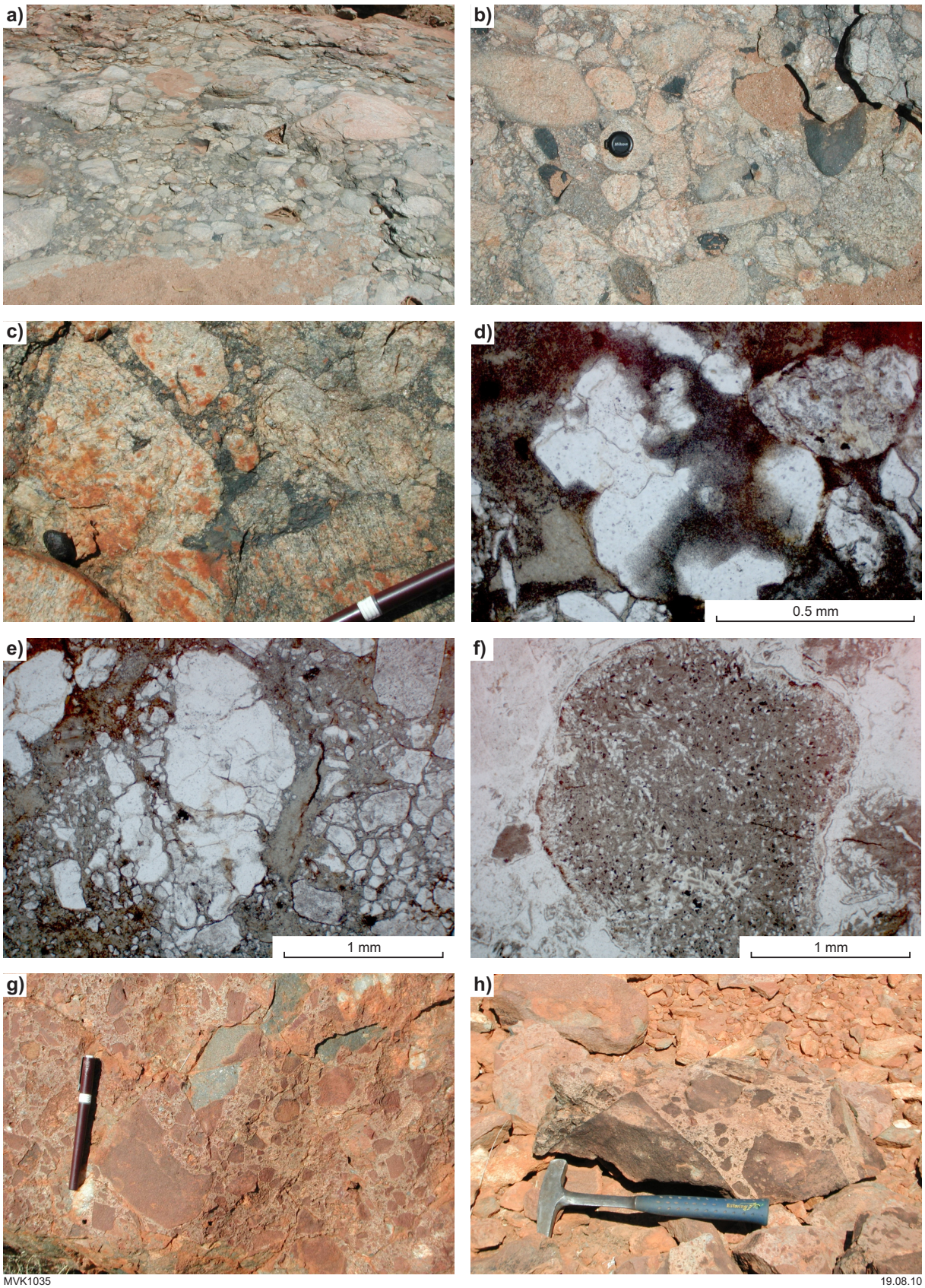

Figure 63. Outcrop features of the phreatomagmatic breccia dyke at Locality 4.4: a) river-washed outcrop of well-rounded granitic boulder conglomerate; b) close-up of granitic boulder conglomerate, showing dispersed basaltic clasts and angular nature of finer grained matrix (top right); c) area of dark rock-flour matrix between granite cobbles; d) photomicrograph (plane-polarized light) showing dissolution of quartz clasts by matrix; e) photomicrograph (plane-polarized light) showing in situ disaggregation of granitic clasts, suggestive of seismic shaking; f) photomicrograph (plane-polarized light) of basaltic droplet with chilled margin defined by inward-radiating plagioclase crystallites; g) dark-coloured breccia along the margin of the phreatomagmatic dyke, consisting predominantly of angular basaltic clasts, but including scattered granitic clasts; h) basaltic breccia at the contact with basaltic lavas on the edge of the phreatomagmatic dyke

Originally likened to round-pebble vent agglomerate, the boulder conglomerates within the narrow zone in front of the Black Range dyke are unusual because they contain:

- no evidence of bedding (Fig. 63a)
- clasts that show an ***increasing*** angularity with ***decreasing*** grain size, opposite to that in conglomerates of sedimentary origin (Fig. 63b)
- well-rounded basaltic pebbles within granitic boulder conglomerates, which would probably not have survived in a sedimentary environment (Fig. 63b)
- biotite-rich granitic clasts with dark alteration rinds (Fig. 63b)
- a matrix that varies from sand-size rock crystal grains to rock flour (Fig. 63c)
- a component of the matrix that consists of chlorite, which shows reaction with, and resorption of, granitic clasts, indicative of a hot matrix component (Fig. 63d)
- clasts showing evidence of in situ disaggregation, indicative of some sort of intense shaking (Fig. 63e)
- rounded basaltic clasts with chilled rinds (Fig. 63f)
- lateral changes in the composition of the conglomerate, from dominantly granitic clasts in the core of the zone to hybrid basalt–granite conglomerates near the margins of the zone, and basaltic breccias with sparse granitic clasts at the very edges of the zone, in contact with basaltic lavas (Fig. 63g,h).

These conglomerates show a variety of textures and compositions across strike and have peperitic contacts with remnants of basaltic lava flows, indicating contemporaneity of formation with basalt eruption. Contemporaneity is supported by a U–Pb zircon date of 2767 ± 3 Ma from an intermediate tuffaceous sandstone that flanks the linear zone of conglomerate (Fig. 62; Van Kranendonk et al., 2006a).

For these reasons, Van Kranendonk et al. (2006a) concluded that the conglomerates were caused by phreatomagmatic brecciation of the granitic country rocks during emplacement of the Black Range dyke, through one of two ways (Fig. 64a). In this model, the Black Range dyke was emplaced laterally into a developing fracture, the propagation tip of which was filled by disaggregated country rock and basaltic droplets sourced from the intruding magma. Rounding of the country rock boulders developed as a result of turbulent milling during gas/magma (phreatic) eruptions, which resulted in chipping off of angular fine fragments, development of matrix rock flour, alteration/resorption of fragments by hot matrix, and in situ clast disaggregation. Perhaps this type of linear zone is equivalent to the Lunar rilles, which have been interpreted as graben developed over intrusive dykes (Fig. 64b).

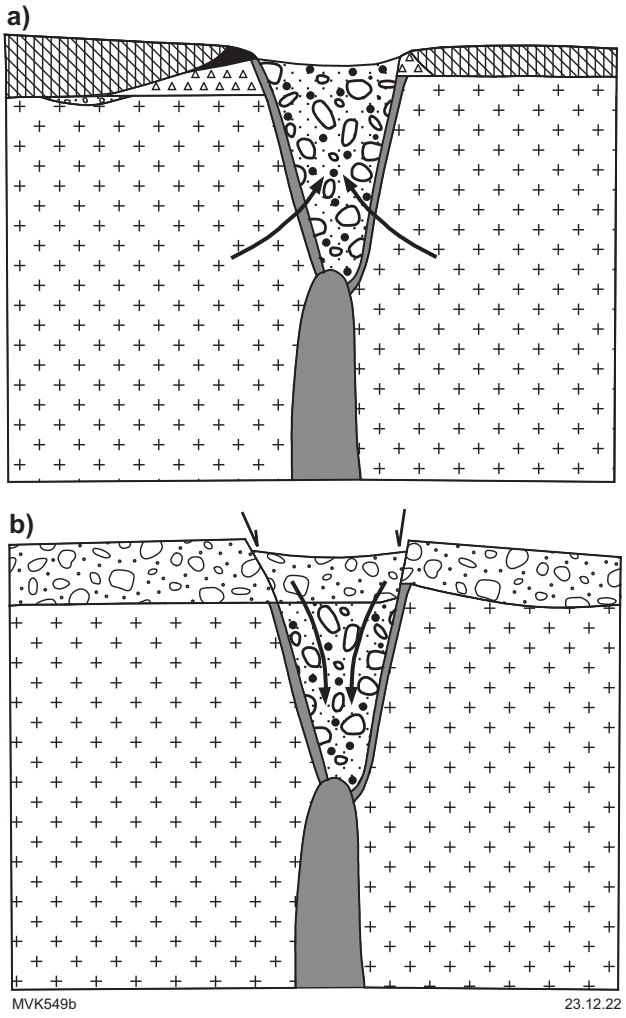

Figure 64. Two possible models of formation of the phreatomagmatic breccia dyke at Locality 4.4: a) phreatomagmatic brecciation at the propagation tip of the Black Range dyke in granitic country rocks, through steam-generated milling of country rocks and with the addition of basaltic droplets from the incoming magma; b) phreatomagmatic brecciation at the propagation tip of the Black Range dyke emplaced beneath a pre-existing sedimentary cover (from Van Kranendonk et al., 2006a)

Locality 4.5: North Shaw Tonalite, Shaw Granitic Complex (Zone 50, 754745E 7636561N)

This outcrop near the northern tip of the Shaw Granitic Complex (Fig. 65) is typical of the North Shaw Tonalite, an essentially undeformed mafic quartz diorite–tonalite containing 5–10% quartz and 10–15% hornblende and dated at 3468 ± 5 Ma (Nelson, 2005b). At this locality, it contains angular xenoliths of amphibolite spalled off from the adjacent country rocks, and an intrusive contact for this unit is apparent. Smithies et al. (2009) showed that Archean Pilbara tonalite–trondhjemite–granodiorite (TTG) like this derived from infracrustal hydrous melting of enriched basalt.

Locality 4.6: Coolyia Creek Granodiorite, Shaw Granitic Complex (Zone 50, 756241E 7632122N)

The outcrops of the Coolyia Creek Granodirite in the creek at this locality are more siliceous and leucocratic than the older North Shaw Tonalite to the north. The Coolyia Creek Granodiorite is characterized by a distinctive clotty texture defined by 15–20% of 1–3 cm-sized, elongate and flattened (L–S) clots of mafic minerals. In thin section, the mafic clots are composed of green biotite–epidote–chlorite — opaque minerals (trace) within a medium-grained, recrystallized groundmass of plagioclase and quartz, with <5% myrmekite and K-feldspar. Bickle et al. (1993) described the local development of cumulate igneous layering and presented geochemical data for the Coolyia Creek Granodiorite. This unit has intrusive contacts with the North Shaw Tonalite and with greenstones along its western contact where it cuts across bedding.

The originally spherical mafic clots have clearly been affected by regional tectonic strain and deformed into prolate spheroids. The origin of the clotty texture is enigmatic and cannot be explained by assimilation of xenoliths alone because their distribution and size are too even over most of the unit, and they have fuzzy or weakly gradational margins. Instead, this texture is interpreted to be either the product of mingling and mixing of comagmatic basaltic and granitic liquids (Pitcher, 1993), or of quenching.

A sample of the Coolyia Creek Granodiorite was collected for SHRIMP U–Pb dating of zircon from the same locality where Bickle et al. (1993) obtained a Pb–Pb isochron age of 3338 ± 52 Ma. Results indicate a single population of zircons and an igneous age of 3469 ± 2 Ma (Nelson, 2000b), indicating that the younger Pb–Pb age must reflect a period of metamorphic alteration and recrystallization.

Locality 4.7: Post-tectonic, c. 2.85 Ga, Cooglegong Monzogranite, Shaw Granitic Complex (Zone 50, 748900E 7618404N)

Good exposure in Cooglegong Creek reveals the undeformed, coarse-grained nature that is typical of the post-tectonic monzogranites of the Split Rock Supersuite, emplaced across the craton at between 2870 and 2830 Ma. Here in the creek, a sample was collected for geochronology and returned an age of 2851 ± 2 Ma (Nelson, 1998a).

Also visible in outcrops here are thin greisen veins with tantalite mineralization, which was mined extensively in dry creek beds from further east of this locality from 1957 to the 1970s.

Locality 4.8: Orthogneiss, schlieric leucogranite and Mulgandinnah Monzogranite; Shaw Granitic Complex. Heritage Site — not visited (Zone 50, 743068E 7622484N)

A dark-brown weathering, homogeneous, fine-grained body of the 2928 ± 2 Ma (Nelson, 1998b) Mulgandinnah Monzogranite forms the small hill at this locality. The monzogranite has an equigranular to weakly feldspar–porphyritic texture and a characteristic spotted appearance due to sparse, but relatively large, magnetite crystals that are rimmed by haloes of feldspar. This body is one of several that together appear as a 'string of pearls' across the Shaw Granitic Complex at this latitude (Fig. 65).

On the western flank of the Mulgandinnah Monzogranite are low outcrops of older migmatitic orthogneiss and intrusive sheets of schlieric leucogranite. The precursor to the orthogneiss was a commonly even-grained to weakly feldspar phyric, blue-grey tonalite that locally shows evidence of having been an intrusive complex of multiple, slightly texturally variable sheets. Elsewhere, these rocks contain xenoliths and rafts of amphibolite, meta-anorthosite and metasedimentary rocks. Zegers (1996) dated the precursor components of migmatitic orthogneisses in two places from the southern part of the Shaw Granitic Complex, and these yielded identical ages of c. 3467 Ma, similar to that of the Coolyia Creek Granodiorite of the North Shaw Suite at Locality 4.6.

The schlieric leucogranite was previously interpreted as the third igneous layer of the North Shaw Suite (Bettenay et al., 1981; Bickle et al., 1993). However, detailed mapping of the leucogranite shows that it is an impure, highly variable unit that is clearly less of a purely magmatic body than the older North Shaw Tonalite and Coolyia Creek Granodiorite to the north.

Instead, at this locality and elsewhere, the leucogranite can be seen to have been emplaced as a series of irregular intrusive sheets into the older blue-grey orthogneisses, and they contain a discontinuous ghost layering (schlieren) that was inherited from the host orthogneiss. Deeper within the core of the granitoid complex, leucogranite is present as heterogeneous, schlieric diatexite and as leucosome veins in tonalitic orthogneiss. At higher structural levels, with increasing amounts of segregation and transfer, the leucogranite is a homogeneous intrusive sheet with straight margins (Fig. 65).

Overall, the leucogranite forms a lensoid sill within the northern part of the Shaw Granitic Complex that was emplaced along the contact between migmatitic orthogneiss at deeper structural levels (to the south), and better-preserved plutonic components of the North Shaw Suite at higher structural levels (to the north) (Fig. 65). Geochronological data from two samples of leucogranite give slightly different results. Zircons from a leucogranite diatexite near the structural base of the unit contained

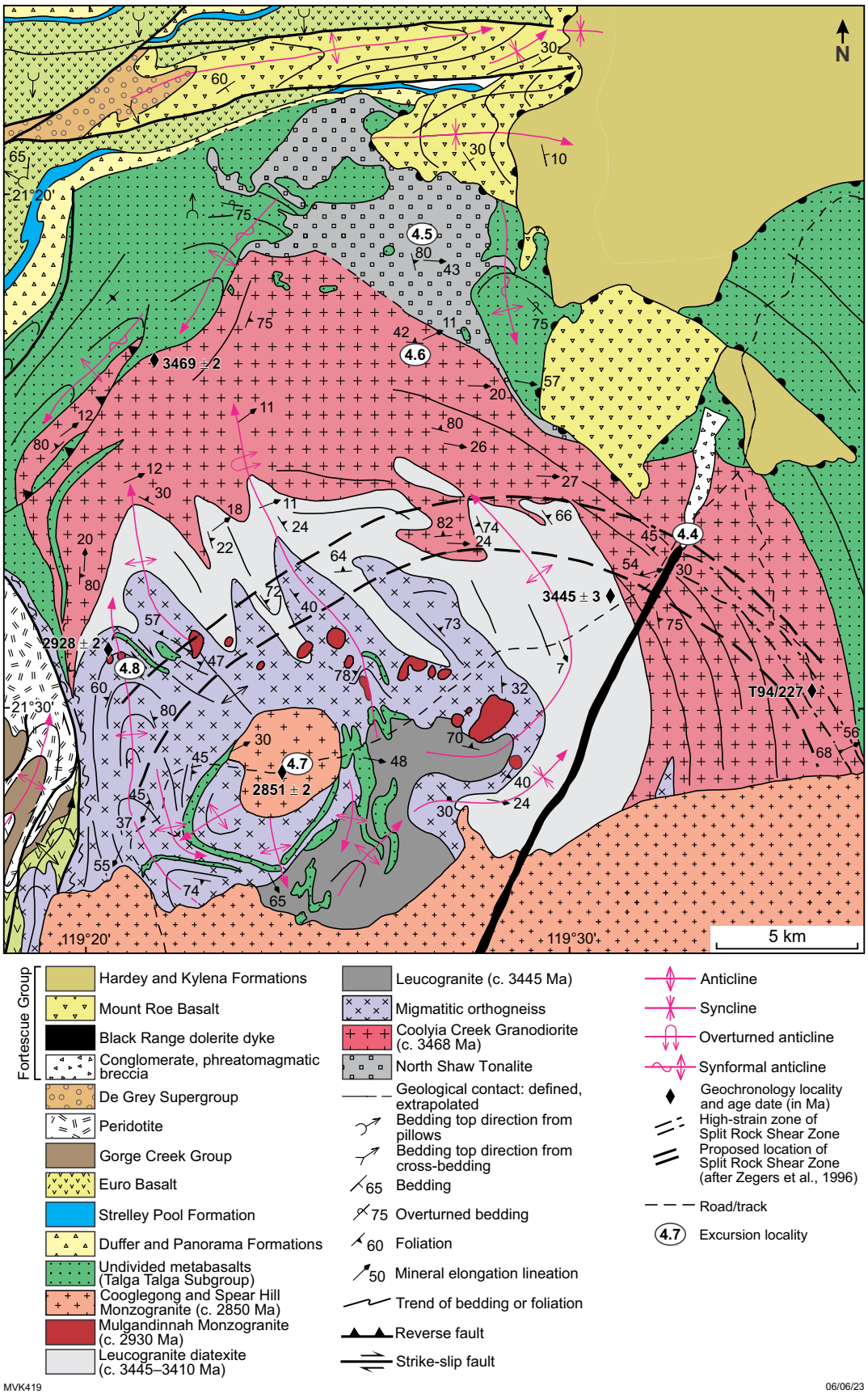

Figure 65. Geological map of the northern part of the Shaw Granitic Complex showing excursion localities. Modified from Van Kranendonk et al. (2004)

rims that crystallized at 3410–3400 Ma on cores that were c. 3450 Ma (GSWA, unpublished data; Nelson, 2000c). A sample from a homogeneous leucogranite dyke at a structurally higher level in the granitoid complex yielded a single zircon population with an age of 3445 ± 3 Ma (Nelson, 1998c). The evidence that tonalitic rocks of similar age lie above and below the leucogranite, combined with evidence that the leucogranite was derived from these rocks through anatexis, suggests that the leucogranite may not be a third component of the igneous North Shaw Suite. Instead, the leucogranite is interpreted to represent a melt derived from the older plutonic components at deeper structural levels within the Shaw Granitic Complex that ponded in the tonalites as a lensoid sill during an early period of structural doming at c. 3410 Ma. A schematic model showing the interpreted evolution of the Shaw Granitic Complex is presented in Van Kranendonk et al. (2004) (Fig. 66).

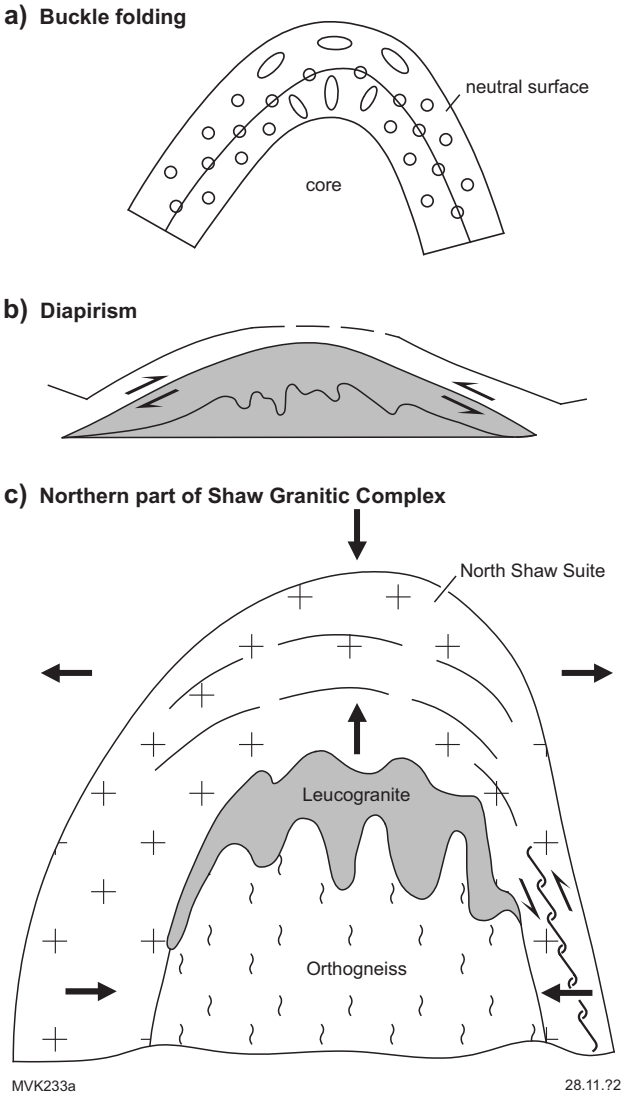

Figure 66. Schematic diagrams of folds, showing strain distribution: a) cross-section of a buckle fold, showing the distribution of strain (circles and ellipses); b) cross-section through centrifuge model of a diapir, showing upright buckle folds in diapiric core material (grey stipple) resulting from east–west compression, and horizontal boudinage of a stiff marker bed (black dashed line) in stretched overburden. The boundary between the diapiric material and cover rock may be a shear zone. Traced from Ramsay (1967); c) highly simplified geological cross-section of the North Shaw area at c. 3440 Ma, showing the simultaneous development of upright buckle folds in leucogranite and arcuate foliations in the North Shaw Suite (crosses) due to vertical flattening. From Van Kranendonk et al. (2004)

Field trip localities: Part 2 West Pilbara and Central Pilbara Tectonic Zone — rifted margin, subduction-related 'arc' magmatism and accretion and collisional orogeny

In stark contrast to the Paleoarchean East Pilbara Terrane, where the regional evidence from stratigraphic, structural, metamorphic, geochronological and geochemical studies indicates that Phanerozoic-style plate tectonic processes did not play a significant role (Green et al., 2000; Smithies, 2000; Smithies and Champion, 2000; Hickman and Van Kranendonk, 2004; Van Kranendonk and Pirajno, 2004; Smithies et al., 2005a, 2007a; Van Kranendonk et al., 2007a), a large amount of accumulated evidence indicates that there was a major change in crustal processes and tectonic environments in the western part of the Pilbara Craton between c. 3220 and c. 3070 Ma (Hickman, 2001b, 2004, 2016, 2021; Smithies et al., 2003, 2004, 2005a,b, 2007b; Van Kranendonk et al., 2006b, 2007a, 2010). Here, the Mesoarchean volcanic and sedimentary successions provide perhaps the best evidence on Earth that subduction-like processes with similarities to those of today were operating, at least locally, by c. 3200 Ma. Figures 67–69 provide an overview of this region. Field localities described in this section of the guide provide some of the evidence for interpreting this region as an active margin from 3220 to 2900 Ma. This region evolved through stages, outlined below, that have collectively been interpreted to represent a Mesoarchean Wilson cycle (Van Kranendonk et al., 2010):

- rifted continental margins with continental shelf deposition (3220–3165 Ma)
- formation of MORB-like crust (3200–3150 Ma)
- convergence, subduction of primitive mafic crust, and formation of an intra-oceanic volcanic arc (3135–3100 Ma)
- accretion and collisional orogeny (3070–3060 Ma)
- peneplanation, post-orogenic extension, and subsidence, with development of a continental basin (3050–3016 Ma)
- subduction northwest of the present craton margin with a southeast-dipping slab, and the establishment of a magmatic arc and back-arc basin parallel to the northwestern margin of the craton (3010–2980 Ma)
- post-subduction removal (break-off) of the fossil slab, and southeastward migration of hot mantle material, with melting of subduction-modified mantle beneath the central part of the western Pilbara, and granitic intrusion into overlying clastic sediments in strike-slip basins (2950–2940 Ma)
- final convergence, closure of all basins, and major orogeny, completing cratonization (2940–2900 Ma).

Day 5: Central Pilbara Tectonic Zone — post-subduction basins and remobilized lithospheric mantle / De Grey Superbasin (Whim Creek and Mallina Basins and contemporaneous intrusions)

The following stops visit two of the four basins that form part of the De Grey Superbasin (Fig. 67). These include the Whim Creek Basin (3010–2990 Ma Whim Creek Group) and the Mallina Basin (2970–2940 Ma Croydon Group). Time will not permit examination of the Gorge Creek Basin (3050–3020 Ma Gorge Creek Group) or the Mosquito Creek Basin (2970–2930 Ma Mosquito Creek Formation).

The 3010–2990 Ma Whim Creek Basin is entirely composed of the Whim Creek Group, which comprises volcanic, intrusive and volcaniclastic rocks of the Warambie Basalt and Red Hill Volcanics (Fig. 70). The group is unconformably overlain by 2970–2930 Ma sedimentary and volcanic formations of the Croydon and Bookingarra Groups. Together, the Whim Creek, Croydon and Bookingarra Groups form the supracrustal succession that makes up the east-northeast trending, 150 km-long Whim Creek greenstone belt, located between Roebourne and Port Hedland. The boundary between this greenstone belt and the Mallina Basin is defined by three faults: i) the western section of the Mallina Shear Zone in the south; ii) the Loudens Fault in the southeast; iii) the eastern section of the Sholl Shear Zone in the northeast (Fig. 68). The depositional setting of the Whim Creek Group was interpreted as a pull-apart basin by Barley (1987), but Pike and Cas (2002) suggested it may have formed in an ensialic back-arc basin, based on examination of its volcanic and sedimentary facies.

The 2970–2930 Ma Mallina Basin (Figs 67, 68) is 100 km wide, over 250 km long, and filled by a 2–4 km-thick succession of conglomerate, sandstone and shale, deposited in submarine fans (Eriksson, 1981). The basin overlies the 3070 Ma collision zone between the East Pilbara Terrane and the West Pilbara Superterrane and is unconformably underlain by metamorphosed, c. 3200 Ma oceanic crust, bimodal volcanics of the 3130–3110 Ma Whundo Group arc complex, and the 3050–3015 Ma Gorge Creek Group. Along its northwestern margin, the basin unconformably overlies the Whim Creek Group and Maitland River Supersuite, but there is no evidence that these 3010–2980 Ma units extend to the southeastern side of the basin.

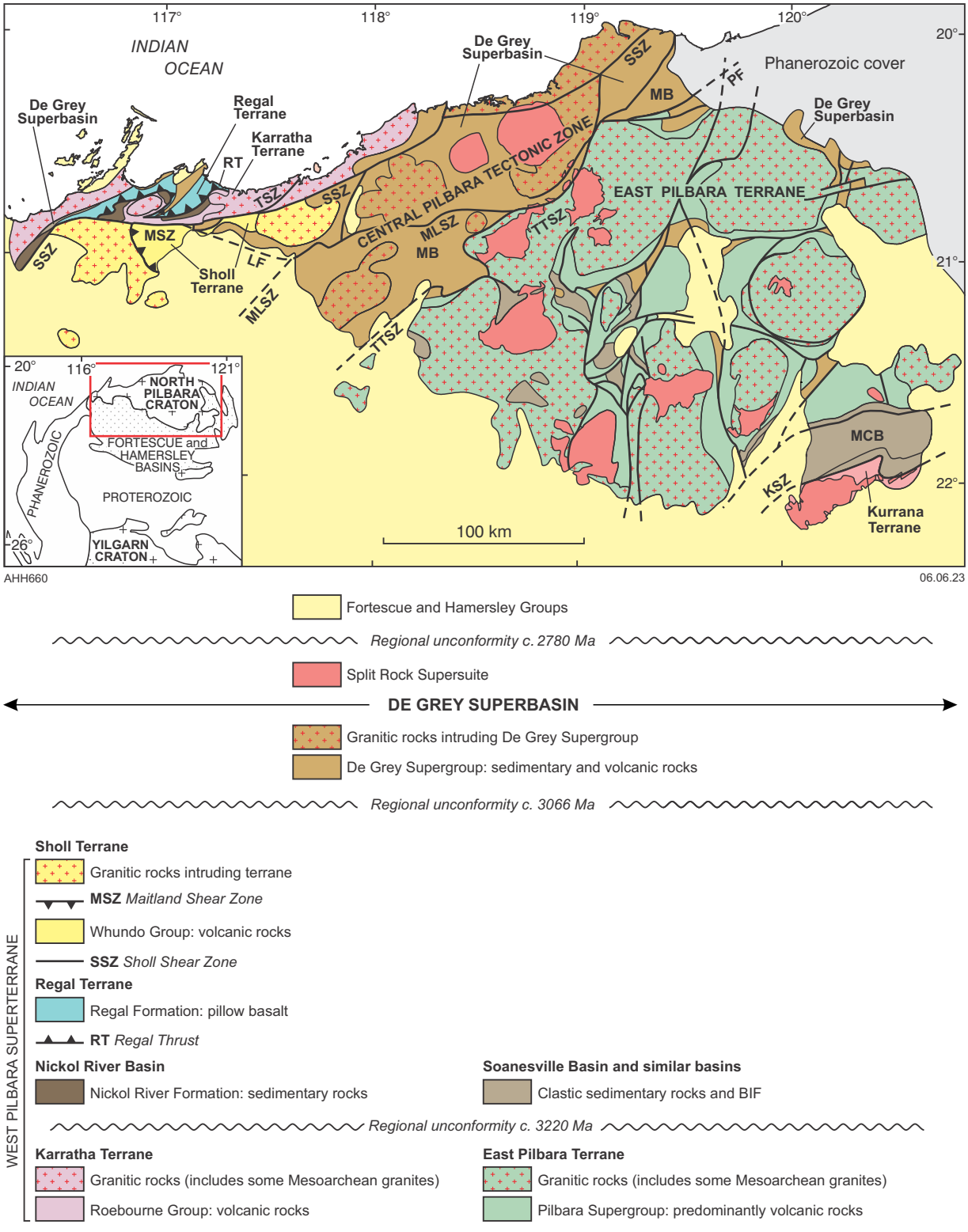

Figure 67. Simplified geological map of the northwestern Pilbara Craton, showing terranes plus the De Grey Superbasin. Abbreviations: LF = Loudens Fault; MB = Mallina Basin; MCB = Mosquito Creek Basin; MLSZ = Mallina Shear Zone; MSZ = Maitland Shear Zone; SSZ = Sholl Shear Zone; TSZ = Terenar Shear Zone; TTSZ = Tabba Tabba Shear Zone; KSZ = Kurrana Shear Zone; PF = Pardoo Fault; RT = Regal Thrust

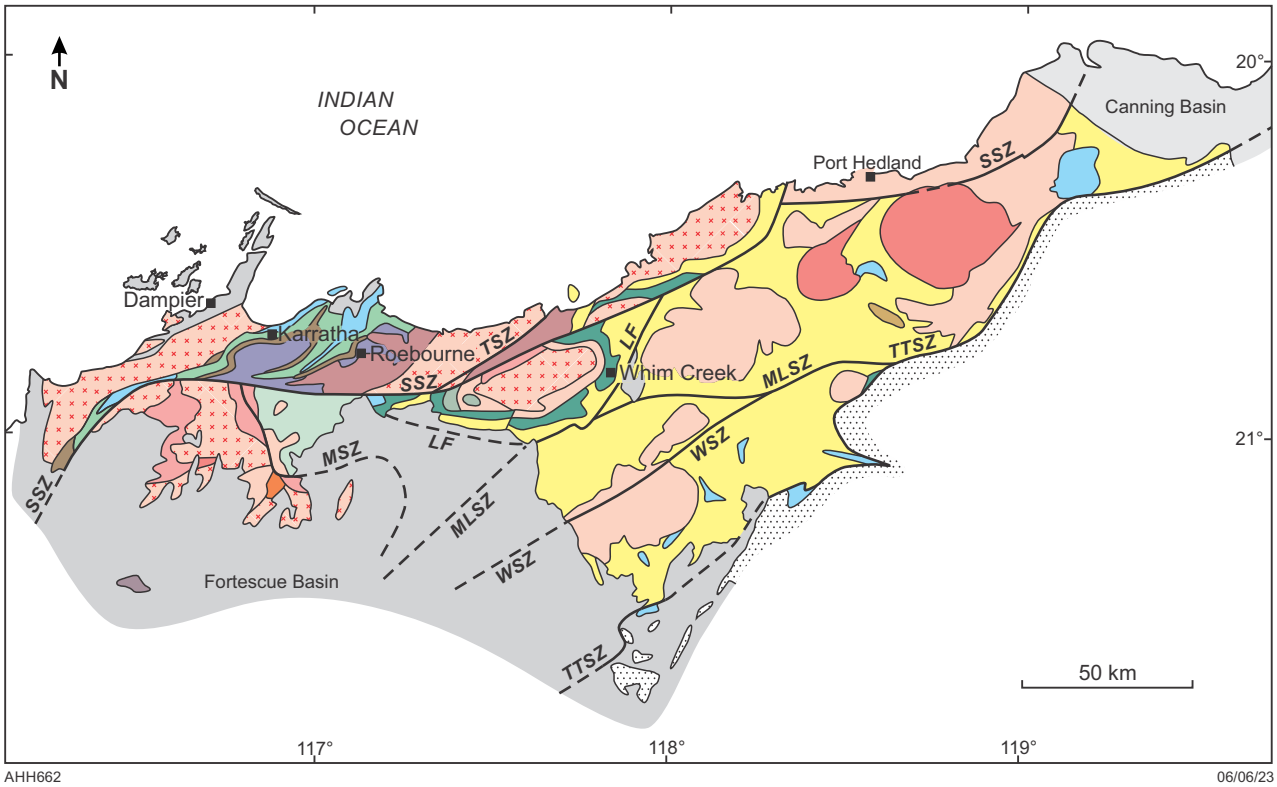

Figure 68. Geological map showing basins and supersuites of the northwest Pilbara Craton. Ages and contact relationships are summarized in Figure 69. Note that the supersuites (predominantly granitic) are distributed in east-northeast trending linear zones with decreasing intrusive ages towards the southeast. Abbreviations: LF = Loudens Fault; MLSZ = Mallina Shear Zone; MSZ = Maitland Shear Zone; SSZ = Sholl Shear Zone; TSZ = Terenar Shear Zone; TTSZ = Tabba Tabba Shear Zone; WSZ = Wohler Shear Zone

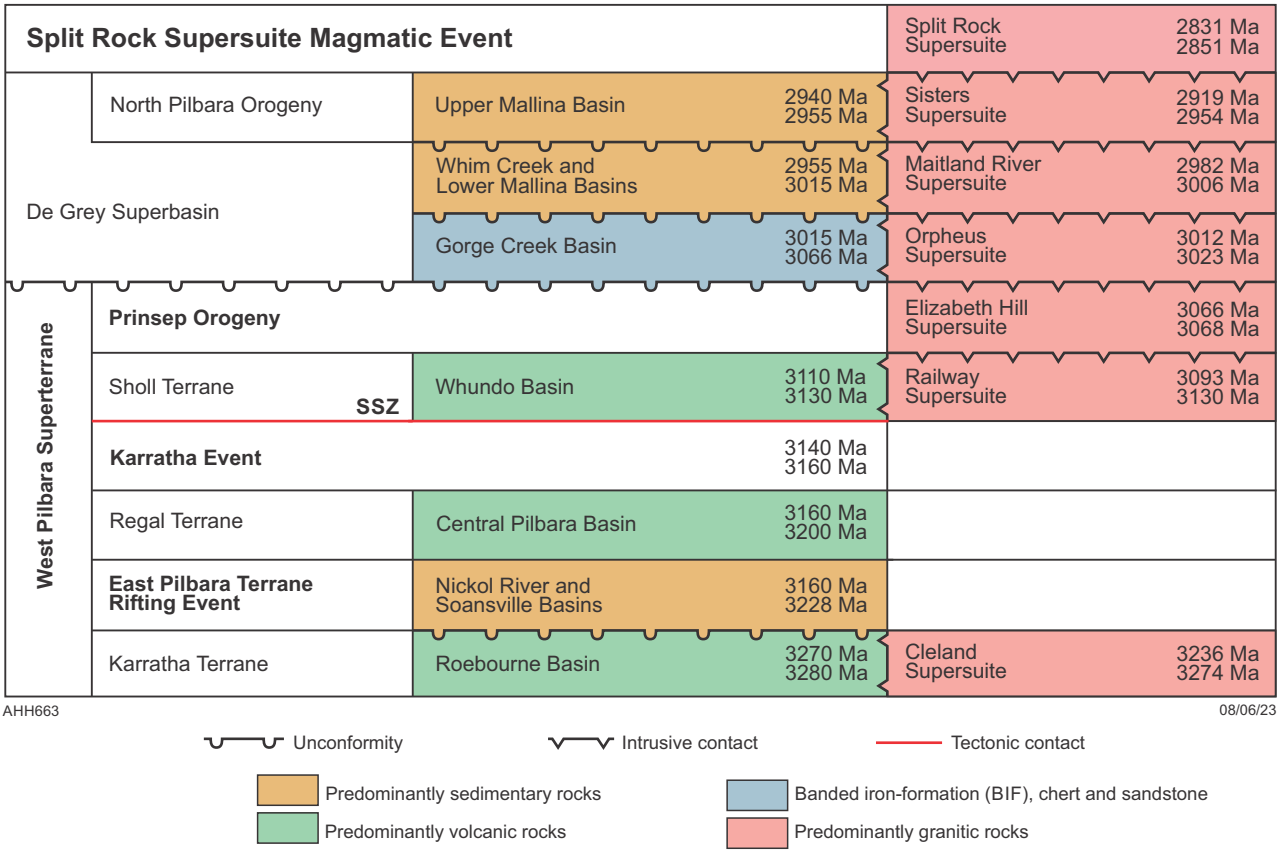

Figure 69. Diagrammatic illustration of the ages and contact relationships of terranes, basins, supersuites and events in the northwest Pilbara Craton. The tectonic contact between the Nickol River Basin and the Central Pilbara Basin (Regal Terrane) is the Regal Thrust, whereas that between the Regal Terrane and the Sholl Terrane is the Sholl Shear Zone. Regional unconformities at c. 3220, 3066 and c. 2955 Ma coincide with periods of erosion during major rifting or following collision orogeny. Deposition in volcanic and sedimentary basins was generally accompanied by supersuite intrusion

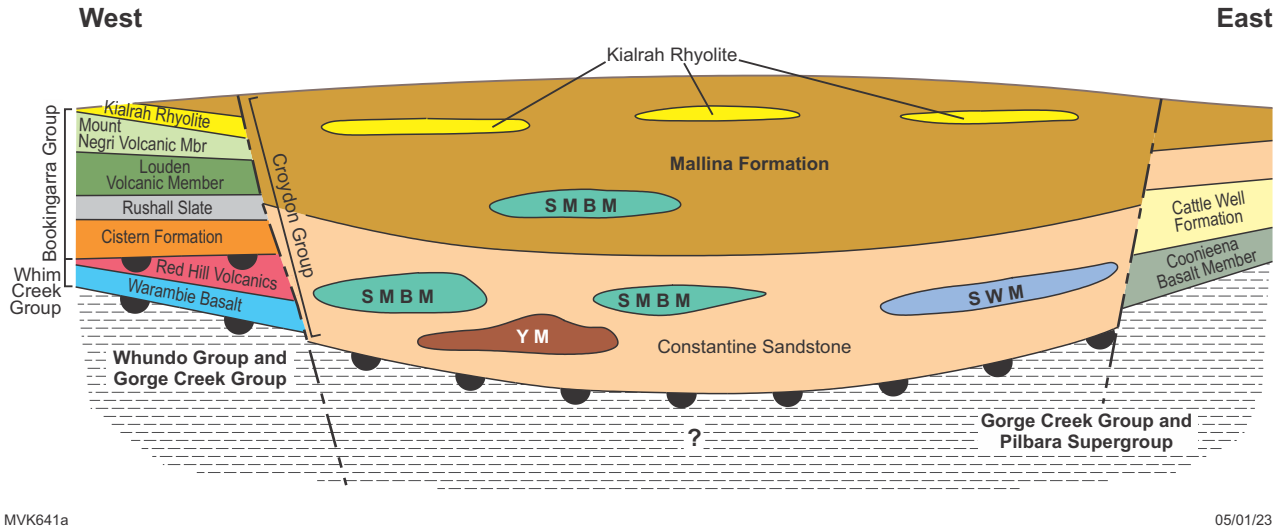

Figure 70. Diagrammatic cross-section of the Mallina Basin, showing units of the Whim Creek, Bookingarra and Croydon Groups. The Louden Volcanics, Mount Negri Volcanics and South Mallina Basalt Member (SMBM), Salt Well Member (SWM), Yareweeree Member (YM), and Coonieena Basalt Member are all components of the Bookingarra and Croydon Groups

Where it occurs in the Whim Creek greenstone belt, the Bookingarra Group is represented by three volcanic and two clastic formations — with possible lithostratigraphic equivalents to the southeast, within the Croydon Group of the Mallina Basin. The basal Cistern Formation in the Whim Creek greenstone belt is an upward-fining succession of subaqueous fanglomerate, breccia and sandstone, deposited unconformably on uplifted and eroded rocks of the Whim Creek Group (Pike and Cas, 2002). This formation is overlain by shale (Rushall Slate) deposited in isolated half graben sub-basins (Pike and Cas, 2002). Overlying the Rushall Slate are two siliceous high-Mg basalt formations — the Mount Negri Volcanics and the Louden Volcanics, followed by the Kialrah Rhyolite.

In the Whim Creek greenstone belt, the Cistern Formation has been dated at 2964 ± 6 Ma (Huston et al., 2002), whereas the Kialrah Rhyolite at the top of the Bookingarra Group gives a maximum depositional age of 2943 ± 7 Ma (GSWA 144261: Nelson, 1998a). Here, volcanogenic massive sulfide mineralization in rocks of both the Whim Creek and Bookingarra Groups is dated at between 2950 and 2920 Ma (Huston et al., 2002). To the southeast of the Whim Creek greenstone belt, in the Mallina Basin, detrital zircons from the fine- to coarse-grained siliciclastic rocks of the Croydon Group (Mallina Formation and Constantine Sandstone) yield a maximum depositional age of 2994 ± 4 Ma (GSWA 142942: Nelson, 2000a), although a study of xenocrystic zircons from granites that intrude the basin indicates a more realistic maximum depositional age of c. 2970 Ma (Smithies et al., 2001). The main sedimentary fill was folded prior to intrusion of granites, beginning at c. 2955 Ma. However, detrital zircons from a shale in the eastern part of the basin indicate a second depositional cycle (a later basin) at 2941 ± 9 Ma (GSWA 142188: Nelson, 1999). This is corroborated by a depositional age of 2948 ± 3 Ma (GSWA 169025: Nelson 2000a) from a rhyolitic unit in the same region.

The stratigraphy and structural history of the Mallina Basin records periods of extension and rift-related deposition (clastic sediments), intrusion (ultramafic–mafic sills) and minor basaltic magmatism, alternating with folding, strike-slip faulting, and thrusting during northwest–southeast compression. The intensity of deformation increases in a southeasterly direction, towards the Tabba Tabba Shear Zone, along the tectonic contact with the East Pilbara Terrane (Fig 67). Minor basaltic lava flows, locally including hyaloclastite breccias, are of siliceous high-Mg basalt (Smithies et al., 2004). Between 2950 and 2940 Ma, intrusion of the Sisters Supersuite included alkali granites, high-Mg diorites (sanukitoids) and monzogranites (Smithies and Champion, 2000). The high-Mg diorites followed emplacement of mafic subvolcanic sills with boninite-like compositions, and collectively provide evidence for the partial melting of subduction-enriched mantle (Smithies et al., 2004). Nd_{TDM} model ages from the Croydon Group and Sisters Supersuite within the main part of the basin are younger than c. 3280 Ma (Smithies et al., 2007b).

The first stops of this field trip look at units within the Mallina Basin and intrusions belonging to the Sisters Supersuite. We then visit volcanic units within the upper part of the Bookingarra Group in the Whim Creek area before moving to the western part of the Whim Creek Basin to examine spectacular volcanic rocks of the Whim Creek Group.

Locality 5.1: Sanukitoids (High-Mg diorites) of the Sisters Supersuite (Zone 50, MGA 626237E 7688762N or 688800E 7704500N)

Siliciclastic and mafic intrusive and extrusive rocks of the Mallina Basin were intruded by high-Mg diorites (sanukitoids) of the Sisters Supersuite between 2955 and 2945 Ma (Smithies and Champion, 2000). The sanukitoids form a northeast-trending chain of high-level intrusions extending for over 150 km along the axis of the Mallina Basin (Fig. 71). In the east of the basin, the sanukitoids were emplaced into zones of active dilation related to extension along crustal-scale basin-parallel faults; most of the intrusions are stocks of <20 km² in areal extent. The Peawah Granodiorite is the largest intrusion, covering an area of approximately 180 km², and is a composite body that can be geochemically subdivided into the Peawah Granodiorite (east) and the Peawah Granodiorite (west). The Peawah Granodiorite (west) has been dated at 2948 ± 5 Ma (GSWA 118967: Nelson, 1997b). Many of the intrusions are partially surrounded by earlier intrusions of gabbro. Most intrusions also contain abundant rounded enclaves up to 30 cm in diameter, mostly cognate inclusions of diorite and gabbro. Some intrusions preserve a chilled margin of fine-grained melanodiorite, which also occurs in 1–2 m-thick dykes and sills in country rock.

The sanukitoids range from diorite and monzodiorite, to tonalite and granodiorite. Mesocratic granodiorite is the most common rock type and ranges in texture from equigranular to seriate to porphyritic, with plagioclase phenocrysts up to 1 cm long. Plagioclase forms a connected framework of euhedral crystals, many of which show well-developed compositional zoning from inner zones of An_{35} to sodic rims of An_{18}. Small sericite- and calcite-altered cores suggest compositions more calcic than An_{35}. Hornblende is the dominant mafic mineral, and in most granodiorites contains cores of diopside ($Wo_{45–47}En_{40–41}Fs_{13–14}$ – $Mg^{\#}$ ~75), variably altered to actinolite. The abundance of these cores indicates the rocks were initially clinopyroxene rich. Biotite mantles hornblende or forms an anhedral intergranular phase. Quartz and minor microcline are intergranular phases. Accessory minerals include magnetite, sphene, apatite and zircon, all of which are concentrated in hornblende and biotite. Mafic clots, up to 1 cm in diameter, are locally abundant and contain hornblende with lesser diopside, biotite, plagioclase and magnetite.

Fine-grained melanodiorite forms a chilled margin to some intrusions. It contains 2–4 mm-long phenocrysts of euhedral plagioclase (An_{43} cores to rims of An_{21}), diopside ($Wo_{41}En_{42}Fs_{17}$ – $Mg^{\#}$ ~72) and hornblende ($Mg^{\#}$ = 65) ± orthopyroxene, within a flow-aligned groundmass of plagioclase and hornblende, with lesser biotite ($Mg^{\#}$ = 52), quartz and magnetite. Orthopyroxene occurs as discrete subhedral crystals, as granoblastic clots containing minor diopside and plagioclase, or as anhedral cores in diopside. Analysis of coexisting clinopyroxene and orthopyroxene give equilibration temperatures of approximately 1020 °C.

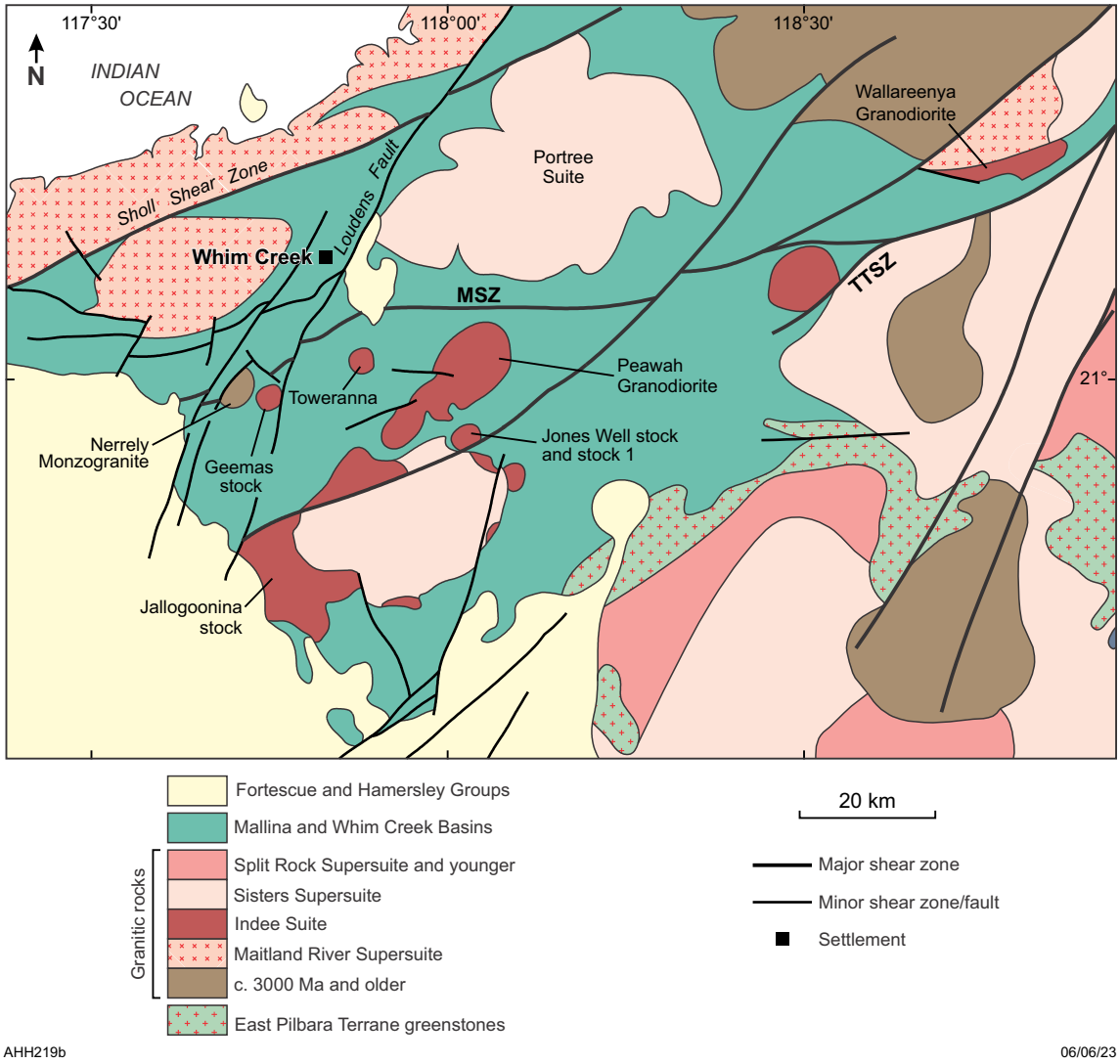

Figure 71. Simplified geological map of the western part of the De Grey Superbasin, showing major faults. Abbreviations: MSZ = Mallina Shear Zone; TTSZ = Tabba Tabba Shear Zone

The term 'Archean Sanukitoid suite' was first used by Shirey and Hanson (1984) to describe a suite of dioritic to granodioritic rocks, the more mafic of which (60% SiO_2 or less) having $Mg^{\#}$ >60, and Ni and Cr >100 ppm, coupled with high concentrations of large ion lithophile elements (LILE), light rare earth elements (LREE), Th, Na_2O and K_2O, low concentrations of high field strength elements (Figs 72, 73) and high LREE / heavy rare earth elements (HREE) ratios [e.g. $(La/Yb)_{PM}$ ~15–55]. Such compositions required a mantle source region to achieve the high $Mg^{\#}$, Cr and Ni, but also a significantly enriched component to explain the high LILE, Th and LREE. Archean sanukitoids are now recognized as a widespread, but minor (probably <<5% of Archean granitic rocks), component of many Archean terranes younger than c. 2.8 Ga (Shirey and Hanson, 1984; Stern and Hanson, 1991). The only older documented examples are the sanukitoids of the Sisters Supersuite (Smithies and Champion, 2000). In the case of these sanukitoids, Smithies and Champion (2000) showed that the high LILE content could not be a result of varying degrees of either magma mixing or assimilation of felsic crust. The enriched source component was most likely an addition to the mantle source region.

Smithies et al. (2004) suggested that c. 3120 Ma Whundo-like mafic crust and homogeneous sediment derived from old (>3.3 Ga) Archean terrains was subducted to the southeast beneath the protocrust of the Whim Creek and Mallina Basins, and that partial melts derived from the subducted sediments infiltrated the mantle wedge. Compared to the source for the boninite-like rocks and the siliceous high-Mg basalts, contamination of the source for the sanukitoids was by a component with a considerably lower ratio of old Pilbara-like crust to basaltic Whundo-like crust. The mantle source for the sanukitoids was metasomatized by the addition of up to 40% of slab-derived melt that would explain the more radiogenic Nd-isotopic compositions and the higher LREE concentrations and LREE/HREE ratios of the sanukitoids (Fig. 74), particularly if melting of the slab occurred at pressures high enough to stabilize garnet. If this is the case, then by c. 2950 Ma two distinct enriched mantle sources had developed beneath the central part of the Pilbara Craton. Since the combined geographical extent of the boninite-like rocks, siliceous high-Mg basalts, and sanukitoids shows complete geographical overlap and the entire magmatic period probably occurred within the narrow interval, between c. 2.955 Ga and c. 2.945 Ga, it is likely that the respective mantle source regions overlapped in space and time.

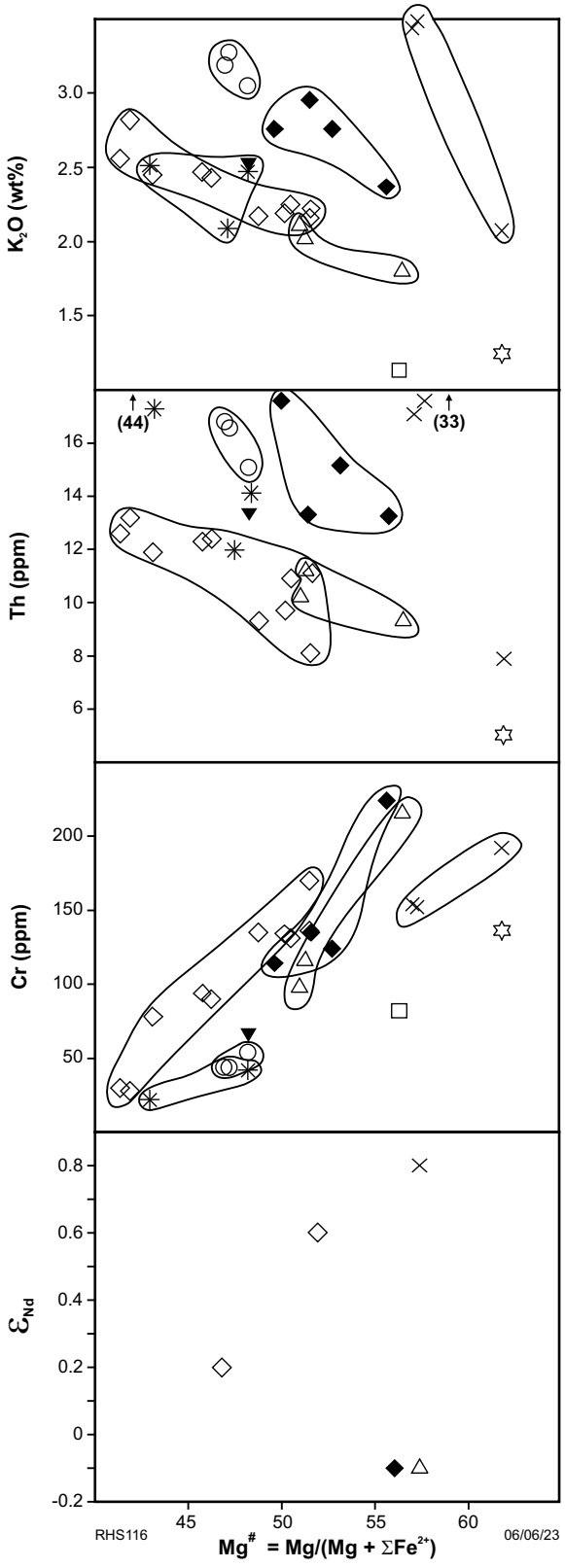

Figure 72. Compositional variation diagrams plotting $Mg^{\#}$ against K_2O, Th, Cr and $\varepsilon_{Nd(2.95\ Ga)}$ for high-Mg diorite (sanukitoids) of the Sisters Supersuite. Symbols define specific plutons as described by Smithies and Champion (2000): circles = Jallagoonina; open diamond = Peawah West; closed diamond = Peawah East; double cross = Mallindra; triangle = Jones Well; cross = Wallareenya; star = Stock 1; TTG = Tonalite–Trondhjemite–Granodiorite series (Smithies and Champion, 2000)

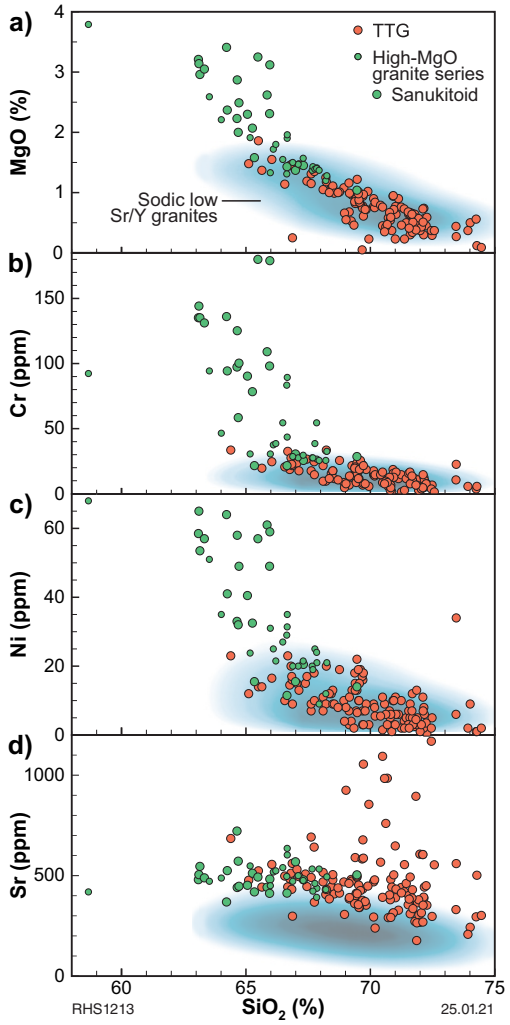

Figure 73. Compositional variation in MgO, Cr, Ni and Sr against SiO_2 for TTG and hornblende-bearing rocks of the high-MgO granite series. The blue field in each panel is a kernel density field enclosing 90% of the data for sodic low Sr/Y granites. Mesoarchaean (c. 2.95 Ga) hornblende diorite and granodiorite identified as sanukitoid (larger green dots) form the more primitive, mafic part of the high-MgO granite series, but also overlap extensively with Paleoarchaean hornblende granodiorites (smaller green dots) (after Smithies et al., 2021)

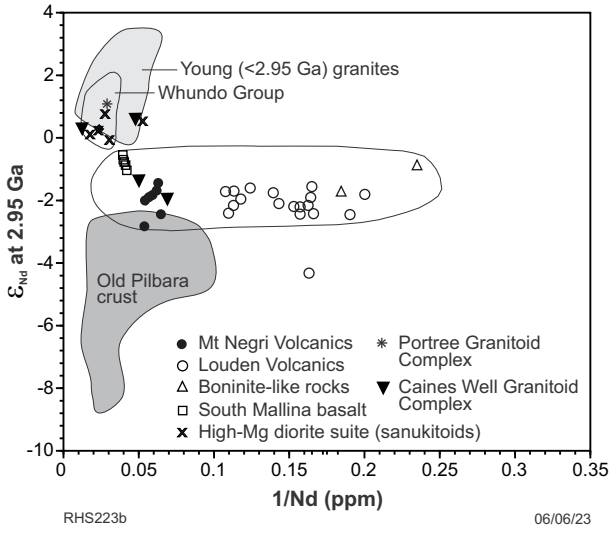

Figure 74. $\varepsilon_{Nd(2.95\,Ga)}$ vs 1/Nd diagram, comparing the isotopic compositions of the Mallina igneous rocks with regional sources of potential contamination. Errors are typically ±0.5 epsilon units (Smithies et al., 2004)

Enrichment of the mantle source regions might have occurred at c. 3010 Ma, the depositional age of the Whim Creek Group, but might be as old as c. 3120 Ma, the age of the subduction-related Whundo Group. The variably metasomatized sub-Mallina mantle remained essentially inert between c. 55 and 165 Ma until, at c. 2955 Ma, it was remobilized. Smithies and Champion (2000) attributed the late tectonothermal anomaly that caused this magmatism to either a plume or to active rifting of the Mallina Basin, whereas Smithies et al. (2004) and Van Kranendonk et al. (2007b) suggest it more likely relates to break-off of a fossil slab. The observation that slightly later (2940–2930 Ma) monzogranitic magmatism of the Sisters Supersuite becomes less voluminous and younger away from the Mallina Basin indicates that this tectonothermal anomaly was centred on the Mallina Basin.

Locality 5.2: Louden Volcanics (Bookingarra Group) in the Whim Creek greenstone belt (Zone 50, MGA 594288E 7702618N or 588557E 7688054N)

In the Whim Creek greenstone belt, the upper part of the Bookingarra Group is dominated by siliceous high-Mg basalt flows. Included within this unit are thin and discontinuous layers of laminated mudstone, and medium- to coarse-grained quartz sandstone. Two mafic volcanic formations are recognized — a lower Mount Negri Volcanics, and the upper Louden Volcanics. They show slight, but persistent, geochemical differences and are typically easily distinguished in the field — the Mount Negri Volcanics is variolitic and characterized by only fine spinifex texture, whereas the Louden Volcanics is never variolitic and forms units that include coarsely spinifex-textured varieties. In both cases, the spinifex texture is formed by acicular clinopyroxene, often with cores of either orthopyroxene or olivine. Deposition of both volcanic formations was almost entirely subaqueous, and although pillow structures are common, non-pillowed rocks are equally abundant, reflecting rapid rates of extrusion.

These localities provide a range of examples of pyroxene–spinifex textured flows, including rare examples of an ultramafic flow unit (Fig. 75). Although the two volcanic formations do show slight, but persistent, geochemical differences (Fig. 76), together they define a remarkably narrow range in various incompatible trace element ratios (e.g. La/Nb, La/Sm and La/Zr; Fig. 77). Other basaltic flows, interleaved with siliciclastic rocks in the southeastern part of the Croydon Group of the Mallina Basin (i.e. in the Mallina Formation and Constantine Sandstone), also share this distinct geochemical feature.

Locality 5.3: Roadside stop — unconformity between the Mallina Basin and the Fortescue Group (Zone 50, MGA 593972E 7695680N)

This is a quick roadside stop where, looking south, an angular unconformity can be seen between the folded rocks of the Mallina Basin and the flat-lying sedimentary rocks at the base of the Mount Roe Basalt, at the base of the Fortescue Group.

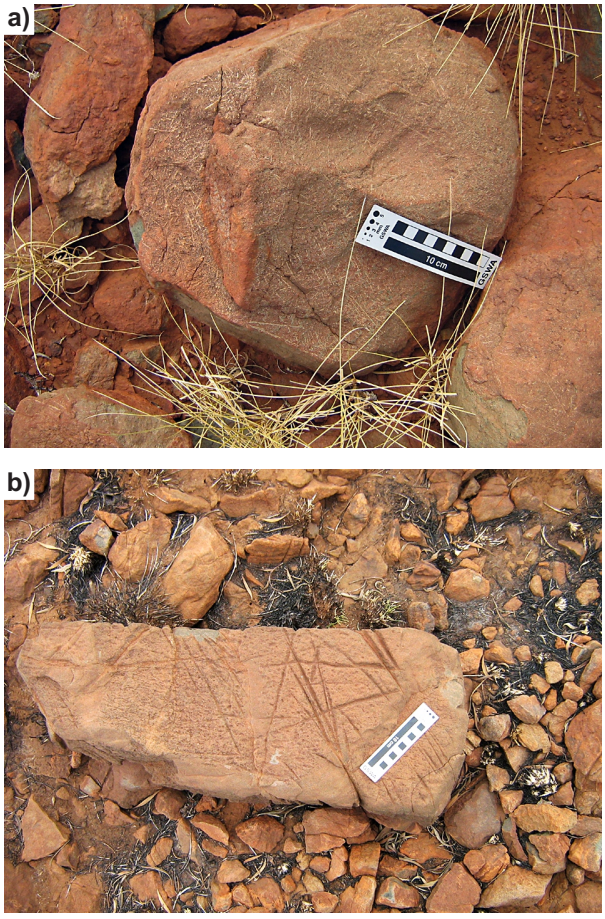

Figure 75. Coarse spinifex in rocks of the Louden Volcanics: a) mafic; b) ultramafic

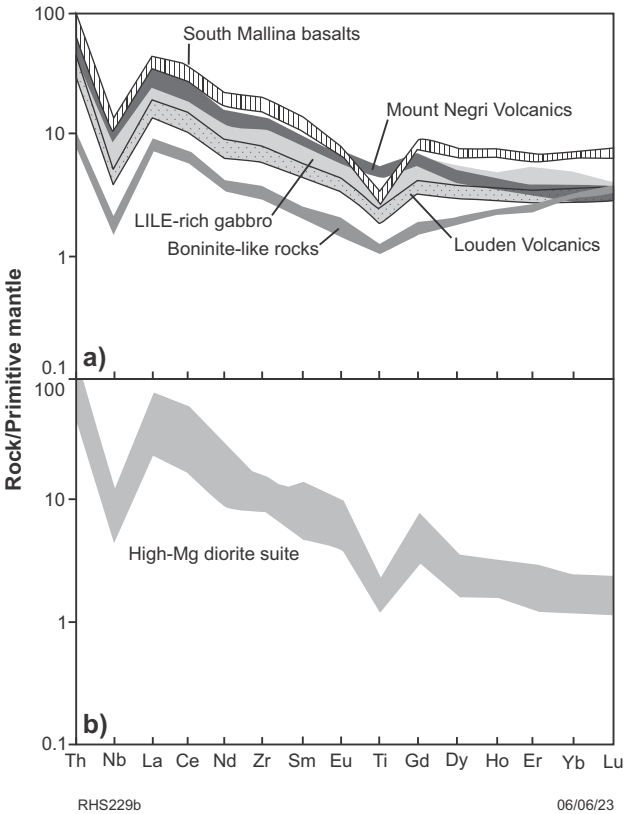

Figure 76. Primitive mantle normalized trace element diagrams for: a) the mafic lavas and intrusions of the Croydon Group; b) high-Mg diorite (sanukitoids) of the Sisters Supersuite. LILE = large ion lithophile element (Smithies et al., 2004)

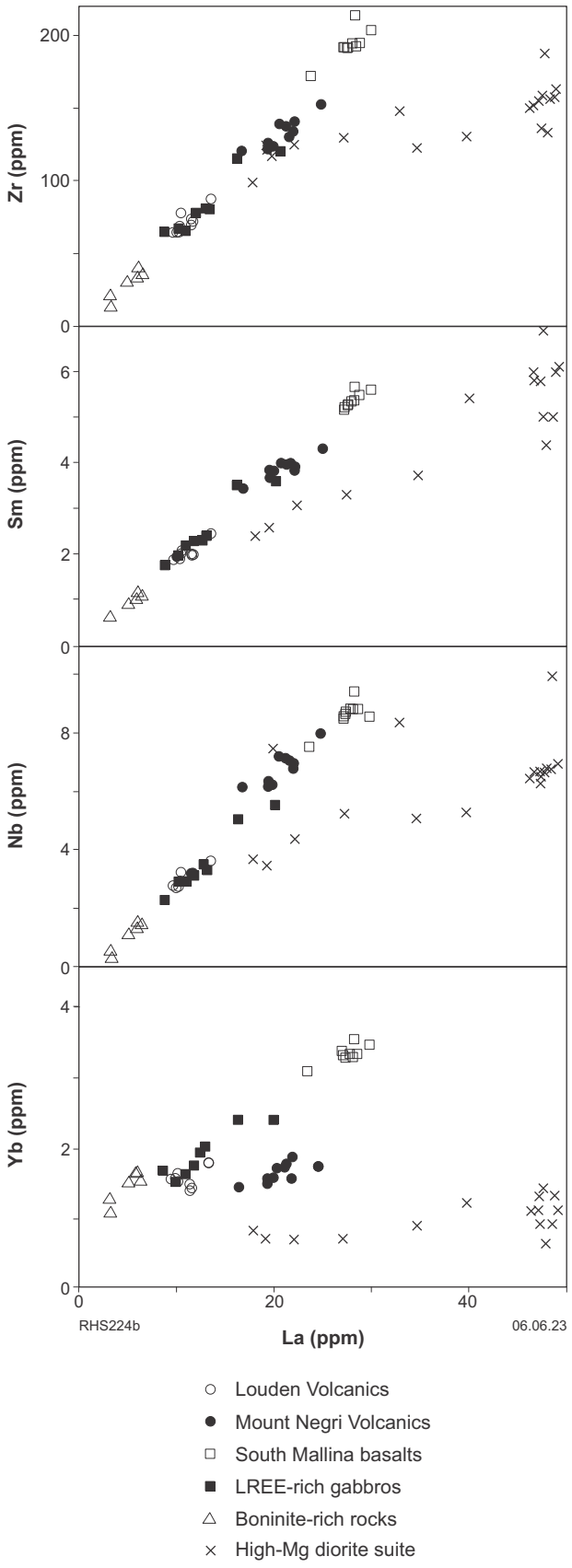

Figure 77. La vs Zr, Sm, Nb and Yb diagrams for the igneous rocks of the Mallina Basin. LREE = light rare earth element (Smithies et al., 2004)

Locality 5.4: (optional — time permitting) Siliceous high-Mg basalt flows in the Mallina Basin (South Mallina Basalt Member) — Croydon Group (Zone 50, MGA 586063E 7680635N)

Siliceous high-Mg basalt, interlayed with siliciclastic rocks of the Mallina Formation, forms a minor but important part of the Mallina Basin stratigraphy southeast of the Whim Creek greenstone belt. These high-Mg basalts range from massive to vesicular (Fig. 78) and locally show autobrecciation, both as flow-tops, and more commonly as hyaloclastite. Although these rocks can be distinguished geochemically from the mafic volcanic formations of the Bookingarra Group (Fig. 76), they share several important geochemical similarities with volcanic rocks from the Whim Creek greenstone belt. In particular, all of these lavas have a common, narrow range in various incompatible trace element ratios (e.g. La/Nb, La/Sm and La/Zr; Fig. 77).

To the southeast, within the core of the Croydon Anticline, the thickly developed Constantine Sandstone of the Croydon Group is tightly folded about a north-trending axis. In this area, two additional geochemically specialized mafic magma types — low-Ti tholeiitic intrusions and rocks with boninite-like compositions — are present within the contact areole of the c. 2935 Ma Satirist Monzogranite and the c. 2950 Ma Peawah Granodiorite. The rocks at this locality are typically strongly deformed and the nature of most contacts is not clear. Nevertheless, the low-Ti tholeiites are typically medium grained and appear to have intruded both the quartzite and the boninite-like rocks.

The boninite-like rocks outcrop over a strike length of more than 50 km, but their original extent has been obscured by intrusion of the Satirist Granite. They are typically a schistose assemblage of actinolite, chlorite and serpentine, with accessory epidote, talc, plagioclase and quartz. At other localities (e.g. on the southeastern edge of the Satirist Granite) that replicate this structural and stratigraphic setting, rarely preserved fine-grained quench textures, or, more commonly, medium-grained olivine-cumulate textures are preserved. The former include possible hopper-textured actinolite (after clinopyroxene) in a weakly metamorphosed plagioclase-bearing rock, and oriented pyroxene–spinifex textures. Despite evidence for quenching, no definitive evidence for an extrusive origin was found. The extensive continuity of this thin unit within coarse-grained sedimentary rocks that were deposited in a high-energy environment favours an intrusive (subvolcanic) origin.

According Smithies (2002), low-Ti tholeiites and boninites form an association typical of arc settings, with geological evidence suggesting that the Mallina Basin formed in an intracontinental setting. Smithies (2002) and Smithies et al. (2004) suggest that mantle source regions for these rocks were locally to regionally modified during a previous subduction event (perhaps related to formation of the Whundo Group, or subduction of Whundo-type material during formation of the Whim Creek Group), and remelted during a subsequent event, perhaps related to removal of a fossil slab at c. 2955 Ma (e.g. Van Kranendonk et al., 2007b).

The low-Ti tholeiite relates to a mantle source already depleted during a previous mantle melting event, whereas the source for the boninite-like rocks suggests that this depleted source was modified by addition of an enriched, subduction-related, component prior to mantle melting. Trace element data show that the component that enriched the mantle source of the boninite-like rocks was the same component identified in the mantle source for the mafic lavas of the Bookingarra Group and for the South Mallina Basalt Member (Smithies et al., 2004). This same enriched component can also be identified in the source of similarly aged siliceous high-Mg basalts and dolerites as far northwest as the Cleaverville area (Smithies et al., 2004), to the east and northeast across the northern margin of the East Pilbara Terrane (Salt Well Member), and on the northeastern margin of the East Pilbara Terrane (Smithies et al., 2007b; Van Kranendonk et al., 2007b; Pease et al., 2008).

Smithies et al. (2004) suggested that c. 3.12 Ga Whundo-like mafic crust and homogeneous sediment derived from old (>3.3 Ga) Archean terrains was subducted to the southeast, and that partial melts derived from the subducted sediments infiltrated the mantle wedge. Resulting metasomatism was homogeneous in regards to ratios involving LREE and Zr, at least over an area large enough to provide the source that later produced the boninite-like rocks and the siliceous high-Mg basalts.

AHH410 06.08.10

Figure 78. Rarely preserved volcanic structures in siliceous high-Mg basalt flows of the South Mallina Basalt Member

Day 6: West Pilbara Superterrane

Locality 6.1: Warambie Basalt and Red Hill Volcanics, Whim Creek Basin, near Red Hill (Zone 50, MGA 555230E 7682950N)

Localities 6.1 and 6.2 are located in the Whim Creek greenstone belt, which contains all exposures of the Whim Creek Group and the most northwesterly exposures of the Bookingarra Group. The geology of the Red Hill area is shown in Figure 79. Coarse basal breccia at this locality represents the lowest part of the Warambie Basalt, composed of angular boulders of basalt and granite within a poorly sorted coarse sandstone/granulestone matrix (Fig. 80). The granite boulders were derived from the adjacent Caines Well Granite, which elsewhere includes rocks as old as 3090 Ma (GSWA 118965: Nelson, 1997a). Approximately 1.5 km to the west, the Warambie Basalt unconformably overlies amphibolite facies metabasalt of the 3130–3110 Ma Whundo Group. The basal breccia is interpreted to be derived from basement uplift and erosion, and may be proximal to a syndepositional fault related to 3010 Ma extension. Transport of the granite blocks was likely to have been by clast rolling and sliding.

The Warambie Basalt contains a range of sheet lava types, including thick (~24 m) tabular flows and thin (0.5 – 2 m) irregular flows. At this level, the Warambie Basalt is dominated by coherent lava with lesser autobreccia and rare hyaloclastite. Vesicle layers occur within the basaltic lavas, which also include aphanitic and many plagioclase–glomeroporphyritic types.

Dark grey dacitic rocks of the Mons Cupri Dacite Member of the Red Hill Volcanics are encountered about 200 m southwest of the basal Warambie Basalt (at MGA 555150 7682800). The dacite is wholly coherent and contains a spherulitic matrix indicative of high-temperature devitrification of volcanic glass. The dacite also contains plagioclase phenocrysts and abundant, cherty fragments that may be early formed crystals.

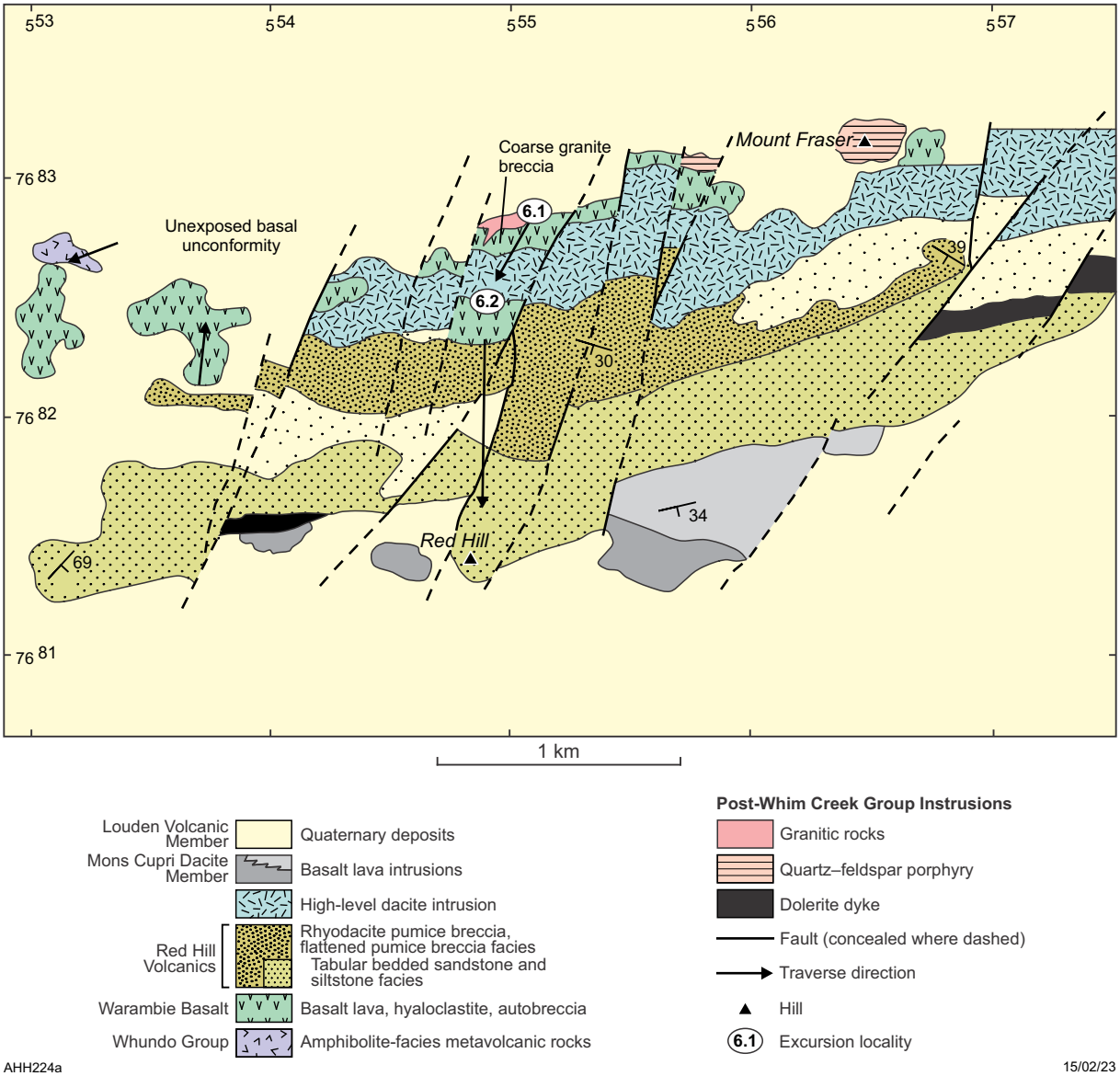

Figure 79. Simplified geological map of the Red Hill area in the Whim Creek greenstone belt, showing Excursion Localities 6.1 and 6.2

AHH411 06.08.10

Figure 80. Coarse basal breccia of the Warambie Basalt at Locality 6.2. Angular boulders of basalt and granite are set in a poorly sorted sandstone/granulestone matrix

Locality 6.2: Traverse across the Red Hill Volcanics at Red Hill (Zone 50, MGA 554950E 7682450N)

At the beginning of the short (a few hundred metres) traverse, dark grey basaltic breccia has an irregular contact with the upper surface of the dacite observed at the last locality. Tracing out the contact reveals a lobate upper margin to the dacite that may be original topography. However, the preferred interpretation (Pike, 2001) is that this highly irregular contact is the result of injection of dacite into the basaltic breccia. If this interpretation is correct, then the presence of spherulitic matrix in the dacite suggests a relatively high level of emplacement (subvolcanic sill?). The basaltic breccia is jigsaw-fit and is composed of dark grey aphanitic clasts with distinct, margin-parallel banding. There are rare, wispy apophyses of the same material that are clearly not clasts. The breccia is an excellent example of hyaloclastite in which basaltic magma has undergone quenching in the presence of water. The clasts have rapidly contracted and shattered in situ. Clast-rotated breccias may indicate limited movement. The basaltic apophyses represent 'fingers' of basaltic magma that have remained whole, perhaps protected by the breccia carapace.

The flat ground at the start of the 500-m traverse from Locality 6.2 to a position (MGA 554950E 7681950N) 300 m northwest of Red Hill (Fig. 79) is underlain by centimetre- to decimetre-scale tabular beds of shard-rich volcaniclastic rocks. These rocks outcrop only in deep creek beds and are easily overlooked when overgrown. Interpretation is difficult due to limited outcrop, but they appear to be the medial to distal products of turbidity currents. Pumice-rich breccia underlies much of the traverse. The first outcrops contain both dense and pumiceous breccia in massive beds. This volcaniclastic material is rhyodacitic in composition. This angular volcaniclastic breccia represents the onset of felsic volcanism and probably resulted from debris flows derived from adjacent volcanic areas.

To the south, Red Hill is composed entirely of angular tube pumice breccia. The matrix to the pumice breccia is glass-shard sandstone. The pumice breccia lacks bedding, has a monomictic composition and represents synvolcanic sedimentation. The large amount of pumiceous material points to an ignimbrite origin, as does the presence of relic shard textures. A sample of the breccia, collected 50 m west of the fence line and 300 m northwest of Red Hill, gave a U–Pb SHRIMP zircon an age of 3009 ± 4 Ma (GSWA 141936: Nelson, 1998e). Individual concordant or slightly discordant zircon grains gave $^{207}Pb/^{206}Pb$ ages between 3150 and 2995 Ma, confirming a significant detrital component in the rock, with possible sources including the Whundo Group and Railway Supersuite.

West Pilbara Superterrane — rifted margin and subduction-related 'arc' magmatism

The West Pilbara Superterrane forms the northwestern 20% of the exposed Pilbara Craton, and outcrops between Port Hedland and Cape Preston (Fig. 67). The superterrane is a collage of the 3270–3250 Ma Karratha Terrane (containing the Ruth Well Formation and Cleland Supersuite, and is interpreted to be a rifted fragment of the East Pilbara Terrane), the c. 3220 Ma Nickol River Formation, the c. 3200 Ma Regal Terrane (a 2 km-thick basalt succession of the Regal Formation), and the 3130–3100 Ma Sholl Terrane (containing the Whundo Group volcanics and Railway Supersuite). These terranes accreted during collision with the East Pilbara Terrane at 3070 Ma (Van Kranendonk et al., 2010). This collision, accompanied by granitic magmatism forming the Elizabeth Hill Supersuite and various types of deformation, is referred to as the Prinsep Orogeny.

The most distinctive tectonic feature of the West Pilbara Superterrane is a northeasterly structural grain, defined by the elongation of granitic complexes and the trend of greenstone belts, and by numerous closely spaced east and northeast-striking strike-slip faults. The Karratha and Sholl Terranes are separated by the 1–2 km-wide Sholl Shear Zone that bisects the West Pilbara Superterrane over an exposed length of 250 km (Fig. 67). The Sholl Shear Zone is steeply inclined to the northwest and is composed of mylonite and schist derived from granitic, volcanic and intrusive rocks. The Karratha Terrane and the overlying Regal Terrane outcrop north of the Sholl Shear Zone and are everywhere separated by the Regal Thrust (Fig. 67). The structural geology of the West Pilbara Superterrane and the geochemistry of its volcanic and granitic rocks suggests processes at least superficially similar with Phanerozoic-style plate tectonic processes (Van Kranendonk et al., 2007b, 2010).

The Whundo Group (Sholl Terrane), in particular, remains exceptional among Archean volcanic sequences (other than perhaps the Mesoarchean sequences of the Youanmi Terrane in the Yilgarn Craton; Lowrey et al., 2019) in that it preserves a range of independent geological and geochemical features that together provide compelling evidence of modern-style subduction processes (Smithies et al., 2005a, 2007c). The group includes boninites, interlayered tholeiitic and calc-alkaline volcanics, Nb-enriched basalts and adakites. Decreasing La/Sm and La/Yb ratios correlate with decreasing LILE, Cr, Ni and $Mg^{\#}$ values, and with increasing values of Nb, Zr and Yb, providing evidence for flux melting of an Archean mantle wedge. Although high Ba/La ratios reflect fluid-mediated source metasomatism, a systematic decrease in Ba/La suggests an increasing slab melt component up the stratigraphic pile of calc-alkaline volcanics, culminating in the eruption of adakitic rocks and Nb-enriched basalts. Low Th/La (0.07 – 0.14) and Ce/Yb

(<40) ratios, and a lack of evidence for a felsic basement to the Whundo Group, point to a setting free of significant compositionally evolved contaminants (e.g. 'continental crust') as might be found, in a modern plate tectonic context, in an intra-oceanic arc setting.

Karratha Terrane

The main components of the Karratha Terrane are the >3270 Ma Ruth Well Formation (Roebourne Group) and the 3270–2760 Ma Karratha Granodiorite that intrudes this formation (Fig. 67). The Karratha Granodiorite is the same age as the oldest granitic intrusions of the Cleland Supersuite in the East Pilbara Terrane. In the Cherratta Granitic Complex, south of the Sholl Shear Zone, the 3236 Ma Tarlwa Pool Tonalite is the same age as younger granites of the Cleland Supersuite in the East Pilbara Terrane and is therefore also included in this supersuite (Van Kranendonk et al., 2006b). The Ruth Well Formation, which is almost entirely composed of undated ultramafic–mafic volcanic rocks, is unconformably overlain by the sedimentary Nickol River Formation (Hickman, 2016).

The Ruth Well Formation is up to 2000 m thick and consists of metamorphosed ultramafic and mafic volcanic rocks (peridotite to tholeiitic basalt) with a few thin chert intercalations. No stratigraphic base is preserved, lower contacts being either tectonic or intrusive. As it is intruded by the Karratha Granodiorite, the formation must be older than 3270 Ma. Its maximum depositional age is currently very poorly constrained, but likely less than c. 3450 Ma, based on depleted mantle extraction (Nd T_{DM} model) ages (Arndt et al., 2001; Smithies et al., 2007b).

The c. 3270 Ma Karratha Granodiorite ranges from tonalite to granodiorite (GSWA 142433: Nelson, 1998f; Smith et al., 1998). Much older Nd T_{DM} model ages of 3480–3430 Ma from this intrusion (Sun and Hickman, 1998) indicate that magma generation involved older crust or enriched lithospheric mantle, as for the Cleland Supersuite in the East Pilbara Terrane (data in Smithies et al., 2007b). For these reasons, the Karratha Terrane has been interpreted as a rifted fragment of the East Pilbara Terrane.

Nickol River Formation

From its type area around Roebourne and the Nickol River, the Nickol River Formation outcrops almost continuously for 100 km southwestwards, where it extends beneath the Fortescue Group within 25 km of the Fortescue River. The stratigraphy of the formation is dislocated by numerous low-angle thrusts within a regional-scale zone of tectonic transport, referred to as the Regal Thrust (Hickman, 2001a). The formation is well exposed south of Mount Regal, where basal quartzite and chert are overlain by metamorphosed ferruginous shale, banded iron-formation (BIF) and carbonate rocks. The sedimentary rocks are extensively sheared, and mesoscopic recumbent folds are visible in outcrop. Near the Lower Nickol mining area, 20 km east of Mount Regal, Kiyokawa et al. (2002) referred to the same formation as the 'Lydia Mine complex' (informal name), and reached the same conclusion as Hickman (2001a) that these rocks underlie a major thrust. They interpreted the formation to have originated as a continental shelf deposit unconformably overlying the Karratha Granodiorite and recorded the presence of metamorphosed pebbly sandstone in the formation, in agreement with Hickman and Smithies (2001). Metasandstones of the formation contain rounded clasts of black chert and altered volcanic rocks most likely derived from erosion of the Ruth Well Formation. Black chert conglomerate mapped on the northwestern coast at Cleaverville (Kiyokawa and Taira, 1998) underlies pillow basalts of the Regal Formation, suggesting that the Nickol River Formation may also be present on the northwest limb of the Cleaverville Synform (Fig. 81).

In the Lower Nickol area, schistose metasandstone of the formation was dated at 3269 ± 2 Ma (GSWA 136819: Nelson, 1998d), a date consistent with the derivation of detrital zircon by erosion of the underlying Karratha Granodiorite. Southeast of Mount Regal, metamorphosed carbonate rocks and ferruginous chert found locally at the base of the formation (in tectonic contact with the underlying Ruth Well Formation) contain metamorphosed porphyritic rhyolite (probably a deformed intrusion). Using the SHRIMP U–Pb zircon method, the crystallization age of this rock was interpreted as 3251 ± 6 Ma (GSWA 118975: Nelson, 1997c), with older zircons, of similar age to the Karratha Granodiorite, interpreted to represent a xenocrystic population. Nelson (1997c) interpreted concordant and slightly discordant zircons younger than the 3251 Ma population as having lost radiogenic Pb, but an alternative interpretation is that the 3251 Ma population is xenocrystic, and the crystallization age is closer to that of the youngest concordant zircon dated at c. 3217 Ma. Deposition of the Ruth Well and the Nickol River Formations was probably separated by at least 20 million years, and possibly more than 50 million years. During that time, the Karratha Granodiorite was intruded into the Ruth Well Formation and then eroded, suggesting that the Ruth Well Formation and Nickol River Formation should not be assigned to the same group (Roebourne Group). The Nickol River Formation could be an analogue of the c. 3200 Ma Soanesville Group, a volcanic+clastic succession that unconformably overlies the northwestern margin of the East Pilbara Terrane (Van Kranendonk et al., 2010) on the opposite side of the inferred c. 3200 Ma oceanic basin consumed and sutured beneath the Mallina Basin.

Regal Terrane and the Regal Thrust

The Regal Terrane is composed of the Regal Formation, a 2–3 km-thick sequence of metamorphosed pillow basalt, local basal komatiitic peridotite and rare chert. Sills of dolerite and gabbro intrude the formation. In all areas except Cleaverville, the formation has been metamorphosed to amphibolite or upper greenschist facies. Lower-grade metamorphism in the succession at Cleaverville is attributed to separation from the main outcrop area by large faults, resulting in only the topmost part of the formation being exposed. Pillow basalt units at Cleaverville, here also assigned to the Regal Formation, were informally named as different formations by Kiyokawa and Taira (1998).

The Regal Terrane is separated from the underlying Karratha Terrane by the Regal Thrust zone, which is mainly composed of tectonically deformed slices of the Nickol River Formation. Nd-isotopic data (Smithies et al., 2007b) indicate an approximate depositional age of 3200 Ma for the Regal Formation (Van Kranendonk et al., 2007b), in agreement with a U–Pb zircon age of c. 3195 Ma obtained from a thin felsic tuff unit in the correlative, informally named, Dixon Island Formation at Cleaverville (Kiyokawa et al., 2002). The Dixon Island Formation has been recognized only on Dixon

Island and in isolated exposures on Cleaverville Beach, where it underlies pillow basalts of the Regal Formation. The minimum age of the Regal Formation is c. 3160 Ma, based on the age of a thermal event that metamorphosed it, the Karratha Granodiorite and the Ruth Well Formation (Kiyokawa, 1993; Smith et al., 1998; Beintema, 2003).

The lithological composition (pillow basalt and rare thin chert units) and geochemistry (MORB-like) of the Regal Formation are suggestive of oceanic crust (Ohta et al., 1996; Kiyokawa and Taira, 1998; Sun and Hickman, 1998; Beintema, 2003), although the absence of sheeted dykes casts doubt on a mid-ocean ridge origin. Interpretation of the Regal Formation as a slice of oceanic crust (ophiolite) is consistent with its flat REE patterns, lack of evidence of crustal contamination, and ε_{Nd} of +3.5, which is close to the depleted mantle value (3.2) at 3200 Ma (Smithies et al., 2007b).

Across 3000 km^2 of the northwest Pilbara, the Regal Formation is sandwiched between the underlying Karratha Terrane and the overlying Cleaverville Formation. Although this is probably not the case at Cleaverville, the Cleaverville Formation overlies continental crust elsewhere in the Pilbara Craton, potentially suggesting that, despite being composed of BIF, chert and generally fine-grained clastic sedimentary rocks, the Cleaverville Formation might not be considered a deep-water oceanic deposit.

The Regal Thrust forms the contact between the Regal Formation and the Karratha Terrane (Hickman, 2001a; Hickman and Smithies, 2001) over the entire west Pilbara north of the Sholl Shear Zone (Figs 81, 82). Way-up evidence from pillow structures in the Regal Formation confirms the continuity of the structural succession over a strike length of at least 100 km (Fig. 82). The uppermost thrust plane immediately underlies tectonically stretched and flattened basaltic rocks of the Regal Formation and includes several mylonite units several metres thick. Below this level, there is a zone of tectonic lensing up to 1 km thick in which the Nickol River Formation is broken into numerous tectonic slices bound by mylonites. These mylonites contain refolded isoclinal folds, the orientation of which led Hickman (2001b, 2004) to suggest that transport (obduction of oceanic crust) of the Regal Terrane was from the north or northwest. However, Kiyokawa et al. (2002) and Van Kranendonk et al. (2006b) instead suggested that the Regal Formation could have been thrust across the Karratha Terrane from the south or southeast, the direction where oceanic crust is interpreted to have existed after 3200 Ma. Establishing the direction of tectonic transport of the Regal Thrust is complicated by the effects of several later phases of deformation (described below), which added shearing and folding to the thrust-related fabrics.

The age of the Regal Thrust must be between 3160 and 3070 Ma. If thrusting occurred at 3160–3150 Ma (Hickman et al., 2001; Hickman, 2001b; Beintema, 2003), it is unlikely to have been from the south or southeast, because at that time the southeastern area was in an extensional setting. However, if the thrusting occurred during the Prinsep Orogeny at 3070 Ma, it would have been related to the plate collision that formed the West Pilbara Superterrane. Kiyokawa et al. (2002) suggested that thrusting could have occurred as late as 3020 Ma, although that seems improbable given that it must then also have involved the 3130–3110 Ma Whundo Group, which was in tectonic contact with the Karratha Terrane from 3070 Ma. After c. 3010 Ma, and most probably at c. 2950 Ma, the Regal Thrust was folded by major upright folds, so that the thrust and the overlying Regal Formation outcrop on three fold limbs (Figs 81, 82).

Sholl Terrane

The Sholl Terrane comprises the 3130–3110 Ma Whundo Group (see below) and the 3130–3110 Ma Railway Supersuite (Figs 81, 82). Most Railway Supersuite outcrops are within the Cherratta Granitic Complex, but mafic and felsic intrusions of the supersuite also intrude the lower stratigraphic levels of the Whundo Group. The Sholl Terrane was intruded by granitic rocks of the Elizabeth Hill Supersuite during its collision with the Karratha Terrane at 3070 Ma (Prinsep Orogeny).

Prinsep Orogeny and Elizabeth Hill Supersuite

Plate convergence, signalled by the eruption of the 3130–3110 Ma Whundo Group and intrusion of the Railway Supersuite, eventually led to accretion of three terranes (Karratha, Regal and Sholl) to form the West Pilbara Superterrane at 3070 Ma (Van Kranendonk et al., 2006b). At the same time, the West Pilbara Superterrane collided with the East Pilbara Terrane, accompanied by extensive intrusion of 3070 Ma granites (Elizabeth Hill Supersuite) along the northwestern margin of the East Pilbara Terrane. This northwest–southeast collision resulted in the Prinsep Orogeny, which included low-angle thrusting on the Regal Thrust and Maitland Shear Zone, and major sinistral strike-slip movement (at least 200 km) on the Sholl Shear Zone. The Elizabeth Hill Supersuite intrudes both the West Pilbara Superterrane and the western part of the East Pilbara Terrane, and is defined as separate from either of these older, major tectonic units. In the west Pilbara, the Elizabeth Hill Supersuite is represented by the Cliff Pool Tonalite, which outcrops over 70 km^2 as part of the Cherratta Granitic Complex east of the Munni Munni Intrusion, and possibly also by gneiss in the Caines Well Granitic Complex. A sample of the Cliff Pool Tonalite (GSWA 142661: Nelson, 1998a), collected approximately 6 km south-southeast of the Elizabeth Hill mine, was dated by Nelson (1998g) at 3068 ± 4 Ma. The Cliff Pool Tonalite is a foliated biotite tonalite, which includes xenocrystic zircons of Railway Supersuite age, supporting the field observation of an intrusive relationship to the c. 3130 Ma Pinnacle Hill Gneiss. Its northern contact with this gneiss is diffuse and interlayered, with sheets of the tonalite intruding rafts of the gneiss. The southern contact of the tonalite is intruded by granitic rocks of the 3000–2980 Ma Maitland River Supersuite.

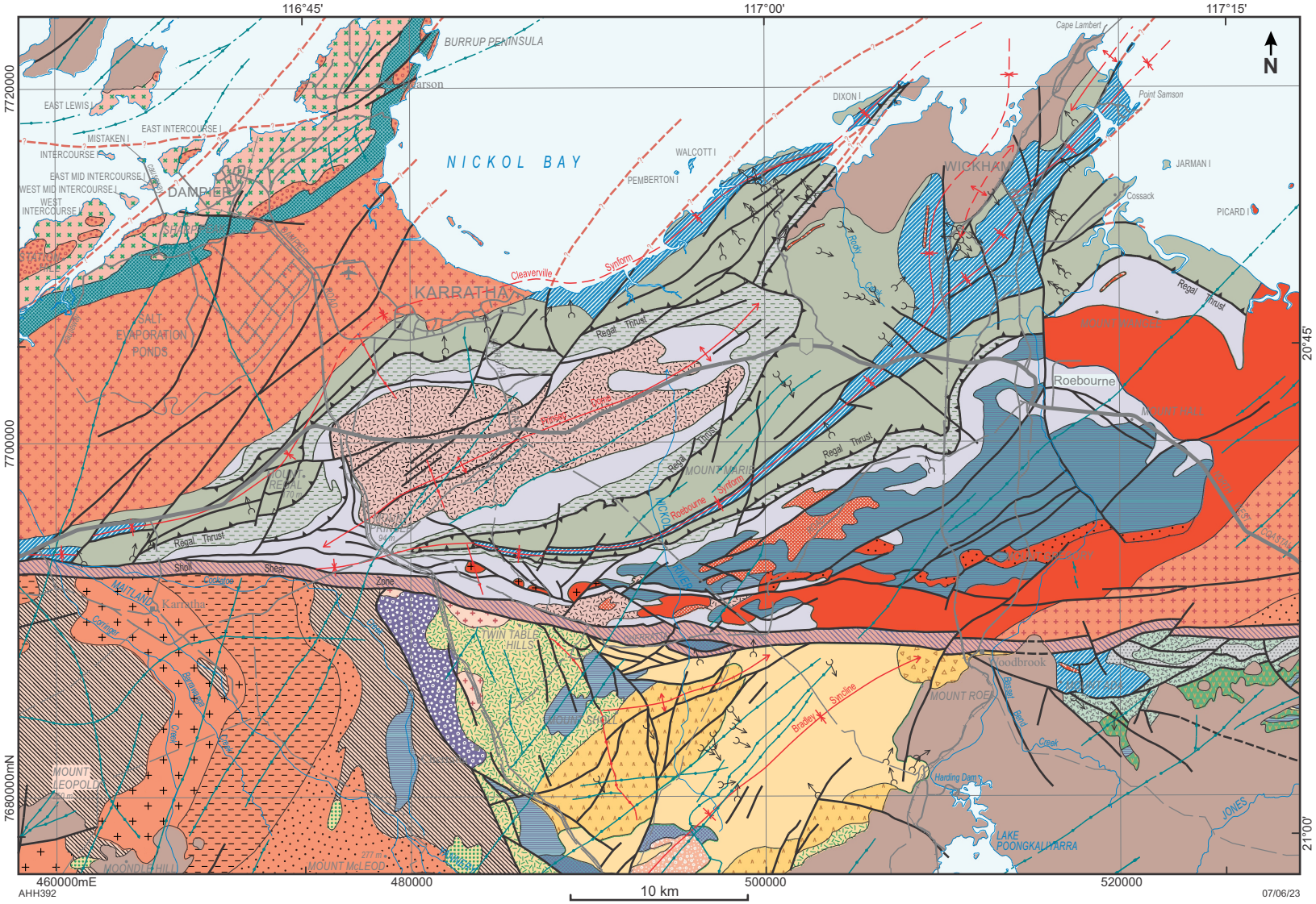

Figure 81. Geological map of the Roebourne–Karratha area, showing major structures and way-up evidence (from pillow structures) in the Regal Formation

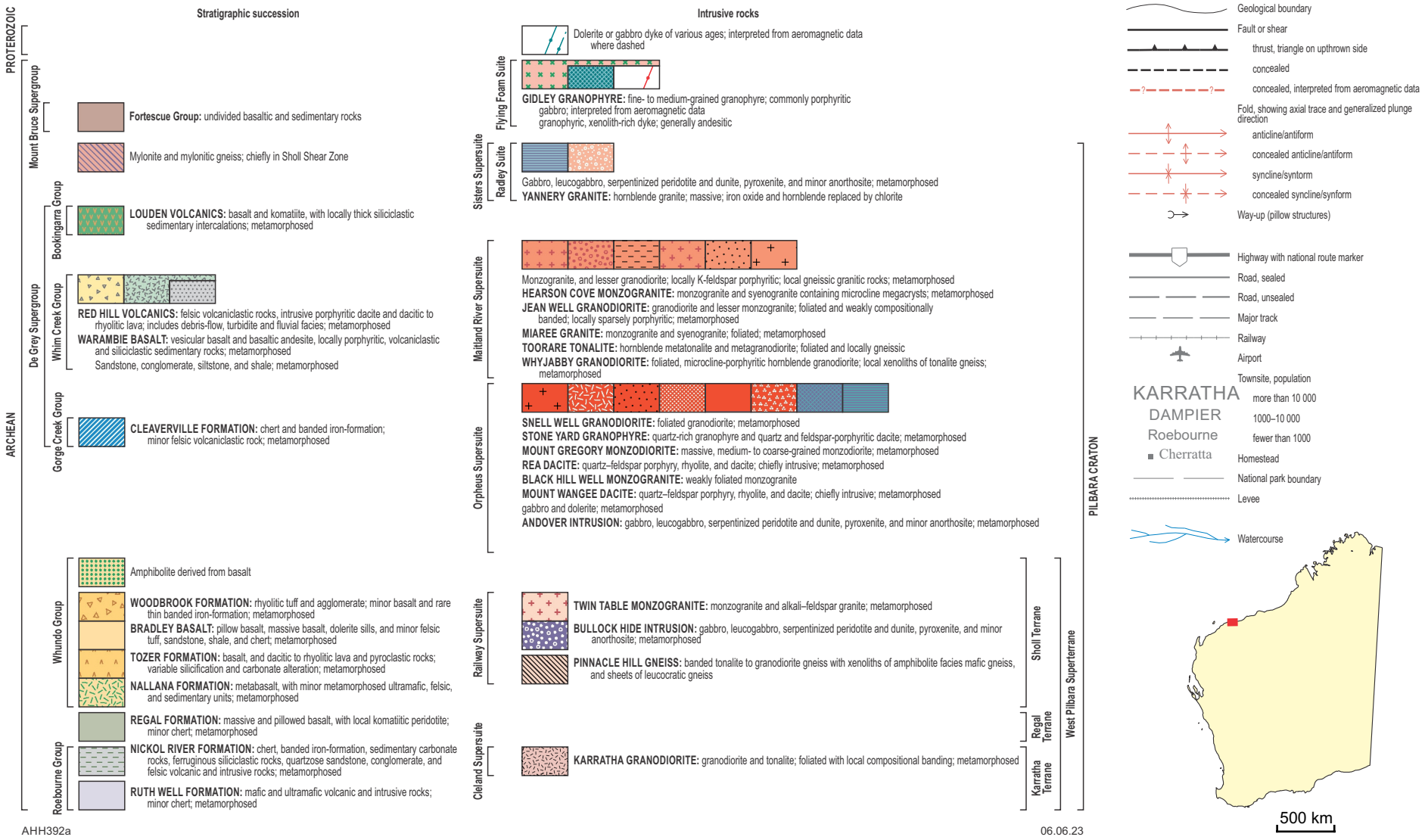

Figure 81. continued

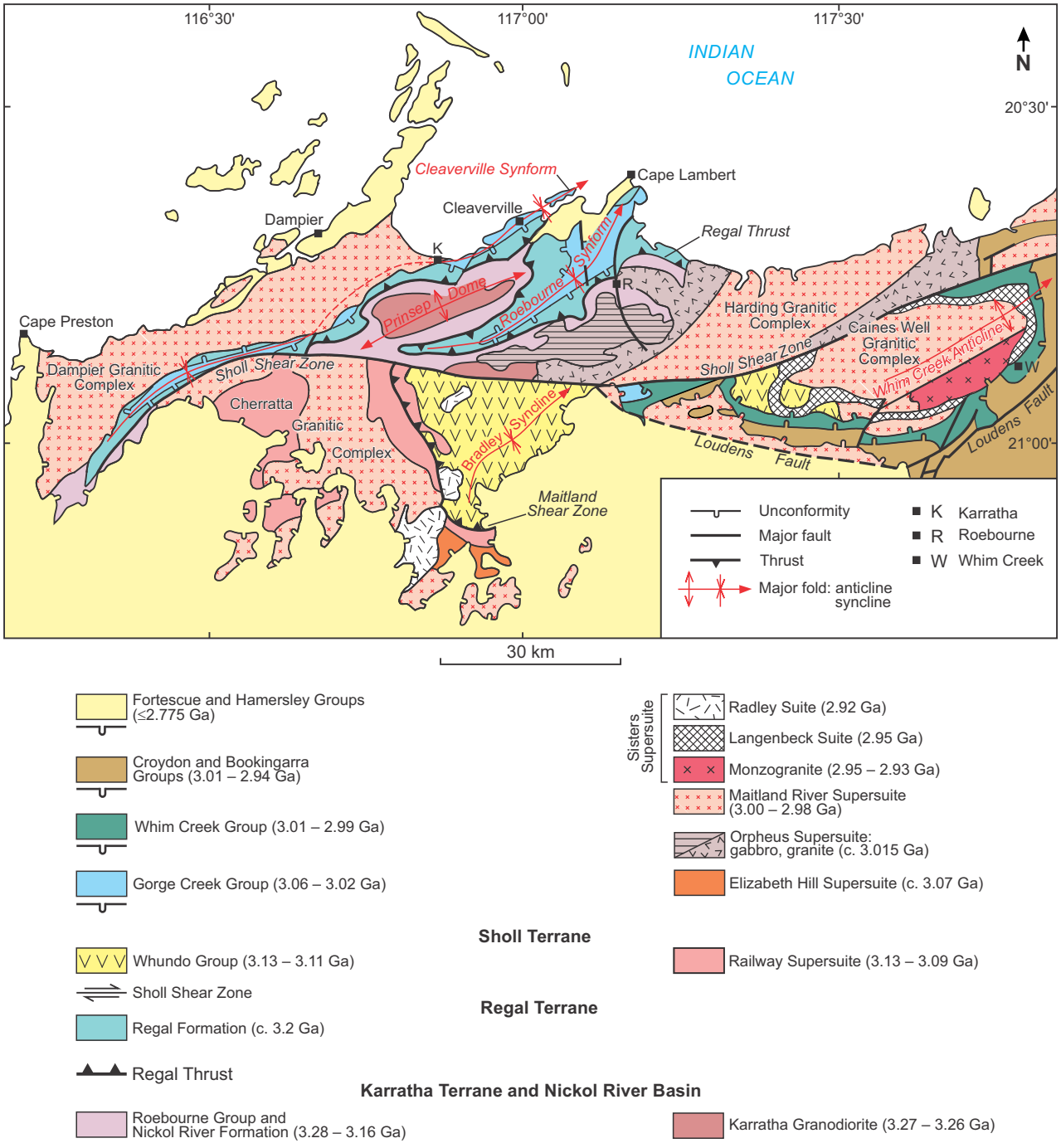

Figure 82. Simplified geological map of the northwestern Pilbara Craton, showing lithostratigraphy, tectonic units and major structures

Locality 6.3: Komatiite flows in the Ruth Well Formation, Roebourne Group, at Mount Hall (Zone 50, MGA 520770E 7701337N)

Roadside exposures at Mount Hall provide one of the few accessible exposures of well-preserved sheaf and random spinifex-textured ultramafic komatiite flows in the Ruth Well Formation. Olivine plates (pseudomorphed by serpentine and tremolite) are up to 50 cm long (Fig. 83). Microscopic examination of the sheaf spinifex texture reveals a highly magnesian rock comprised mainly of tremolite, serpentine, chlorite, and a pale yellow, birefringent phyllosilicate (probably vermiculite). Serpentine, and tremolite or vermiculite has replaced olivine blades. Tremolite and serpentine also form very fine intergrowths, and chlorite forms randomly oriented flakes. Opaque minerals are disseminated through the rock as anhedral grains and granular aggregates, and as discontinuous linings along narrow fractures or veinlets. Some of the opaques have a translucent, reddish-brown character around their outer margins, suggesting they are iron oxides such as hematite. Layers of different spinifex texture indicate that the ultramafic flows are about 2 m thick.

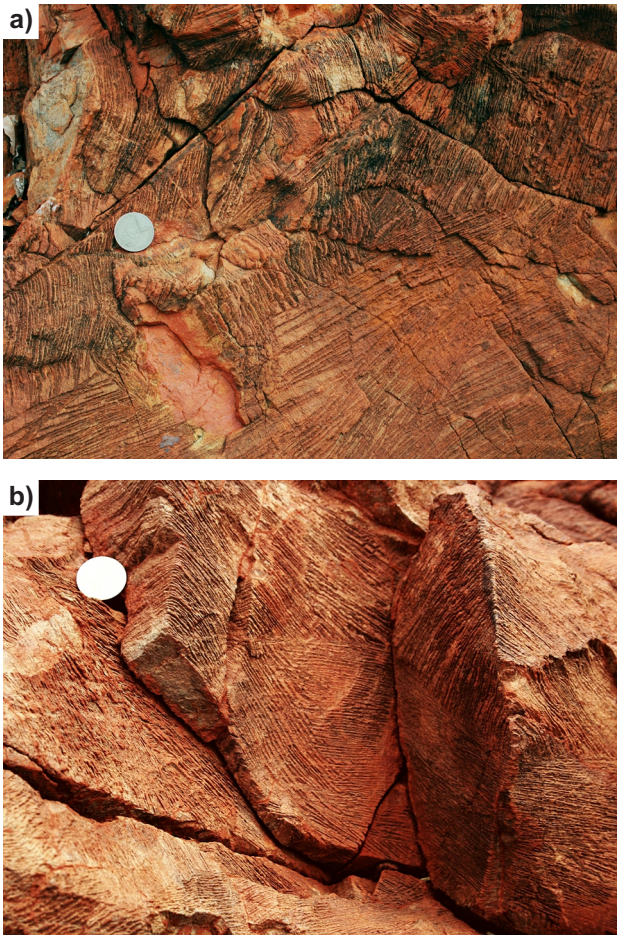

Figure 83. Bladed olivine–spinifex texture in a komatiite flow of the Ruth Well Formation at Mount Hall: a) platy olivine crystals, pseudomorphed by serpentine, tremolite and chlorite, up to 50 cm long; b) close-up of interlocking olivine crystals. Scale in both images: 3 cm-diameter coin

The komatiitic flows are overlain by a thin unit of quartzite and ferruginous chert, the bedding in which shows that the succession dips 30 to 50° southwards. Further south, this is overlain by amphibolite (metabasalt), with gabbro, pyroxenite and serpentinized peridotite of the Andover Intrusion. At Mount Wangee, 7 km to the north, similar spinifex-textured ultramafic flows are overlain by massive and pillowed basalts of the Regal Formation, but the succession in that area dips northwestward. There are no Archean exposures between these localities, but aeromagnetic data indicate that the Harding Granitic Complex underlies Cenozoic deposits of the coastal plain. The opposing inclinations of the Ruth Well Formation at Mount Hall and Mount Wangee indicate that the Harding Granitic Complex occupies the core of an anticline in the Ruth Well Formation.

The Sholl Terrane: 3130–3115 Ma arc volcanics (Whundo Group) accreted against the Karratha and Regal Terranes along the Sholl Shear Zone

The Whundo Group is divided into four lithostratigraphic formations (Fig. 81). No stratigraphic base is exposed, but the group is interpreted to have been deposited above c. 3200 Ma oceanic crust. The exposed basal contact is the Maitland Shear Zone, which separates the Whundo Group from the Railway Supersuite of the Cherratta Granitic Complex, and which was a low-angle thrust prior to folding at c. 2950 Ma. The northern contact of the group is defined by the Sholl Shear Zone and the group is unconformably overlain by the Gorge Creek, Whim Creek and Fortescue Groups.

The lowest formation preserved is the >2.0 km-thick Nallana Formation of metabasalt, ultramafic rocks, intermediate pyroclastic rocks and dolerite sills. The conformably overlying Tozer Formation is 2.5 km thick and contains basalt, andesite, dacite, rhyolite and thin metasedimentary units. The conformably overlying Bradley Basalt is more than 4 km thick and consists of metamorphosed, and massive and pillowed basalt, with komatiitic basalt near its base. The Bradley Basalt is conformably overlain by felsic volcanic rocks of the Woodbrook Formation, which comprises weakly metamorphosed rhyolite tuff and agglomerate, and only minor metabasalt.

A detailed chemostratigraphic analysis of the Whundo Group (Smithies et al., 2005a) revealed that it developed from a more complex set of igneous processes than can be identified from lithological mapping (Figs 84, 85). A lower volcanic package (Nallana and lower Tozer Formations) contains calc-alkaline and boninite-like rocks; the middle package (upper Tozer Formation and lower Bradley Basalt) consists of tholeiitic and minor boninite-like rocks, and rhyolites; and the upper package (upper Bradley Basalt and Woodbrook Formation) contains calc-alkaline rocks, including adakites, Mg-rich basalts, Nb-enriched basalts and rhyolites.

Geochronological data from all stratigraphic levels of the group provide a well-constrained depositional age range between 3126 and 3112 Ma (Hickman et al., 2006). Nd-isotopic compositions show that the Whundo Group represents juvenile crustal addition with values that lie very close to depleted mantle values (ε_{Nd}~+1.5–2.0 at c. 3120 Ma; Smith et al., 1998; Sun and Hickman, 1998; Smithies et al., 2005a).

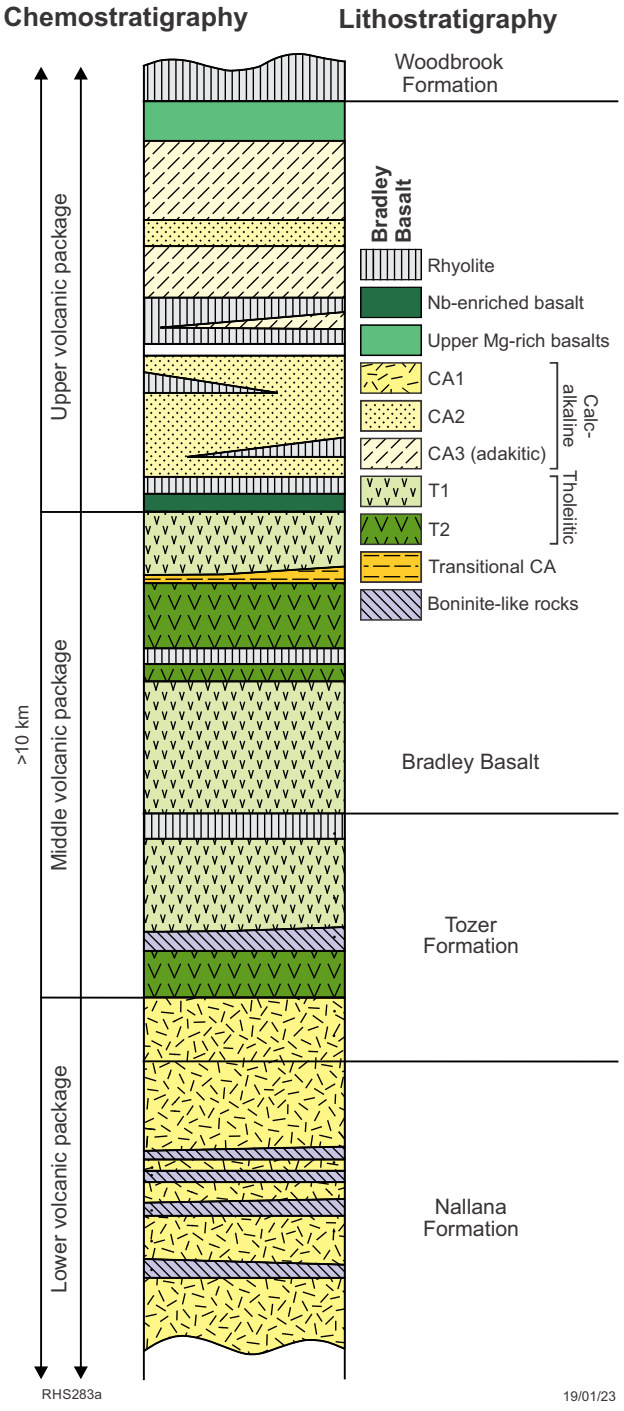

Figure 84. Chemostratigraphic column of the Whundo Group, with lithostratigraphic formation boundaries shown for comparison

Smithies et al. (2005a) outlined numerous features of the Whundo Group that might be interpreted in terms of processes similar to those that produce magmas in modern-style subduction-zone settings. Although many of these features could be individually interpreted in terms of processes not necessarily related to modern-style plate tectonics or to subduction, together they provide a compelling case for a convergent margin setting at 3120 Ma — and probably the best direct early evidence for the operation of processes resembling those operating during modern-style subduction processes (Pearce, 2008). These features include:

- the fine- and broad-scale intercalation of discrete tholeiitic and calc-alkaline volcanics (Fig. 84)
- Nd-isotopic compositions that lie very close to depleted mantle values
- the presence of rocks with a strong boninite affinity (Fig. 85a) near the base of the sequence
- the presence of Nb-enriched basalts (Figs 84, 85) near the top of the sequence, and the close association of these with lavas of adakitic affinity
- the recognition that assimilation of crust is an unlikely cause of LREE-enrichments in the boninite-like lavas and calc-alkaline lavas
- the identification of a range of source regions, from depleted to undepleted and enriched
- the mixing of source regions and/or primitive magmas derived from undepleted, depleted, calc-alkaline and tholeiitic (MORB) sources, with distinct periods characterized by enhanced interaction and magmatic diversity
- the recognition that the calc-alkaline lavas are the result of flux melting
- the absence of any intervening sequences containing exotic ‘continental’ material
- the absence of evidence for continental (felsic) basement material, and the possibility that the sequence was developed over arc-like mid-level crust of similar age.

Krapež and Eisenlohr (1998), Smith (2003) and Smith et al. (1998) all suggested a back-arc setting for the Whundo Group. However, the lack of evidence for felsic basement, the presence of boninites, and low Th/La, La/Nb and Ce/Yb ratios are more likely indicative of an intra-oceanic arc setting (Smithies et al., 2005a). Van Kranendonk et al. (2006b, 2007b, 2010) suggested that the arc lay adjacent to a subduction zone within the post-3200 Ma basaltic basin between the East Pilbara Terrane and the Karratha Terrane, revealing a change from spreading to plate convergence at about 3130 Ma.

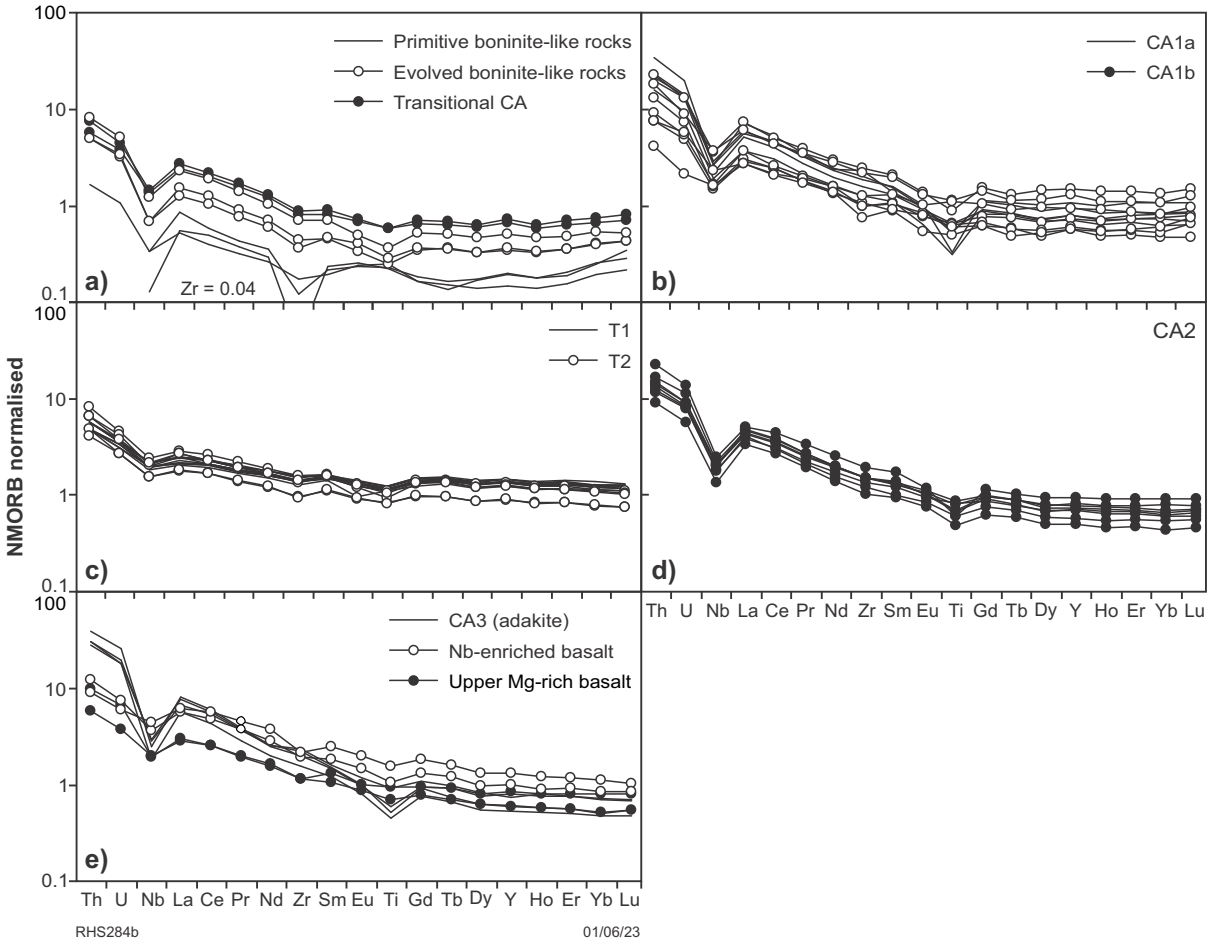

Figure 85. Trace element plots normalized to primitive mantle for various volcanic rocks of the Whundo Group (from Smithies et al., 2007a): a) boninite-like rocks mainly from the lower volcanic package; b) calc-alkaline basalts from the lower volcanic package; c) tholeiitic basalts from the middle volcanic package; d) calc-alkaline basalts from the upper volcanic package; e) adakitic rocks and Nb-enriched basalts from the upper volcanic package. CA = calc-alkaline; T = tholeiitic. Normalizing factors after Sun and McDonough (1989)

Locality 6.4: Lower volcanic package — first calc-alkaline basalt and boninites (Zone 50, MGA 486086E 7685229N and 485258E 7685226N (boninite) and 485639E 7684529N)

The lower volcanic package is dominated by calc-alkaline basaltic to andesitic lavas (CA1) (Figs 85b, 86), but also includes 1–10 m-thick flow units with boninitic compositions, which are interbedded throughout; these boninites form up to 15% of the overall package. This package forms the most deformed and metamorphosed part of the Whundo Group. Large-scale depositional features such as hyaloclastite layers, pillows and flow-top breccias are only locally preserved. These locally schistose rocks comprise a greenschist-facies assemblage of quartz–actinolite–chlorite–epidote–plagioclase. Little of the primary ***mineralogy*** is preserved, although primary ***textures*** are commonly well preserved; later alteration resulted in locally extensive development of a quartz–carbonate–sericite assemblage. Locally preserved original igneous textures show the boninitic lavas to have been vesicular, extremely fine-grained, glass-rich rocks containing phenocrysts of subhedral olivine (now chlorite and serpentine) and acicular pyroxene (now actinolite).

Locality 6.5: Middle volcanic package — lower volcanolithic conglomerates (Zone 50, MGA 500859E 7687959N)

This is a quick roadside stop to observe volcanolithic conglomeratic deposits within the Bradley Basalt.

Locality 6.6: Middle volcanic package — lower tholeiitic pillow basalts, Harding Dam (Zone 50, MGA 508900E 7682000N)

This locality provides excellent 3D exposure of pillow basalt (Fig. 87) in the middle volcanic package (Bradley Basalt) of the Whundo Group. Pillow structures show that the lava flows, which dip 55° towards the northeast, are the right way up.

Tholeiitic lavas (T1 of Smithies et al., 2005a) dominate the middle volcanic package (Figs 84, 85c), although rare flows of boninite-like lavas persist into the lower parts of this package and rocks compositionally transitional between these and overlying calc-alkaline lavas are found in the upper parts of the section. Large-scale primary features (pillow structures, hyaloclastite, vesicle-rich layers

and flow-top breccias) are common, as are fine-scale igneous textures; however, the original mineralogy shows a moderate to high level of replacement, and fine calcite veining is a locally prominent feature. The tholeiitic rocks are plagioclase-phyric, although the euhedral laths (up to 2 mm long) are typically replaced by calcite, sericite and epidote. Groundmass plagioclase is better preserved, and locally has only a moderate dusting of alteration minerals. Original mafic minerals — dominantly clinopyroxene, both as phenocrysts and a groundmass phase — have been largely replaced by chlorite and lesser actinolite. The tholeiites contain rare clots of serpentine, likely replacing olivine, and abundant leucoxene replacing magnetite.

Upper volcanic package

A now inaccessible track between Localities 5.4 and 5.5 once provided a traverse through the upper volcanic package, which is described here for completeness. This upper volcanic package contains abundant calc-alkaline basaltic (CA2) to dacitic flows of vesicular pillowed units, intercalated with hyaloclastite, flow-top breccias, and reworked volcaniclastic deposits. Large-scale features are extremely well preserved, as are fine-scale igneous textures, and primary mineralogy is also locally well preserved. The area from which these calc-alkaline rocks were sampled is one of the few large outcrops where deformation and overprinting alteration is not significant.

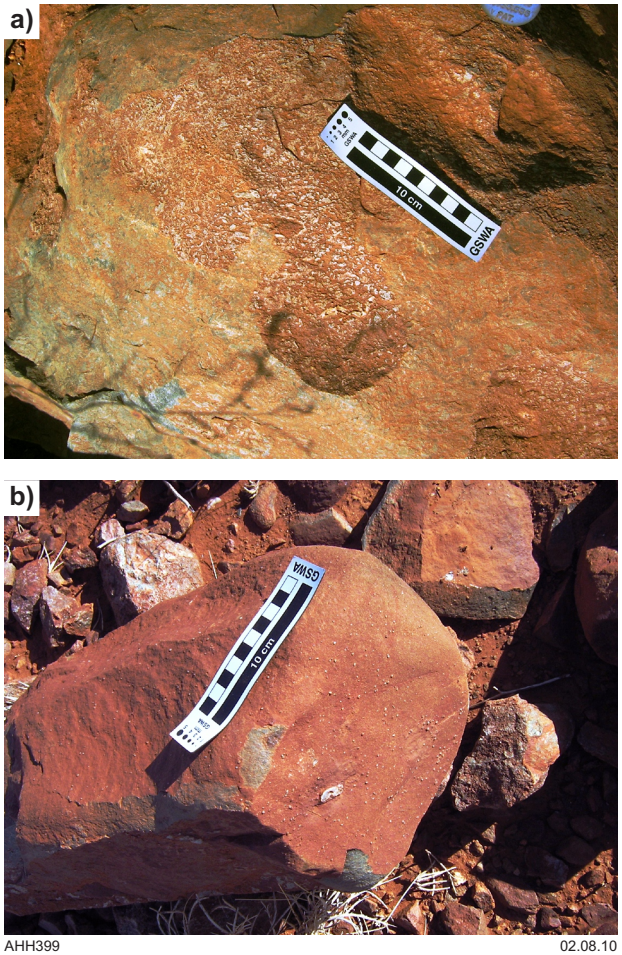

AHH399 02.08.10

Figure 86. Mafic units in the lower volcanic package of the Whundo Group, showing: a) hyaloclastite breccia in boninite; b) weakly amygdaloidal boninite flows

Felsic rocks clearly of a volcanic and volcaniclastic origin first appear within the stratigraphically lower levels of the middle volcanic package. These include laminated ash deposits (Fig. 88a) pumiceous breccia, and porphyritic quartz-plagioclase flows, as well as a felsic volcaniclastic unit showing cyclic grain-size grading (Fig. 88b), well-developed flame structures and slump folding (Fig. 88c), fine-scale cross bedding (Fig.88d), and fragmental coarse-grained volcaniclastic sandstone (Fig. 88e). These rocks show possible rheomorphic structures and sharp contacts with vesicular CA2 basalts. The proportion of felsic volcanic and volcaniclastic rocks increases upwards within the upper volcanic package, and they dominate the poorly preserved uppermost part of that package. These felsic units include the adakitic calc-alkaline CA3 unit (Fig. 84). Near the top of the upper volcanic package, felsic volcanic and volcaniclastic rocks are interbedded with minor flows of Nb-rich basalt and LREE-rich dacite. The adakitic and Nb-enriched rocks are particularly indistinct in outcrop (Fig. 88f), only being recognized on the basis of geochemistry.

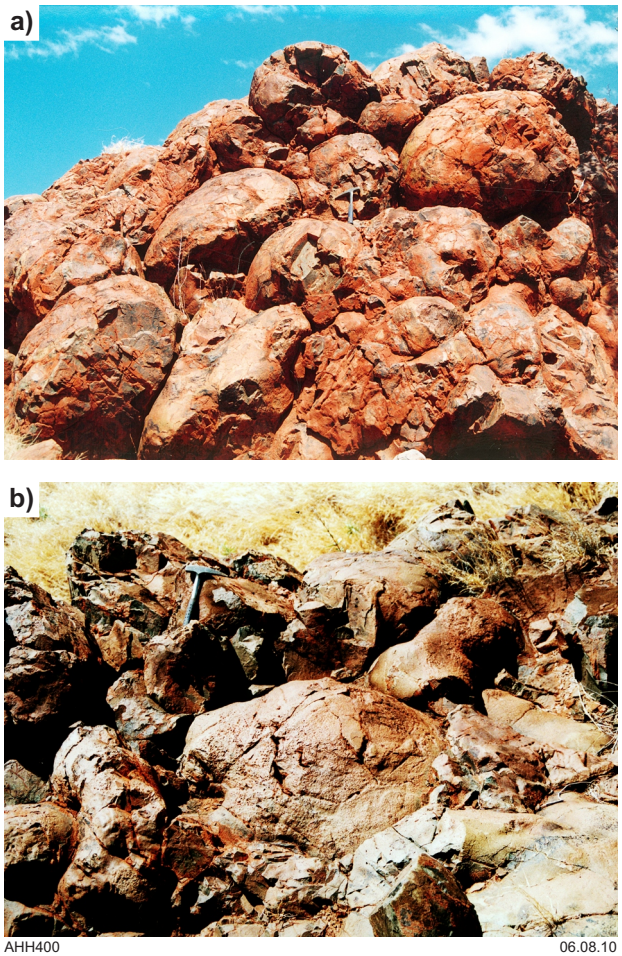

AHH400 06.08.10

Figure 87. Pillow lava in the Bradley Basalt 2.5 km northwest of Harding Dam: a) pillow structures, 1.5 to 2 m in diameter, are exceptionally well exposed on the side of the small hill; b) pillow structures viewed from above, showing irregular flow morphology and vesicular tops

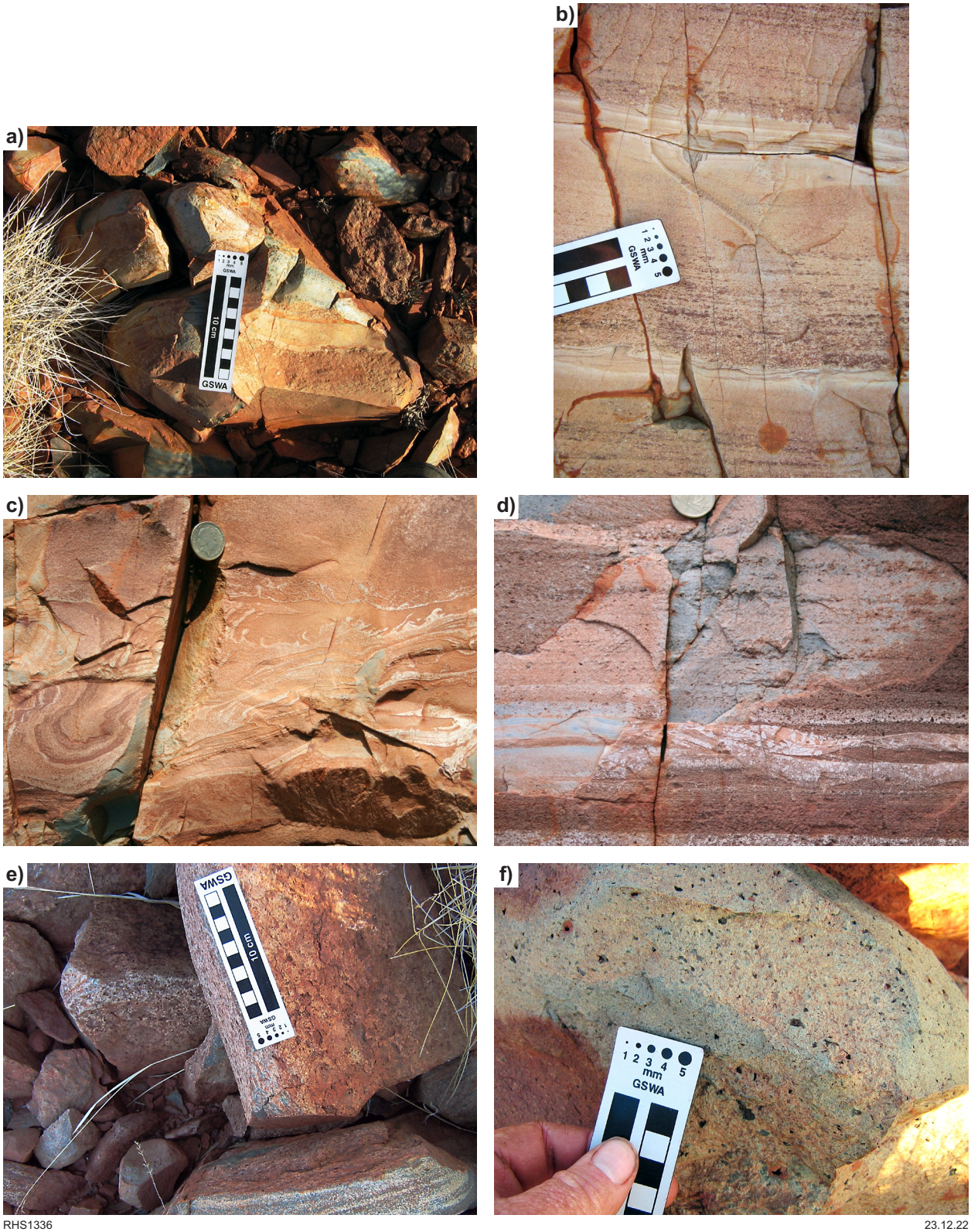

Figure 88. Sedimentary and igneous structures in felsic volcanic and volcaniclastic units of the Bradley Basalt: a) laminated ash deposits; b) cyclic grainsize grading; c) well-developed flame structures (centre and right), and syndepositional slump folding (left), coin 2 cm diameter; d) fine-scale cross bedding in reworked felsic tuffaceous sediment, coin 2 cm diameter; e) fragmental volcaniclastic rocks; (f) Nb-enriched basalts

References

Allwood, AC, Walter, MR, Kamber, BS, Marshall, CP and Burch, IW 2006, Stromatolite reef from the Early Archaean era of Australia: Nature, v. 441, p. 714–717.

Allwood, AC, Walter, MR, Burch, IW and Kamber, BS 2007, 3.43 billion-year-old stromatolite reef from the Pilbara Craton of Western Australia: Ecosystem-scale insights to early life on Earth: Precambrian Research, v. 158, p. 198–227.

Allwood, AC, Grotzinger, JP, Knoll, AH, Burch, IW, Anderson, MS, Coleman, ML and Kanik, I 2009, Controls on development and diversity of Early Archean stromatolites: Proceedings of the National Academy of Sciences, v. 106, p. 9548–9555.

Allwood, AC, Kamber, BS, Walter, MR, Burch, IW and Kanik I 2010, Trace elements record depositional history of an Early Archean stromatolitic carbonate platform: Chemical Geology, v. 270, p. 148–163.

Appel, PWU, Polat, A and Frei, R 2009, Dacitic ocelli in mafic lavas, 3.8 – 3.7 Ga Isua greenstone belt, West Greenland: Geochemical evidence for partial melting of oceanic crust and magma mixing: Chemical Geology, v. 258, p. 105–124.

Arndt, N, Bruzak, G and Reischmann, T 2001, The oldest continental and oceanic plateaus: Geochemistry of basalts and komatiites of the Pilbara Craton, Australia, *in* Mantle plumes: Their identification through time *edited by* RE Ernst and KL Buchan: Geological Society of America, Special Paper 352, p. 359–387.

Ballhaus, C, Fonseca, ROC, Münker, C, Kirchenbaur, M and Zirner, A 2015, Spheroidal textures in igneous rocks – Textural consequences of H_2O saturation in basaltic melts: Geochimica et Cosmochimica Acta, v. 167, p. 241–252.

Barley, ME 1993, Volcanic, sedimentary and tectonostratigraphic environments of the ~3.46 Ga Warrawoona Megasequence: A review: Precambrian Research, v. 60, p. 47–67.

Barley, ME 1987, The Archaean Whim Creek Belt, an ensialic fault-bounded basin in the Pilbara Block, Australia: Precambrian Research, v. 37, no. 3, p. 199–215, doi:10.1016/0301-9268(87)90067-2.

Barley, ME 1997, The Pilbara Craton, *in* Greenstone Belts *edited by* MJ de Wit and L Ashwal: Clarendon Press, Oxford University Monographs on Geology and Geophysics No. 35, p. 657–664.

Barley, ME and Pickard, AL 1999, An extensive, crustally-derived, 3325 to 3310 Ma silicic volcanoplutonic suite in the eastern Pilbara Craton: Evidence from the Kelley Belt, McPhee Dome and Corunna Downs Batholith: Precambrian Research, v. 96, p. 41–62.

Barley, ME, Dunlop, JSR, Glover, JE and Groves, DI 1979, Sedimentary evidence for Archaean shallow-water volcanic-sedimentary facies, eastern Pilbara Block, Western Australia: Earth and Planetary Science Letters, v. 43, p. 74–84.

Baumgartner, R, Van Kranendonk, MJ, Wacey, D, Fiorentini, M, Saunders, M, Caruso, S, Pagès, A, Homann, M and Guagliardo, P 2019, Nano-porous pyrite and organic matter in 3.5 billion-year-old stromatolites record primordial life: Geology, v. 47, p. 1039–1043.

Baumgartner, RJ, Van Kranendonk, MJ, Pagès, A, Fiorentini, ML, Wacey, D and Ryan, C 2020a, Accumulation of transition metals and metalloids in sulfidized stromatolites of the 3.48 billion-year-old Dresser Formation, Pilbara Craton: Precambrian Research, v. 337, 105534.

Baumgartner, RJ, Van Kranendonk, MJ, Fiorentini, ML, Pagès, A, Wacey, D, Kong, C, Saunders, M and Ryan, C 2020b, Formation of micro-spherulitic barite in association with organic matter within sulfidized stromatolites of the 3.48 billion-year-old Dresser Formation, Pilbara Craton: Geobiology, v. 18, p. 415–425.

Baumgartner, R, Caruso, S, Fiorentini, ML, Van Kranendonk, MJ, Martin, L, Jeon, H, Wacey, D and Pagès, A 2020c, Sulfidization of 3.48 billion-year-old stromatolites of the Dresser Formation, Pilbara Craton: Constraints from in-situ sulfur isotope analysis of pyrite: Chemical Geology, v. 538, 119488.

Beintema, KA 2003, Geodynamic evolution of the west and central Pilbara Craton: A mid-Archean active continental margin: Geologica Ultraiectina, Utrecht University, Utrecht, The Netherlands, PhD thesis (unpublished), 248p.

Bettenay, LF, Bickle, MJ, Boulter, CA, Groves, DI, Morant, P, Blake, TS and James, BA 1981, Evolution of the Shaw Batholith – An Archaean granitoid-gneiss dome in the eastern Pilbara, Western Australia: Geological Society of Australia, Special Publication 7, p. 361–372.

Bickle, MJ, Bettenay, LF, Boulter, CA, Groves, DI and Morant, P 1980, Horizontal tectonic intercalation of an Archaean gneiss belt and greenstones, Pilbara Block, Western Australia: Geology, v. 8, p. 525–529.

Bickle, MJ, Morant, P, Bettenay, LF, Boulter, CA, Blake, TS and Groves, DI 1985, Archaean tectonics of the Shaw Batholith, Pilbara Block, Western Australia: Structural and metamorphic tests of the batholith concept, *in* Evolution of Archean Supracrustal Sequences *edited by* LD Ayers, PC Thurston, KD Card and W Weber: Geological Association of Canada, Special Paper 28, p. 325–341.

Bickle, MJ, Bettenay, LF, Chapman, HJ, Groves, DI, McNaughton, NJ, Campbell, IH and de Laeter, JR 1993, Origin of the 3500–3300 Ma calc-alkaline rocks in the Pilbara Archaean: Isotopic and geochemical constraints from the Shaw Batholith: Precambrian Research, v. 60, p. 117–149.

Blewett, RS 2002, Archaean tectonic processes: A case for horizontal shortening in the North Pilbara granite-greenstone terrane, Western Australia: Precambrian Research, v. 113, p. 87–120.

Bontognali, TRR, Sessions, AL, Allwood, AC, Fischer, WW, Grotzinger, JP, Summons, RE and Eiler, JM 2012, Sulfur isotopes of organic matter preserved in 3.45 billion-year-old stromatolites reveal microbial metabolism: Proceedings of the National Academy of Sciences, v. 102, p. 15146–15151.

Boudon, G, Villemant, B, Komorowski, J-C, Ildefonse, P and Semet, MP 1998, The hydrothermal system at Soufriere Hills volcano, Montserrat (West Indies): Characterisation and role in the on-going eruption: Geophysical Research Letters, v. 25, p. 3693–3696.

Boulter, CA, Bickle, MJ, Gibson, B and Wright, RK 1987, Horizontal tectonics pre-dating upper Gorge Creek Group sedimentation, Pilbara Block, Western Australia: Precambrian Research, v. 36, p. 241–258.

Branney, MJ and Kokelaar, P 1994, Volcano-tectonic faulting, soft-state deformation, and orthomorphism of tuffs during development of a piecemeal caldera, English Lake District: Geological Society of America Bulletin, v. 106, p. 507–530.

Brown, AJ, Walter, MR and Cudahy, TJ 2005, Hyperspectral imaging spectroscopy of a Mars analogue environment at the North Pole Dome, Pilbara Craton, Western Australia: Australian Journal of Earth Science, v. 52, p. 353–364.

Buchanan, LJ 1981, Precious metal deposits associated with volcanic environments in the southwest, *in* Relations of Tectonics to Ore Deposits in the Southern Cordillera *edited by* WR Dickson and WD Payne: Arizona Geological Society Digest, v. 14, p. 237–262.

Buick, R 1985, Life and conditions in the early Archaean: Evidence from 3500 M.Y. old shallow-water sediments in the Warrawoona Group, North Pole, Western Australia: Department of Geology, University of Western Australia, PhD thesis (unpublished).

Buick, R and Dunlop, JSR 1990, Evaporitic sediments of Early Archaean age from the Warrawoona Group, North Pole, Western Australia: Sedimentology, v. 37, p. 247–277.

Buick, R, Dunlop, JSR and Groves, DI 1981, Stromatolite recognition in ancient rocks: An appraisal of irregularly laminated structures in an Early Archaean chert–barite unit from North Pole, Western Australia: Alcheringa, v. 5, p. 161–181.

Buick, R, Thornett, JR, McNaughton, NJ, Smith, JB, Barley, ME and Savage, M 1995, Record of emergent continental crust ~3.5 billion years ago in the Pilbara Craton of Australia: Nature, v. 375, p. 574–577.

Byerly, GR, Lowe, DR, Wooden, JL and Xie, X 2002, An Archean impact layer from the Pilbara and Kaapvaal cratons: Science, v. 297, p. 1325–1327.

Cammack, JN, Picuza, MJ, Cavosie, AJ, Van Kranendonk, MJ, Hickman, AH, Kozdon, R, Orland, IJ, Kitajima, K and Valley, JW 2018, SIMS microanalysis of the Strelley Pool Formation cherts and the implications for the secular-temporal oxygen-isotope trend of cherts: Precambrian Research, v. 304, p. 125–139.

Caruso, S, Van Kranendonk, MJ, Baumgartner, RJ, Fiorentini, ML, Forster and MA 2021, The role of magmatic fluids in the ~3.48 Ga Dresser Caldera, Pilbara Craton: New insights from the geochemical investigation of hydrothermal alteration: Precambrian Research, v. 362, 106299.

Casanova, J 1986, Les stromatolites continentaux: Paleoecologie, paleohydrologie, paleoclimatologie application au rift Gregory: Université d'aix-Marseilles, PhD thesis (unpublished), 256p.

Charles, RW, Vidale Buden, RJ and Goff, F 1986, An interpretation of the alteration assemblages at Sulphur Springs, Valles Caldera, New Mexico: Journal of Geophysical Research, v. 91, p. 1887–1898.

Cole, J, Milner, D and Spinks, K 2005, Calderas and caldera structures: A review: Earth-Science Reviews, v. 69, p. 1–26.

Collins, WJ 1989, Polydiapirism of the Archaean Mt. Edgar batholith, Pilbara Block, Western Australia: Precambrian Research, v. 43, p. 41–62.

Collins, WJ and Van Kranendonk, MJ 1999, Model for the development of kyanite during partial convective overturn of Archaean granite-greenstone terranes: The Pilbara Craton, Australia: Journal of Metamorphic Petrology, v. 17, p. 145–156.

Collins, WJ, Van Kranendonk, MJ and Teyssier, C 1998, Partial convective overturn of Archaean crust in the east Pilbara Craton, Western Australia: Driving mechanisms and tectonic implications: Journal of Structural Geology, v. 20, p. 1405–1424.

Delarue, F, Robert, F, Derenne, S, Tartese, R, Jauvion, C, Bernard, S, Pont, S, Gonzalez-Cano, A, Duhamel, R and Sugitani, K 2019, Out of rock: A new look at the morphological and geochemical preservation of microfossils from the 3.46 Gyr-old Strelley Pool Formation: Precambrian Research, v. 336, 105472.

Delor, C, Burg, J-P and Clarke, G 1991, Relations diapirisme-metamorphisme dans la Province du Pilbara (Australie-occidentale): Implications pour les régimes thermiques et tectoniques à la Archéen: Comptes Rendus de l'Academie des Sciences Paris, v. 312, p. 257–263.

DiMarco, MJ and Lowe DR 1989, Stratigraphy and sedimentology of an early Archean felsic volcanic sequence, Eastern Pilbara Block, Western Australia, with special reference to the Duffer Formation and implications for crustal evolution: Precambrian Research, v. 44, p. 147–169.

Dixon, JM and Summers, JM 1983, Patterns of total and incremental strain in subsiding troughs: Experimental centrifuged models of inter-diapir synclines: Canadian Journal of Earth Sciences, v. 20, p. 1843–1861.

Djokic, T, Van Kranendonk, MJ, Campbell, KA, Walter, MR and Ward, CR 2017, Earliest signs of life on land preserved in ca. 3.5 Ga hot spring deposits: Nature Communications, doi:10.1038/ncomms15263.

Djokic, T, Campbell, KA and Van Kranendonk, MJ 2021, A reconstructed subaerial hot spring field in the ~3.5 billion-year-old Dresser Formation, North Pole Dome, Pilbara Craton, Western Australia: Astrobiology, v. 21, no. 1, p. 1–38.

Duda, J-P, Van Kranendonk, MJ, Thief, V, Ionescu, D, Strauss, H, Schäfer, N and Reitner, J 2016, A rare glimpse of Paleoarchean life: Geobiology of an exceptionally preserved microbial mat facies from the 3.4 Ga Strelley Pool Formation, Western Australia: PlosOne, v. 11, doi: 10.1371/journal.pone.0147629.

Duda, J-P, Thiel, V, Bauersachs, T, Missbach, H, Reinhard, M, Schäfer, N, Van Kranendonk, MJ and Reitner, J 2018, Ideas and perspectives: Hydrothermally driven redistribution and sequestration of early Archaean biomass – the 'hydrothermal pump hypothesis': Biogeosciences, v. 15, p. 1535–1548.

Dunlop, JSR and Buick, R 1981, Archaean epiclastic sediments derived from mafic volcanics, North Pole, Pilbara Block, Western Australia: Special Publication of the Geological Society of Australia, v. 7, p. 225–233.

Eriksson, KA 1981, Archaean platform-to-trough sedimentation, East Pilbara Block, Australia, *in* Archaean Geology: Second International Symposium, Perth 1980 *edited by* JE Glover and DI Groves: Geological Society of Australia, Special Publication 7, p. 235–244.

Ferguson, J and Currie, KL 1972, Silicate immiscibility in the ancient 'basalts' of the Barberton Mountain Land, Transvaal: Nature, v. 235, p. 86–89.

Flannery, DT, Allwood, AC, Summons, RE, Williford, KH, Abbey, W, Matys, ED and Ferralis, N 2017, Spatially-resolved isotopic study of carbon trapped in ~3.43 Ga Strelley Pool Formation stromatolites: Geochimica et Cosmochimica Acta, v. 223, p. 21–35.

Foukal, K 2003, Can solar variations in solar luminosity provide missing link between sun and the climate?: Eos, v. 84, p. 205–212.

García-Ruiz, JM, Hyde, ST, Carnerup, AM, Christy, AG, Van Kranendonk, MJ and Welham, NJ 2003, Self-assembled silica-carbonate structures and detection of ancient microfossils: Science, v. 302, p. 1194–1197.

Gardiner, NJ, Wacey, D, Kirkland, CL, Johnson, TE and Jeon, H 2019, Zircon U–Pb, Lu–Hf and O isotopes from the 3414 Ma Strelley Pool Formation, East Pilbara Terrane, and the Palaeoarchaean emergence of a cryptic cratonic core: Precambrian Research, v. 321, p. 64–84.

Glikson, M, Duck, LJ, Golding, SD, Hofmann, A, Bolhar, R, Webb, R, Baiano, JCF and Sly, LI 2008, Microbial remains in some earliest Earth rocks: Comparison with a potential modern analogue: Precambrian Research, v. 164, p. 187–200.

González-Muñoz, MT, Fernández-Luque, P, Martínez-Ruiz, F, Ben Chekroun, P, Arias, JM, Rodríguez-Gallego, M, Martínez-Cañamero, M, De Linares, C and Paytan, A 2003, Precipitation of barite by *Myxococcus xanthus*: Possible implications for the biogeochemical cycle of barium: Applied and Environmental Microbiology, v. 69, p. 5722–5725.

González-Muñoz, MT, Martinez-Ruiz, F, Morcillo, F, Martin-Ramos, JD and Paytan, A 2013, Precipitation of barite by marine bacteria: A possible mechanism for marine barite formation: Geology, v. 40, p. 675–678.

Gramp, JP, Birgham, JM, Sasaki, K and Tuovinen, OH 2007, Formation of Ni- and Zn-sulfides in cultures of sulfate-reducing bacteria: Journal of Geomicrobiology, v. 24, p. 609–614.

Green, MG, Sylvester, PJ and Buick, R 2000, Growth and recycling of early Archaean continental crust: Geochemical evidence from the Coonterunah and Warrawoona Groups, Pilbara Craton, Australia: Tectonophysics, v. 322, no. 1, p. 69–88.

Grey, K 1984, Abiogenic stromatoloids from the Warrawoona Group (Early Archaean): Geological Survey of Western Australia, Palaeontology Report 74/84.

Groves, DI, Dunlop, JSR and Buick, R 1981, An early habitat of life: Scientific American, v. 245, p. 64–73.

Harris, AC, White, NC, McPhie, J, Bull, SW, Line, MA, Skrzeczynski, R, Mernagh, TP and Tosdal, RM, 2009, Early Archean hot springs above epithermal veins, North Pole, Western Australia: New insights from fluid inclusion microanalysis: Economic Geology, v. 104, p. 793–814.

Harris, LV, Hutchinson, IB, Ingley, R, Marshall, CP, Olcott Marshall, O and Edwards, HGM 2015, Selection of portable spectrometers for planetary exploration: A comparison of 532 nm and 785 nm Raman spectroscopy of reduced carbon in Archean cherts: Astrobiology, v. 15, p. 420–429.

Hickman, AH 1975, Precambrian structural geology of part of the Pilbara region: Geological Survey of Western Australia Annual Report, 1974, p. 68–73.

Hickman, AH 1983, Geology of the Pilbara Block and its environs: Geological Survey of Western Australia, Bulletin 127, 268p.

Hickman, AH 1984, Archaean diapirism in the Pilbara Block, Western Australia, *in* Precambrian Tectonics Illustrated *edited by* A Kröner and R Greiling: E. Schweizerbarts'che Verlagsbuchhandlung, Stuttgart, p. 113–127.

Hickman, AH 2001a, Geology of the Dampier 1:100 000 sheet: Geological Survey of Western Australia, 1:100 000 Geological Series Explanatory Notes, 39p.

Hickman, AH 2001b, The West Pilbara granite–greenstone terrane and its place in the Pilbara Craton, *in* Extended Abstracts – 4th International Archaean Symposium, Perth, 24–28 September 2001 *edited by* KF Cassidy, JM Dunphy and MJ Van Kranendonk: AGSO (Geoscience Australia), Record 2001/37, p. 319–321.

Hickman, AH 2004, Two contrasting granite–greenstones terranes in the Pilbara Craton, Australia: Evidence for vertical and horizontal tectonic regimes prior to 2900 Ma: Precambrian Research, v. 131, p. 153–172.

Hickman, AH 2008, Regional review of the 3426–3350 Ma Strelley Pool Formation, Pilbara Craton, Western Australia: Geological Survey of Western Australia, Record 2008/15, 27p.

Hickman, AH 2016, Northwest Pilbara Craton: A record of 450 million years in the growth of Archean continental crust: Geological Survey of Western Australia, Report 160, 104p.

Hickman, AH 2021, East Pilbara Craton: A record of one billion years in the growth of Archean continental crust: Geological Survey of Western Australia, Report 143, 187p.

Hickman, AH and Smithies, RH 2001, Roebourne, Western Australia (2nd edition): Geological Survey of Western Australia, 1:250 000 Geological Series Explanatory Notes, 52p.

Hickman, AH and Van Kranendonk, MJ 2004, Diapiric processes in the formation of Archaean continental crust, east Pilbara granite–greenstone terrane, Australia, *in* The Precambrian Earth: Tempos and events *edited by* PG Eriksson, W Altermann, DR Nelson, WU Mueller and O Catuneanu: Elsevier, Amsterdam, The Netherlands, Developments in Precambrian Geology 12, p. 54–75.

Hickman, AH and Van Kranendonk, MJ 2012, A billion years of Earth history: A geological transect through the Pilbara Craton and the Mount Bruce Supergroup – a field guide to accompany 34th IGC Excursion WA-2: Geological Survey of Western Australia, Record 2012/10, 66p.

Hickman, AH, Smithies, RH, Pike, G, Farrell, TR and Beintema, KA 2001, Evolution of the West Pilbara granite–greenstone terrane and Mallina Basin, Western Australia – a field guide: Geological Survey of Western Australia, Record 2001/16, 65p.

Hickman, AH, Smithies, RH and Strong, CA 2006, Interpreted bedrock geology of the northwestern Pilbara Craton (1:250 000 scale): Geological Survey of Western Australia, Report 92, Plate 1.

Hoashi, M, Bevacqua, DC, Otake, T, Watanabe, YZ, Hickman, AH, Utsunomiya, S and Ohmoto, H 2009, Primary haematite formation in an oxygenated sea 3.46 billion years ago: Nature Geosciences, v. 2, p. 301–306.

Hofmann, HJ, Grey, K, Hickman, AH and Thorpe, R 1999, Origin of 3.45 Ga coniform stromatolites in the Warrawoona Group, Western Australia: Geological Society of America Bulletin, v. 111, p. 1256–1262.

Huerta-Diaz, MA, Delgadillo-Hinojosa, F, Otero, XL, Hernandez-Ayon, JM, Segovia-Zavala, JA, Galindo-Bect, MS and Amaro-Franco, E 2011, Iron and trace metals in microbial mats and underlying sediments: Results from Guerero Negro saltern, Baja California Sur, Mexico: Aquatic Geochemistry, v. 17, p. 603–628.

Huerta-Diaz, MA, Delgadillo-Hinojosa, F, Siqueiros-Valencia, A, Valdivieso-Ojeda, J, Reimer, JJ and Segovia-Zavala, JA 2012, Millimeter-scale resolution of trace metal distributions in microbial mats from a hypersaline environment in Baja California, Mexico: Geobiology, v. 10, p. 531–547.

Huston, DL, Sun, S-S, Blewett, R, Hickman, AH, Van Kranendonk, MJ, Phillips, D, Baker, D and Brauhart, C 2002, The timing of mineralization in the Archean North Pilbara Terrain, Western Australia: Economic Geology, v. 97, p. 733–755.

Johnson, C, Zheng, X-Y, Djokic, T, Van Kranendonk, M, Czaja, A, Roden, E and Beard, B 2022, Early Archean biogeochemical iron cycling and nutrient availability: New insights from a 3.5 Ga land–sea transition: Earth-Science Reviews, v. 228, 103992.

Kemp, AIS, Hickman, AH, Kirkland, CL and Vervoort, JD, 2015, Hf isotopes in detrital and inherited zircons of the Pilbara Craton provide no evidence for Hadean continents: Precambrian Research, v. 261, p. 112–126.

Kitajima, K, Maruyama, S, Utsonomita, S and Liou, JG 2001, Seafloor hydrothermal alteration at an Archaean mid-ocean ridge: Journal of Metamorphic Geology, v. 19, p. 581–597.

Kiyokawa, S 1993, Stratigraphy and structural evolution of a Middle Archean greenstone belt, northwestern Pilbara Craton, Australia: University of Tokyo, PhD thesis (unpublished).

Kiyokawa, S and Taira, A 1998, The Cleaverville Group in the west Pilbara coastal granite–greenstone terrane of Western Australia: An example of a mid-Archaean immature oceanic island-arc succession: Precambrian Research, v. 88, p. 102–142.

Kiyokawa, S, Taira, A, Byrne, T, Bowring, S and Sano, Y 2002, Structural evolution of the middle Archean coastal Pilbara terrane, Western Australia: Tectonics, v. 21, no. 1044, p. 1–24, doi:10.1029/2001TC001296.

Kloppenburg, A, White, SH and Zegers, TE 2001, Structural evolution of the Warrawoona Greenstone Belt and adjoining granitoid complexes, Pilbara Craton, Australia: Implications for Archaean tectonic processes: Precambrian Research, v. 112, p. 107–147.

Krapež, B and Eisenlohr, B 1998, Tectonic settings of Archaean (3325–2775 Ma) crustal–supracrustal belts in the West Pilbara Block: Precambrian Research, v. 88, p. 173–205.

Labrenz, M, Druschel, GK, Thomsen-Ebert, T, Gilbert, B, Wlech, SA, Kremner, KM, Logan, GA, Summons, RE, De Stasio, G, Bond, PL, Lai, B, Kelly, SD and Banfield, JF 2000, Formation of sphalerite (ZnS) deposits in natural biofilms of sulfate-reducing bacteria: Science, v. 290, p. 1744–1747.

Lalonde, SV, Amskold, LA, Warren, LA and Konhauser, KO 2007, Surface chemical reactivity and metal adsorptive properties of natural cyanobacterial mats from an alkaline hydrothermal spring Yellowstone National Park: Chemical Geology, v. 243, p. 36–52.

Lambert, I, Donnelly, T, Dunlop, J and Groves, D 1978, Stable isotopic compositions of early Archaean sulphate deposits of probable evaporitic and volcanogenic origins: Nature, v. 276, p. 808–811.

Li, W, Johnson, CM and Beard, BL 2012, U–Th–Pb isotope data indicate Phanerozoic age for oxidation of the 3.4 Ga Apex Basalt: Earth and Planetary Science Letters, v. 319–320, p. 197–206.

Li, W, Czaja, AD, Van Kranendonk, MJ, Beard, BL, Roden, EE and Johnson, CM 2013, An anoxic, Fe(II)-rich, U-poor ocean 3.46 billion years ago: Geochimica et Cosmochimica Acta, v. 120, p. 65–79.

Lindsay, JF, Brasier, MD, McLoughlin, N, Green, OR, Fogel, M, Steele, A and Mertzman, SA 2005, The problem of deep carbon – an Archaean paradox: Precambrian Research, v. 143, p. 1–22.

Lowe, DR 1980, Stromatolites 3,400-Myr old from the Archaean of Western Australia: Nature, v.284, p. 441–443.

Lowe, DR 1983, Restricted shallow-water sedimentation of Early Archean stromatolitic and evaporitic strata of the Strelley Pool Chert, Pilbara Block, Western Australia: Precambrian Research, v.19, p.239–283.

Lowe, DR 1994, Abiological origin of described stromatolites older than 3.2 Ga: Geology, v. 22, p.387–390.

Lowrey, JR, Wyman, DA, Ivanic, TJ, Smithies, RH and Maas, R 2019, Archean boninite-like rocks of the northwestern Youanmi Terrane, Yilgarn Craton: Geochemistry and genesis: Journal of Petrology, v. 60, no. 11, p. 2131–2168, doi:10.1093/petrology/egaa002.

MacLean, LCW, Tyliszczak, T, Gilbert, PUPA, Zhou, D, Pray, TJ, Onstott, TC and Southam, G 2008, A high-resolution chemical and structural study of framboidal pyrite formed within a low-temperature bacterial biofilm: Geobiology, v. 6, p. 471–480.

Mareschal, J-C and West, GF 1980, A model for Archean tectonism. Part 2. Numerical models of vertical tectonism in greenstone belts: Canadian Journal of Earth Sciences, v. 17, p. 60–71.

Marshall, CP, Love, GD, Snape, CE, Hill, Allwood, AC, Walter, MR, Van Kranendonk, MJ, Bowden, SA, Sylva, SP and Summons, RE 2007, Structural characterization of kerogen in 3.4 Ga Archaean cherts from the Pilbara Craton, Western Australia: Precambrian Research, v. 155, p. 1–23.

Martinez-Ruiz, F, Jroundi, F, Paytan, A, Guerra-Tschuschke, I, Del Mar Abad, MM and González-Muñoz, MT 2018a, Barium bioaccumulation by bacterial biofilms and implications for Ba cycling and use of Ba proxies: Nature Communications, doi:10.1038/s41467-018-04069-z.

Martinez-Ruiz, F, Paytan, A, González-Muñoz, MT, Jroundi, F, Abad, MM, Lam, PJ, Bishop, JKP, Horner, TJ, Morton, PL and Kastner, M 2018b, Barite formation in the ocean: Origin of amorphous and crystalline precipitates: Chemical Geology, v. 511, p. 441–451.

McCollom, TM and Seewald, JS 2006, Carbon isotope composition of organic compounds produced by abiotic synthesis under hydrothermal conditions: Earth and Planetary Science Letters, v. 243, p. 74–84.

Morag, N, Williford, KH, Kitajima, K, Philippot, P, Van Kranendonk, MJ, Lepot, K, Thomazo, C and Valley, JV 2016, Microstructure-specific carbon isotopic signatures of Om from ~3.5 Ga cherts of the Pilbara Craton support a biologic origin: Precambrian Research, v. 275, p. 429–449.

Nelson, DR 1997a, 118965: equigranular biotite monzogranite gneiss, old highway – Sherlock River crossing 457: Geological Survey of Western Australia, 4p.

Nelson, DR 1997b, 118967: equigranular hornblende–biotite tonalite, Ten Foot Well 459: Geological Survey of Western Australia, 4p.

Nelson, DR 1997c, 118975: porphyritic rhyolite, Mount Regal 432: Geological Survey of Western Australia, 4p.

Nelson, DR 1998a, Compilation of SHRIPM U_PB zircon geochronology data, 1997: Geological Survey of Western Australia, Record 1998/2, 242p.

Nelson, DR 1998b, 142882: biotite monzogranite, west of Mulgandinna Hill; Geochronology dataset 351, *in* Compilation of geochronology data, June 2006 update: Geological Survey of Western Australia.

Nelson, DR 1998c, 142878: foliated biotite monzogranite, Hillside Track; Geochronology dataset 349, *in* Compilation of geochronology data, June 2006 update: Geological Survey of Western Australia.

Nelson, DR 1998d, 136819: quartz–mica schist, Lydia Mine 413: Geological Survey of Western Australia, 3p.

Nelson, DR 1998e, 141936: welded tuff, Red Hill; Geochronology Record 396: Geological Survey of Western Australia, 3p.

Nelson, DR 1998f, 142433: tonalite, Mount Regal; Geochronology Record 403: Geological Survey of Western Australia, 3p.

Nelson, DR 1998g, 142661: foliated biotite tonalite, Zebra Hill; Geochronology Record 409: Geological Survey of Western Australia, 3p.

Nelson, DR 1998h, 142836: volcaniclastic sedimentary rock, Gorge Creek *in* Compilation of SHRIMP U–Pb zircon geochronology data, 1997: Geological Survey of Western Australia, Record 1998/2, p. 66–68.

Nelson, DR 1999, Compilation of geochronology data, 1998: Geological Survey of Western Australia, Record 1999/2, 222p.

Nelson, DR 2000a, Compilation of geochronology data, 1999: Geological Survey of Western Australia, Record 2000/2, 251p.

Nelson, DR 2000b, 142962: tonalite, Chocolate Hill; Geochronology dataset 303, *in* Compilation of geochronology data, June 2006 update: Geological Survey of Western Australia.

Nelson, DR 2000c, 142966: heterogeneous schlieric granodiorite, Unices Well; Geochronology dataset 306, *in* Compilation of geochronology data, June 2006 update: Geological Survey of Western Australia.

Nelson, DR 2000d, 142952: porphyritic felsic tuff, Tremain Well; Geochronology dataset 302, *in* Compilation of geochronology data, June 2006 update: Geological Survey of Western Australia.

Nelson, DR 2001, 168913: dacite, Gallop Well, Geochronology dataset 225: Geological Survey of Western Australia.

Nelson, DR 2005a, 178042: altered volcaniclastic sandstone, Table Top Well, Geochronology dataset 564: Geological Survey of Western Australia.

Nelson, DR 2005b, 178044: hornblende-biotite quartz monzodiorite, North Shaw Well; Geochronology dataset 566, *in* Compilation of geochronology data, June 2006 update: Geological Survey of Western Australia.

Nijman, W, De Bruin, K and Valkering, M 1998, Growth fault control of early Archaean cherts, barite mounds, and chert-barite veins, North Pole Dome, Eastern Pilbara, Western Australia: Precambrian Research, v. 88, p. 25–52.

Ohta, H, Maruyama, S, Takahashi, E, Watanabe, Y and Kato, Y 1996, Field occurrence, geochemistry and petrogenesis of the Archaean Mid-Oceanic Ridge Basalts (AMORBs) of the Cleaverville area, Pilbara Craton, Western Australia: Lithos, v. 37, p. 199–221.

Otálora, F, Mazurier, A, García-Ruiz, JM, Van Kranendonk, MJ, Kotopoulou, E, El Albani, A and Garrido, CJ 2018, A crystallographic study of crystalline casts and pseudomorphs from the 3.5 Ga Dresser Formation, Pilbara Craton (Australia): Journal of Applied Crystallography, v. 51, p. 1050–1058.

Pearce, JA 2008, Geochemical fingerprinting of oceanic basalts with applications to ophiolite classification and the search for Archean oceanic crust: Lithos, v. 100, p. 14–48.

Pease, V, Percival, J, Smithies, RH, Stevens, G and Van Kranendonk, MJ 2008, When did plate tectonics begin? Evidence from the orogenic record, *in* When did plate tectonics begin on planet Earth? *edited by* KC Condie and V Pease: Geological Society of America, Special Paper 440, p. 199–228.

Philippot, P, Van Zuilen, M, Lepot, K., Thomazo, C, Farquhar, J and Van Kranendonk, M 2007, Early Archean microorganisms preferred elemental sulphur, not sulphate: Science, v. 317, p. 1534–1537.

Pike, G and Cas, R 2002, Stratigraphic evolution of Archaean volcanic rock-dominated rift basins from the Whim Creek Belt, west Pilbara Craton, Western Australia, *in* Precambrian sedimentary environments: A modern approach to ancient depositional systems *edited by* W Altermann and P Corcoran: Blackwell Science, Oxford, UK, International Association of Sedimentologists, Special Publication 33, p. 213–234.

Pike, GJ 2001, The facies architecture of two contrasting volcano-sedimentary basin successions from the Archaean Whim Creek Belt, North Pilbara Terrain, Western Australia: The intra-continental arc-related Whim Creek Group and plume-related, continental rift-hosted Bookingarra Group: Monash University, Melbourne, PhD thesis (unpublished), 465p.

Pitcher, WS 1993, The nature and origin of granite: London, Blackie Academic and Professional, 321p.

Ramsay, JG 1967, Folding and fracturing of rocks: McGraw-Hill Books, New York.

Rasmussen, B and Muhling, JR 2023, Organic carbon generation in 3.5-billion-year-old basalt-hosted seafloor hydrothermal vent systems: Sci. Advances, vol. 9, no. 5, doi: 10.1126/sciadv.add7925.

Rasmussen, B, Fletcher, IR and Muhling, JR 2007, In situ U–Pb dating and element mapping of three generations of monazite: Unravelling cryptic tectonothermal events in low-grade terranes: Geochimica et Cosmochimica Acta, v. 71, pp. 670–690.

Rasmussen, B, Krapež, B and Muhling, JR 2014, Hematite replacement of iron-bearing precursor sediments in the 3.46-b.-y.-old Marble Bar Chert, Pilbara craton, Australia: GSA Bulletin, v. 126, p. 1245–1258.

Renaut, RW and Jones, B 1997, Controls on aragonite and calcite precipitation in hot spring travertines at Chemurkeu, Lake Bogoria, Kenya: Canadian Journal of Earth Sciences, v. 34, p. 801–818.

Shen, Y, Buick, R and Canfield, DE 2001, Isotopic evidence for microbial sulphate reduction in the early Archaean era: Nature, v. 410, p. 77–81.

Shen, YN, Farquhar, J, Masterson, A, Kaufman, AJ and Buick, R 2009, Evaluating the role of microbial sulfate reduction in the early Archean using quadruple sulfur isotope systematics: Earth and Planetary Science Letters, v. 279, p. 383–391.

Shirey, SB and Hanson, GN 1984, Mantle-derived Archaean monozodiorites and trachyandesites: Nature, v. 310, p. 222–224.

Smith, JB 2003, The episodic development of intermediate to silicic volcano-plutonic suites in the Archaean West Pilbara, Australia: Chemical Geology, v. 194, p. 275–295.

Smith, JB, Barley, ME, Groves, DI, Krapež, B, McNaughton, NJ, Bickle, MJ and Chapman, HJ 1998, The Sholl Shear Zone, West Pilbara; evidence for a domain boundary structure from integrated tectonostratigraphic analysis, SHRIMP U–Pb dating and isotopic and geochemical data of granitoids: Precambrian Research, v. 88, p. 143–172.

Smithies, RH 2000, The Archaean tonalite–trondhjemite–granodiorite (TTG) series is not an analogue of Cenozoic adakite: Earth and Planetary Science Letters, v. 182, p. 115–125.

Smithies, RH 2002, Archaean boninite-like rocks in an intracratonic setting: Earth and Planetary Science Letters, v. 197, no. 1–2, p. 19–34.

Smithies, RH and Champion, DC 2000, The Archaean high-Mg diorite suite: Links to tonalite–trondhjemite–granodiorite magmatism and implications for early Archaean crustal growth: Journal of Petrology, v. 41, no. 12, p. 1653–1671.

Smithies, RH, Nelson, DR and Pike, G 2001, Development of the Archaean Mallina Basin, Pilbara Craton, northwestern Australia; A study of detrital and inherited zircon ages: Sedimentary Geology, 141–142, p. 79–94.

Smithies, RH, Champion, DC and Cassidy, KF 2003, Formation of Earth's early Archaean continental crust: Precambrian Research, v. 127, p. 89–101.

Smithies, RH, Champion, DC and Sun, S-S 2004, Evidence for early LREE-enriched mantle source regions: Diverse magmas from the c. 3.0 Ga Mallina Basin, Pilbara Craton, NW Australia: Journal of Petrology, v. 45, no. 8, p. 1515–1537.

Smithies, RH, Champion, DC, Van Kranendonk, MJ, Howard, HM and Hickman, AH 2005a, Modern-style subduction processes in the Mesoarchaean: Geochemical evidence from the 3.12 Ga Whundo intra-oceanic arc: Earth and Planetary Science Letters, v. 231, no. 3–4, p. 221–237.

Smithies, RH, Van Kranendonk, MJ and Champion, DC 2005b, It started with a plume – early Archaean basaltic proto-continental crust: Earth and Planetary Science Letters, v. 238, no. 3–4, p. 284–297.

Smithies, RH, Champion, DC and Van Kranendonk, MJ 2007a, The oldest well-preserved volcanic rocks on Earth: Geochemical clues to the early evolution of the Pilbara Supergroup and implications for the growth of a Paleoarchean continent, *in* Earth's oldest rocks *edited by* MJ Van Kranendonk, VC Bennett and RH Smithies: Elsevier BV, Burlington, Massachusetts, USA, Developments in Precambrian Geology 15, p. 339–367.

Smithies, RH, Champion, DC, Van Kranendonk, MJ and Hickman, AH 2007b, Geochemistry of volcanic rocks of the northern Pilbara Craton, Western Australia: Geological Survey of Western Australia, Report 104, 47p.

Smithies, RH, Van Kranendonk, MJ and Champion, DC 2007c, The Mesoarchean emergence of modern-style subduction: Gondwana Research, v. 11, no. 1–2, p. 50–68, doi:10.1016/j.gr.2006.02.001.

Smithies, RH Champion, DC and Van Kranendonk, MJ 2009, Formation of Paleoarchean continental crust through infracrustal melting of enriched basalt: Earth and Planetary Science Letters, v. 281, p. 298–306.

Smithies, RH, Lu, Y, Kirkland, CL, Johnson, TE, Mole, DR, Champion, DC, Martin, L, Jeon, H, Wingate, MTD and Johnson, SP 2021, Oxygen isotopes trace the origins of Earth's earliest continental crust: Nature, v. 592, p. 70–75, doi:10.1038/s41586-021-03337-1.

Stern, RA and Hanson, GN 1991, Archean high-Mg granodiorite: A derivative of light rare earth element-enriched monzodiorite of mantle origin: Journal of Petrology, v. 32, p. 201–238.

Strik, G, Blake, TS, Zegers, TE, White, SH and Langereis, CG 2003, Palaeomagnetism of flood basalts in the Pilbara Craton, Western Australia: Late Archaean continental drift and the oldest known reversal of the geomagnetic field: Journal of Geophysical Research, v. 108, no. B12, 2551, doi:10.1029/2003JB002475, 2003.

Sugitani, K, Lepot, K, Mimura, K, Van Kranendonk, MJ, Oehler, D and Walter, MR 2010, Biogenicity of morphologically diverse carbonaceous microstructures from the ca. 3400 Ma Strelley Pool Formation, in the Pilbara Craton, Western Australia: Astrobiology, v. 10, p. 899–920.

Sugitani, K, Mimura, K, Takeuchi, M, Yamaguchi, T, Suzuki, K, Senda, R, Asahara, Y, Wallis, S and Van Kranendonk, MJ 2015a, A Paleoarchean coastal hydrothermal field inhabited by diverse microbial communities: The Strelley Pool Formation, Pilbara Craton, Western Australia: Geobiology, doi: 10.1111/gbi.12150.

Sugitani, K, Mimura, K, Takeuchi, M, Lepot, K and Javaux, EJ 2015b, Early evolution of large micro-organisms with cytological complexity revealed by microanalyses of 3.4 Ga organic-walled microfossils: Geobiology, v. 13, p. 507–521.

Sun, S-S and Hickman, AH 1998, New Nd-isotopic and geochemical data from the west Pilbara – implications for Archaean crustal accretion and shear zone development: Australian Geological Survey Organisation, Research Newsletter, no. 28, p. 25–29.

Sun, S-S and McDonough, WF, 1989, Chemical and isotopic systematics of oceanic basalts: Implications for mantle composition and processes: Geological Society London, Special Publication 42, p. 313–345.

Tadbiri, S and Van Kranendonk, MJ, 2020, Structural analysis of syn-depositional hydrothermal veins of the 3.48 Ga Dresser Formation, Pilbara Craton, Australia: Precambrian Research, v. 347, 105844.

Terabayashi, M, Masuda, Y and Ozawa, H 2003, Archaean ocean floor metamorphism in the North Pole area, Pilbara Craton, Western Australia: Precambrian Research, v. 127, p. 167–180.

Teyssier, C and Collins, WJ 1990, Strain and kinematics during the emplacement of the Mount Edgar Batholith and Warrawoona Syncline, Pilbara Block, Western Australia, *in* Third International Archaean Symposium Extended Abstracts Volume *compiled by* JE Glover and SE Ho: Geoconferences (WA) Inc., Perth, p. 481–483.

Thorne, AM and Trendall, AF 2001, Geology of the Fortescue Group, Pilbara Craton, Western Australia: Geological Survey of Western Australia, Bulletin 124.

Thorpe, RA, Hickman, AH, Davis, DW, Mortensen, JK and Trendall, AF 1992a, U–Pb zircon geochronology of Archaean felsic units in the Marble Bar region, Pilbara Craton, Western Australia: Precambrian Research, v. 56, p. 169–189.

Thorpe, RI, Hickman, AH, Davis, DW, Mortensen, JK and Trendall, AF 1992b, Constraints to models for Archaean lead evolution from precise U–Pb geochronology from the Marble Bar region, Pilbara Craton, Western Australia, *in* The Archaean: Terrains, processes and metallogeny *edited by* JE Glover and S Ho: Geology Department and University Extension, The University of Western Australia, Publication 22, p. 395–408.

Torres-Crespo, N, Martínez-Ruiz, F, González-Muñoz, MT, Bedmar, EJ, De Lange, G and Jroundi, F 2015, Role of bacteria in marine barite precipitation: A case using Mediterranean seawater: Science of the Total Environment, v. 512–513, p. 562–571.

Troll, V, Walter, TR and Schmincke, H-U 2002, Cyclic caldera collapse: Piston or piecemeal subsidence? Field and experimental evidence: Geology, v. 30, p. 135–138.

Ueno, Y, Yoshioka, H, Maruyama, S and Isozaki, Y 2004, Carbon isotopes and petrography in ~3.5 Ga hydrothermal silica dykes in the North Pole area, Western Australia: Geochimica et Cosmochimica Acta, v. 68, p. 573–589.

Ueno, Y, Yamada, K, Yoshida, N, Maruyama, S and Isozaki, Y 2006, Evidence from fluid inclusions for microbial methanogenesis in the early Archaean era: Nature, v. 440, p. 516–519.

Ueno, Y, Ono, S, Rumble, D and Maruyama, S 2008, Quadruple sulfur isotope analysis of ca. 3.5 Ga Dresser Formation: New evidence for microbial sulfate reduction in the early Archean: Geochimica et Cosmochimica Acta, v. 72, p. 5675–5691.

van Haaften, WM and White, SH 1998, Evidence for multiphase deformation in the Archean basal Warrawoona Group in the Marble Bar area, East Pilbara, Western Australia: Precambrian Research, v. 88, p. 53–66.

Van Kranendonk, MJ 1999, North Shaw, WA, Sheet 2755: Geological Survey of Western Australia, 1:100 000 Geological Series.

Van Kranendonk, MJ 2000, Geology of the North Shaw 1:100 000 sheet: Geological Survey of Western Australia, 1:100 000 Geological Series Explanatory Notes, 86p.

Van Kranendonk, MJ 2006, Volcanic degassing, hydrothermal circulation and the flourishing of early life on Earth: New evidence from the Warrawoona Group, Pilbara Craton, Western Australia: Earth-Science Reviews, v. 74, p. 197–240.

Van Kranendonk, MJ 2007, A review of the evidence for putative Paleoarchean life in the Pilbara Craton, *in* Earth's Oldest Rocks. Developments in Precambrian Geology 15 *edited by* MJ Van Kranendonk, RH Smithies and V Bennet: Elsevier, Amsterdam, The Netherlands, pp. 855–896.

Van Kranendonk, MJ 2010, Three and a half billion years of life on Earth: A transect back into deep time: Geological Survey of Western Australia, Record 2010/21, 93p.

Van Kranendonk, MJ 2011, Morphology as an indicator of biogenicity for 3.5 – 3.2 Ga fossil stromatolites from the Pilbara Craton, Western Australia: Lecture Notes in Earth Sciences, v. 131, p. 537–554.

Van Kranendonk, MJ and Morant, P 1998, Revised Archaean stratigraphy of the North Shaw 1:100 000 sheet, Pilbara Craton: Western Australian Geological Survey, Annual Review 1997–1998, p. 55–62.

Van Kranendonk, MJ and Pirajno, F 2004, Geological setting and geochemistry of metabasalts and alteration zones associated with hydrothermal chert ± barite deposits in the ca. 3.45 Ga Warrawoona Group, Pilbara Craton, Australia: Geochemistry: Exploration, Environment, Analysis, v. 4, p. 253–278.

Van Kranendonk, MJ, Hickman, AH, Smithies, RH, Nelson, DN and Pike, G 2002, Geology and tectonic evolution of the Archaean North Pilbara terrain, Pilbara Craton, Western Australia: Economic Geology, v. 97, p. 695–732.

Van Kranendonk, MJ, Webb, GE and Kamber, BS 2003, Geological and trace element evidence for a marine sedimentary environment of deposition and biogenicity of 3.45 Ga stromatolitic carbonates in the Pilbara Craton, and support for a reducing Archean ocean: Geobiology, v. 1, p. 91–108.

Van Kranendonk, MJ, Collins, WJ, Hickman, AH and Pawley, MJ 2004, Critical tests of vertical vs horizontal tectonic models for the Archaean East Pilbara Granite–Greenstone Terrane, Pilbara Craton, Western Australia: Precambrian Research, v. 131, p. 173–211.

Van Kranendonk, MJ, Bleeker, W and Ketchum, J 2006a, Phreatomagmatic boulder conglomerates at the fracture propagation tip of the 2.77 Ga Black Range dolerite dyke, Pilbara Craton, Western Australia: Australian Journal of Earth Sciences, v. 53, p. 617–630.

Van Kranendonk, MJ, Hickman, AH, Smithies, RH, Williams, IR, Bagas, L and Farrell, TR 2006b, Revised lithostratigraphy of Archean supracrustal and intrusive rocks in the northern Pilbara Craton, Western Australia: Geological Survey of Western Australia, Record 2006/15, 57p.

Van Kranendonk, MJ, Hickman, AH, Smithies, RH and Champion, DC 2007a, Paleoarchean development of a continental nucleus: The East Pilbara Terrane of the Pilbara Craton, Western Australia, *in* Earth's oldest rocks *edited by* MJ Van Kranendonk, VC Bennett and RH Smithies: Elsevier BV, Burlington, Massachusetts, USA, Developments in Precambrian Geology 15, p. 307–337.

Van Kranendonk, MJ, Smithies, RH, Hickman, AH and Champion, DC 2007b, Review: Secular tectonic evolution of Archean continental crust: Interplay between horizontal and vertical processes in the formation of the Pilbara Craton, Australia: Terra Nova, v. 19, no. 1, p. 1–38.

Van Kranendonk, MJ, Philippot, P, Lepot, K, Bodorkos, S and Pirajno, F 2008, Geological setting of Earth's oldest fossils in the ca. 3.5 Ga Dresser Formation, Pilbara Craton, Western Australia: Precambrian Research, v. 167, p. 93–124.

Van Kranendonk, MJ, Smithies, RH, Hickman, AH, Wingate, MTD and Bodorkos, S 2010, Evidence for Mesoarchean (~3.2 Ga) rifting of the Pilbara Craton: The missing link in an early Precambrian Wilson cycle: Precambrian Research, v. 177, no. 1–2, p. 145–161, doi:10.1016/j.precamres.2009.11.007.

Van Kranendonk, MJ, Smithies, RH, Griffin, WL, Huston, DL, Hickman, AH, Champion, DC, Anhaeusser, CR and Pirajno, F 2015, Making it thick: A volcanic plateau model for Paleoarchean continental lithosphere of the Pilbara and Kaapvaal cratons, *in* Continent Formation Through Time *edited by* NMW Roberts, M Van Kranendonk, S Parman, S Shirey and PD Clift: Geological Society, London, Special Publications 389, p. 83–112.

Van Kranendonk, MJ, Djokic, T, Poole, G, Tadbiri, S, Steller, L and Baumgartner, R 2019a, Depositional setting of the fossiliferous, c. 3480 Ma Dresser Formation, Pilbara Craton: A review, *in* Earth's Oldest Rocks, 2nd edition *edited by* MJ Van Kranendonk, V Bennett and E Hoffmann: Elsevier, USA, p. 985–1006.

Van Kranendonk, MJ, Smithies, RH and Champion, DC 2019b, Paleoarchean development of a continental nucleus: The East Pilbara Terrane of the Pilbara Craton, Western Australia, *in* Earth's Oldest Rocks, 2nd edition *edited by* MJ Van Kranendonk, V Bennett and E Hoffmann: Elsevier, USA, p.437–462.

Van Kranendonk, MJ, Baumgartner, R, Djokic, T, Ota, T, Steller, L, Garbe, U and Nakamura, E 2021a, Elements for the origin of life on land: A deep-time perspective from the Pilbara Craton of Western Australia: Astrobiology, v. 21, no. 1, p. 39–59, doi: 10.1089/ast.2019.2107.

Van Kranendonk, MJ, Djokic, T, Baumgartner, R, Bontognali, T, Sugitani, K, Kiyokawa, S and Walter, MR 2021b, Life analogue sites for Mars from early Earth: Diverse habitats from the Pilbara Craton and Mount Bruce Supergroup, Western Australia, *in* Mars Geological Enigmas: From the Late Noachian Epoch to the Present Day *edited by* RJ Soare, SJ Conway, DZ Oehler and J-P Williams: Elsevier Inc., USA p. 357–403.

Wacey, D, McLoughlin, N, Stokes, CA, Kilburn, MR, Green, OR and Brasier, MD 2010a, The 3426-3350 Ma Strelley Pool Formation in the East Strelley greenstone belt – a field and petrographic guide: Geological Survey of Western Australia, Record 2010/10, 64p.

Wacey, D, McLoughlin, N, Whitehouse, MJ and Kilburn, MR 2010b, Two coexisting sulfur metabolisms in a ca. 3400 Ma sandstone: Geology, v. 38, p. 1115–1118.

Walter, MR 1983, Archean Stromatolites: Evidence of the Earth's earliest benthos, *in* Earth's Earliest Biosphere *edited by* JW Schopf: Princeton University Press, Princeton.

Walter, MR, Buick, R and Dunlop, JSR 1980, Stromatolites 3400–3500 Myr old from the North Pole area, Western Australia: Nature, v. 284, p. 443–445.

Warren, RG and Ellis, DJ 1996, Mantle underplating, granite tectonics, and metamorphic P-T-t paths: Geology, v.24, p. 663–666.

Williams, IS and Collins, WJ 1990, Granite–greenstone terranes in the Pilbara Block, Australia, as coeval volcano-plutonic complexes; evidence from U–Pb zircon dating of the Mount Edgar batholith: Earth and Planetary Science Letters, v. 97, p. 41–53.

Wingate, MTD 1999, Ion microprobe baddeleyite and zircon ages for Late Archaean mafic dykes of the Pilbara Craton, Western Australia: Australian Journal of Earth Sciences, v. 46, p. 493–500.

Zegers, TE, White, SH, de Keijzer, M and Dirks, P 1996, Extensional structures during deposition of the 3460 Ma Warrawoona Group in the eastern Pilbara Craton, Western Australia: Precambrian Research, v. 80, p. 89–105.

Zegers, TE, Nelson, DR, Wijbrans, JR and White, SH 2001, SHRIMP U–Pb zircon dating of Archean core complex formation and pancratonic strike-slip deformation in the East Pilbara Granite–Greenstone Terrain: Tectonics, v.20, p. 883–908.

RECORD 2023/6

6IAS: Pilbara Craton, evolving Archean tectonic styles — field guide

MJ Van Kranendonk and RH Smithies

Access GSWA products

All products
All GSWA products are free to download as PDFs from the DMIRS eBookshop <www.dmirs.wa.gov.au/ebookshop>.
View other geoscience information on our website <www.dmirs.wa.gov.au/gswa>.

Hard copies
Limited products are available to purchase as hard copies from the First Floor Counter at Mineral House or via the DMIRS eBookshop <www.dmirs.wa.gov.au/ebookshop>.

Fieldnotes
Fieldnotes is a free digital-only quarterly newsletter which provides regular updates to the State's exploration industry and geoscientists about GSWA's latest programs, products and services.
Access by subscribing to the GSWA eNewsletter <www.dmirs.wa.gov.au/gswaenewsletter> or downloading the free PDF from the DMIRS eBookshop <www.dmirs.wa.gov.au/ebookshop>.

GSWA eNewsletter
The GSWA eNewsletter is an online newsletter that contains information on workshops, field trips, training and other events.
To keep informed, please subscribe <www.dmirs.wa.gov.au/gswaenewsletter>.

Further details of geoscience products are available from:

First Floor Counter
Department of Mines, Industry Regulation and Safety
100 Plain Street
EAST PERTH WESTERN AUSTRALIA 6004
Phone: +61 8 9222 3459 Email: publications@dmirs.wa.gov.au
www.dmirs.wa.gov.au/GSWApublications